Abstract

Title of Dissertation: SUPERFLUIDITY IN A DEGENERATE ATOMIC FERMI GAS

Nicolai Nygaard, Doctor of Philosophy, 2003

Dissertation directed by: Professor Millard H. Alexander
Chemical Physics Program
Dr. Charles W. Clark
National Institute of Standards and Technology

Dilute atomic gases have become a powerful tool for studying many-body quantum mechanics. The best example of this is the achievement of Bose-Einstein condensation in 1995 in a gas of Bose atoms, a discovery which has invoked a confluence of ideas from condensed matter, atomic and nuclear physics. Now a concerted research effort is focused on creating and studying a BCS superfluid in an atomic Fermi gas.

In the work presented here we study in detail pairing superfluidity in a Fermi gas of atoms, by self-consistently solving the Bogoliubov-de Gennes equations, both for bulk systems, and for atoms in a harmonic confining potential. A critical part of this work is the derivation of a regularized theory, which is formulated entirely in terms of physically measurable quantities, such that a quantitative

comparison between theory and experiment is possible with no adjustable parameters. The resulting equations form a non-linear problem, and the accurate numerical solution of this poses a formidable challenge. A major component of this thesis is the development of efficient computational approaches to overcome these difficulties.

Based on the linear response of the gas to a twisting of the order parameter phase, the superfluid density can be defined as a generalized elasticity of the system. Using finite temperature perturbation theory we calculate the superfluid density in an inhomogeneous system.

We investigate the structure and thermodynamic properties of a singly quantized vortex line in a gas of superfluid fermionic atoms, making the first quantitative determination the critical rotation frequency for thermodynamic stability of the vortex state, and study the nature of the bound states in the vortex core. These excitations fill the core, making direct imaging of the vortex unlikely. Instead, we propose an experiment to indirectly probe the vortex density of states with laser fields, in a scheme analogous to Scanning Tunneling Microscopy. Furthermore, it is shown that the vortex state causes a shift of the superfluid transition temperature, which can be understood as a finite size effect.

SUPERFLUIDITY IN A DEGENERATE ATOMIC FERMI GAS

by

Nicolai Nygaard

Dissertation submitted to the Faculty of the Graduate School of the
University of Maryland at College Park in partial fulfillment
of the requirements for the degree of
Doctor of Philosophy
2003

Advisory Committee:

Professor Millard H. Alexander, Chairman/Advisor
Dr. Charles W. Clark, Advisor
Professor William D. Phillips
Professor Wendell T. Hill III
Professor Steven Anlage

Til mine forældre

Acknowledgements

It is a pleasure to lead this thesis off by giving thanks to those who have helped making it possible. Though it represents the sum of my work, many people have left their imprint on it, and deserve recognition.

I extend my deepest appreciation to Charles Clark, for giving me the opportunity to come to NIST and work with the best and the brightest. He has been an inspiration through his passion for physics and his ability to identify interesting and important problems. I am grateful to him for making my years in graduate school a gratifying and rewarding experience. I feel like I have been blessed with several advisors, who have helped to guide and shape my research and learning. I want to thank Millard Alexander for serving as my University of Maryland supervisor, and for his advice and guidance. Georg Bruun and David Feder have been invaluable sources of knowledge and assistance. It has been a true pleasure to work with both of them. Likewise, it is a joy to thank Barry Schneider for teaching me all I know about the intricacies of the discrete variable representation and for his mentoring. I cannot leave out Klaus Mølmer, who guided me through my master's education in Aarhus. He set up the initial contact with the research group at NIST, which I have been able to

call my home for the past four years. I owe him great thanks for his strong engagement in my career.

Everybody in the Physics Laboratory at NIST, in particular those in the Radiation Physics Building, deserve a heartfelt appreciation for creating a warm and friendly environment. As a scientific institution NIST is a truly amazing place, where critical thinking and scientific curiosity are nurtured. Everyone I have interacted with has affected me with their contagious enthusiasm. In particular Blair Blakie, Zach Dutton, Ana Maria Rey, Marianna Safranova, and Jamie Williams should be pointed out for being wonderful friends and colleagues, and for always volunteering their time and advice when I had questions. Jamie Williams deserves special recognition for at least pretending to keep his sanity while sharing an office with me. Also a special thanks to Blair Blakie for not just reading the manuscript, but offering valuable comments and suggestions in the process.

Additionally, I want to thank all of my friends outside the world of physics. They have helped me to stay connected to life outside the bubble, and to keep an eye on the truly important things in life. The same holds true for my parents and my sister. I love them dearly and cannot thank them enough for helping me grow into the person I am today.

Finally, I want to give my most affectionate thanks to Judith Gayle. No words could sufficiently describe the joy and happiness she has brought into my life. Without her love and unending support the completion of this work would not have been possible.

Table of Contents

List of Figures

Chapter 1

Introduction

Historical context

For the last century superconductors and superfluids have been among the most fascinating systems in physics, due to their almost "magical" properties. It is our view that the two phenomena are not disparate, but rather connected at a fundamental level. This will be a recurring theme in the thesis. The purpose of this first Chapter is to set the stage for the ensuing discussion, and to provide a historical context for our work.

Since the first observation of superconductivity in mercury by Onnes [1], the phenomenon has been the object of intense scrutiny in a wide range of materials. The vast experimental effort has uncovered a large variety of unique properties associated with the superconducting phase. One of the most spectacular of these is of course the vanishing of the resistivity as the the transition point is traversed from the normal state, but just as important is the perfect diamagnetism of a superconductor, *i.e.* the ability of the sample to exclude a weak magnetic field. This is known as the Meissner effect [2]. In 1938 Kapitza [3] and Allen and

Misener [4] discovered superfluidity in liquid ^{4}He. They found that at the so-called λ-point ($T = 2.19$ K) the liquid undergoes a phase transition to a new state with bizarre properties. Whereas the liquid above the λ-point (known as helium I) behaves like a normal fluid, the phase below the λ-point, helium II, is characterized by unique *superfluid* properties. These are expressed most dramatically in the suppression of the coefficient of viscosity by a factor of 10^6 or more compared with helium I [3, 4]. Other manifestations include the fountain effect [5], and the existence of temperature waves or second sound [6].

Both superconductivity and superfluidity can be associated with the existence of a macroscopic wavefunction for the system, and for this reason they are manifestations of quantum mechanics on a scale visible to the naked eye. London was the first to realize that such macroscopic coherence could be responsible for superfluid behavior [7]. Based on this idea, Tisza introduced a qualitative two-fluid model in which the special properties of helium II are ascribed to the existence of a zero entropy, superfluid component flowing without friction, intermixing with a normal fluid component comprising the rest of the liquid [8]. A similar two-fluid model was formulated for superconductors by Gorter and Casimir [9]. Independently of Tisza, Landau derived two-fluid hydrodynamics based on a phenomenological picture of the superfluid liquid being composed of weakly-interacting quasi-particles [10].

Landau also introduced the important concept of an order parameter to describe phase transitions such as those to the superconducting and superfluid states. The order parameter was later related to the macroscopic wavefunction, and significant work was done in the 1950's and 1960's in parallel by Ginzburg and Landau on superconductors [11] and by Pitaevskii [12] and Gross [13] on su-

perfluids, with a spatially nonuniform order parameter. Anderson was a pioneer in clarifying the role played by the macroscopic wavefunction, and in elucidating how the phase of this object determines the dynamic properties of superflow [14].

While a microscopic theory of superfluidity was proposed in 1947 by Bogoliubov [15], the underlying theory of superconductivity remained largely a mystery until 1957, when Bardeen, Cooper and Schrieffer explained the phenomena as essentially a superfluid flow of charged electron pairs [16]. The concept of pairing, while irrelevant for ^{4}He, was a fundamental element in understanding the emergence of coherence in the superconducting systems at the phase transition, and underscores an important basic difference between electrons and ^{4}He atoms. Several other systems have since been found where superfluidity arises due to pairing of particles. Most notable among these are liquid ^{3}He, which was first cooled below its superfluid transition temperature of 2.7 mK in 1972 by Osheroff, Richardson and Lee [17], and the novel class of ceramic superconductors with an extremely high transition temperature discovered in 1986 by Bednorz and Müller [18]. Likewise pairing between nucleons in atomic nuclei is known to give rise to superfluid effects.

Ultracold quantum gases provide a novel system for studying low temperature phenomena in many-body physics. Produced by applying atomic physics techniques to cool dilute atomic vapors to sub-microkelvin temperatures, they have generated a lot of excitement due to the large degree of control exerted by experimentalists over such vital system properties as the density, interactions, temperature and composition. While superfluidity was achieved in a dilute gas in 1995 in the labs of Cornell and Wieman [19], Ketterle [20], and Hulet [21], a superfluid phase based on pairing as in a superconductor has yet to be observed.

The production of such a system is the goal of an ongoing research effort, and is interesting from a fundamental perspective since it could ultimately shed light on other pairing systems, like high temperature superconductors, for which the pairing mechanisms are not well understood. The pairing superfluid state in an atomic gas is the topic of this thesis.

Overview of the thesis

The overall goal of the thesis is to describe the physics of a neutral Fermi superfluid in the context of the ongoing experimental effort to achieve a phase transition to this state in an atomic gas. We start in Chapter 2 with an introduction to the physics of Fermi gases in the normal (non-superfluid) state, both ideal and weakly interacting. To describe the latter we introduce a mean-field description, where the pairwise atomic collisions are replaced by a static effective single-particle potential encapsulating the net effect of the the interactions of a single atom with all the other particles in the gas at the neglect of correlation effects. This mean-field approach is our platform for doing computations of properties like the density distribution and single-particle excitation spectra. We consider numerically two specific examples: a Fermi gas trapped in a harmonic potential, directly relevant to the typical experimental setups, and the case of a Fermi gas enclosed in a cylinder, which mimics a homogeneous system provided the volume of the confining vessel is large enough that finite size effects are negligible. These two different situations will be used recurrently in the thesis to illustrate the predictions of the theory. While the discussion in Chapter 2 is

well-known it introduces the fundamental concepts of fermion physics relevant for the remaining Chapters.

In Chapter 3 we go through the derivation of the weak-coupling BCS theory of a superfluid Fermi gas. As in Chapter 2 this is a mean-field theory, now including the possibility that the particles form phase coherent pairs below a critical temperature T_c, marking the transition from the normal state to the superfluid phase. In general the superfluid state is described by a set of non-linear differential equations, which has to be solved numerically. This is quite challenging, and a large component of this work involves the development of efficient numerical procedures for solving the mean-field equations. However, for a bulk gas the equations allow for an analytical solution, and we place a particular emphasis on comparing the properties of a superfluid Fermi gas in a cylinder with those of a homogeneous medium. The key element of the theory is the proper regularization of the pairing amplitude, linking the many-body treatment with two-body scattering physics. This leads to a first principles theory formulated entirely in terms of physically measurable quantities, and consequently the predictions of the theory can be directly related to experiments with no adjustable parameters. This is different from the typical situation in superconductivity theory, where such direct comparison is usually not possible. The regularization of the pairing theory builds on earlier work, but in the present discussion we clarify the systematic introduction of an energy cutoff into the theory, discussing how to truncate the numerical sums over the eigenstates of the system in such a way that all observables are independent of the particular value of this upper energy. Furthermore, we emphasize the importance of including self-energy effects in the regularization procedure in order to optimize the numerical convergence of the

scheme.

Chapter 4 discusses the nature of superfluidity in the system. As is customary we formulate the description of the phase transition in terms of a broken symmetry leading to the establishment of a macroscopic phase coherence in the sample. That is, the superfluid state is characterized by the emergence of a macroscopic wavefunction for the pairs with a well defined phase encapsulating the appearance of a microscopic ordering in the system. This underscores the view of superfluidity as a manifestation of the underlying quantum relations between the particles. We show how the phase coherence leads directly to a macroscopic rigidity of the system, related to the stiffness of the phase of the pair wavefunction. The persistent currents of superfluid flow arise due to energy barriers separating thermodynamic (quasi)-equilibrium states corresponding to different values of the quantized circulation. Based on the tendency of the gas to resist a strain on the phase parameter we calculate the local superfluid density under very general assumptions. We find that at zero temperature the entire gas is superfluid regardless of the details of the potential or strength of interactions, provided the paired superfluid state is the ground state of the system. In the limit of a bulk system we recover the usual result for a homogeneous gas.

In Chapter 5 we investigate in detail the vortex state of a superfluid atomic Fermi gas. Due to the quantization of circulation the gas will resist an attempt to put it into rotational motion, unless the rotation is fast enough to excite the system to a state with exactly one half unit of angular momentum per particle. This is the vortex state, which represents the first excited state of the macroscopic wavefunction. The rotation frequency at which the vortex is thermodynamically stabilized is known as the critical frequency, and has not been accurately deter-

mined until now. We calculate this quantity numerically, confirming a particular phenomenological model of the vortex structure, while ruling against another. This result is of importance not only for degenerate atomic Fermi gases, but for a broader range of physical systems where vortices occur. Calculating the critical frequency requires very accurate numerical techniques, since it involves finding a small difference between two large numbers. We furthermore investigate the detailed microscopic structure of the vortex state and its thermodynamic properties. Finding an unambiguous signature of superfluidity in a dilute atomic Fermi gas is one of the outstanding questions of the field. Since quantized vortices is one of the hallmarks of superfluids, observing a vortex is a potential candidate for detecting the transition to the superfluid state. We discuss the feasibility of probing the quantized currents associated with the flow around the vortex structure with a spectroscopic method.

The final chapter addresses the determination of the transition point, *i.e.* the temperature at which the gas goes from the normal to the superfluid state. This temperature can be accurately determined from a linearization of the equations governing the superfluid. Again the regularization procedure plays an important role, and when implementing this we find perfect agreement with the analytical bulk result for a Fermi gas held in a cylinder. We also investigate the influence of a vortex state on the transition temperature and find a significant shift, which we attribute to a finite size effect related to the swelling of the vortex structure as temperature is increased, such that at high temperatures it becomes impossible to 'fit' the vortex into the finite box.

The appendices contain some of the mathematical and numerical details not necessary in the main text. These include a discussion of the pseudopotential

method , which is an effective low energy replacement of the true interaction potential by a model one, designed to reproduce the correct two-body scattering physics, and an overview of the methodology of finite temperature field theory.

Chapter 2

Fermions

2.1 Spin and Statistics

In classical mechanics we can follow the individual phase space trajectories of identical particles. Quantum mechanics on the other hand introduces a fundamental uncertainty in the identification of identical particles, making them *indistinguishable*: interchange of any two identical particles in a system leaves it unchanged. In physical terms this means that all observables are invariant under such permutations, which in turn implies that the many-body wavefunction, Ψ, of the system can only change by a global phase factor θ, when the spatial coordinates and spin variables of two particles are interchanged

$$\Psi(\ldots, \mathbf{x}_i, \ldots, \mathbf{x}_j, \ldots) = \theta\, \Psi(\ldots, \mathbf{x}_j, \ldots, \mathbf{x}_i, \ldots). \tag{2.1}$$

Here we use $\mathbf{x}_i = (\mathbf{r}_i, \sigma_i)$ as a short-hand notation for the position and spin of the i'th particle. Since two consecutive permutations return the system to the original state, the phase factor must be either $+1$ or -1, corresponding to a wavefunction that is symmetric or anti-symmetric, respectively, under interchange of particle labels. The appropriate symmetry is determined exclusively

by the spin of the particles in question. This is the spin-statistics theorem, which states that the fundamental constituents of matter can be divided into two distinct groups according to the value of their intrinsic spin [22]. Particles with integer spin (in units of $\hbar = h/2\pi$, where h is Planck's constant) are *bosons*, and are required to have $\theta = +1$. On the other hand, particles with half-integer spin, called *fermions*, are described by wavefunctions that are anti-symmetric under permutations, *i.e.* $\theta = -1$. The spin-statistics theorem is a consequence of very general field theoretical considerations based on the assumption of microscopic causality [23]. From the anti-symmetry of the many-body wavefunction of a system of indistinguishable fermions it follows immediately that two identical fermions can not occupy the same single-particle state, a rule of Nature known as the Pauli exclusion principle. In contrast, any number of bosons can occupy the same single-particle state with no restrictions other than those placed by thermal equilibrium. To show the exclusion principle we write the many-body wavefunction as a product over single-particle states

$$\Psi_0(\ldots, \mathbf{x}_i, \ldots, \mathbf{x}_j, \ldots) = \mathcal{A}\psi_1(\mathbf{x}_1) \cdots \psi_\alpha(\mathbf{x}_i) \cdots \psi_\beta(\mathbf{x}_j) \cdots, \tag{2.2}$$

where $\mathcal{A}$ is an anti-symmetrization operator. In general this is only possible in the absence of interactions, but supposing the single-particle states form a complete set, we can expand Ψ for an interacting system in terms of states like Ψ_0. If we interchange the labels of particles i and j the wavefunction has to change sign in order to comply with the spin-statistics theorem. However, if the two fermions are both in the same single-particle state, *i.e.* $\alpha = \beta$, such a permutation obviously leaves the wavefunction unchanged. We therefore infer that states with $\alpha = \beta$ are not permissible. The importance of the Pauli principle can not be overemphasized, it is the foundation of the periodic table

of the elements, and hence all of chemistry [24, 25].

From these considerations on enumerating the allowed many-body states one derives by purely combinatorial means the statistical laws governing thermal equilibrium of a quantum gas. For bosons one finds that they follow a Bose-Einstein distribution, whereas fermions are described by Fermi-Dirac statistics [26]. We are interested in systems with well defined average energy and mean particle number, for which the grand canonical ensemble is appropriate (we are thus assuming that the system is in contact with a heat bath and a reservoir with which it can exchange particles). Hence the mean occupation number of a single-particle state with translational energy ϵ is

$$f(\epsilon) = \frac{1}{e^{\beta(\epsilon-\mu)} \mp 1}, \tag{2.3}$$

where the upper (lower) sign is for bosons (fermions). We will use this convention throughout the thesis, whenever we specifically quote results for both types of particles. We have defined as usual $\beta = 1/k_{\mathrm{B}}T$, where k_{B} is Boltzmann's constant, and T is the temperature. Additionally, μ is the chemical potential, defined as the change in the total energy E when another particle is added to a system containing N particles, keeping both the volume V, and the entropy S fixed [27]

$$\mu = \left(\frac{\partial E}{\partial N}\right)_{VS}. \tag{2.4}$$

It is interesting to note that while most modern treatments of quantum statistics assume translational invariance, as appropriate for homogeneous systems like the electron gas, Enrico Fermi's original derivation of Fermi-Dirac statistics focused on an ideal gas in a harmonic oscillator potential, thereby presaging the current experiments cooling fermionic atoms to degeneracy in harmonic trapping potentials [28, 29].

Strictly speaking the spin-statistics theorem only applies for elementary particles. However, one can show that aggregates of elementary particles are bosons (fermions) when they contain an even (odd) number of fermionic entities, provided the interaction between such clusters is small enough that their internal structure can be neglected [30]. Therefore the many-body wavefunction of a system, written in terms of the coordinates of these composite objects, must be symmetric under the interchange of any two clusters, if these contain an even number of fermions, and anti-symmetric otherwise. That is, a composite object can be a boson or a fermion, depending on its internal structure. For example the atom ^{6}Li is a fermion, since it contains an odd number of fermions (3 electrons, and 6 nucleons), while the isotope ^{7}Li obeys Bose-Einstein statistics (because of the extra nucleon). As we shall see below this means that the properties of the two isotopes are dramatically different at low temperatures.

2.1.1 Quantum Degeneracy

At high temperature (or equivalently low densities) the effects of quantum statistics are entirely negligible, and the thermal properties of a system are determined by the Boltzmann distribution

$$f(\epsilon) = e^{\beta(\mu-\epsilon)} \tag{2.5}$$

regardless of whether said system is a collection of bosons or fermions. This follows from taking the low occupation number limit of (2.3). However, as we pass below a crossover temperature scale $T_{\rm deg}$ the quantum mechanical nature of the particles manifests itself on a macroscopic scale. In this regime the quantum statistical effects are of central importance as the (thermal) de Broglie waves of

the atoms begin to overlap. For a gas of particles of mass m_a at temperature T the de Broglie wavelength is

$$\lambda_{\mathrm{dB}} = \frac{h}{\sqrt{2\pi m_a k_{\mathrm{B}} T}}. \tag{2.6}$$

When λ_{dB} becomes comparable to, or larger than the inter-particle spacing $d \sim n^{-1/3}$, where $n = N/V$ is the number density, the wavepackets describing quantum states of the individual particles begin to significantly overlap, and the indistinguishability of the particles becomes important. This defines the crossover between classical (Boltzmann) and quantum (Fermi-Diarc/Bose-Einstein)) statistics. The condition for quantum degeneracy can be written as

$$k_{\mathrm{B}} T_{\mathrm{deg}} \sim \frac{\hbar^2}{m_a n^{2/3}}, \tag{2.7}$$

or alternatively in terms of the phase space density Λ

$$\Lambda = n\lambda_{\mathrm{dB}}^3 \sim 1. \tag{2.8}$$

The effects of quantum degeneracy depend crucially on whether the particles are bosons or fermions. At a temperature on the order of the degeneracy temperature bosons undergo a phase transition to a state where a macroscopic number of particles occupy the lowest single-particle eigenstate of the system. The particles in this state form a coherent matter wave called a *Bose-Einstein condensate* [31]. First predicted in 1925 by Albert Einstein [32] building on earlier work by Satyendra Nath Bose [33], Bose-Einstein condensation (BEC) is generally believed to be the mechanism responsible for superfluidity in liquid ^{4}He [7]. In 1995 BEC was achieved in ultracold, dilute atomic gases [19, 20, 21], which marked the culmination of a research effort beginning in the late 1970's with cooling and trapping experiments on spin-polarized hydrogen [34]. Since then

a host of beautiful experiments have investigated the properties and peculiarities of this new quantum state of matter (for a fairly recent review of the field see [35]).

The effect of quantum degeneracy on fermions will be the topic of the remainder of this chapter. But before we get to that, the next section will briefly discuss the elements of a typical ultracold atom experiment. This will serve to introduce some of the terminology of the field, and to acquaint the reader with the physical systems of interest.

2.2 A Theorist's Ultracold Atomic Gas How-To

The cooling and trapping techniques for neutral atoms developed in the quest to reach BEC in an atomic Bose gas have been applied with few modifications to obtain degeneracy in a gas of fermionic atoms. We can not possibly do justice to this vast research field spanning almost three decades. Instead we very briefly touch on the most important aspects of an ultracold gas experiment, with the aim to introduce the key concepts relevant for the ensuing discussion on dilute atomic Fermi gases. The interested reader is urged to consult one of many existing reviews, *e.g.* [31, 36, 37, 38, 39] and references therein.

The first step in most ultracold gas experiments is laser cooling of the sample. The basic principle can be posed as follows: consider a a two-level atom with states $|g\rangle$ and $|e\rangle$, connected by a closed transition with energy $\hbar\omega_a = E_e - E_g$, where $E_e > E_g$. If an atom in the lower state absorbs a photon on resonance it is excited and the photon is lost. Momentum conservation causes the atom to recoil in the direction of the incoming light and changes its velocity by an amount

$\hbar\mathbf{k}/m_a$, where $\mathbf{k}$ is the wavevector of the electromagnetic field. As the atom returns to the state $|g\rangle$ by spontaneous emission it gets a second momentum kick in the direction opposite that of the emitted photon. However, as spontaneous emission is a random process with a symmetric angular distribution, the atom will get no net momentum transfer from the emission when we average over many absorption/emission cycles. Thus on average the atomic velocity is changed by $\hbar\mathbf{k}/m_a$ each time such a cycle is completed. This effect was first demonstrated by Frisch in 1933, who used a sodium lamp to slightly deflect an atomic beam. However, not until the advent of the laser did we have a narrow band, intense light source, capable of generating a substantial scattering force. In a setup with six laser beams counterpropagating along three orthogonal axes, all detuned below resonance, one can achieve cooling of an atomic vapor. Due to the Doppler shift an atom preferentially absorbs laser light with a wavevector opposite to its velocity. The result is a compression of the atomic cloud, and a reduction of the mean velocity, which amounts to cooling. Combining the lasers with a quadrupole magnetic field a stable trap for neutral atoms can be created. In such a magneto-optical trap (MOT) phase space densities on the order of 10^{-5} can be achieved.

When cold enough, atoms with magnetic moments can be trapped by magnetic forces alone, due to the interaction of their intrinsic magnetic dipole moment $\boldsymbol{\mu}_m$ with an external magnetic field $\mathbf{B}$, giving rise to a potential $-\boldsymbol{\mu}_m \cdot \mathbf{B}$. If the field is nonuniform, the atoms experience a force proportional to the magnetic field gradient. An atom in a state with $g_F m_F < 0$ is attracted towards regions of field minimum. Here g_F is the g-factor, and m_F is the projection of the total spin $\mathbf{F} = \mathbf{L} + \mathbf{S} + \mathbf{I}$ unto the axis defined by the local direction of the

magnetic field (**L** is the orbital angular momentum, **S** the electron spin, and **I** is the nuclear spin). On the other hand if $g_F m_F$ is positive, the atoms are pushed by the magnetic force towards regions of a higher field. In constructing a magnetic trap a serious restriction is imposed by the impossibility of a local field maxima. So a magnetic trap can only hold atoms in 'low-field seeking' states, *i.e.* atomic states with negative value of $g_F m_F$ This sets a serious limitation on the operation of traps based on the magnetic force, as there will be several untrapped states which are thus unavailable in such experiments. Additionally, if a magnetic trap holds a combination of different spin states one must worry about spin changing collisions, which can lead to trap loss, if an atom is flipped from a 'low-field seeking' to 'high-field seeking' Zeeman state where $g_F m_F$ is positive.

Alternatively, one can hold the atoms trapped using only optical forces. The simplest example is a Gaussian, focused red-detuned laser beam, and uses the dipole force to restrict the atomic motion. In contrast to the dissipative force used in laser cooling above, this is a conservative force arising due to the ac Stark shift. For negative detuning an atom is attracted towards regions of high intensity, while for blue detuned light the force is in the opposite direction. An optical trap is particularly useful in that it will hold any spin state, or combination of spin states.

Holding the atoms in a magnetic or optical trap, further cooling and increase in phase space density can be accomplished by a process known as evaporative cooling. By lowering the depth of the trapping potential the hottest atoms are allowed to escape. This selective removal of atoms in the high energy tail of the thermal distribution causes the remaining atoms to cool under collisional equili-

bration. A key point here is that this rethermalization process is inhibited for a spin polarized Fermi gas, since at low temperatures it becomes non-interacting, as we discuss in the next section. Therefore evaporative cooling becomes ineffective for fermions at low temperatures. To circumvent this difficulty one can trap simultaneously fermions in two different internal states, as these remain interacting as the temperature approaches zero. This sympathetic cooling also works well for a spin polarized Fermi gas immersed in a sea of bosonic atoms, which can be cooled to form a BEC. The collisions between the two species can establish thermal equilibrium on a time scale short enough to cool the fermionic component.

It is important to note that at low energies atoms in both magnetic and optical traps feel a harmonic restoring force. Therefore calculations for harmonic oscillator potentials hold a special relevance in comparing theory with experiments. Furthermore, the strength and depth of the trapping potential can be continuously varied by ramping either the magnetic field gradient and strength or the laser focusing and intensity. This provides an effective control over the density of the gas, and by a periodic variation of the trap strength collective oscillations of the trapped cloud can be induced. Similarly, the position of the trap minimum is subject to experimental control. Displacements of the trap center can be used to measure the spring constant of the harmonic restoring force, since in a harmonic potential the dipole modes have the special property that the center of mass and relative motion are separable for systems interacting through forces that depend only on the relative distance between scattering particles. Therefore dipole, or Kohn modes, are undamped by interactions or finite temperature effects, and simply observing the oscillatory motion of the center of

mass of the atomic cloud along different axes, gives a measure of the harmonic trapping frequencies of single particles.

Detection of the atoms is direct. It involves taking a picture of the atomic density distribution using either shadow or non-destructive phase-contrast imaging. The cloud can be observed while sitting in the trap or after a short ballistic expansion, *i.e.* by turning off the external potential and allowing the gas to expand freely, while falling under gravity. The latter method is often preferred to enlarge features too small to be observable in-situ.

Using the techniques described above a number of fermionic isotopes are currently being trapped and cooled in several laboratories worldwide. They include ^{6}Li ($I = 1$), ^{40}K ($I = 4$), ^{84}Rb ($I = 2$, and which is radioactive), and ^{53}Cr ($I = \frac{3}{2}$), but the list of atoms (bosons and fermions alike) which have been successfully cooled to degeneracy is growing and a new species seems to be added every few months.

Throughout this thesis we will focus on ^{6}Li, whenever it is relevant to quote specific numerical examples. The reason for this choice does not reflect any particular bias, but it is the element being used in the majority of the experiments on Fermi gases. At 7.5% the natural abundance is quite high. It has an optical transition frequency of 671 nm, at which diode lasers provide a reliable light source for laser cooling. Typically, experiments on ^{6}Li are conducted with a 50-50 mixture of atoms in the two Zeeman sublevels of the lower hyperfine state $|F = 1/2; m_F = \pm 1/2\rangle$. Since the $m_F = 1/2$ state is a 'high-field seeker' this combination of states require an optical trapping potential. The reason for choosing these specific states is the tunability of interatomic scattering potential (see Section 3.5 below), and the stability of this mixture against spin-exchange

collisions. These conserve the total magnetic quantum number $m_F^{\rm tot} = m_F^1 + m_F^2$, where $m_F^{\rm tot} = 0$ for the $|F = 1/2; m_F = \pm 1/2\rangle$ states. Since there are no two-particle spin states with $m_F^{\rm tot} = 0$ at lower energies, spin-exchange collisions are suppressed.

We end this section by emphasizing the importance of the dilute nature of the gases under scrutiny. At the temperatures and pressures of the experiments just accounted for, the stable thermodynamic ground state of the atoms is a solid. Hence the gaseous form is only a meta-stable state of the system. However, there is an energy barrier between the two phases which may keep the system in a local minimum of the free energy corresponding to the gas phase. The gas-solid phase transition is characterized by nucleation; droplets of the new phase (liquid or crystal) form either from thermodynamic fluctuations, on a surface, or around impurity particles and then grow to encompass the entire system. In a high vacuum the influence of impurities can be minimized, and since the magnetic and optical trapping methods described above hold the atomic cloud suspended far away from the walls of the vacuum chamber, the dominant loss mechanism determining the lifetime of the sample is three-body recombination. The rate of this process is strongly suppressed at low densities, as it scales as n^2, where n is the atomic density. Depending on the particular system, the lifetime of the trapped gas can be as long as a few minutes.

2.3 Microscopic Theory of an Atomic Fermi Gas

As stated in the previous section this thesis will primarily be concerned with a Fermi gas consisting of atoms in two different Zeeman sublevels, which we label

as $|\uparrow\rangle$ and $|\downarrow\rangle$. Due to the extremely low energies involved in atomic collisions, the Zeeman levels are well separated (the exact splitting within a given hyperfine manifold will depend on the strength of the magnetic bias field, but in typical experiments it is on the order of several MHz, equivalent to temperatures of hundreds of μK). Therefore we can consider the two component Fermi gas as a two level, or spin-1/2 system, and from this point onward we will simply refer to the two internal states as spin states.

To write down the many-body Hamiltonian it is convenient to invoke the formalism of quantum field theory. In this second quantization language the symmetry properties of the many-body state is incorporated in a very elegant way, through the commutation rules of the creation and annihilation operators, $\hat{c}_i^\dagger$ and $\hat{c}_i$, which creates and destroys a particle in the single-particle state $|\psi_i\rangle$, respectively (we will use a hat on an operator to indicate that it acts on a many-body state). The index i labels both the external (orbital) and internal state of the particles. For fermions these operators obey anti-commutation relations:

$$\begin{aligned} \{\hat{c}_i, \hat{c}_j^\dagger\} &\equiv \hat{c}_i\hat{c}_j^\dagger + \hat{c}_j^\dagger\hat{c}_i = \delta_{ij}, \\ \{\hat{c}_i, \hat{c}_j\} &= \{\hat{c}_i^\dagger, \hat{c}_j^\dagger\} = 0. \end{aligned} \tag{2.9}$$

Defining the vacuum state $|0\rangle$ as the state containing no particles such that

$$\hat{c}_i|0\rangle = 0, \tag{2.10}$$

we obtain a state vector for a system of N fermions by acting on $|0\rangle$ consecutively with N different $\hat{c}_i^\dagger$'s, in an abstract sense creating the particles out of the vacuum. To describe continuum quantum fields we introduce the field operators

$$\hat{\psi}_\sigma(\mathbf{r}) = \sum_i \psi_i(\mathbf{r}, \sigma)\hat{c}_i,$$

$$\hat{\psi}^{\dagger}_{\sigma}(\mathbf{r}) \;=\; \sum_{i} \psi^{*}_{i}(\mathbf{r},\sigma)\hat{c}^{\dagger}_{i}, \tag{2.11}$$

where the mode function $\psi_i(\mathbf{r},\sigma) = \langle \mathbf{r},\sigma|\psi_i\rangle$ is the projection of the single particle state $|\psi_i\rangle$ onto the coordinate eigenstate $|\mathbf{r}\rangle$ and the state of spin projection $|\sigma\rangle$. The physical meaning of the operator $\hat{\psi}^{\dagger}_{\sigma}(\mathbf{r})$ is revealed by acting with it on the vacuum state:

$$\begin{aligned}
\hat{\psi}^{\dagger}_{\sigma}(\mathbf{r})\,|0\rangle \;&=\; \sum_{i} \psi^{*}_{i}(\mathbf{r},\sigma)\,\hat{c}^{\dagger}_{i}\,|0\rangle = \sum_{i}\langle\psi_i|\mathbf{r},\sigma\,\rangle|\psi_i\rangle \\
&=\; \sum_{i} |\psi_i\rangle\langle\psi_i|\mathbf{r},\sigma\rangle = |\mathbf{r},\sigma\rangle,
\end{aligned} \tag{2.12}$$

exploiting the fact that the single particle states $\{|\psi_i\rangle\}$ form a complete basis set. It is then clear that the action of $\hat{\psi}^{\dagger}_{\sigma}(\mathbf{r})$ is to create a fermion at $\mathbf{r}$ in the spin state $|\sigma\rangle$. In a similar manner it can be shown that $\hat{\psi}_{\sigma}(\mathbf{r})$ annihilates a fermion at $\mathbf{r}$. The field operators satisfy the anti-commutation relations:

$$\begin{aligned}
\left\{\hat{\psi}_{\alpha}(\mathbf{r}),\hat{\psi}^{\dagger}_{\beta}(\mathbf{r}')\right\} \;&=\; \delta(\mathbf{r}-\mathbf{r}')\delta_{\alpha\beta}, \\
\left\{\hat{\psi}_{\alpha}(\mathbf{r}),\hat{\psi}_{\beta}(\mathbf{r}')\right\} \;&=\; \left\{\hat{\psi}^{\dagger}_{\alpha}(\mathbf{r}),\hat{\psi}^{\dagger}_{\beta}(\mathbf{r}')\right\} = 0,
\end{aligned} \tag{2.13}$$

which follow directly from (2.9) and (2.11).

In a typical experimental regime the trapped gases are so dilute that collisions involving more than two particles are highly improbable. Hence we can safely restrict the interactions to include only binary collisions between fermions. To be definite we consider two fermions in spin states $|\sigma\rangle$ and $|\sigma'\rangle$, interacting via a short range potential $V_{\sigma\sigma'}(\mathbf{r})$. Furthermore, since the Pauli exclusion principle dictates that the scattering wave function of two indistinguishable fermions be anti-symmetric, only odd angular momentum partial waves are allowed, when the scattering particles are in the same internal state $|\sigma\rangle$. But the centrifugal barrier effectively shuts down all non-zero angular momentum channels for

collisions in the degenerate regime. In particular, at the temperatures we are interested in only s-wave scattering is of any significance, and as a consequence only particles in different spin states interact. A spin polarized Fermi gas, where only a single spin state is occupied, is therefore close to ideal. The suppression of p-wave scattering was observed experimentally by DeMarco *et al.*, who demonstrated that at low temperatures the p-wave elastic cross section was significantly suppressed compared with the contribution from the s-wave channel [40]. We can therefore take $\sigma' = -\sigma$ in the interaction potential, and include only s-wave contributions. Here we are using the notational convention that $-\sigma = \downarrow$ if $\sigma = \uparrow$, and vice versa. With these considerations the many-body Hamiltonian becomes

$$\begin{aligned} \hat{H} &= \sum_{\sigma} \int d^3r\, \hat{\psi}^{\dagger}_{\sigma}(\mathbf{r}) \mathcal{H}_{\sigma} \hat{\psi}_{\sigma}(\mathbf{r}) \\ &+ \frac{1}{2} \sum_{\sigma} \int d^3r \int d^3r'\, \hat{\psi}^{\dagger}_{\sigma}(\mathbf{r}) \hat{\psi}^{\dagger}_{-\sigma}(\mathbf{r}') V(\mathbf{r}-\mathbf{r}') \hat{\psi}_{-\sigma}(\mathbf{r}') \hat{\psi}_{\sigma}(\mathbf{r}). \end{aligned} \tag{2.14}$$

The first term includes the single-particle Hamiltonian

$$\mathcal{H}_{\sigma} = -\frac{\hbar^2}{2m_a}\nabla^2 + V_{\mathrm{ext},\sigma}(\mathbf{r}), \tag{2.15}$$

and is the many-body Hamiltonian for a non-interacting system. We have included an external potential, which may be different for the two spin states. In the second term describing the interactions we have dropped the subscripts on the two-body potential since $V_{\sigma-\sigma} = V_{-\sigma\sigma}$. It is also instructive to write the Hamiltonian in terms of the mode operators

$$\hat{H} = \sum_{mn\sigma} \langle m|\mathcal{H}_{\sigma}|n\rangle \hat{c}^{\dagger}_{m\sigma}\hat{c}_{n\sigma} + \frac{1}{2}\sum_{klmn\sigma} \langle kl|V|mn\rangle \hat{c}^{\dagger}_{k\sigma}\hat{c}^{\dagger}_{l-\sigma}\hat{c}_{m-\sigma}\hat{c}_{n\sigma}, \tag{2.16}$$

where the spin states have been explicitly indicated.

In writing the Hamiltonian (2.14) we have left out the energy splitting between the two spin states, $\hbar\omega_{\mathrm{a}} \equiv \epsilon_{\uparrow} - \epsilon_{\downarrow}$. While this energy offset is important in

establishing the true thermodynamic ground state of the system, we can safely neglect it here, since we are interested only in solving for a quasi-equilibrium state. As explained above low-energy collisions are incapable of changing the relative populations of the two states. Additionally, radiative transitions can usually be disregarded on the time scale of typical experiments. Hence we can take the population of either state to be a fixed thermodynamic variable, set by the exact preparation of the experiment, and the difference in internal energy between the two spin levels is consequently irrelevant for our discussion. This is equivalent to applying the transformation $\mathcal{U}_\sigma = \exp(i\epsilon_\sigma t/\hbar)$ to the field operator $\hat{\psi}_\sigma$. It is easily seen that the dynamical equations for $\hat{\psi}'_\sigma = \mathcal{U}_\sigma \hat{\psi}_\sigma$ are independent of $\hbar\omega_{\rm a}$. These considerations are all moot if the states are directly coupled through an external field, or if the Zeeman splitting varies spatially, as is the case if the gas is immersed in an inhomogeneous magnetic field if the magnetic moments of the two states are different. Under these circumstances one has to include explicitly the energy offset in the Hamiltonian.

2.4 The Ideal Fermi Gas

We now consider the properties of a non-interacting Fermi gas. At temperatures below $T_{\rm deg}$ the lowest single-particle states of the many-body system have occupancies close to unity, the maximum allowed under the Pauli exclusion principle. In the limit of $T = 0$ the Fermi distribution function reduces to a step function where all states with energy lower than the chemical potential have mean occupation number one, and all other states are empty

$$\lim_{T\to 0} \frac{1}{e^{\beta(\epsilon-\mu)}+1} = \theta(\mu-\epsilon). \tag{2.17}$$

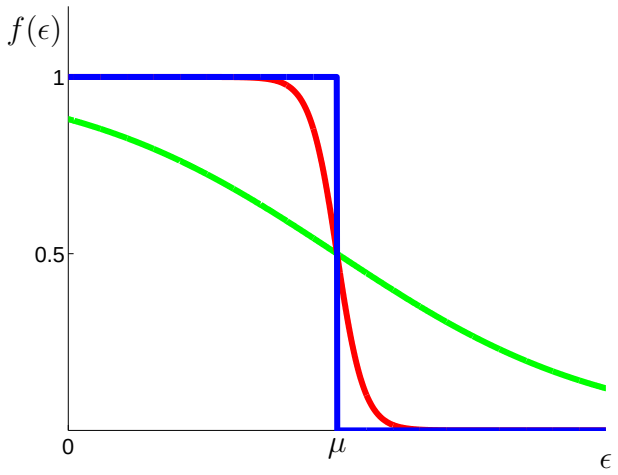

Figure 2.1: The Fermi distribution function for an ideal Fermi gas at $T = 0$ (*blue*), $0 < T \ll E_{\rm F}/k_{\rm B}$ (*red*), and for $T = E_{\rm F}/2k_{\rm B}$ (*green*).

This shows that at zero temperature the chemical potential of a Fermi gas is a positive number (recall that $\beta\mu \to -\infty$ for $T \to \infty$ for both bosons and fermions). It is customary to call this the Fermi energy $E_{\rm F}$

$$E_{\rm F} = \mu(T = 0). \tag{2.18}$$

The Fermi distribution function at zero temperature, at a temperature small compared to $E_{\rm F}/k_{\rm B}$, and $k_{\rm B}T = E_{\rm F}/2$ are sketched in Fig. 2.1.

2.4.1 Free Fermions

To derive an expression for the Fermi energy we consider a Fermi gas enclosed in a cubic box of volume $V = L^3$. In the thermodynamic limit the size and shape of the container is irrelevant. As we shall later see one finds finite size effects for mesoscopic systems, but for now we will neglect these. Assuming periodic (Born-von Karman) boundary conditions the wavefunctions are plane

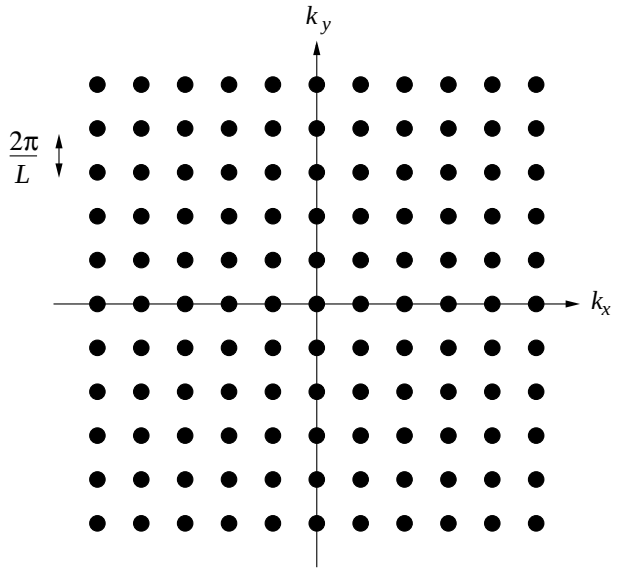

Figure 2.2: Allowed eigenstates for a particle in a box represented in momentum space. For clarity only the states in the plane defined by $k_z = 0$ are shown.

waves with wavevectors given by

$$\mathbf{k} = (\hat{e}_x n_x + \hat{e}_y n_y + \hat{e}_z n_z)\frac{2\pi}{L}, \quad \text{with} \quad n_i \in \mathbb{Z}, \tag{2.19}$$

and energies $\epsilon_{\mathbf{k}} = \hbar^2\mathbf{k}^2/2m_a$. As is seen from (2.19) the allowed quantum states of the system can be represented by a grid of equidistant points in $\mathbf{k}$-space, with a separation between points of $2\pi/L$. This is shown in Fig. 2.2. Therefore the density of points in momentum space is $(L/2\pi)^3$. At zero temperature all states with an energy less than the Fermi energy are filled. We define the Fermi surface as the constant energy surface $\epsilon_{\mathbf{k}} = E_{\mathrm{F}}$. It is the surface of a sphere with radius k_{F}, called the Fermi vector. In an inhomogeneous system the Fermi surface can have a topology of arbitrary complexity.

The total number of states inside the Fermi surface numbers $(4\pi k_{\mathrm{F}}^3/3)(L/2\pi)^3$.

This must equal the number of particles, and we thus have

$$k_{\mathrm{F}} = \left(6\pi^2 \frac{N}{V}\right)^{1/3}. \tag{2.20}$$

The Fermi energy is given by

$$E_{\mathrm{F}} = \frac{\hbar^2 k_{\mathrm{F}}^2}{2m_a} = \frac{\hbar^2}{2m_a}\left(6\pi^2 \frac{N}{V}\right)^{2/3}. \tag{2.21}$$

The filled states below E_{F} are usually termed the Fermi sea. In a multi-component system each component will fill its own Fermi sea giving rise to separate Fermi energies $E_{F\sigma}$, assuming no interactions between the two components. In this case we replace N in (2.21) by N_σ, the number of particles in state σ.

The total energy of the gas is defined as $E = \langle \hat{H} \rangle$, where we take $\langle \cdots \rangle$ to mean the ensemble (thermal) average (see Appendix C). For the non-interacting two-component Fermi gas we find

$$E_0 = \sum_{\mathbf{k}\sigma} \epsilon_{\mathbf{k}\sigma} \langle \hat{c}^\dagger_{\mathbf{k}\sigma} \hat{c}_{\mathbf{k}\sigma} \rangle = 2 \sum_{\mathbf{k}} \epsilon_{\mathbf{k}} f(\epsilon_{\mathbf{k}}). \tag{2.22}$$

The factor of 2 is the spin degeneracy, and we have assumed an equal number of particles in each spin state $N_\uparrow = N_\downarrow$ such that $E_{F\uparrow} = E_{F\downarrow} = E_{\mathrm{F}}$. At zero temperature the total energy can be related to the Fermi energy and the number of particles

$$E_0 = 2 \sum_{k<k_{\mathrm{F}}} \frac{\hbar^2 k^2}{2m_a} = \frac{3}{5}\, nV\, \frac{\hbar^2 k_{\mathrm{F}}^2}{2m_a} = \frac{3}{5}\, N E_{\mathrm{F}}, \tag{2.23}$$

where $N = N_\uparrow + N_\downarrow$ is the total number of atoms, and we have used the conversion of the sum to an integral $\sum_{\mathbf{k}} \to V/(2\pi)^3 \int d^3k$, which is valid in the limit of a sufficiently large quantization volume, where $\mathbf{k}$ can be treated as a continuous variable. Since the gas is non-interacting this energy represents a

pure quantum pressure, $P = 2E_0/3V$ (or $P = E_0/3V$ for relativistic particles), since $P = -\partial E/\partial V$. This Fermi pressure remains non-vanishing even at zero temperature, and arises from the Pauli exclusion principle. It is responsible for stabilizing white dwarfs and neutron stars against gravitational collapse [41]. In the experiments on ultracold Fermi gases the onset of degeneracy is marked by the gas achieving a minimum size below which it can not shrink as temperature is lowered further [42]. Additionally, a measurement of the total energy of the gas reveals that in the degenerate regime, the system posses an excess energy compared with a classical gas at the same temperature [43].

2.4.2 Local-Density Approximation

When the Fermi gas is spatially inhomogeneous the solution of the many-body problem in the absence of interactions is found by diagonalizing the single-particle Hamiltonian (2.15), and populating the resulting eigenstates according to the Fermi distribution function. In general this can only be done numerically, and is a somewhat tedious process. For a harmonic oscillator potential this was done by Schneider and Wallis [44], who demonstrated that for a relatively small number of particles the gas shows pronounced finite size effects related to the closing of shells in the energy spectrum of the oscillator. The importance of the discrete nature of the spectrum diminishes as the size of the system grows, or as the temperature is increased.

If the external potential is slowly varying it may be possible to partition the gas into cells of linear dimension d, and neglect the variation of the potential within each cell. In this case we can locally replace the exact solutions of the Hamiltonian with plane wave states. Provided the number of particles in each

cell is large

$$n(\mathbf{r})d^3 \gg 1, \tag{2.24}$$

we can introduce a local degenerate Fermi sea, characterized by a spatially varying Fermi vector $k_{\mathrm{F}}(\mathbf{r})$ given by a generalization of Eq. (2.20)

$$n(\mathbf{r}) = \frac{k_{\mathrm{F}}^3(\mathbf{r})}{6\pi^2}. \tag{2.25}$$

In equilibrium the Fermi energy must be position independent, otherwise it would be energetically favorable for particles to migrate to areas with a lower value of E_{F}. Hence we must have [45]

$$E_{\mathrm{F}} = \frac{\hbar^2 k_{\mathrm{F}}^2(\mathbf{r})}{2m_a} + V_{\mathrm{ext}}(\mathbf{r}). \tag{2.26}$$

This is known as the local density approximation (LDA), or sometimes the Thomas-Fermi approximation. In order to estimate the range of applicability we must specify what we mean by "slowly varying". Provided the strength of the potential is small compared with the local Fermi level, $|V_{\mathrm{ext}}(\mathbf{r})| \ll \hbar^2 k_{\mathrm{F}}^2(\mathbf{r})/2m_a$, only particles in the vicinity of the Fermi surface are affected by the potential. Hence the condition for neglecting the spatial variation of the potential over a cell is $d|\nabla V_{\mathrm{ext}}| \ll \hbar^2 k_{\mathrm{F}}^2(\mathbf{r})/2m_a$. The potential is roughly constant on the scale of the oscillations in the single-particle wavefunctions. Therefore we require

$$d|\nabla V_{\mathrm{ext}}| \ll \frac{\hbar^2}{2m_a}[6\pi^2 n(\mathbf{r})]^{2/3}. \tag{2.27}$$

Combining this with (2.24) we find the variations in the potential must be such that

$$|\nabla V_{\mathrm{ext}}(\mathbf{r})| \ll \frac{\hbar^2}{2m_a}(6\pi^2)^{2/3} n(\mathbf{r}), \tag{2.28}$$

in order for the local density approximation to be valid. It is clear that the LDA must fail wherever the atomic density vanishes, for example at the edge

of a cloud confined in an external potential. Since the LDA involves treating the position and momentum coordinates of the particles as classical variables, while including the effects of quantum statistics it constitutes a semi-classical approximation to the full quantum mechanical problem.

2.5 The Interacting Fermi Gas

As we have already argued, the diluteness of a quantum gas means that only two-body collisions are relevant. Additionally, at ultralow temperatures the details of the two-body interaction potential are unimportant. Instead we can replace the exact atomic potential by a model one, parameterized by the s-wave scattering length a. This so-called *pseudopotential* is discussed in some detail in Appendix A. Here it suffices to say that in the absence of pairing correlations, all quantities are well behaved at the origin, and we can neglect the regularization operator, modeling the atomic potential as

$$V(\mathbf{r}-\mathbf{r}') = \frac{4\pi\hbar^2 a}{m_a}\,\delta(\mathbf{r}-\mathbf{r}') = g\delta(\mathbf{r}-\mathbf{r}'). \tag{2.29}$$

Even so the Hamiltonian can only be diagonalized for a small number of particles. In general one has to rely on many-body perturbation theory to find the spectrum of quasi-particle modes or the ground state energy of the gas. This requires summation of a large (possibly infinite) number of Feynman diagrams [27, 46, 47]. Here we shall take a different approach and neglect correlations altogether by working in a *mean-field* picture. Also known as the independent particle model, it entails replacing the pair-wise interactions with an effective potential in the single-particle Hamiltonian due to the combined effect on a single atom of the

multitude of interactions with the $N-1$ other atoms in the gas

$$g\int d^3r\,\hat{\psi}^\dagger_\uparrow(\mathbf{r})\hat{\psi}^\dagger_\downarrow(\mathbf{r})\hat{\psi}_\downarrow(\mathbf{r})\hat{\psi}_\uparrow(\mathbf{r}) \rightarrow \quad g\ \sum_\sigma \int d^3r\, n_{-\sigma}(\mathbf{r})\hat{\psi}^\dagger_\sigma(\mathbf{r})\hat{\psi}_\sigma(\mathbf{r}) \\ -\quad g\ \int d^3r\, n_\uparrow(\mathbf{r})n_\downarrow(\mathbf{r}), \tag{2.30}$$

where the density of atoms in state $|\sigma\rangle$ is $n_\sigma(\mathbf{r}) = \langle\hat{\psi}^\dagger_\sigma(\mathbf{r})\hat{\psi}_\sigma(\mathbf{r})\rangle$. This is the Hartree-Fock approximation, which is widely used in atomic physics, though here we are using a contact potential, as opposed to the long range Coulomb interaction. As a consequence the direct and exchange terms are identical. The mean-field approach is equivalent to the Weiss molecular field approximation in the Ising model [26]. Note that in a LDA sense we can define the following relationship between the local Fermi wavevector and Fermi energy in the presence of interactions

$$E_{F\sigma} = \frac{\hbar^2 k^2_{\rm F}(\mathbf{r})}{2m_a} + V_{\rm ext}(\mathbf{r}) + gn_{-\sigma}(\mathbf{r}). \tag{2.31}$$

The mean-field $gn_{-\sigma}$ is called the Hartree field, and can give rise to both a positive and negative shift of the single-particle energies, depending on the sign of the coupling constant g. As discussed in Appendix A $g > 0$ corresponds to repulsive interactions, while a negative coupling constant means that the mean-field interaction is attractive. In the following we will consider exclusively the case of attractive interactions.

Within the mean-field approximation the Hamiltonian (2.14) can be solved exactly. As an example we consider a two-component Fermi gas with attractive interactions in a spherically symmetric harmonic oscillator potential of frequency ω, pertinent to current experiments on degenerate atomic Fermi gases. In spherical coordinates the external potential is

$$V_{\rm ext}(\mathbf{r}) = \frac{1}{2}m_a\omega^2 r^2, \tag{2.32}$$

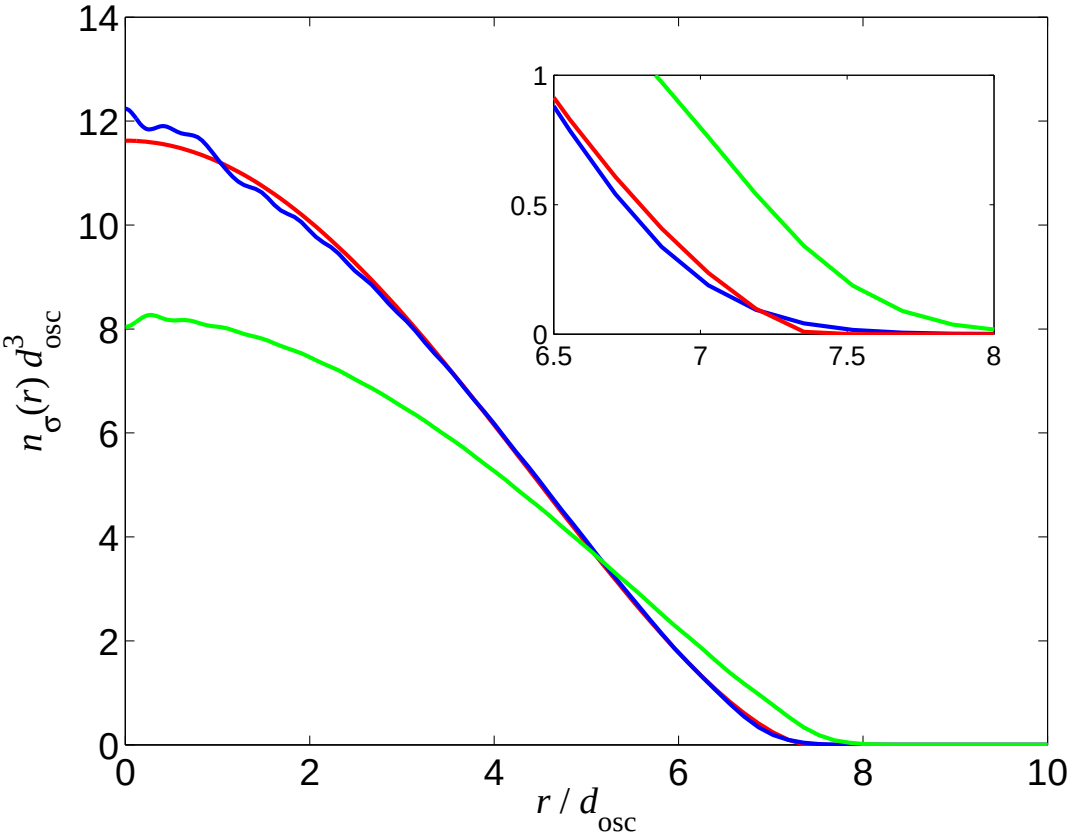

Figure 2.3: Plot of the density profile of a Fermi gas trapped in a harmonic oscillator potential. The number of particles is $N_\sigma = 4988$ in each spin state. The blue curve is the result of a full quantum mechanical mean-field calculation for $g = -1.0\ \hbar\omega d^3_{\rm osc}$. The red curve is the LDA solution for the same parameters, which is seen to be an excellent approximation, except at the edge of the cloud as shown in the inset, and in the trap center where Friedel oscillations are clearly visible in the exact density profile. These are missed by the semi-classical calculation. The density of an ideal gas ($g = 0$) with approximately the same number of particles is plotted in green. The attractive interaction causes the gas to contract, increasing the central density.

where $r = \sqrt{x^2 + y^2 + z^2}$ is the distance from the trap center. It is convenient to introduce the harmonic oscillator length $d_{\rm osc} = \sqrt{\hbar/m_a\omega}$, which sets the characteristic length scale of the problem. Given the number of particles the zero temperature density profile can be calculated by filling all single-particle orbitals with energy less than the Fermi level. The result is shown in Fig. 2.3 for $N_\uparrow = N_\downarrow = 4988$ (corresponding to $\mu = 27.3\ \hbar\omega$), and a coupling strength of $g = -1\ \hbar\omega d_{\rm osc}^3$. If the scattering length and particle mass are chosen appropriate to ^{6}Li, that is $a = -2160\ a_0$ and $m_a = 6$ a.m.u., this corresponds to a trap frequency of $2\pi \times 820$ Hz. The experimental range of frequencies is from tens of Hz to a few kHz. In the figure the quantum result is compared to the density profile as found in a LDA calculation, as well as the density of a noninteracting gas. We see that due to the attractive mean-field interactions the cloud shrinks, thereby increasing the central density. The density of the Fermi gas exhibits small amplitude oscillations near the center of the trap with a wavelength on the order of $k_{\rm F}^{-1}$. These so-called Friedel oscillations reflect the matter wave modulation of the density due the particles in the highest occupied shell [44]. For more detailed calculations of the effect of interactions on the properties of a Fermi gas in harmonic potential we refer to the work of Bruun and Burnett [48]. The LDA density profile is determined by (2.26), and for a non-interacting gas it is given by

$$n_\sigma^{\rm LDA}(\mathbf{r}) = \frac{1}{6\pi^2}\left\{\frac{2m_a}{\hbar^2}\left[E_{\rm F} - \frac{1}{2}m_a\omega^2 r^2\right]\right\}^{3/2}. \tag{2.33}$$

The edge of the cloud, where $n_\sigma^{\rm LDA}$ vanishes, is called the Thomas-Fermi radius, $R_{\rm TF}$. It is

$$R_{\rm TF} = \sqrt{\frac{2E_{\rm F}}{\hbar\omega}}\, d_{\rm osc}. \tag{2.34}$$

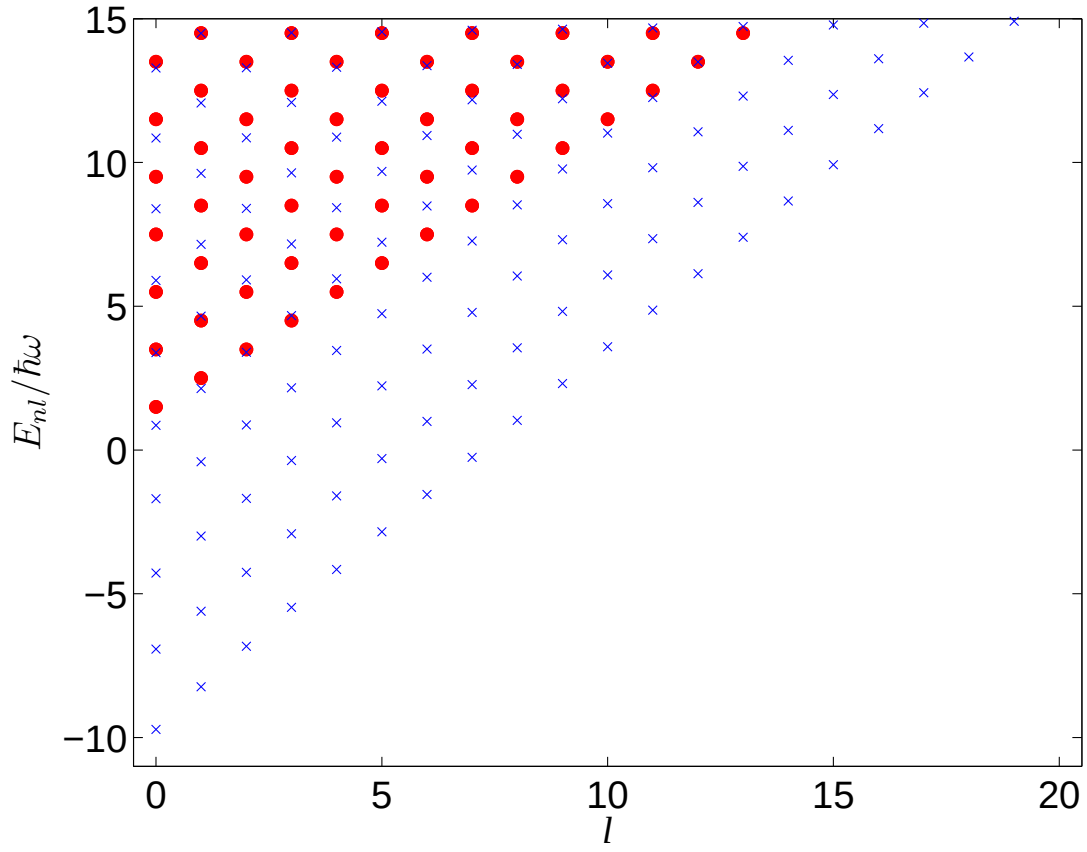

Figure 2.4: The quasi-particle spectrum of a Fermi gas in a harmonic oscillator potential in units of $\hbar\omega$, the level spacing of the trap. The •'s are the energies for a noninteracting gas, while ×'s mark the quasi-particle energies for the case of attractive interactions. The parameters are the same as in Fig. 2.3.

For an ideal gas the Fermi energy can be found to be $E_{\rm F} = (6N)^{1/3}\hbar\omega$ [31], and hence we have $R_{\rm TF} = (48N)^{1/6}d_{\rm osc}$ for that system.

It is interesting to examine the influence of the interaction on the quasi-particle spectrum of the gas. This is graphed in Fig. 2.4 as a function of the angular momentum l, which remains a good quantum number, since the interaction is synmmetric under rotations. For comparison the noninteracting energies,

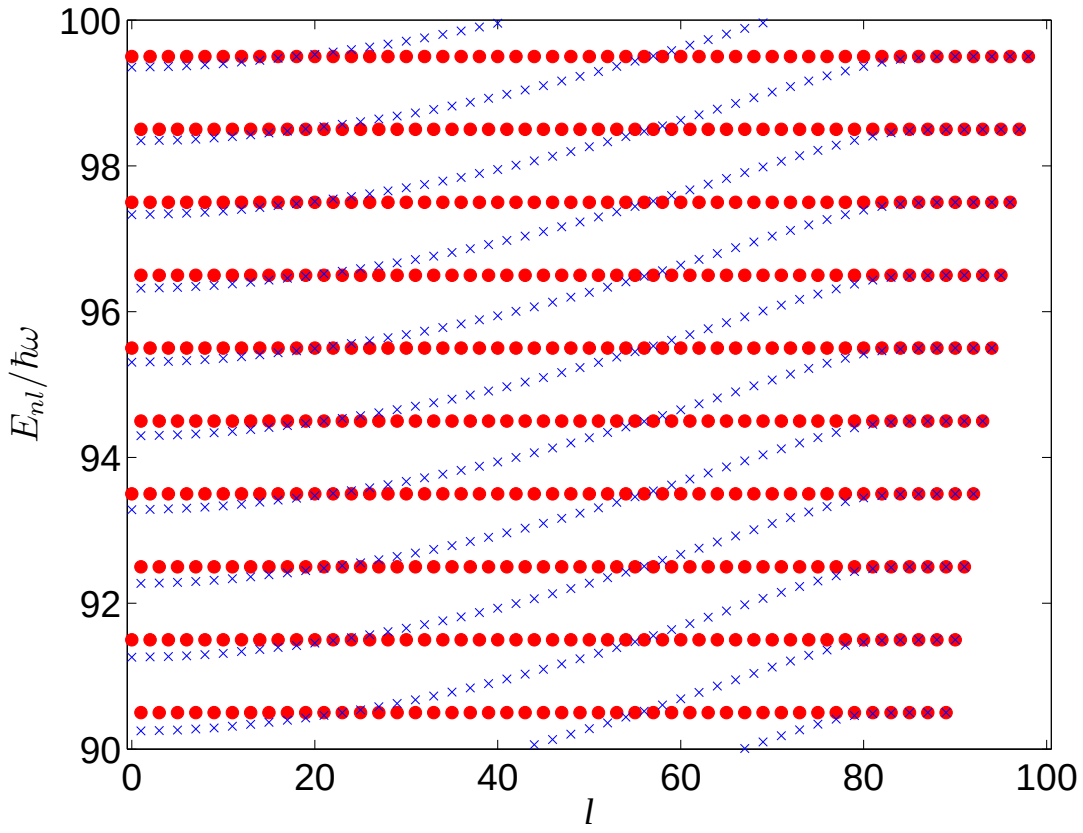

Figure 2.5: The same quasi-particle spectrum as in Fig. 2.4, but at higher energies.

$E_{nl} = \hbar\omega(2n + l + 3/2)$ with $\{n = 0, 1, 2, \ldots\}$, are also plotted. As is seen the effect of the attractive interaction is to lower all the quasi-particle energies by several $\hbar\omega$, this is the mean-field shift. Also the shell structure due to the degeneracy of the ideal gas levels with the same value of $\nu = 2n + l$ is lost. The states with the lowest values of l have a larger amplitude in the center of the trap, where the Hartree field is strongest, and hence the mean-field shift is largest, than the high l states. Therefore the trend is for the quasi-particle energies to rise with increasing l for a fixed value of ν [48]. The largest shift is roughly equal to $gn_\sigma(r = 0)$, the value of the Hartree field at the center of the trap.

As the energy increases the influence of the Hartree field on the single-particle state is weakened. However, as is seen in Fig. 2.5 it is still substantial at energies $\sim 100\ \hbar\omega$. However, the agreement with the non-interacting eigenvalues dramatically improves at an l-value on the order of $(R_{\rm TF}/d_{\rm osc})^2$. To understand this we consider the effective potential made up of the external trap and the centrifugal potential. For a given value of the angular momentum, l, this combined potential has a minimum $r_{\rm min}$ at approximately $\sqrt{l}$ oscillator lengths from the trap center. Thus the lowest eigenstate of the effective potential will be localized at $r \simeq r_{\rm min}$. If $r_{\rm min} > R_{\rm TF}$ the Hartree field will not have a significant influence on this quantum state, and its energy will be unchanged from the non-interacting case. Fig. 2.5 supports this conclusion. In a homogeneous system all single-particle levels feel the Hartree field equally, and the mean-field shift persists at high energies.

Next, we calculate the ground state energy of a homogeneous interacting two-component Fermi gas with Hartree-Fock theory, noting that the effect of interactions is to shift the single-particle energies of the spin state σ by $gn_{-\sigma}$ (apart from an overall shift of $-gn_\uparrow n_\downarrow V$):

$$E_{\rm HF} = \sum_\sigma \sum_{k<k_{F\sigma}} \left(\frac{\hbar^2 k^2}{2m_a} + gn_{-\sigma} \right) - gn_\uparrow n_\downarrow V = \frac{3}{5} \sum_\sigma N_\sigma E_{F\sigma} + gn_\sigma^2 V. \quad (2.35)$$

In Fig. 2.6 this expression for the total energy at $T = 0$ is compared with that of an ideal gas at the same density, Eq. (2.23), as a function of the dimensionless number $k_{\rm F}|a|$. Again we use parameters for ^{6}Li (see above). As expected the negative shift of the energy relative to the noninteracting state increases with $k_{\rm F}|a|$, *i.e.* with increasing particle density. Also plotted is the result of a diagonalization of the mean-field Hamiltonian for an interacting Fermi gas held in a cylindrical confining vessel of radius $R = 28.5\ \mu$m $\simeq 250\ a$, and length

$L = 11.4$ μm. With this values of $k_{\mathrm{F}}a$ used the density is on the order of 10^{12} cm^{-3} (see inset), which is quite reasonable for the current experiments on ultracold Fermi gases. Clearly, the bulk expression (2.35) is a good approximation to the energy in this case. Here and in the following chapters the numerical calculations for a Fermi gas in a cylinder are done in dimensionless units. To convert to physical units we choose the length scale d_{cyl} such that the scattering length has the desired value. The unit of energy is then set by $\hbar^2/m_a d_{\mathrm{cyl}}^2$.

2.5.1 Mechanical Stability

In the mean-field approximation a Fermi gas with attractive interactions is unstable against collapse if the density or interaction strength is too large. In that case the Fermi pressure is incapable of matching the inward force of the interparticle attraction, and the metastable gas phase ceases to exist [49, 50, 51]. To see this we consider the LDA expression for the local Fermi vector, assuming for simplicity the densities of the two components to be identical

$$E_{\mathrm{F}} - V_{\mathrm{ext}}(\mathbf{r}) = \frac{\hbar^2 k_{\mathrm{F}}^2(\mathbf{r})}{2m_a} + g\frac{k_{\mathrm{F}}^3(\mathbf{r})}{6\pi^2}. \tag{2.36}$$

The right hand side of this equation has a maximum for $g < 0$, at $k_{\mathrm{F}}(\mathbf{r}) = k_{\mathrm{F}}^{\max} = \pi/2|a|$. Consequently, if the local Fermi vector is larger than $k_{\mathrm{F}}^{\max}$ (or equivalently $E_{\mathrm{F}} > E_{\mathrm{F}}^{\max} = (\pi^2/24)\hbar^2/m_a|a|^2 + V_{\mathrm{ext}}(\mathbf{r})$), no stable solution to (2.36) exists. For a given trap geometry and strength of attraction this results in an upper bound $N^{\max}$ on the number of particles for which the system is stable. In our numerical calculations we make sure to always input particle numbers $N < N^{\max}$ such that convergence to solutions with a finite density is ensured.

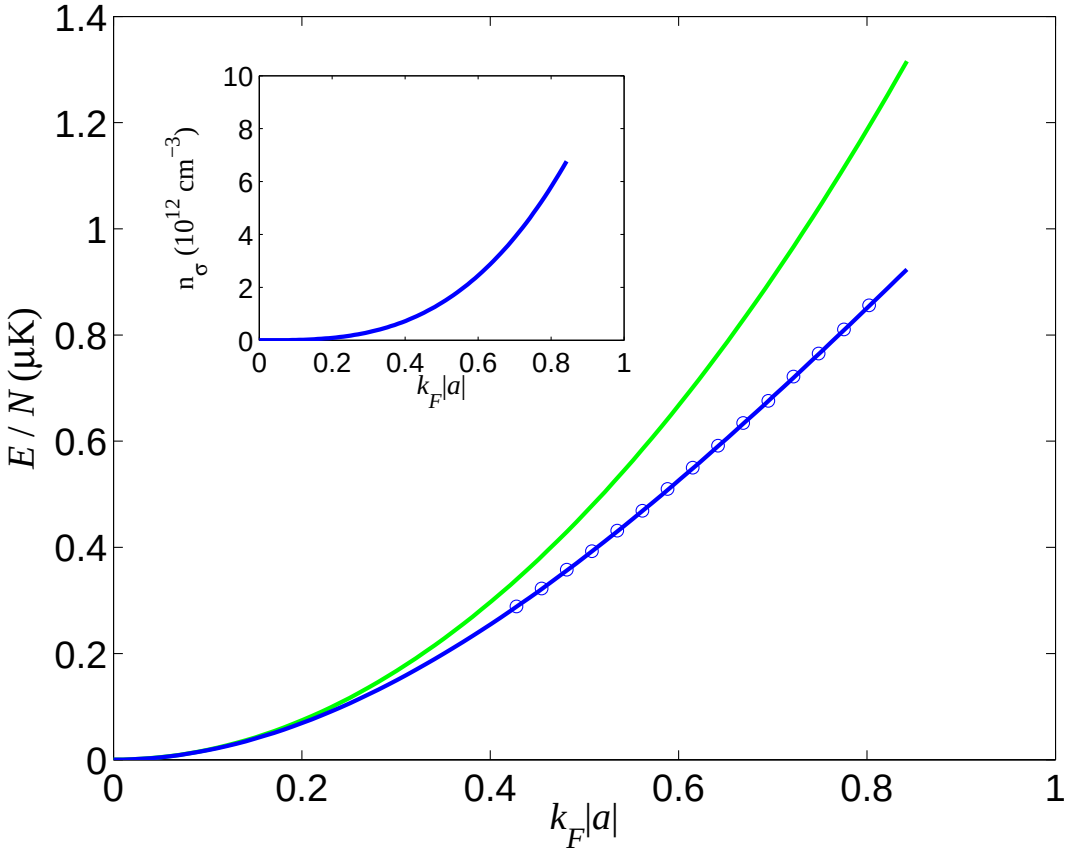

Figure 2.6: Energy per particle of a two-component Fermi gas with attractive interactions (*blue line*) and in the ideal gas case (*green line*). The circles are the numerical results for a gas trapped in a cylinder. See text for parameters. The inset shows the density per spin state as a function of $k_{\mathrm{F}}|a|$.

The above arguments depend on the validity of mean-field theory, which breaks down exactly around the point of the instability. Consequently, more sophisticated reasoning based on many-body physics is required to determine the range of stability. Indeed, one finds that a two-component Fermi gas is unconditionally stable against collapse, when the energy dependence of the coupling strength is taken into account [52]. This prediction has been substantiated by

experiments creating a strongly interacting Fermi gas by tuning the effective coupling by a Feshbach resonance. Stable configurations were observed at densities in excess of those predicted above for the onset of the instability [53].

Chapter 3

Pairing Theory for Atomic Fermi Gas

When Fermi particles interact through an attractive two-body potential, the low temperature ground state changes character. The normal state (Fermi sea) becomes unstable, and a new vacuum emerges. This is characterized by a finite energy gap for single-particle excitations and a modified collective mode spectrum. The mechanism for this profound change in the system properties is the formation of bound states between pairs of particles. These so-called *Cooper pairs* behave like (quasi) composite bosons, and can condense into the pair state with zero center of mass momentum giving rise to superfluidity. The pairing theory was first worked out by Bardeen, Cooper and Scrieffer (BCS) [16], who showed it to be the underlying mechanism of superconductivity. For this work they were awarded the 1972 Nobel Prize in physics. The idea that pairs of electrons behaving like bosons were responsible for superconductivity had previously been advanced by Schafroth and Blatt [54, 55, 56]. However, these authors considered the electron pairs to be localized bosonic molecules. As we shall see, this picture is invalid in the limit of weak coupling, where instead such pairs overlap substantially, and therefore can not be considered as separate entities. Rather

one should think of pair correlations existing in the system.

The concept of pairing in Fermi systems is profound and universal. Cooper pairing gives rise to superfluid phenomena in a host of different physical systems. The one most akin to the dilute atomic gas we are considering is liquid ^{3}He. A superfluid phase was found to exist at temperatures below 2.6 mK in this rare helium isotope in 1972 by Lee, Osheroff, and Richardson, a discovery which earned them the Nobel prize in 1996 [17, 57]. Leggett generalized the BCS theory to treat this new superfluid system, where the ^{3}He atoms form pairs with a more complicated symmetry than the electron pairs of BCS theory [58]. For this work he shared the 2003 Nobel prize with Abrikosov and Ginzburg, who in turn made seminal contributions to the theory of superconductivity. Fermi superfluidity is also observed experimentally in atomic nuclei, where it gives rise to an asymmetry in the excitation energies between even-even and odd-A nuclei, and a reduction of the moment of inertia [59, 60]. Contrary to the condensed matter systems mentioned above, atomic nuclei are inherently finite sized, and the manifestations of superfluidity due to nucleon pairing are not as pronounced as in a bulk system. Similarly, the cores of neutron stars, which can in some sense be regarded as a giant nucleus, are predicted to be superfluid due to the pairing between neutrons [41]. The presence of a fermion condensate has important consequences for the thermal properties and the hydrodynamics of these compact objects. Finally, we mention dense quark matter as an even more exotic system where fermion pairing is predicted to occur [61]. This has implications for phase transitions of matter in the early universe [62].

The purpose of the present chapter is to give a self-contained derivation of the pairing theory for an atomic Fermi gas within a mean-field approximation.

We will formulate the theory for a general neutral Ferm i system assuming only a contact form of the interaction potential. A crucial element of the theory is its proper regularization, which connects the coupling constant of the model potential with the physical scattering parameters of the system. After calculating the transition temperature, we comment on the possibility of attaining Fermi superfluidity in the current generation of ultracold gas experiments. Finally, we conclude the chapter by applying the theory to a Fermi gas trapped in two specific geometries.

3.1 Cooper Pairing

In 1956 Leon Copper had the brilliant insight that a filled Fermi sea is unstable against any attractive force, no matter how weak, between the particles [63]. We reproduce the argument here to introduce the concepts which form the basis of the ensuing discussion. Consider a pair of fermions interacting above a quiescent Fermi sea at $T = 0$. For reasons of simplicity we assume a contact potential

$$V(\tilde{\mathbf{r}}) = g_0 \delta(\tilde{\mathbf{r}}), \tag{3.1}$$

where $g_0 < 0$ is the bare coupling strength and the relative coordinate of the pair is $\tilde{\mathbf{r}} = \mathbf{r}_1 - \mathbf{r}_2$ (we shall reserve the symbol $\mathbf{r}$ without the tilde for a general particle coordinate). To investigate the propensity of the particles to form a bound state we need only consider their relative motional state, which in the case of translational invariance has a Fourier decomposition in terms of the relative momentum $\hbar\mathbf{q} = \hbar(\mathbf{k}_1 - \mathbf{k}_2)/2$

$$\psi_{\rm rel}(\tilde{\mathbf{r}}) = \frac{1}{V} \sum_{\mathbf{q}}{}' \psi_{\mathbf{q}} e^{i\mathbf{q}\cdot\tilde{\mathbf{r}}}. \tag{3.2}$$

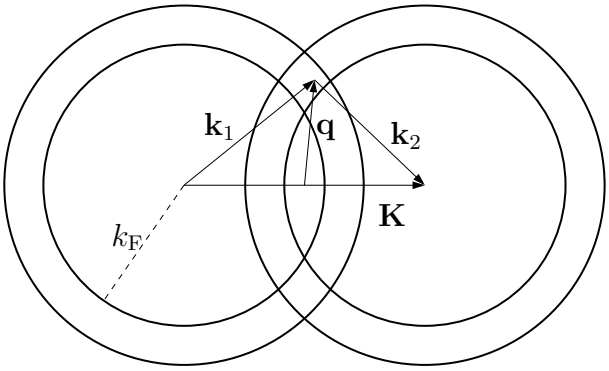

Figure 3.1: Cross-section of overlap in k-space. The inner circles have radius k_F, while the outer circles give the size of some cutoff in momentum space.

The momentum sum is is restricted to have $k_1, k_2 > k_\mathrm{F}$ due to the filled Fermi sphere, which makes low lying states inaccessible due to Pauli blocking. We are implicitly assuming that the two fermions are in an anti-symmetric spin state, since this is the most relevant situation for the physical systems we are interested in (*cf.* the discussion in Section 2.2). The Schrödinger equation for the relative motion reads

$$\frac{1}{V}\sum_{\mathbf{q}}{}' \left(\frac{\hbar^2 q^2}{m_a} + \frac{\hbar^2 K^2}{4m_a} - E\right)\psi_{\mathbf{q}} e^{i\mathbf{q}\cdot\tilde{\mathbf{r}}} = -\frac{g_0}{V}\sum_{\mathbf{q}}{}'\psi_{\mathbf{q}} e^{i\mathbf{q}\cdot\tilde{\mathbf{r}}}\delta(\tilde{\mathbf{r}}), \tag{3.3}$$

where m_a is the mass of the particles, and $\hbar\mathbf{K} = \hbar(\mathbf{k}_1 + \mathbf{k}_2)$ is the center of mass momentum. If the fermions form a bound state their total energy E will be less than $2E_\mathrm{F}$. Multiplying both sides by $\exp(-i\mathbf{k}\cdot\tilde{\mathbf{r}})$ and integrating over all space we obtain

$$\sum_{\mathbf{q}}{}' \left(\frac{\hbar^2 q^2}{m_a} + \frac{\hbar^2 K^2}{4m_a} - E\right)\psi_{\mathbf{q}}\delta_{\mathbf{qk}} = -\frac{g_0}{V}\sum_{\mathbf{q}}{}'\psi_{\mathbf{q}}. \tag{3.4}$$

The restriction on possible momentum states is shown in Fig. (3.1). Given a center of mass momentum $\mathbf{K}$ the momenta must be chosen such that $\mathbf{q}$ lies in the regions of overlap between the rings. The binding energy is largest when

the number of allowable momentum states is maximized. The maximum overlap possible is for $\mathbf{K} = 0$, corresponding to a pair at rest. In this case the particles have equal and opposite momenta $\mathbf{k}_1 = -\mathbf{k}_2$, and the restriction on the summation is $q > k_{\mathrm{F}}$. Defining $\alpha = \sum_{q>k_{\mathrm{F}}} \psi_{\mathbf{q}}$ the eigenvalue equation becomes

$$\psi_{\mathbf{q}} = -\frac{g_0}{V}\,\alpha \left(\frac{\hbar^2 q^2}{m_a} - E \right)^{-1}, \tag{3.5}$$

summing over $q > k_{\mathrm{F}}$ on both sides of this expression we find

$$-\frac{1}{g_0} = \frac{1}{V} \sum_{q>k_{\mathrm{F}}} \left(\frac{\hbar^2 q^2}{m_a} - E \right)^{-1}. \tag{3.6}$$

Unfortunately, the momentum sum is ultraviolet divergent, due to the absence of a high energy cutoff in the contact potential. To remedy this problem, we have to express the bare coupling constant in terms of the (zero-energy) two-body scattering matrix $T^{2B} = 4\pi a \hbar^2/m_a \equiv g$, which contains the physically measured quantity a, the s-wave scattering length (see Appendix A). From the Lippman-Schwinger equation one finds [50, 64]

$$\frac{1}{g} = \frac{1}{g_0} + \frac{1}{V} \sum_{q>k_{\mathrm{F}}} \frac{1}{2\epsilon_{\mathbf{q}}}, \tag{3.7}$$

where $\epsilon_{\mathbf{k}} = \hbar^2 k^2/2m_a$ are the free particle energies, and the sum is again restricted to reflect the presence of the inert Fermi sea. Another way to state the relationship between g_0 and g is that the former represents the first Born approximation to the low energy scattering amplitude, whereas g results from formally summing the Born series to all orders. With this regularized interaction the eigenvalue equation can now be written as

$$-\frac{1}{g} = \frac{1}{2\pi^2} \int_{k_{\mathrm{F}}}^{\infty} dq\, q^2 \left(\frac{1}{\frac{\hbar^2 q^2}{m_a} - E} - \frac{1}{\frac{\hbar^2 q^2}{m_a}} \right) = \frac{m_a \kappa^2}{2\pi^2 \hbar^2} \int_{k_{\mathrm{F}}}^{\infty} \frac{dq}{q^2 - \kappa^2}, \tag{3.8}$$

introducing $\kappa^2 = m_a E/\hbar^2$. The integral is now convergent and easily done. The result is

$$\frac{1}{g} = \frac{m_a \kappa}{4\pi^2\hbar^2} \ln\left(\frac{k_{\rm F} - \kappa}{k_{\rm F} + \kappa}\right). \tag{3.9}$$

Since we are anticipating a state with an energy lower than two non-interacting particles above the Fermi sea we define the binding energy Δ by the relation $E = 2E_{\rm F} - \Delta$. In the limit of a weak interaction the energies are not changed by much, and we can assume $\Delta \ll 2E_{\rm F}$. Substituting $\kappa \simeq k_{\rm F}$ outside the logarithm, and expanding the numerator and denominator of the argument to first order in $\Delta/2E_{\rm F}$ we find for the binding energy of the pair

$$\Delta = 8E_{\rm F} e^{-2/N(0)|g|}, \tag{3.10}$$

with $N(0) = m_a k_{\rm F}/2\pi^2\hbar^2$ the density of states per unit volume at the Fermi level for a uniform Fermi gas. Since $\Delta > 0$ this constitutes the proof of the instability of the Fermi sea in the case of an attractive two-body interaction. A few things are worth noting. First, it is clear from (3.10) that while the binding energy decreases exponentially when the strength of the interaction decreases, any attractive force regardless of its strength will lead to the formation of a bound pair. The reason for this is the filled Fermi sea. If the two particles were instead in a vacuum we would have $E_{\rm F} = 0$ and Δ would vanish. This is just another way of stating that a delta function potential in three dimension does not give rise to any scattering, as shown in Appendix A. The presence of the Fermi sea effectively restricts the Hilbert space of the two particles under consideration to states on the two dimensional Fermi surface, and in two dimensions the delta function potential does indeed have a bound state.

Secondly, we have used a contact potential to model the interaction between the fermions. This is slightly different from the approach usually used in the

superconductivity community. Here the source of the potential at play is the electron-phonon coupling, which in conjunction with the screened Coulomb repulsion gives rise to an effectively attractive potential between the electrons at low momenta. However, the coupling to lattice vibrations introduces a natural energy cutoff in the guise of the Debye frequency $\hbar\omega_D$. In that case the prefactor in (3.10) becomes proportional to $\hbar\omega_D$ instead of E_F, but the exponential remains unchanged. In both cases the weak-coupling limit is characterized by the pairing taking place exclusively in a narrow energy band around the Fermi level. It is interesting to note that while a typical superconductor has $\hbar\omega_D \ll E_\mathrm{F}$, ultracold gases have Fermi energies several orders of magnitude lower than in a metal. As a result the predicted transition temperature in ^{6}Li is on the order of 100 nK, which is to be contrasted with a T_c of a few Kelvin for a superconducting metal. Another crucial result of the calculation is that the bound state energy is a non-analytic function of the coupling strength. Therefore in an expansion of Δ in powers of $N(0)g$ every term will be infinite in the limit of $g \to 0$ (see *e.g.* expression (3.10)). This means that a perturbation series for the ground state energy does not exist, and the Cooper paired state can not be obtained by perturbation theory on the normal state. The superfluid vacuum is orthogonal to the state with no pairing [65]. The last point we wish to make is that while the calculation shows that pairing is possible from a two particle point of view, it completely neglects many-body effects. These are crucial in determining at what temperature pairing sets in for a realistic system. The derivation of the many-body pairing theory is the topic of the remainder of this chapter.

We conclude this section by calculating the size of a Cooper pair defined

through

$$\langle \tilde{r}^2 \rangle = \frac{\int d^3\tilde{r}\, |\psi_{\rm rel}(\tilde{\mathbf{r}})|^2 \tilde{r}^2}{\int d^3\tilde{r}\, |\psi_{\rm rel}(\tilde{\mathbf{r}})|^2}. \tag{3.11}$$

A simpler way to write this expression is in terms of the Fourier components of the relative wavefunction

$$\langle \tilde{r}^2 \rangle = \frac{\sum_{q>k_{\rm F}} |\nabla_{\mathbf{q}} \psi_{\mathbf{q}}|^2}{\sum_{q>k_{\rm F}} |\psi_{\mathbf{q}}|^2}. \tag{3.12}$$

This is easily seen if one uses the relations

$$\begin{aligned} \psi_{\mathbf{q}} &= \int d^3\tilde{r}\, e^{-i\mathbf{q}\cdot\tilde{\mathbf{r}}} \psi_{\rm rel}(\tilde{\mathbf{r}}), \\ \nabla_{\mathbf{q}} \psi_{\mathbf{q}} &= -i \int d^3\tilde{r}\, \tilde{\mathbf{r}} e^{-i\mathbf{q}\cdot\tilde{\mathbf{r}}} \psi_{\rm rel}(\tilde{\mathbf{r}}), \end{aligned} \tag{3.13}$$

in (3.12). Converting the sums into integrals we have (from Eq. (3.5))

$$\langle \tilde{r}^2 \rangle = \frac{4\hbar^4}{m_a^2} \frac{\int_{k_{\rm F}}^{\infty} dq\, q^4 \left(\frac{\hbar^2 q^2}{m_a} - E \right)^{-4}}{\int_{k_{\rm F}}^{\infty} dq\, q^2 \left(\frac{\hbar^2 q^2}{m_a} - E \right)^{-2}}. \tag{3.14}$$

The integrals are straightforward, but tedious to calculate, and we shall only state the final result here. We find for the mean square radius of a Cooper pair

$$\langle \tilde{r}^2 \rangle \simeq \frac{4}{3} \frac{\hbar^4 k_{\rm F}^2}{m_a^2 \Delta^2}, \tag{3.15}$$

where we have used that $\Delta \ll E_{\rm F}$, and neglected terms of order $1/\Delta$ and $1/E_{\rm F}$ compared with terms of order $E_{\rm F}/\Delta^2$. We use the mean radius of a pair to define the *coherence length* ξ of the gas, the characteristic length scale over which pairing correlations extend

$$\xi = \sqrt{\langle \tilde{r}^2 \rangle} = \frac{2}{\sqrt{3}} \frac{\hbar v_F}{\Delta}, \tag{3.16}$$

with $v_F = \hbar k_{\rm F}/m_a$ the Fermi velocity. Comparing this length scale with the average spacing between the particles $d \sim n_\sigma^{-1/3}$, we find that

$$\frac{\xi}{d} \sim e^{2/N(0)g} \gg 1, \tag{3.17}$$

in the weak-coupling limit. Here we have used that $n_\sigma = k_{\rm F}^3/6\pi^2$. Hence the Cooper pairs are extremely large compared with the inter-particle spacing, and each pair is necessarily overlapping with a huge number of other pairs. Therefore in the weak coupling limit we should not think of the pairs as localized bosonic molecules. The fact that they overlap in space means that Cooper pairs retain some of the fermionic nature of their constituent atoms. However, the large density of pairs does simplify the many-body description, in the sense that a large concentration gives us the perfect conditions for the development of a mean-field theory.

3.2 Mean-Field Theory

In principle the Hamiltonian as written in Eq. (2.14) contains all the correct microscopic physics of the system. However, we cannot hope to extract the relevant information without making further approximations. In particular, it is well-known [66] that if $\hat{H}$ can be reduced to a quadratic form, it can be easily diagonalized by a canonical transformation to a basis of non-interacting quasi-particles. This amounts to a mean-field approximation, where operator pairs are developed around their (c-number) mean value. By requiring the ensemble average of the mean-field Hamiltonian $\langle \hat{H}_{\rm MF} \rangle$ to be equal to that of the original Hamiltonian $\langle \hat{H} \rangle$ when both are evaluated in the quadratic ensemble, and using Wick's theorem (see Appendix D) to evaluate the latter, a self-consistent mean-field theory is obtained by substituting

$$\begin{aligned} \hat{\psi}_\sigma^\dagger(\mathbf{r})\hat{\psi}_\sigma(\mathbf{r}') &= \langle \hat{\psi}_\sigma^\dagger(\mathbf{r})\hat{\psi}_\sigma(\mathbf{r}') \rangle + \delta(\hat{\psi}_\sigma^\dagger(\mathbf{r})\hat{\psi}_\sigma(\mathbf{r}')), \\ \hat{\psi}_{-\sigma}(\mathbf{r})\hat{\psi}_\sigma(\mathbf{r}') &= \langle \hat{\psi}_{-\sigma}(\mathbf{r})\hat{\psi}_\sigma(\mathbf{r}') \rangle + \delta(\hat{\psi}_{-\sigma}(\mathbf{r})\hat{\psi}_\sigma(\mathbf{r}')), \end{aligned} \tag{3.18}$$

in the Hamiltonian (neglecting the "magnetic" terms $\langle\hat{\psi}^\dagger_\sigma(\mathbf{r})\hat{\psi}_{-\sigma}(\mathbf{r}')\rangle$). Keeping only term to first order in the fluctuations, and using the regularized pseudopotential defined in Appendix A for the two-body interaction, we obtain for the mean-field Hamiltonian

$$\begin{aligned}\hat{H}_{\rm MF} &= \int d^3r \Big\{\sum_\sigma \hat{\psi}^\dagger_\sigma(\mathbf{r})\mathcal{H}^{\rm HF}_\sigma\hat{\psi}_\sigma(\mathbf{r}) \\ &\quad +\Delta(\mathbf{r})\hat{\psi}^\dagger_\uparrow(\mathbf{r})\hat{\psi}^\dagger_\downarrow(\mathbf{r}) + \Delta^*(\mathbf{r})\hat{\psi}_\downarrow(\mathbf{r})\hat{\psi}_\uparrow(\mathbf{r}) \\ &\quad -gn_\uparrow(\mathbf{r})n_\downarrow(\mathbf{r}) + \Delta^*(\mathbf{r})F(\mathbf{r},\mathbf{r})\Big\}. \end{aligned} \tag{3.19}$$

The Hartree-Fock (HF) Hamiltonian $\mathcal{H}^{\rm HF}_\sigma = \mathcal{H}_\sigma + gn_{-\sigma}(\mathbf{r})$ incorporates the mean-field shift of the single-particle energy levels. Whereas the density distribution of particles in state σ, $n_\sigma(\mathbf{r}) = \langle\hat{\psi}^\dagger_\sigma(\mathbf{r})\hat{\psi}_\sigma(\mathbf{r})\rangle$, is relatively unchanged when going from the superfluid to the normal state, the superfluid phase is characterized by a non-vanishing value of the anomalous average $F(\mathbf{r},\mathbf{r}') = \langle\hat{\psi}_\uparrow(\mathbf{r})\hat{\psi}_\downarrow(\mathbf{r}')\rangle$ which is a measure of pairing correlations in the gas. In the normal phase the anomalous average is zero. The pair potential is defined as

$$\Delta(\mathbf{r}) = -g\lim_{\tilde{r}\to 0}\partial_{\tilde{r}}[\tilde{r}F(\mathbf{r},\mathbf{r}')] = -g\lim_{\tilde{r}\to 0}\partial_{\tilde{r}}[\tilde{r}\,\langle\hat{\psi}_\uparrow(\mathbf{r})\hat{\psi}_\downarrow(\mathbf{r}')\rangle], \tag{3.20}$$

where again we define the relative coordinate as $\tilde{\mathbf{r}} = \mathbf{r} - \mathbf{r}'$. For a homogeneous Fermi superfluid $\Delta(\mathbf{r}) = \Delta_0$ is related to the gap in the single-particle excitation spectrum.

Since the density expression is convergent the regularization operator,$\partial_{\tilde{r}}[\tilde{r}\cdot]$, in the pseudopotential does not affect n_σ. However, the anomalous average is inherently ultraviolet divergent, as will be demonstrated below, but the regularization operator exactly removes the divergent part, making a $\Delta(\mathbf{r})$ a well-defined quantity.

3.2.1 The Nature of the Divergence

Before we work out the practical implementation of the regularization procedure, we need to understand the precise form of the divergence of the pairing field. We do this by exploiting that in the the steady state limit, F is a thermodynamic variable of the system, and thus a constant of the motion.

From the MF Hamiltonian we can derive the Heisenberg equations of motion for the field operators. They read

$$\begin{aligned} i\hbar\frac{d}{dt}\hat{\psi}_\uparrow(\mathbf{r}) &= \mathcal{H}_\uparrow^{\mathrm{HF}}\hat{\psi}_\uparrow(\mathbf{r}) + \Delta(\mathbf{r})\hat{\psi}_\downarrow^\dagger(\mathbf{r}), \\ i\hbar\frac{d}{dt}\hat{\psi}_\downarrow(\mathbf{r}) &= \mathcal{H}_\downarrow^{\mathrm{HF}}\hat{\psi}_\downarrow(\mathbf{r}) - \Delta(\mathbf{r})\hat{\psi}_\uparrow^\dagger(\mathbf{r}). \end{aligned} \tag{3.21}$$

It is now possible to evaluate the time derivative of the anomalous average, which must vanish in the steady state limit:

$$\begin{aligned} 0 &= \frac{d}{dt}\left\langle \hat{\psi}_\uparrow\left(\mathbf{R}+\frac{\tilde{\mathbf{r}}}{2}\right)\hat{\psi}_\downarrow\left(\mathbf{R}-\frac{\tilde{\mathbf{r}}}{2}\right)\right\rangle \\ &= \frac{1}{i\hbar}\left[\left\{T_{\mathrm{tot}} + V_{\mathrm{eff},\uparrow}\left(\mathbf{R}+\frac{\tilde{\mathbf{r}}}{2}\right) + V_{\mathrm{eff},\downarrow}\left(\mathbf{R}-\frac{\tilde{\mathbf{r}}}{2}\right)\right\}\right. \\ &\times \left\langle \hat{\psi}_\uparrow\left(\mathbf{R}+\frac{\tilde{\mathbf{r}}}{2}\right)\hat{\psi}_\downarrow\left(\mathbf{R}-\frac{\tilde{\mathbf{r}}}{2}\right)\right\rangle \\ &+ \Delta\left(\mathbf{R}+\frac{\tilde{\mathbf{r}}}{2}\right)\left\langle \hat{\psi}_\downarrow^\dagger\left(\mathbf{R}+\frac{\tilde{\mathbf{r}}}{2}\right)\hat{\psi}_\downarrow\left(\mathbf{R}-\frac{\tilde{\mathbf{r}}}{2}\right)\right\rangle \\ &- \left.\Delta\left(\mathbf{R}-\frac{\tilde{\mathbf{r}}}{2}\right)\left\langle \hat{\psi}_\uparrow\left(\mathbf{R}+\frac{\tilde{\mathbf{r}}}{2}\right)\hat{\psi}_\uparrow^\dagger\left(\mathbf{R}-\frac{\tilde{\mathbf{r}}}{2}\right)\right\rangle\right]. \end{aligned} \tag{3.22}$$

Here we have defined an effective single-particle potential $V_{\mathrm{eff},\sigma}(\mathbf{r}) \equiv V_{\mathrm{ext},\sigma}(\mathbf{r}) + gn_{-\sigma}$ and the total kinetic energy operator of a pair

$$T_{\mathrm{tot}} \equiv -\frac{\hbar^2}{2m_a}\left[\nabla^2_{\mathbf{R}+\frac{\tilde{\mathbf{r}}}{2}} + \nabla^2_{\mathbf{R}-\frac{\tilde{\mathbf{r}}}{2}}\right], \tag{3.23}$$

with $\mathbf{R} = \frac{1}{2}(\mathbf{r}+\mathbf{r}')$ the center of mass position, and $\mathbf{r} = \mathbf{R} + \tilde{\mathbf{r}}/2$, while $\mathbf{r}' = \mathbf{R} - \tilde{\mathbf{r}}/2$. We want to rewrite the kinetic operator in terms of $\tilde{\mathbf{r}}$ and $\mathbf{R}$. Using

the chain rule we trivially obtain

$$T_{\rm tot} = -\frac{\hbar^2}{2m_a}\left[\nabla^2_{\mathbf{r}} + \nabla^2_{\mathbf{r}'}\right] = -\frac{\hbar^2}{m_a}\left[\nabla^2_{\tilde{\mathbf{r}}} + \frac{1}{4}\nabla^2_{\mathbf{R}}\right]. \tag{3.24}$$

By using the anti-commutativity of the field operators we then get from (3.22):

$$\begin{aligned}
0 &= \left[-\frac{\hbar^2}{m}\left(\nabla^2_{\tilde{\mathbf{r}}} + \frac{1}{4}\nabla^2_{\mathbf{R}}\right) + V_{\rm eff,\uparrow}\left(\mathbf{R}+\frac{\tilde{\mathbf{r}}}{2}\right) + V_{\rm eff,\downarrow}\left(\mathbf{R}-\frac{\tilde{\mathbf{r}}}{2}\right)\right] \\
&\times \left\langle \hat{\psi}_\uparrow\left(\mathbf{R}+\frac{\tilde{\mathbf{r}}}{2}\right)\hat{\psi}_\downarrow\left(\mathbf{R}-\frac{\tilde{\mathbf{r}}}{2}\right)\right\rangle \\
&+ \Delta\left(\mathbf{R}+\frac{\tilde{\mathbf{r}}}{2}\right)\left\langle \hat{\psi}^\dagger_\downarrow\left(\mathbf{R}+\frac{\tilde{\mathbf{r}}}{2}\right)\hat{\psi}_\downarrow\left(\mathbf{R}-\frac{\tilde{\mathbf{r}}}{2}\right)\right\rangle \\
&+ \Delta\left(\mathbf{R}-\frac{\tilde{\mathbf{r}}}{2}\right)\left\langle \hat{\psi}^\dagger_\uparrow\left(\mathbf{R}-\frac{\tilde{\mathbf{r}}}{2}\right)\hat{\psi}_\uparrow\left(\mathbf{R}+\frac{\tilde{\mathbf{r}}}{2}\right)\right\rangle \\
&- \Delta(\mathbf{R})\delta(\tilde{\mathbf{r}}),
\end{aligned} \tag{3.25}$$

where we have used that $\Delta(\mathbf{R}-\tilde{\mathbf{r}}/2)\delta(\tilde{\mathbf{r}}) = \Delta(\mathbf{R})\delta(\tilde{\mathbf{r}})$. From this result it is clear that the diagonal part of the anomalous average must contain a term diverging as $1/\tilde{r}$ (this follows from the identity $\nabla^2(1/\tilde{r}) = -4\pi\delta(\tilde{\mathbf{r}})$, and the fact that the terms proportional to $\Delta(\mathbf{R}+\tilde{\mathbf{r}}/2)$ and $\Delta(\mathbf{R}-\tilde{\mathbf{r}}/2)$ both remain regular in the limit of vanishing $\tilde{r}$). We write the anomalous average F as the sum of a divergent and a regular part [67]

$$F(\mathbf{r},\mathbf{r}') = \frac{m_a}{4\pi\hbar^2\tilde{r}}\,\Delta(\frac{\mathbf{r}+\mathbf{r}'}{2}) + F_{\rm reg}(\frac{\mathbf{r}+\mathbf{r}'}{2}) + \mathcal{O}(\tilde{r}). \tag{3.26}$$

But the regularization operator $\partial_{\tilde{r}}[\tilde{r}\cdot]$ of the pseudo-potential acts to remove the divergence, leaving only the regular part $F_{\rm reg}(\mathbf{r}) = \lim_{\tilde{r}\to 0}\partial_{\tilde{r}}\left[\tilde{r}F(\mathbf{r},\mathbf{r}')\right]$. Hence we can define the superfluid pair potential as $\Delta(\mathbf{r}) \equiv -gF_{\rm reg}(\mathbf{r})$. In section 3.4 we will detail how the regularization procedure is carried out in practice.

3.2.2 Diagonalizing the Mean-Field Hamiltonian

Since the mean-field Hamiltonian does not commute with the particle number operator

$$\hat{N} = \sum_{\sigma} \int d^3r \, \hat{\psi}^{\dagger}_{\sigma}(\mathbf{r}) \hat{\psi}_{\sigma}(\mathbf{r}), \tag{3.27}$$

we must work in the grand canonical ensemble, and the relevant thermodynamic quantity to minimize in order to establish the nature of the ground state is the grand canonical potential $\Omega = \langle \hat{H} \rangle - TS - \sum_{\sigma} \mu_{\sigma} \langle \hat{N}_{\sigma} \rangle$. The chemical potential μ_{σ} then serves as a Lagrange multiplier to fix the average particle number in spin state σ to be $N_{\sigma} = \langle \hat{N}_{\sigma} \rangle$. The non-conservation of particle number is due to the pairing terms in $\hat{H}_{\mathrm{MF}}$ ($\Delta(\mathbf{r}) \hat{\psi}^{\dagger}_{\uparrow}(\mathbf{r}) \hat{\psi}^{\dagger}_{\downarrow}(\mathbf{r})$ and its hermitian conjugate), which create and destroy two atoms. We can interpret this as a particle exchange with a Cooper pair "condensate" acting as a particle reservoir. In this sense we can think of the Cooper pairs as forming a Bose-Einstein condensate, but for the reasons outlined in section 3.1 we must be careful to not take this analogy too far. Besides, the exact interpretation of the source of the pairing terms in the mean-field Hamiltonian will be of little relevance. The physics is, as we shall see, entirely determined by the nature of the elementary excitations.

The quadratic mean-field Hamiltonian (3.19) is diagonalized by the Bogoliubov-Valatin transformation [68, 69, 70]

$$\begin{aligned} \hat{\psi}_{\uparrow}(\mathbf{r}) &= \sum_{\eta} \left[u_{\eta}(\mathbf{r}) \hat{\gamma}_{\eta\uparrow} - v^{*}_{\eta}(\mathbf{r}) \hat{\gamma}^{\dagger}_{\eta\downarrow} \right], \\ \hat{\psi}^{\dagger}_{\downarrow}(\mathbf{r}) &= \sum_{\eta} \left[u^{*}_{\eta}(\mathbf{r}) \hat{\gamma}^{\dagger}_{\eta\downarrow} + v_{\eta}(\mathbf{r}) \hat{\gamma}_{\eta\uparrow} \right]. \end{aligned} \tag{3.28}$$

From the structure of the new operators it is easy to assess their physical meaning: The action of $\hat{\gamma}^{\dagger}_{\eta\sigma}$ is to create a particle with orbital and spin quantum

numbers (η, σ) with amplitude $u_\eta(\mathbf{r})$ and destroy a particle, or equivalently create a hole, $(\eta, -\sigma)$ with amplitude $v_\eta(\mathbf{r})$. It thus creates a fermionic excitation. However, in general this excitation is not a real particle as $\hat{\gamma}^\dagger_{\eta\sigma}$ mixes bare particle and hole operators of opposite spins. Instead, $\hat{\gamma}^\dagger_{\eta\sigma}$ is a dressed or quasi-particle creation operator. Likewise, $\hat{\gamma}_{\eta\sigma}$ annihilates a fermionic quasi-particle. The superfluid ground state $|\Psi_0\rangle$ is the vacuum of the quasi-particle operators: $\hat{\gamma}_{\eta\sigma}|\Psi_0\rangle = 0$. Since the quasi-particle operators are themselves fermionic they must obey anti commutation relations just like the field operators. In order to have both the old and the new operators comply with Fermi-Dirac statistics the amplitude functions of the Bogoliubov-Valatin transformation must satisfy the completeness relations

$$\sum_\eta \left[u_\eta(\mathbf{r})u^*_\eta(\mathbf{r}') + v_\eta(\mathbf{r}')v^*_\eta(\mathbf{r})\right] = \delta(\mathbf{r}-\mathbf{r}'), \tag{3.29}$$

$$\sum_\eta \left[u_\eta(\mathbf{r})v^*_\eta(\mathbf{r}') - u_\eta(\mathbf{r}')v^*_\eta(\mathbf{r})\right] = 0, \tag{3.30}$$

as well as the orthogonality relations

$$\int d^3\mathbf{r}\ \left[u_\eta(\mathbf{r})u^*_\nu(\mathbf{r}) + v_\eta(\mathbf{r})v^*_\nu(\mathbf{r})\right] = \delta_{\eta\nu}, \tag{3.31}$$

$$\int d^3\mathbf{r}\ \left[u_\eta(\mathbf{r})u_\nu(\mathbf{r}) - v_\eta(\mathbf{r})v_\nu(\mathbf{r})\right] = 0. \tag{3.32}$$

Because the Bogoliubov-Valatin transformation diagonalizes the mean-field Hamiltonian, in the quasi-particle basis we have

$$\hat{H}_{\mathrm{MF}} - \sum_\sigma \mu_\sigma \hat{N}_\sigma = \Omega_G + \sum_{\eta\sigma} E_{\eta\sigma}\hat{\gamma}^\dagger_{\eta\sigma}\hat{\gamma}_{\eta\sigma}. \tag{3.33}$$

The ground state grand canonical potential is given by

$$\Omega_G = \int d^3r \left\{ -\sum_{\eta\sigma} E_{\eta\sigma}|v_\eta(\mathbf{r})|^2 - g n_\uparrow(\mathbf{r})n_\downarrow(\mathbf{r}) + \Delta^* F(\mathbf{r},\mathbf{r}) \right\}. \tag{3.34}$$

By using the commutation relations

$$\begin{aligned}[\hat{H}_{\rm MF}, \hat{\gamma}_{\eta\sigma}] &= -E_{\eta\sigma}\hat{\gamma}_{\eta\sigma}, \\ [\hat{H}_{\rm MF}, \hat{\gamma}^{\dagger}_{\eta\sigma}] &= E_{\eta\sigma}\hat{\gamma}^{\dagger}_{\eta\sigma},\end{aligned} \tag{3.35}$$

along with the commutators between $\hat{H}_{\rm MF}$ and the field operators we obtain a set of non-linear eigenvalue equations for the quasi-particle amplitudes (u_η, v_η) known as the Bogoliubov-de Gennes (BdG) equations [70]:

$$\begin{pmatrix} \mathcal{L}_\sigma & \Delta(\mathbf{r}) \\ \Delta^*(\mathbf{r}) & -\mathcal{L}^*_{-\sigma} \end{pmatrix} \begin{pmatrix} u_\eta(\mathbf{r}) \\ v_\eta(\mathbf{r}) \end{pmatrix} = E_{\eta\sigma} \begin{pmatrix} u_\eta(\mathbf{r}) \\ v_\eta(\mathbf{r}) \end{pmatrix}. \tag{3.36}$$

The generalized single-particle Hamiltonian explicitly includes the chemical potential $\mathcal{L}_\sigma = \mathcal{H}^{\rm HF}_\sigma - \mu_\sigma$. In thermal equilibrium the occupation numbers of the quasi-particle states are given by the Fermi distribution

$$f(E_{\eta\sigma}) = \langle \hat{\gamma}^{\dagger}_{\eta\sigma}\hat{\gamma}_{\eta\sigma}\rangle = \frac{1}{\exp(E_{\eta\sigma}/k_{\rm B}T)+1}. \tag{3.37}$$

This implies that the self-consistent density is given by

$$n_\sigma(\mathbf{r}) = \sum_\eta \left[|u_\eta(\mathbf{r})|^2 f(E_{\eta\sigma}) + |v_\eta(\mathbf{r})|^2 \left(1 - f(E_{\eta-\sigma})\right)\right], \tag{3.38}$$

and that the gap equation for the pair potential is

$$\Delta(\mathbf{r}) = -g \lim_{\tilde{r}\to 0} \partial_{\tilde{r}} \left[\tilde{r} \sum_\eta u_\eta(\mathbf{r}) v^*_\eta(\mathbf{r}') \left(1 - f(E_{\eta\uparrow}) - f(E_{\eta\downarrow})\right)\right]. \tag{3.39}$$

It is implied that all quasi-particle sums extend over positive energies only, since solutions with $E_{\eta\sigma} < 0$ are related to the positive branch of the spectrum through the transformation:

$$E_{\eta\sigma} \to -E_{\eta-\sigma}, \quad \begin{pmatrix} u_\eta \\ v_\eta \end{pmatrix} \to \begin{pmatrix} v^*_\eta \\ -u^*_\eta \end{pmatrix}. \tag{3.40}$$

We refer to Appendix E for the proof.

It should be emphasized that the BdG equations describe the *single-particle* excitations of the Fermi superfluid gas. In order to characterize the collective modes where the gas responds as a whole to an external perturbation one needs to go beyond our Hartree-Fock approach, for example by invoking the machinery of the random phase approximation (RPA). Within this framework, which represents the next order approximation, one can work out the linear response of the gas to an external perturbation [71, 72, 73, 74, 75]. This is in contrast with the theory of a dilute Bose gas where the equivalent of the BdG equations describe both single-particle and collective excitations of the Bose-Einstein condensate ground state [76].

It is possible to obtain an equation for the energy difference between creating a quasi-particle excitation in one spin state compared with the other,

$$E_{\eta\uparrow} - E_{\eta\downarrow} = -\delta\mu + \int d^3r \, \left(|u_\eta(\mathbf{r})|^2 + v_\eta(\mathbf{r})|^2\right) \left(\delta V_{\text{ext}} + g\delta n_\sigma\right), \tag{3.41}$$

defining the differences in chemical potential $\delta\mu = \mu_\uparrow - \mu_\downarrow$, external potential $\delta V_{\text{ext}} = V_{\text{ext},\uparrow} - V_{\text{ext},\downarrow}$, and density $\delta n_\sigma = n_\uparrow - n_\downarrow$. For a homogeneous gas this becomes $E_{\eta\uparrow} - E_{\eta\downarrow} = -\delta\mu + g\delta n_\sigma$. In the limit of weak coupling only particles in a thin energy shell around the Fermi energy can participate in the pairing. The atoms deep inside the Fermi sea are dormant, Pauli blocking means that they are essentially unaffected by the interaction. As a consequence the transition temperature decreases rapidly if there is a mismatch of the chemical potential of the two components of the gas. Any offset $\delta\mu$ between the Fermi surfaces of the two Fermi seas translates into fewer states available for pairing. Only for a sufficiently small difference $\delta\mu$ will the critical temperature be finite. In particular for a homogeneous gas one finds that a necessary condition for pairing

is $|\delta n_\sigma|/n < 3k_{\rm B}T_c/2E_{\rm F}$, where T_c is the transition temperature in the case of equal populations, $n = n_\uparrow + n_\downarrow$ is the total density and $E_{\rm F} = (\mu_\uparrow + \mu_\downarrow)/2$ [49]. Because experiments are likely to be done at conditions, which optimize the prospects for achieving pairing, and for reasons of computational convenience, we will choose the populations of the two hyperfine states to be equal from here on, *i.e.* $n_\uparrow = n_\downarrow = n_\sigma$. Also we shall take the trapping potential of both states to be identical. As a consequence of these assumptions the chemical potentials will also be equal $\mu_\uparrow = \mu_\downarrow = \mu$, and we can drop the spin subscript on the quasi-particle energies.

3.3 Thermodynamics

We consider now the thermodynamic properties of the gas in the superfluid state. Within our mean-field approach the quasi-particles form an ensemble of non-interacting fermions for which the entropy is easily evaluated [26]:

$$S = -k_{\rm B} \sum_\eta \left[f(E_\eta) \ln f(E_\eta) + (1 - f(E_\eta)) \ln(1 - f(E_\eta)) \right], \tag{3.42}$$

and the energy of the gas, $E = \langle \hat{H}_{\rm MF} \rangle$, is

$$\begin{aligned} E &= \int d^3r \Big\{ 2 \sum_\eta E_\eta \left[|u_\eta(\mathbf{r})|^2 f(E_\eta) - |v_\eta(\mathbf{r})|^2 (1 - f(E_\eta)) \right] \\ &\quad - g n_\uparrow(\mathbf{r}) n_\downarrow(\mathbf{r}) + \Delta(\mathbf{r}) \sum_\eta u_\eta^*(\mathbf{r}) v_\eta(\mathbf{r}) (1 - 2 f(E_\eta)) \\ &\quad + \sum_\sigma \mu_\sigma n_\sigma(\mathbf{r}) \Big\}. \end{aligned} \tag{3.43}$$

It should be noted that even though both sums over η in the energy expression are manifestly ultraviolet divergent, the energy expression is free of divergences. To see this we examine the high energy behavior of the quasi-particle sums,

neglecting the HF mean-field term $gn_\uparrow(\mathbf{r})n_\downarrow(\mathbf{r})$ and μN which are well behaved. In this regime the Fermi factors are negligible, and the divergent contributions to the energy are

$$\int d^3r \sum_\eta \Big\{ -2E_\eta |v_\eta(\mathbf{r})|^2 + \Delta(\mathbf{r}) u_\eta^*(\mathbf{r}) v_\eta(\mathbf{r}) \Big\}.$$

In the high energy limit the pair potential can be treated as a perturbation, and we expand the quasi-particle amplitudes in the complete set of normalized eigenstates $\phi_n(\mathbf{r})$ of the Hartree-Fock single-particle Hamiltonian

$$(\mathcal{H}_\sigma^{\mathrm{HF}} - \mu)\phi_n(\mathbf{r}) = \xi_n \phi_n(\mathbf{r}), \tag{3.44}$$

by writing them as $u_\eta(\mathbf{r}) = \sum_n u_n \phi_n(\mathbf{r})$ and $v_\eta(\mathbf{r}) = \sum_n v_n \phi_n(\mathbf{r})$. Adopting the diagonal approximation

$$\langle \phi_n | \Delta(\mathbf{r}) | \phi_m \rangle \simeq \delta_{nm} \Delta_n, \tag{3.45}$$

which is reasonable when $\Delta_n/\xi_n \ll 1$ (such that the quasi-particles behave essentially like the bare particles), the BdG equations split into a 2×2 matrix equation for each unperturbed quantum state $|\phi_n\rangle$. The solutions are $u_n^2 = (1+\xi_n/E_n)/2$, $v_n^2 = (1-\xi_n/E_n)/2$ with quasi-particle energies $E_n = (\xi_n^2 + |\Delta_n|^2)^{1/2}$. The divergent parts of the energy then become

$$\sum_n \left(\xi_n - E_n + \frac{|\Delta_n|^2}{2\xi_n \sqrt{1 + |\Delta_n|^2/\xi_n^2}} \right).$$

Expanding in the small parameter $|\Delta_n|^2/\xi_n^2$ and keeping terms to first order we see that the leading high energy contribution to the energy is $-\sum_n |\Delta_n|^4/4\xi_n^3$. This sum is seen to be convergent without further considerations, provided the density of states is $g(\xi) \propto \xi^\alpha$ with $\alpha < 3$. If $\alpha \geq 3$ (for the important case of a spherical harmonic oscillator $\alpha = 3$) we can appeal to the fact that the

matrix elements Δ_n decrease with increasing n, and hence the energy expression of Eq.(3.43) is well behaved. In Eq. (3.72) below we present the final energy expression taking the regularization of the anomalous average into account.

In the absence of a external confining potential the quasi-particle amplitudes can be expanded on a plane wave basis, and the diagonal approximation becomes exact, with $\Delta_n = \Delta_0$, $\forall n$. The Fourier components are

$$\begin{aligned} |u_{\mathbf{k}}|^2 &= \frac{1}{2}\left(1 + \frac{\xi_{\mathbf{k}}}{E_{\mathbf{k}}}\right), \\ |v_{\mathbf{k}}|^2 &= \frac{1}{2}\left(1 - \frac{\xi_{\mathbf{k}}}{E_{\mathbf{k}}}\right), \\ \text{with} \qquad E_{\mathbf{k}} &= \sqrt{\xi_{\mathbf{k}}^2 + \Delta_0^2}, \qquad \xi_{\mathbf{k}} = \frac{\hbar^2 k^2}{2m_a} - \mu. \end{aligned} \tag{3.46}$$

For a normal state Fermi gas, where $\Delta_0 = 0$, the quasi-particle energy is $E_{\mathbf{k}} = |\xi_{\mathbf{k}}|$, and $\{|u_{\mathbf{k}}|^2 = 0, |v_{\mathbf{k}}|^2 = 1\}$ for $k < k_{\mathrm{F}}$, while $\{|u_{\mathbf{k}}|^2 = 1, |v_{\mathbf{k}}|^2 = 0\}$ for $k > k_{\mathrm{F}}$. The dispersion relation is shown in Fig. 3.2, and Fig. 3.3 is a plot of the quasi-particle mode functions. Note that since $\Delta_0/\mu \ll 1$ in the weak-coupling limit we are treating, the pairing only affects the single-particle states in close proximity of the Fermi surface. For energies several Δ_0 removed from the Fermi energy $|u_{\mathbf{k}}|^2$ and $|v_{\mathbf{k}}|^2$ revert to their values in the normal state.

With the above relations the energy expression for a homogeneous gas can be evaluated exactly, and we find that compared with the normal state the energy of the gas in the superfluid phase is lower by an amount called the condensation energy. The bulk value of the condensation energy per unit volume is $\mathcal{E}_{\mathrm{cond}} = N(0)\Delta_0^2/2$, where $N(0)$ is the density of states per unit volume at the Fermi level defined in Section 3.1. The energy in the superfluid phase is therefore [77]

$$E_{\mathrm{SF}} = E_{\mathrm{HF}} - \frac{N(0)\Delta_0^2 V}{2}, \tag{3.47}$$

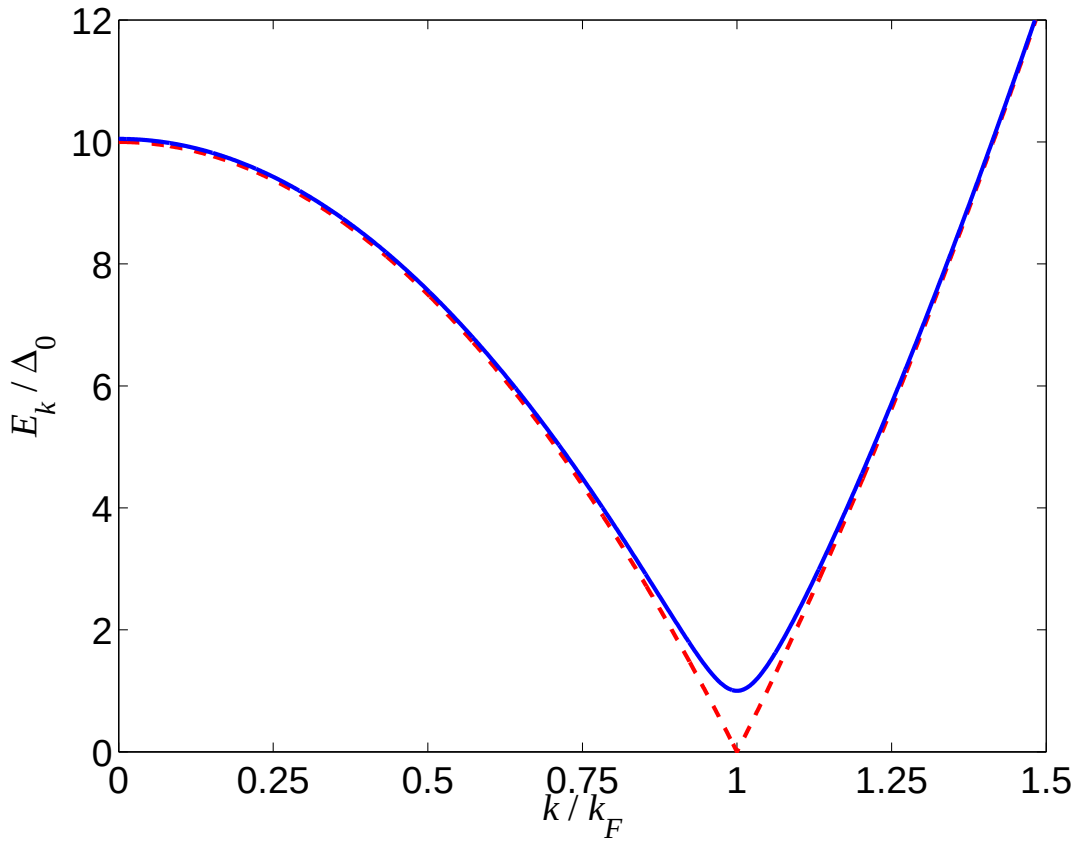

Figure 3.2: The quasi-particle spectrum of a homogeneous BCS superfluid (*blue line*) compared with $|\xi_k|$ (*red dashed line*).

where V is the volume of the system. To calculate the bulk value of the gap Δ_0 we need to carry out the regularization of the pair potential as indicated in (3.39). This is the topic of the next section.

3.4 Regularizing the Gap Equation

A major component of this work is the derivation of a properly regularized expression for the gap function. In the absence of the regularization operator the gap equation would be divergent. However, in numerical calculations the

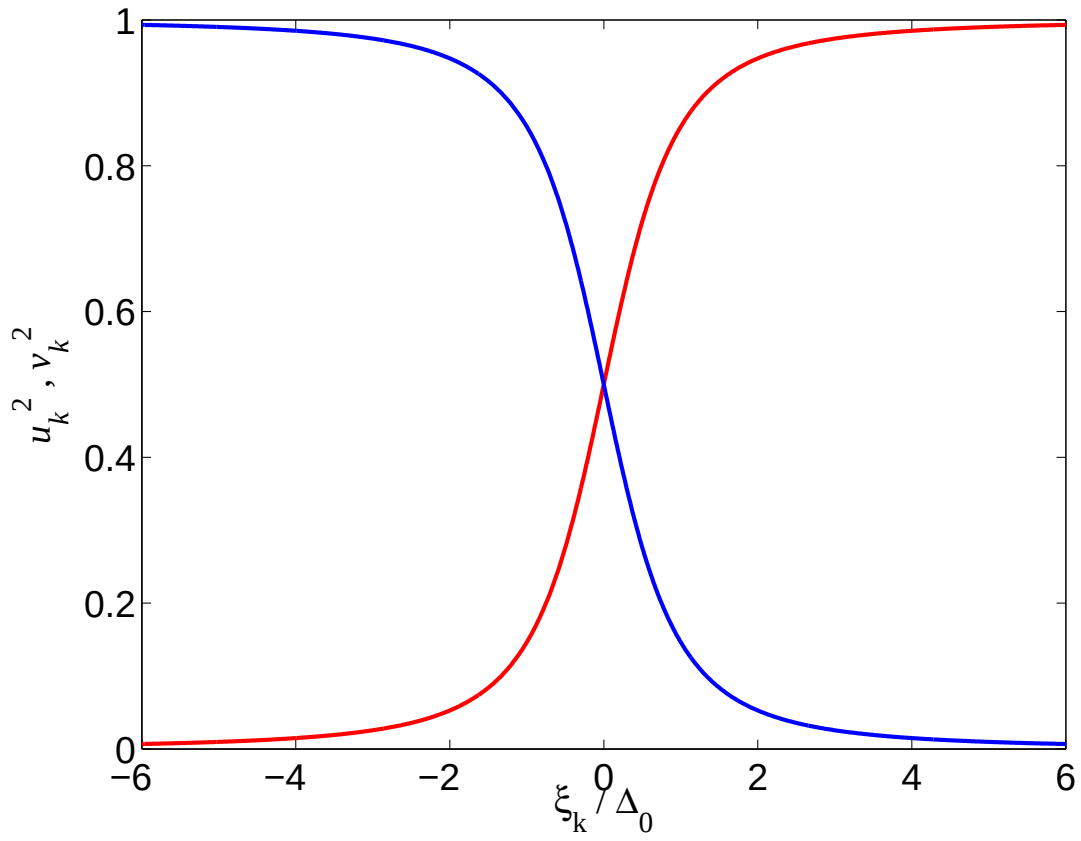

Figure 3.3: The generic form of the squared quasi-particle amplitudes u_k^2 (*red line*) and v_k^2 (*blue line*) around the Fermi energy.

infinite sum over quasi-particle states in (3.39) has to be truncated at some cutoff energy E_c, and since the exact $\tilde{r}^{-1}$ divergence of the anomalous average is only obtained in the limit of $E_c \to \infty$, the value of the sum will depend linearly on the cutoff. Thus in order to perform quantitative calculations, such that the results can be compared with future experiments with no adjustable parameters, we need a regularization procedure to render the predictions of the theory independent of E_c.

Although the gap equation as written in Eq. (3.39) is formally regular,

the practical implementation of the regularization operator $\lim_{\tilde{r}\to 0}\partial_{\tilde{r}}\tilde{r}[\cdot]$ is not straightforward. In this section we describe in detail how the limit $\tilde{r}\to 0$ in the regularization operator can be carried out in numerical calculations, and how an energy cutoff can be introduced in a systematic way. Our approach to the regularization is related to those of [67] and [78], and employs a mathematical trick involving the single-particle Green's function $G_\mu(\mathbf{r},\mathbf{r}')$

$$G_\mu(\mathbf{r},\mathbf{r}') \equiv \left\langle \mathbf{R}+\frac{\tilde{\mathbf{r}}}{2}\left|\frac{1}{\mathcal{H}_\sigma^{\mathrm{HF}}-\mu}\right|\mathbf{R}-\frac{\tilde{\mathbf{r}}}{2}\right\rangle, \tag{3.48}$$

to regularize the numerical sum. For a particle moving in an effective potential, which is the sum of an external potential $V_{\mathrm{ext}}(\mathbf{r})$ and a HF mean-field, the Green's function satisfies the equation

$$\left(\mathcal{H}_\sigma^{\mathrm{HF}}-\mu\right)G_\mu(\mathbf{r},\mathbf{r}') = \delta(\mathbf{r}-\mathbf{r}'). \tag{3.49}$$

We can thus express G_μ for $\tilde{r}\to 0$ (*i.e.* $\mathbf{r}\to\mathbf{r}'$) as

$$G_\mu(\mathbf{r},\mathbf{r}') = \frac{m_a}{2\pi\hbar^2\tilde{r}} + G_\mu^{\mathrm{reg}}(\mathbf{r}) + \mathcal{O}(\tilde{r}), \tag{3.50}$$

observing that the presence of delta function imposes a $m_a/2\pi\hbar^2\tilde{r}$ divergence on $G_\mu(\mathbf{r},\mathbf{r}')$ in the limit where $\mathbf{r}\to\mathbf{r}'$, since $\nabla^2_{\mathbf{r}}(1/\tilde{r}) = -4\pi\delta(\mathbf{r}-\mathbf{r}')$. The form of the divergent part is independent of the details of the potential, and $G_\mu^{\mathrm{reg}}(\mathbf{r})$ represents the regular part of the Green's function, *i.e.* $G_\mu^{\mathrm{reg}}(\mathbf{r})$ remains finite as $\tilde{r}\to 0$. A useful representation of the Green's function is found by expanding it on the eigenstates, $\phi_n(\mathbf{r})$, of the single-particle HF Hamiltonian defined in (3.44). By substituting the expansion

$$G_\mu(\mathbf{r},\mathbf{r}') = \sum_n a_n(\mathbf{r}')\phi_n(\mathbf{r}) \tag{3.51}$$

into the differential equation for $G_\mu(\mathbf{r},\mathbf{r}')$, and using the completeness of the eigenstates $\sum_n \phi_n(\mathbf{r})\phi_n^*(\mathbf{r}') = \delta(\mathbf{r}-\mathbf{r}')$ we get

$$\sum_n a_n(\mathbf{r}')\xi_n = \sum_n \phi_n(\mathbf{r})\phi_n^*(\mathbf{r}'). \tag{3.52}$$

Multiplying by $\phi_m^*(\mathbf{r})$ and integrating over $\mathbf{r}$ the expansion coefficients are seen to be equal to $a_m(\mathbf{r}') = \phi_m^*(\mathbf{r}')/\xi_m$, by using the orthonormality of the eigenstates. The Green's function therefore has the expansion

$$G_\mu(\mathbf{r},\mathbf{r}') = \sum_n \frac{\phi_n^*(\mathbf{r})\phi_n(\mathbf{r}')}{\xi_n}. \tag{3.53}$$

The sum runs over both positive and negative values of ξ_n, corresponding to energies above and below the Fermi level.

The trick now is to write the gap equation as [67]

$$\begin{aligned}
\Delta(\mathbf{r}) &= -g \lim_{\tilde{r}\to 0} \partial_{\tilde{r}} \left[\tilde{r} \left(\left\langle \hat{\psi}_\uparrow(\mathbf{r})\hat{\psi}_\downarrow(\mathbf{r}') \right\rangle - \frac{\Delta(\mathbf{r})}{2} G_\mu(\mathbf{r},\mathbf{r}') + \frac{\Delta(\mathbf{r})}{2} G_\mu(\mathbf{r},\mathbf{r}') \right) \right] \\
&= -g \left[\sum_\eta u_\eta(\mathbf{r}) v_\eta^*(\mathbf{r})(1-2f(E_\eta)) - \frac{\Delta(\mathbf{r})}{2} \sum_n \frac{\phi_n(\mathbf{r})\phi_n^*(\mathbf{r})}{\xi_n} \right] \\
&\quad -\frac{g\Delta(\mathbf{r})}{2} G_\mu^{\mathrm{reg}}(\mathbf{r}).
\end{aligned} \tag{3.54}$$

That is, simply adding and subtracting $\Delta(\mathbf{r})G_\mu(\mathbf{r},\mathbf{r}')/2$ to the anomalous average. On the right hand side the term in the brackets is regular; the $1/\tilde{r}$ divergences of the two sums exactly cancel each other, and the action of the regularization operator on $G_\mu(\mathbf{r},\mathbf{r}')$ extracts from this its regular part ($\lim_{\tilde{r}\to 0}\partial_{\tilde{r}}[\tilde{r}G_\mu(\mathbf{r},\mathbf{r}')]$ as is seen from (3.50)).

The divergence we are trying to remove is ultraviolet in nature, that is it arises from the high energy terms in the sums. However, sufficiently far from the Fermi surface the pairing has essentially no influence on the quasi-particle

energies, and the high energy parts of the sums cancel each other term by term, *i.e.*

$$u_\eta(\mathbf{r})v_\eta^*(\mathbf{r}) - \frac{\Delta(\mathbf{r})}{2}\frac{\phi_\eta(\mathbf{r})\phi_\eta^*(\mathbf{r})}{\xi_\eta} \to 0, \quad \text{for } E_\eta, \xi_\eta \to \infty \tag{3.55}$$

(the Fermi factors are negligible at high energy, and can be dropped). This allows us to introduce an explicit finite energy cutoff E_c, above which the cancellation can be taken to be approximately valid. With this cutoff we can write the gap equation in the form

$$\begin{aligned}\Delta(\mathbf{r}) &= -g\left[\sum_{E_\eta \le E_c} u_\eta(\mathbf{r})v_\eta^*(\mathbf{r})(1-2f(E_\eta)) - \frac{\Delta(\mathbf{r})}{2}\sum_{E_n \le E_c}\frac{\phi_n(\mathbf{r})\phi_n^*(\mathbf{r})}{\xi_n}\right] \\ &\quad -\frac{g\Delta(\mathbf{r})}{2}G_\mu^{\text{reg}}(\mathbf{r}).\end{aligned} \tag{3.56}$$

The final results will be independent of E_c, provided this is chosen high enough. For all the calculations presented in this thesis we have used an energy cutoff of $E_c = 3\mu$. We remark here that we could in principle use any "regulator"-function with a divergent term of the form

$$\frac{m_a\Delta(\mathbf{r})\mathcal{A}(\mathbf{r},\mathbf{r}')}{2\pi\hbar^2\tilde{r}}, \tag{3.57}$$

if $\mathcal{A}(\mathbf{r},\mathbf{r}) = 1$, *i.e.* the general functional form of $\mathcal{A}(\mathbf{r}_1,\mathbf{r}_2)$ is irrelevant. However, the approach we take here is to use the Green's function associated with the effective single-particle potential, $V_{\text{eff}}(\mathbf{r}) = V_{\text{ext}}(\mathbf{r}) + gn_\sigma(\mathbf{r})$, which includes both the external potential and the mean-field (Hartree) potential (see (3.48)). This ensures that the one to one correspondence between the single-particle states with $\Delta(\mathbf{r}) = 0$ and the eigenstates of the BdG Hamiltonian can be established at the lowest possible value of E_c. If instead one chooses the non-paired wavefunctions $\phi_n(\mathbf{r})$ to be plane waves as in [78], the cutoff energy must be taken at a higher value, significantly degrading the convergence of the scheme. The

same conclusion was reached by Grasso and Urban [79], who present a detailed analysis of the convergence properties.

Although the gap equation (3.56) is formally divergence free, we still have to determine the regular part of the single-particle Green's function, defined as

$$G_\mu^{\rm reg}(\mathbf{r}) = \lim_{\tilde{r}\to 0}\left(G_\mu(\mathbf{r},\mathbf{r}') - \frac{m_a}{2\pi\hbar^2\tilde{r}}\right). \tag{3.58}$$

In general, this is a non-trivial procedure which has only been implemented for a limited number of specific cases. However, if the energy cutoff is sufficiently large, that the states above E_c are well approximated by plane waves, we can employ a local density approximation (LDA) to replace the high energy part of the Green's function expansion (3.53) by an integral, such that

$$G_\mu^{\rm reg}(\mathbf{r}) = \lim_{\tilde{r}\to 0}\left(\sum_{E_n\le E_c}\frac{\phi_n(\mathbf{r}')\phi_n^*(\mathbf{r})}{\xi_n} + \int_{k_c(\mathbf{r})}^{\infty}\frac{dk}{2\pi^2}\,\frac{k^2}{\frac{\hbar^2k^2}{2m_a}+V_{\rm eff}(\mathbf{r})-\mu-i\gamma} - \frac{m_a}{2\pi\hbar^2\tilde{r}}\right), \tag{3.59}$$

where the local cutoff wavevector $k_c(\mathbf{r})$ is defined through

$$E_c = \frac{\hbar^2k_c^2(\mathbf{r})}{2m_a} + V_{\rm eff}(\mathbf{r}) - \mu. \tag{3.60}$$

The factor $i\gamma$ is inserted in the denominator to lift the poles off the real axis. At the end of the calculation we take the limit $\gamma\to 0^+$. The criteria for using the LDA is that $2\pi/k_c$ is much smaller than the length scale over which the effective single-particle potential varies. If this is fulfilled then the high energy states "see" the effective potential as locally constant. This is distinct from the convergence criteria of the gap equation. Observing that

$$\frac{1}{2\pi^2}\int_0^\infty dk k^2\,\frac{e^{i\mathbf{k}\cdot\tilde{\mathbf{r}}}}{\frac{\hbar^2k^2}{2m_a}+V_{\rm eff}(\mathbf{r})-\mu-i\gamma} = \frac{m_a}{2\pi\hbar^2}\,\frac{e^{ik_{\rm F}(\mathbf{r})\tilde{r}}}{\tilde{r}}, \tag{3.61}$$

with the local Fermi wavevector given by

$$\mu = \frac{\hbar^2k_{\rm F}^2(\mathbf{r})}{2m_a} + V_{\rm eff}(\mathbf{r}), \tag{3.62}$$

the regular part of the Green's function may be approximated as

$$\begin{aligned} G_\mu^{\rm reg}(\mathbf{r}) &= \sum_{E_n\le E_c}\frac{\phi_n(\mathbf{r})\phi_n^*(\mathbf{r})}{\xi_n}+\int_0^{k_c(\mathbf{r})}\frac{dk}{2\pi^2}\,\frac{k^2}{\mu-\frac{\hbar^2k^2}{2m_a}-V_{\rm eff}(\mathbf{r})+i\gamma} \\ &\quad +\frac{im_ak_{\rm F}(\mathbf{r})}{2\pi\hbar^2}, \end{aligned} \tag{3.63}$$

as is seen by expanding the exponential on the right hand side of (3.61) to first order in $k_{\rm F}(\mathbf{r})\tilde{r}$. The integral over k is evaluated in Appendix F. It is

$$\begin{aligned} I_1 &= \int_0^{k_c(\mathbf{r})}\frac{dk}{2\pi^2}\,\frac{k^2}{\mu-\frac{\hbar^2k^2}{2m_a}-V_{\rm eff}(\mathbf{r})+i\gamma} \\ &= -\frac{m_a}{\pi^2\hbar^2}\left(k_c(\mathbf{r})-\frac{k_{\rm F}(\mathbf{r})}{2}\ln\frac{k_c(\mathbf{r})+k_{\rm F}(\mathbf{r})}{k_c(\mathbf{r})-k_{\rm F}(\mathbf{r}}\right)-\frac{im_ak_{\rm F}(\mathbf{r})}{2\pi\hbar^2} \end{aligned} \tag{3.64}$$

Hence the final expression for the regular part of the Green's function is

$$G_\mu^{\rm reg}(\mathbf{r})=\sum_{E_n\le E_c}\frac{\phi_n(\mathbf{r})\phi_n^*(\mathbf{r})}{\xi_n}-\frac{m_a}{\pi^2\hbar^2}\left(k_c(\mathbf{r})-\frac{k_{\rm F}(\mathbf{r})}{2}\ln\frac{k_c(\mathbf{r})+k_{\rm F}(\mathbf{r})}{k_c(\mathbf{r})-k_{\rm F}(\mathbf{r}}\right). \tag{3.65}$$

Combining all the parts we at long last arrive at the expression for the regularized gap function [78, 80]

$$\begin{aligned} \Delta(\mathbf{r}) &= -g\sum_{E_\eta\le E_c}u_\eta(\mathbf{r})v_\eta^*(\mathbf{r})(1-2f(E_\eta)) \\ &\quad +\frac{g\Delta(\mathbf{r})m_a}{2\pi^2\hbar^2}\left(k_c(\mathbf{r})-\frac{k_{\rm F}(\mathbf{r})}{2}\ln\frac{k_c(\mathbf{r})+k_{\rm F}(\mathbf{r})}{k_c(\mathbf{r})-k_{\rm F}(\mathbf{r}}\right), \end{aligned} \tag{3.66}$$

where the sums over the eigenstates of $\mathcal{H}_\sigma^{\rm HF}$ have cancelled. It is convenient to interpret the regularization procedure in terms of a renormalized, position dependent, coupling strength, $\tilde{g}$:

$$\Delta(\mathbf{r})=-\tilde{g}(\mathbf{r})\sum_{E_\eta\le E_c}u_\eta(\mathbf{r})v_\eta^*(\mathbf{r}), \tag{3.67}$$

defining $\tilde{g}$ in terms of the unregularized coupling parameter in a way suggestive of the Lippman-Schwinger equation

$$\frac{1}{\tilde{g}(\mathbf{r})}=\frac{1}{g}-\frac{m_ak_c(\mathbf{r})}{2\pi^2\hbar^2}\left[1-\frac{k_{\rm F}(\mathbf{r})}{2k_c(\mathbf{r})}\ln\frac{k_c(\mathbf{r})+k_{\rm F}(\mathbf{r})}{k_c(\mathbf{r})-k_{\rm F}(\mathbf{r}}\right]. \tag{3.68}$$

Indeed we find that in the limit of $k_c(\mathbf{r}) \to \infty$, where terms on the order of $k_F(\mathbf{r})/k_c(\mathbf{r})$ can be neglected, our expression for the regularized coupling constant reduces to the result one obtains by combining the Lippman-Schwinger equation for the two-body T-matrix of a delta function potential with the LDA. Further details of this correspondence are given in Appendix A. While the calculation we have just gone through is exceedingly technical and in a certain sense an abstraction, since the ultraviolet divergence is an unphysical relic of the contact interaction potential, it is gratifying to note that the end result for the regularized gap equation is both simple and easy to implement numerically.

To add one last wrinkle we consider what happens in the classically forbidden region where $\mu < V_{\text{eff}}$. Here the local Fermi wavevector becomes purely imaginary

$$k_{\text{F}}(\mathbf{r}) = i\kappa_F(\mathbf{r}), \quad \kappa_F(\mathbf{r}) = \frac{2m_a}{\hbar^2}\sqrt{V_{\text{eff}} - \mu}. \tag{3.69}$$

It is easy to show that in this case one recovers exactly the same expression for $\tilde{g}$. By using the form of the logarithm function with a complex argument we can show that $\tilde{g}$ is still real:

$$\begin{aligned}
\ln\frac{k_c(\mathbf{r}) + k_{\text{F}}(\mathbf{r})}{k_c(\mathbf{r}) - k_{\text{F}}(\mathbf{r})} &= \ln\left(k_c(\mathbf{r}) + k_{\text{F}}(\mathbf{r})\right) - \ln\left(k_c(\mathbf{r}) - k_{\text{F}}(\mathbf{r})\right) \\
&= \ln\left(\sqrt{k_c^2(\mathbf{r}) + \kappa_F^2(\mathbf{r})}\right) + i\tan^{-1}\frac{\kappa_F(\mathbf{r})}{k_c(\mathbf{r})} \\
&\quad - \ln\left(\sqrt{k_c^2(\mathbf{r}) + \kappa_F^2(\mathbf{r})}\right) + i\tan^{-1}\frac{\kappa_F(\mathbf{r})}{k_c(\mathbf{r})} \\
&= 2i\tan^{-1}\frac{\kappa_F(\mathbf{r})}{k_c(\mathbf{r})},
\end{aligned} \tag{3.70}$$

meaning that the renormalized coupling strength in this case can be written as

$$\frac{1}{\tilde{g}(\mathbf{r})} = \frac{1}{g} - \frac{m_a}{2\pi^2\hbar^2}\left[k_c(\mathbf{r}) + \kappa_F(\mathbf{r})\tan^{-1}\frac{\kappa_F(\mathbf{r})}{k_c(\mathbf{r})}\right]. \tag{3.71}$$

We end the discussion of the regularization by writing the final expression for the total energy of the gas, which is free of any divergences. With the procedure discussed above (3.43) becomes

$$\begin{aligned} E &= \int d^3r \Big\{ 2 \sum_{E_\eta \leq E_c} E_\eta \left[|u_\eta(\mathbf{r})|^2 f(E_\eta) - |v_\eta(\mathbf{r})|^2 (1 - f(E_\eta)) \right] \\ &\quad - g n_\uparrow(\mathbf{r}) n_\downarrow(\mathbf{r}) - \frac{|\Delta(\mathbf{r})|^2}{\tilde{g}(\mathbf{r})} + \sum_\sigma \mu_\sigma n_\sigma(\mathbf{r}) \Big\}. \end{aligned} \tag{3.72}$$

This is the experssion for the energy we use in calculations. The important thing to note is that the regularized coupling constant appears explicitly in the energy experssion, such that a properly regularized theory is essential for an accurate calculation of E.

3.4.1 Local-Density Approximation

In the limit of a sufficiently large system, we can again treat the gas as being locally homogeneous. In the superfluid state the LDA entails replacing the quasi-particle wavefunctions by plane waves, with the amplitudes given by (3.46). For this to make sense, we must require that the variation of the potential over the extent of a Cooper pairs, given by the BCS coherence length $\xi_{\rm BCS}$ is small. In this case the sum over discrete states in the gap equation (3.66) can be replaced by an integral over a continuous momentum variable, and we have

$$\begin{aligned} -\frac{1}{g} &= \frac{1}{2\pi^2} \int_0^{k_c(\mathbf{r})} dk\, k^2 \, \frac{\tanh(\frac{\beta E(\mathbf{r},\mathbf{k})}{2})}{2E(\mathbf{r},\mathbf{k})} \\ &\quad - \frac{m_a}{2\pi^2\hbar^2} \left(k_c(\mathbf{r}) - \frac{k_{\rm F}(\mathbf{r})}{2} \ln \frac{k_c(\mathbf{r}) + k_{\rm F}(\mathbf{r})}{k_c(\mathbf{r}) - k_{\rm F}(\mathbf{r}} \right), \end{aligned} \tag{3.73}$$

using that locally we can replace $u_{\mathbf{k}}(\mathbf{r}) v^*_{\mathbf{k}}(\mathbf{r})$ with $\Delta(\mathbf{r})/2E(\mathbf{r},\mathbf{k})$. The local Hartree-Fock and quasi-particle energies are given by (assuming equal popula-

tions of the two components)

$$\epsilon(\mathbf{r},\mathbf{k}) = \frac{\hbar^2 k^2}{2m_a} + V_{\rm ext}(\mathbf{r}) + g n_\sigma(\mathbf{r}), \tag{3.74}$$

$$E(\mathbf{r},\mathbf{k}) = \sqrt{(\epsilon(\mathbf{r},\mathbf{k})-\mu)^2 + |\Delta(\mathbf{r})|^2}. \tag{3.75}$$

We can find the gap function at zero temperature by setting $\tanh(\beta E(\mathbf{r},\mathbf{k})/2) = 1$. In this case (3.73) can be solved analytically in the weak-coupling limit of $\Delta(\mathbf{r})/\mu(\mathbf{r}) \ll 1$, defining a local chemical potential

$$\mu(\mathbf{r}) = \frac{\hbar^2 k_{\rm F}^2(\mathbf{r})}{2m_a} = \mu - V_{\rm ext}(\mathbf{r}) - g n_\sigma(\mathbf{r}). \tag{3.76}$$

We find to lowest order in $\Delta(\mathbf{r})/\mu(\mathbf{r})$ for the pairing field at $T = 0$ (see Appendix F)

$$\Delta(\mathbf{r}, T=0) = \frac{8}{e^2}\,\mu(\mathbf{r}) e^{-1/N(\mathbf{r},0)|g|} = \frac{8}{e^2}\,\mu(\mathbf{r}) e^{-\pi/2k_{\rm F}(\mathbf{r})|a|}, \tag{3.77}$$

with $N(\mathbf{r},0) = m_a k_{\rm F}(\mathbf{r})/2\pi^2\hbar^2$. This result is the LDA generalization of the standard formula for the bulk value of the gap in Fermi superfluid with s-wave pairing [81]. The bulk result is derived by regularizing the gap equation through the Lippman-Schwinger equation for the two-body scattering matrix, as we did in section 3.1. The present calculation therefore shows that the regularized pseudo-potential method is equivalent to replacing the bare coupling strength with the two-body T-matrix (using a local chemical potential), when we are applying a semi-classical approximation to describe the quasi-particle amplitudes.

Within the LDA the critical temperature is a local quantity $T_c = T_c(\mathbf{r})$. As usual it is determined by setting $\Delta(\mathbf{r}) = 0$ in (3.73). The transition temperature of the system will correspond to the largest value of $T_c(\mathbf{r})$. Again, in this limit the equation allows for an analytical solution, and we find that

$$k_{\rm B} T_c(\mathbf{r}) = \frac{8e^{\gamma-2}}{\pi}\,\mu(\mathbf{r}) e^{-\pi/2k_{\rm F}(\mathbf{r})|a|} \simeq 0.57\Delta(\mathbf{r}, T=0). \tag{3.78}$$

Here $\gamma = 0.577\ldots$ is Euler's constant. The bulk value of the gap Δ_0, and the transition temperature for a homogeneous sample are simply given by (3.77) and (3.78) with $V_{\rm ext}(\mathbf{r}) = 0$.

In calculating both the LDA value of the pairing gap and the transition temperature we have neglected the effect of induced interactions. In particular we have used a two-body potential corresponding to fermion-fermion scattering *in vacuo*. The fact that the interacting particles are embedded in a many-body system produces medium effects, by a process closely related to screening in an electron gas. If these are included, the transition temperature and the gap are reduced by a factor $(4e)^{1/3} \simeq 2.2$ for a two-component gas [82, 83].

3.5 Towards Fermi Superfluidity

To our knowledge the lowest temperature attained in Fermi gas experiments to the present day is 0.05 $T_{\rm F}$ [84], and it seems that this may be close to the limit set by the currently available cooling methods (though we mention that a new standard for low temperatures was recently set by cooling a Bose condensed gas to temperatures below 500 picokelvin using a method of adiabatic decompression, while changin the shape of the trap [85]. The extent to which this technique can be applied to cool fermionic gases remains to be seen). The predicted transition temperature in the BCS theory described above is roughly an order of magnitude smaller.

As the calculation of the transition temperature shows, T_c depends exponentially on the dimensionless parameter $k_{\rm F}|a|$, which serves as an effective measure of the interaction strength. The Fermi wavevector is an indicator of the den-

sity of states available for pairing, while the scattering length a is a measure of the force of the attractive potential responsible for pairing. Several theoretical proposals suggest methods for increasing the value of T_c to bring it within experimental reach, by increasing the value of $k_{\mathrm{F}}|a|$. We will briefly mention the main contenders:

- Loading degenerate fermions into an optical lattice, which is a periodic potential formed by the intersection of two or more laser beams. Such light crystals can trap atoms in the potential minima of the dipole force, and give rise to band structure phenomena as in solid state physics. By controlling the intensity of the laser fields this can lead to a substantial increase of the density of states, as the bands flatten when the lattice becomes deeper, and an enhancement of pairing is predicted to result [86]. This system is described by the Hubbard model with negative on-site interaction [87]. As the lattice depth is increased the tunneling rate is exponentially suppressed and eventually the ability to establish phase coherence between Cooper pairs at different lattice sites is lost, and the system converts to Mott insulator state as has already been observed for a Bose gas [88].

- By immersing the Fermi gas in a bath of condensed bosonic atoms, there is a component of the effective fermion-fermion interaction due to the exchange of density fluctuations in the boson component. This is very much reminiscent of the electron-phonon coupling in superconducting metals, and is predicted to increase the attractive forces between pairs of fermions, thus raising the critical temperature for pairing [89]. Experiments have demonstrated how this induced interaction can lead to an instability of the fermion cloud above a critical particle number [90]. It is hoped that

this avenue for manipulating the scattering properties can give rise to pairing in the system, if it is on the verge of the collapse, where the interatomic forces are most attractive.

- The scattering length can be tuned via a Feshbach resonance [91, 92]. This involves a resonant coupling of the scattering continuum states with a bound, bosonic molecular state of the interatomic potential. The difference in magnetic moments of the molecule and the free atoms allows their relative energy to be tuned to resonance by adjusting an external magnetic field. Since the scattering length diverges and changes sign, when a new bound state enters the potential, the Feshbach resonance provides researchers with a powerful tool to vary the effective interactions over a wide range, including both repulsive and attractive forces [93, 94]. If the bound state is tuned above threshold only virtual occupation of the closed channel is allowed, but on the other side of the resonance a substantial fraction of the atoms can be converted into molecules. In an astonishing series of experiments reversible formations of molecules has been demonstrated with a conversion efficiency exceeding 50%, and molecular lifetimes as long as one second [94, 95, 96, 97, 98]. A similar experiment starting from a gas of Bose atoms hints that quantum degeneracy and ultimately BEC of these molecules may be possible (see below) [99].

- Similarly, the molecular bound states can be created directly out of the atomic gas by a photoassociation process. This is also predicted to lead to a resonant increase in the effective interaction of the fermions [100]. The creation of ultracold molecules via photoassociation was recently demon-

strated for an atomic BEC [101].

Mathematically identical, both of the resonance methods (Feshbach and photoassociation) are neutral-particle realizations of the boson-fermion model, which has been widely studied in the context of high-temperature superconductors [102, 103]. It has been shown that the resonant coupling between Fermi atoms and Bose molecules leads to a novel superfluid phase, where mutual macroscopic coherence between Cooper pairs and molecules leads to a transition temperature as high as a few tenths of the Fermi temperature [104, 105]. By tuning the interaction strength across the resonance it is possible to realize the BCS-BEC crossover, going from a limit where only weakly bound Cooper pairs exist, to a strongly coupled regime of localized molecular bosons, which can undergo Bose-Einstein condensation [106, 107]. Just before the completion of this thesis the observation of a molecular Bose-Einstein condensate in a gas of Fermi atoms near a Feshbach resonance was reported by Jin and co-workers [108], and in the laboratory of Grimm [109].

A further intriguing aspect of the strongly interacting Fermi gas, is that as the scattering length becomes larger than the interparticle spacing the interactions become unitarity limited. In this limit the energy per particle and the size of the pairing gap is expected to approach a constant fraction of the Fermi energy [52]. The value of this fundamental many-body parameter is universal, and we can therefore potentially use an atomic Fermi gas as a model system for studying the effects of strong interactions in a wide class of physical systems, notably including nuclear matter and high-temperature superconductors. The wide tunability of the interactions, densities, spin states and temperatures of dilute quantum gases makes them an attractive tool for probing fundamental

physical phenomena outside the realm of atomic physics.

In the strongly interacting limit more sophisticated theoretical tools are needed to augment our mean-field approach, which is only valid when $na^3 \ll 1$. The treatment of this regime lies beyond the scope of this work. The remainder of this thesis will therefore concentrate on the effects of superfluidity on an atomic Fermi gas in the weak-coupling limit.

3.6 Fermi Gas in a Harmonic Trap

With the regularization procedure in place we can solve the BdG equations self-consistently. In general this is an iterative procedure, which must be carried out numerically. The details of our numerical scheme are are deferred to Appendix B, and at this point we focus our attention on the results. As in Chapter 2 we consider two types of confinement; an isotropic harmonic oscillator potential, and a cylindrical box potential. As in Section 2.5 we use parameters appropriate to ^{6}Li taking the scattering length to be $a = -2160\ a_0$. Fig. 3.4 shows the zero temperature variation of the density of the gas in the superfluid phase as a function of distance from the center of the trap (both in harmonic oscillator units). The number of particles is $N_\sigma = 4996$ in each hyperfine state. For comparison the density profile as calculated by the LDA is also plotted, and again we find quite good agreement between the two curves. Finally, the density of a normal state gas with (almost) the same number of particles is shown. As is evident, the density is almost unchanged when going through the superfluid transition. The only visible effect is a smoothening of the oscillations close to $r = 0$ (see inset). In the weak-coupling limit we expect the variation of the

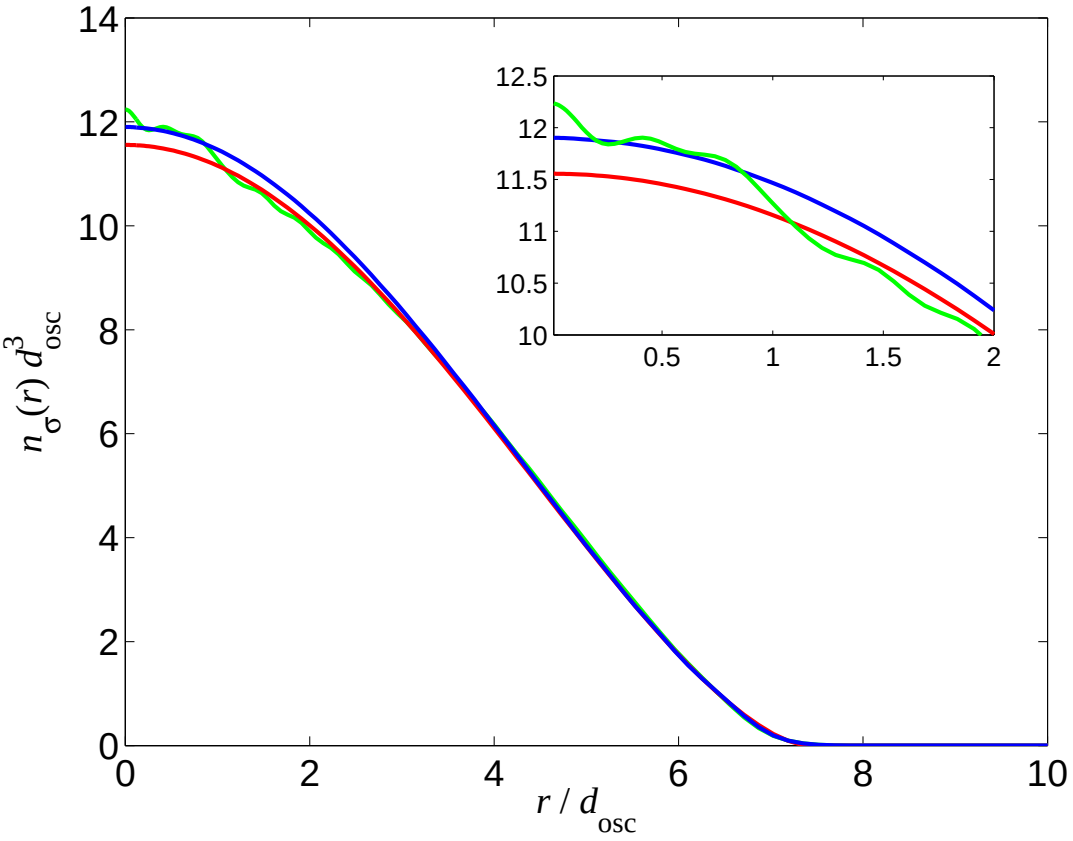

Figure 3.4: Density distribution of Fermi gas in isotropic harmonic trap at $T = 0$. The blue line is the density in the superfluid state with $N_\sigma = 4996$, while the density of the normal state ($\Delta(\mathbf{r}) = 0$, $N_\sigma = 4988$) is shown by the green line. The local-density approximation to the superfluid state density is also plotted (*red line*). The inset shows the behavior of all three curves close the origin. The chemical potential is $\mu = 27.3\ \hbar\omega$.

density due to the finite value of the pairing field to be on the order of $\Delta/E_\mathrm{F} \ll 1$. With the parameters chosen we are in the so-called inter shell pairing regime, where the interaction is strong enough that Cooper pairs can form between atoms in different harmonic oscillator shells. This means that effects due to the shell

structure of the external potential are not pronounced, and the coherence length is small compared to the size of the system [110, 111].

The spatial variation of the pairing field is plotted in Fig. 3.5 for the same parameters. At zero temperature, Cooper pairing occurs throughout the trapped atomic cloud, as is reflected by the density and gap function vanishing at the same distance from the trap center. However, as the temperature is increased the gas will first undergo the transition to the normal phase at the edge of the cloud, where the density, and correspondingly the local transition temperature, is smallest. At finite temperatures the gas will therefore consist of a superfluid core surrounded by a shell of atoms in the normal state where $\Delta(\mathbf{r})$ vanishes, since the density is nearly temperature independent in the range $0 < T < T_c$. This is illustrated in Fig. 3.6 where $\Delta(\mathbf{r})$ at $T = T_c/2$ is compared to the density profile at that temperature. As is evident the pairing field exhibits strong temperature dependence, whereas the density profile is essentially unchanged.

In Fig. 3.5 we also plot the solution of the LDA expression for the pairing field, Eq. 3.77. We see again, that the LDA generally provides a good description of the spatial variation of the full self-consistent solution. However, it fails to capture the shoulder of the gap function close to the surface of the cloud. This feature is due to low energy excitations localized in the potential well formed by the pairing field (on the inside) and the external trapping potential (on the outside). These so-called "in-gap excitations" all have energies significantly lower than $\Delta(r = 0)$. As in seen in the energy spectrum Fig. 3.7 the in-gap modes have virtually no l dependence. This is because these states, being localized in the minimum of $\Delta(r)+V_{\rm ext}(r)-\mu$, are suppressed in the region where the centrifugal barrier $\hbar^2 l(l+1)/2m_a r^2$ is significant [110]. They therefore correspond to surface

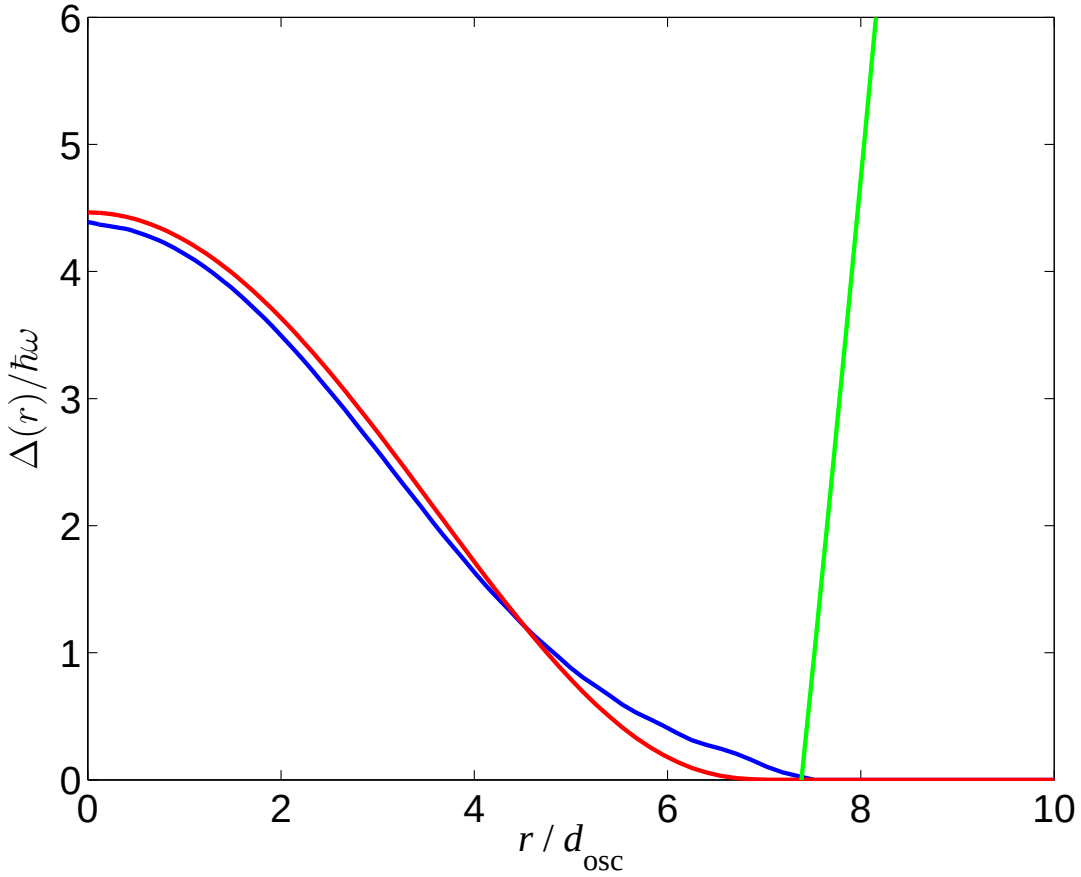

Figure 3.5: The pairing field in a spherical harmonic oscillator potential (*blue line*), compared with the LDA expression Eq. (3.77) (*red line*). The green curve indicates $V_{\mathrm{ext}}(r) - \mu$. The parameters are the same as in Fig. 3.4.

modes of the cloud. We mention that the energies of the in-gap excitations can be determined from a semi-classical analysis of a particle moving in the effective potential formed by the pairing field and the trap [75]. Bogoliubov wavefunctions with energies larger than $\Delta(r = 0)$ penetrate closer to the center of the trap and thus feel the full centrifugal potential. Therefore E_{nl} does depend on the angular momentum for these higher modes.

Among the interesting prospects for achieving pairing in a trapped Fermi

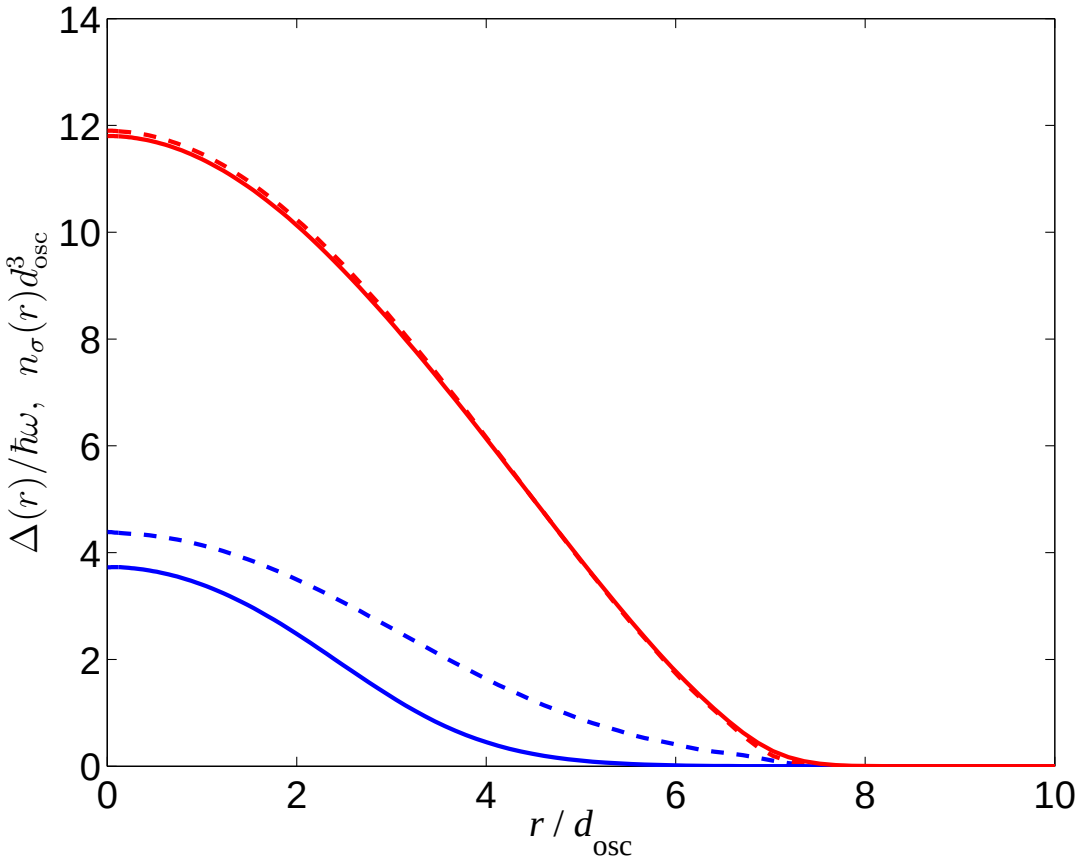

Figure 3.6: The pairing field at $T = T_c/2$ (*blue line*) compared with $\Delta(\mathbf{r})$ at zero temperature (*dashed blue line*), and the density profile (*red line*), which is virtually unchanged from its zero temperature from shown by the dashed red line. The parameters are identical to those used in Fig. 3.4.

gas are the experimental possibilities of tuning the parameters of the system allowing a systematic exploration of finite size effects on pairing. By adjusting either the density or the interaction strength, several different pairing regimes can be identified [110, 112]. In the limit of very weak coupling the shell structure of the trapping potential has a pronounced influence on the pairing, as Cooper pairs only form between particles in the same harmonic oscillator shell. This

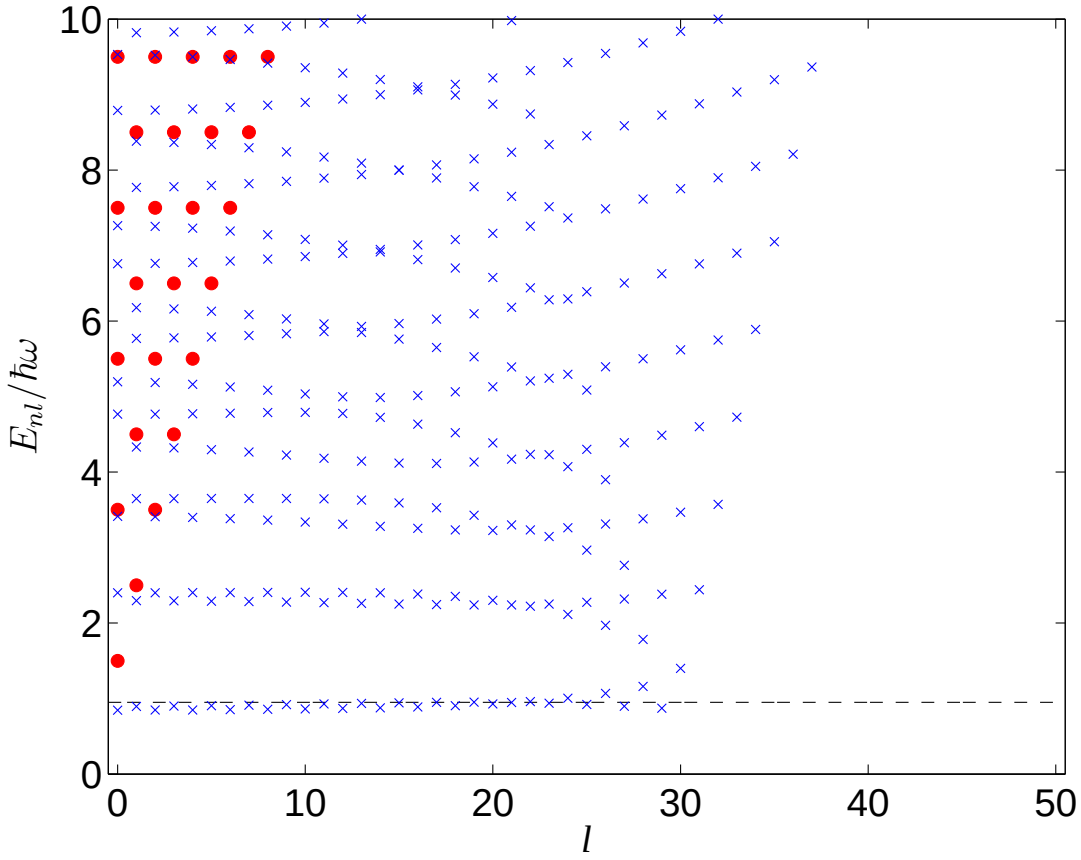

Figure 3.7: Quasi-particle spectrum of a superfluid Fermi gas in a harmonic oscillator potential at zero temperature (×'s). The energies for a non-interacting gas are shown for comparison (•'s). The chemical potential for the superfluid gas is $\mu = 27.3\ \hbar\omega$. The average bulk gap Eq. (3.79) is show by a dashed line.

corresponds to the gap being small compared with the trap level spacing $\hbar\omega$. For stronger interactions and larger systems, one finds that $\Delta \gg \hbar\omega$, and the coherence length is smaller than the size of the cloud. In this limit the gas behaves like a bulk system, and is consequently well described by the LDA. The calculation presented above was done in an intermediate regime, where shell effects are still important, but where interactions are strong enough to cause

pairing between atoms in different shells. In this case the spectral gap is to be understood as the spatially averaged quantity [113]

$$\langle \Delta \rangle \simeq 2 n_F \hbar\omega e^{-\hbar\omega/2G}, \tag{3.79}$$

where n_F is related to the chemical potential by $\mu = (n_F + 3/2)\hbar\omega$, and the parameter G is defined by

$$G = \frac{32\sqrt{2E_{\rm F}}}{15\pi^2} \frac{|a|}{d_{\rm osc}} \hbar\omega. \tag{3.80}$$

The average gap is indicated in Fig. 3.7 by a dashed line, and we observe that the agreement with the lowest numerical quasi-particle energies is good. Due to their experimental flexibilty the trapped atomic gases thus provide a model system for studying Fermi superfluidity in a context bridging bulk condensed matter systems and atomic nuclei, in which finite size effects are important.

3.7 Fermi Gas in a Cylinder

To estimate the degree to which a gas contained in a cylinder can be considered a bulk sample we have performed numerical calculations on such a system. Results for the energy per particle of the gas are plotted in Fig. 3.8 for cylinders of length $L = 11.4\,\mu$m, and two different radii, $R = 28.5\,\mu$m, and $R = 99.7\,\mu$m. This figure is the equivalent of Fig. 2.6, but now includes pairing effects. Also plotted are the bulk expressions for the energy per particle of a gas in the superfluid and the normal phase. We see that the gas in the cylinder to a good approximation can be described by the bulk expression for the energy (3.47). It is also evident that the difference between this energy and the corresponding one for a normal state gas (2.35) is very small. This energy difference, termed the condensation energy,

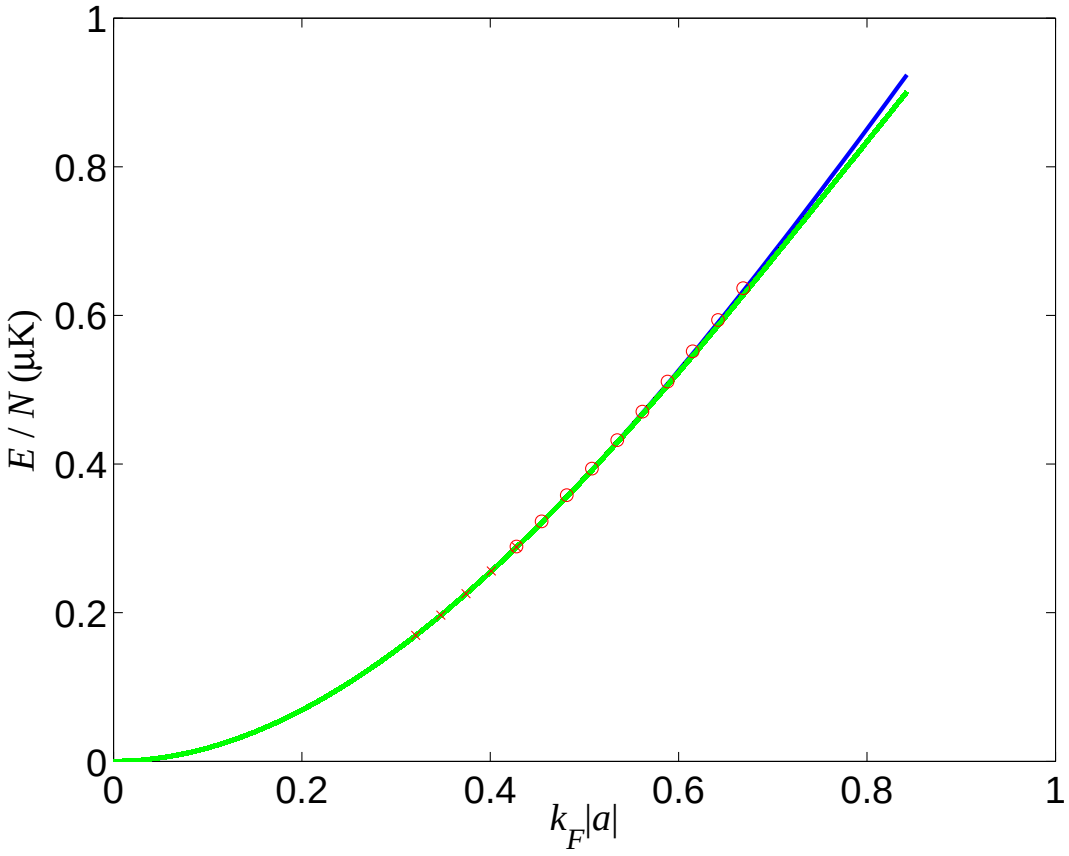

Figure 3.8: Energy per particle in Fermi superfluid as a function of the interaction strength. The green line gives the bulk expression (3.47), which is compared to the energy of a gas in the normal phase (2.35), *i.e.* $\Delta = 0$, with the same parameters (*blue line*). The numerical results from solving the BdG equations for a gas held in a cylinder of length radius R are also plotted. Two different radii were used; $R = 28.5$ μm ($\circ$'s) and $R = 99.7$ μm ($\times$'s).

is $E_{\rm cond} = -N(0)V\Delta_0^2/2 = -3\Delta_0^2 N_\sigma/4E_{\rm F}$, as is seen from (3.47). Its bulk value is plotted in Fig. 3.9, along with the numerical result for the gas in a cylinder, and again we find satisfactory agreement, demonstrating that, for the particular cylinder size chosen, the gas behaves largely as a bulk system, meaning finite size effects are of little importance. The smallness of the condensation energy can be attributed to the fact that we are in the weakly interacting regime, where only a small fraction of the particles participate in the pairing, and hence change their energy. It is remarkable that such a tiny decrease of the ground state energy of the system is accompanied by the dramatic effect on the transport properties that is characteristic of the superfluid phase. This will be the focus of the next chapter.

The spatial variation of the gap function is plotted in Fig. 3.10, as a function of the distance from the symmetry axis of the cylinder, $\rho = \sqrt{x^2 + y^2}$. Also shown is the density profile of the gas. Both are divided by their values in a bulk system with the same number of particles N_σ per spin state, Δ_0, and $n_\sigma = k_{\rm F}^3/6\pi^2 = N_\sigma/V$, respectively. Except in a small boundary layer the gas closely resembles a bulk superfluid. The boundary exists because the Bogoliubov wavefunctions must vanish at $\rho = R$ in order to satisfy the boundary condition at the wall of the cylinder. Due to the suppression of the atomic density close to the cylinder wall, $n_\sigma(\rho)$ is slightly higher than N_σ/V in the interior region. We remark that the feature close at the origin is a numerical artifact.

For a more quantitative comparison with the bulk expression, we show in Fig. 3.11 the value of $\Delta(\mathbf{r})$ halfway to the edge of the cylinder, where boundary effects are negligible, as a function of $k_{\rm F}|a|$. The agreement between the numerical results and Δ_0 provides further confirmation that in the parameter regime

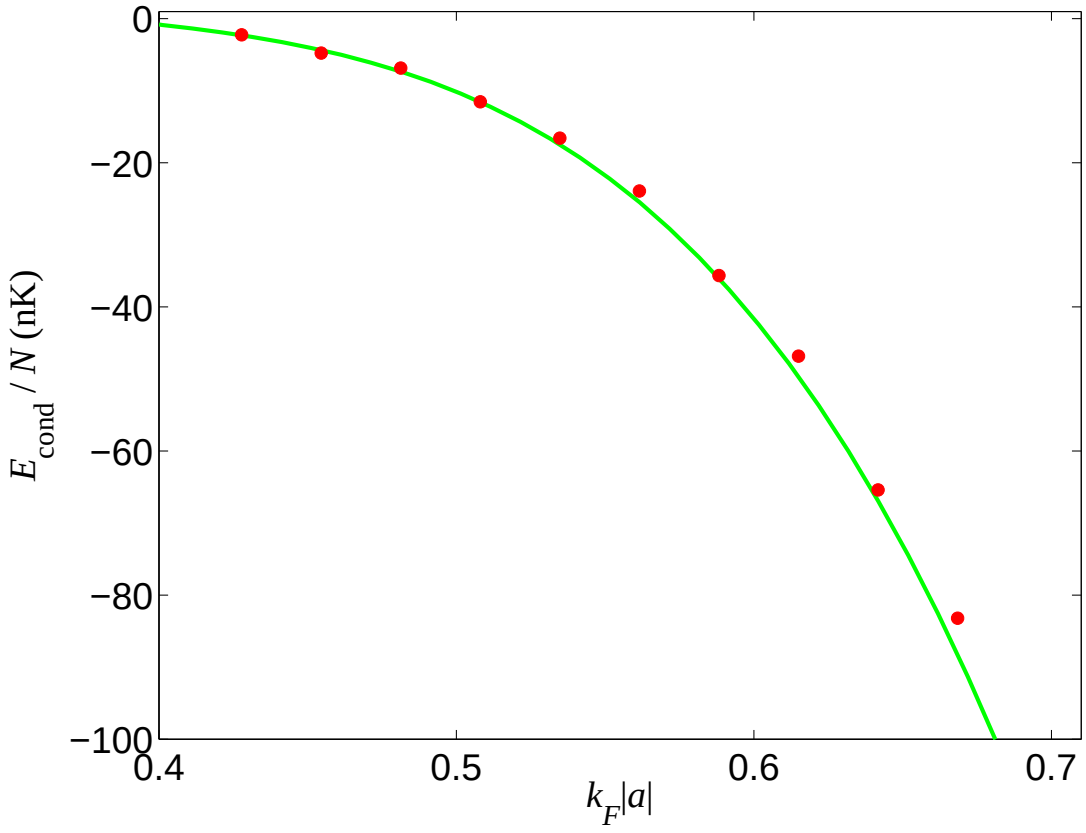

Figure 3.9: Comparison of the condensation energy per particle of a superfluid Fermi gas in a cylinder of radius $R = 28.5$ μm (•'s) with the bulk expression $-N(0)\Delta_0^2/2$ (*dashed green line*). Notice the change of scale from Fig. 3.8.

studied the gas behaves as a bulk superfluid.

Since the pairing field has essentially no spatial variation, except for the sharp drop off at the surface of the cylinder, there are no in-gap excitations as in the case of a harmonic confining potential. We illustrate this point in Fig. 3.12 by plotting the density of states (DOS) $N(E)$ in the vicinity of the Fermi level. It is defined as the spatial integral of the local density of states (LDOS):

$$N(E) = \int d^3r\, N(\mathbf{r}, E), \tag{3.81}$$

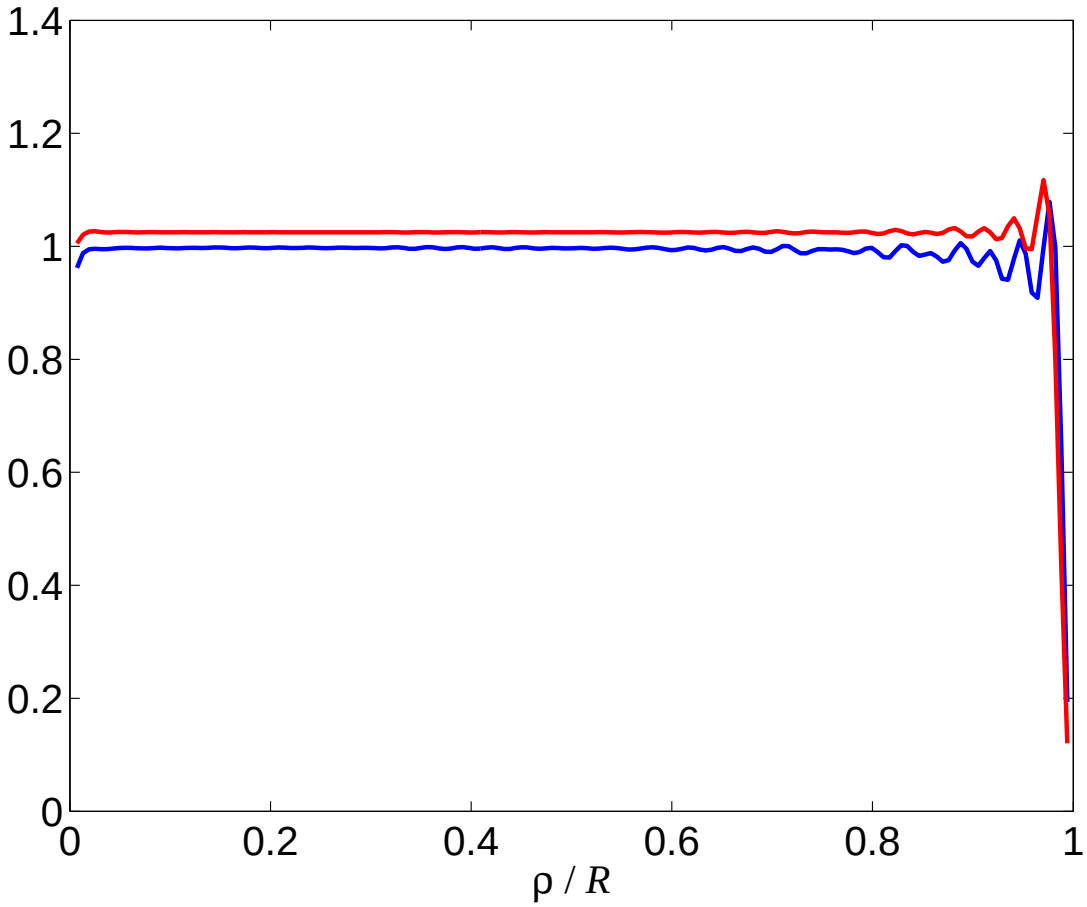

Figure 3.10: The spatial profile of the atomic density (*red line*) and the pairing field (*blue line*) in a cylinder for $k_{\mathrm{F}}|a| = 0.43$, corresponding to about 25 000 atoms per spin state. Both are normalized to their respective bulk values, $n_\sigma = k_{\mathrm{F}}^3/6\pi^2$ and Δ_0.

where

$$N(\mathbf{r}, E) = \sum_\eta \left[|u_\eta(\mathbf{r})|^2 \delta(E - E_\eta) + |v_\eta(\mathbf{r})|^2 \delta(E + E_\eta) \right]. \tag{3.82}$$

When calculating the sum numerically we add a small imaginary component Γ to the quasi-particle energies, thus changing the delta functions $\delta(x)$ into

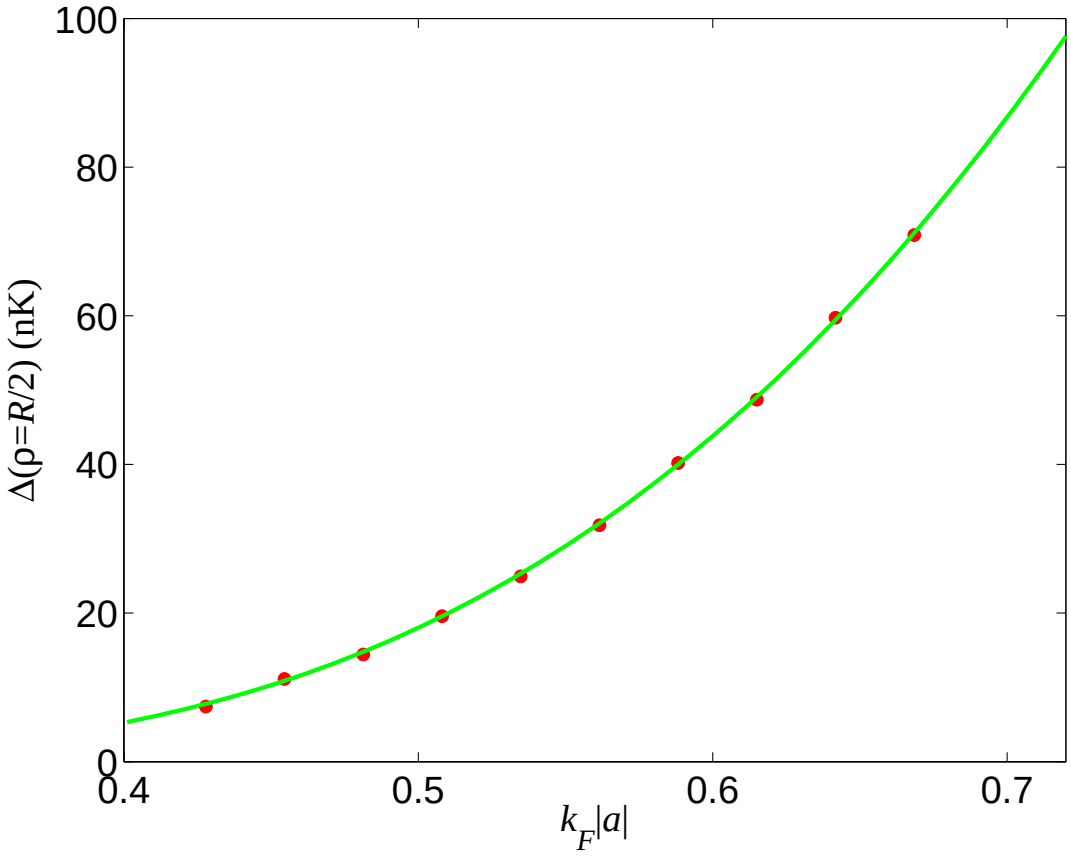

Figure 3.11: Value of delta at $\rho = R/2$ compared with the bulk expression for a cylinder of radius $R = 28.5$ μm.

Lorentzians of width Γ

$$\delta(x) \to \frac{\Gamma/2}{\pi(x^2 + (\Gamma/2)^2)} \quad \text{for} \quad E_\eta \to E_\eta + i\Gamma.$$

The DOS in the superfluid phase is divided by the value in the normal state $N(0)$ (since $\Delta_0/E_\mathrm{F} \ll 1$ we can neglect the variation of the normal state DOS over an energy range on the order of Δ_0, and replace it with its value at the Fermi surface). The superfluid state is characterized by a gap in the single-particle spectrum. There are no excitations with energies between $-\Delta_0$ and $+\Delta_0$. This demonstrates the existence of bound pairs of atoms with binding energy

$2\Delta_0$. To excite a fermion one needs to break a pair, supplying as a minimum the binding energy for the process to be energetically allowed. Since spectral weight is conserved, the opening of a superfluid gap results in the appearance of *coherence peaks* at $\pm\Delta_0$. With increasing $k_{\rm F}|a|$ both the gap and the coherence peaks grow. The oscillations are once again of the Friedel type, and one notices that their (relative) amplitude decreases with increasing $k_{\rm F}$ (with $|a|$ held fixed), since $N(0) \propto k_{\rm F}$.

The equality between the spectroscopic gap and the pairing field only holds in the weak-coupling limit. In the limit of strong coupling the pairs become tightly bound, localized bosonic molecules with a binding energy $\hbar^2/m_a a^2$. The superfluid phase transition occurs when phase coherence is established between the pairs, leading to a BEC of molecules. But the energy scale for pair formation is higher than that for pair condensation, and hence there is a region in the phase diagram, where pre-formed phase incoherent pairs exist. Since the bound pairs result in a single-particle gap equal to their binding energy, this is referred to as the *pseudo-gap* to clarify that it opens up at temperatures above the superfluid transition temperature [81, 114].

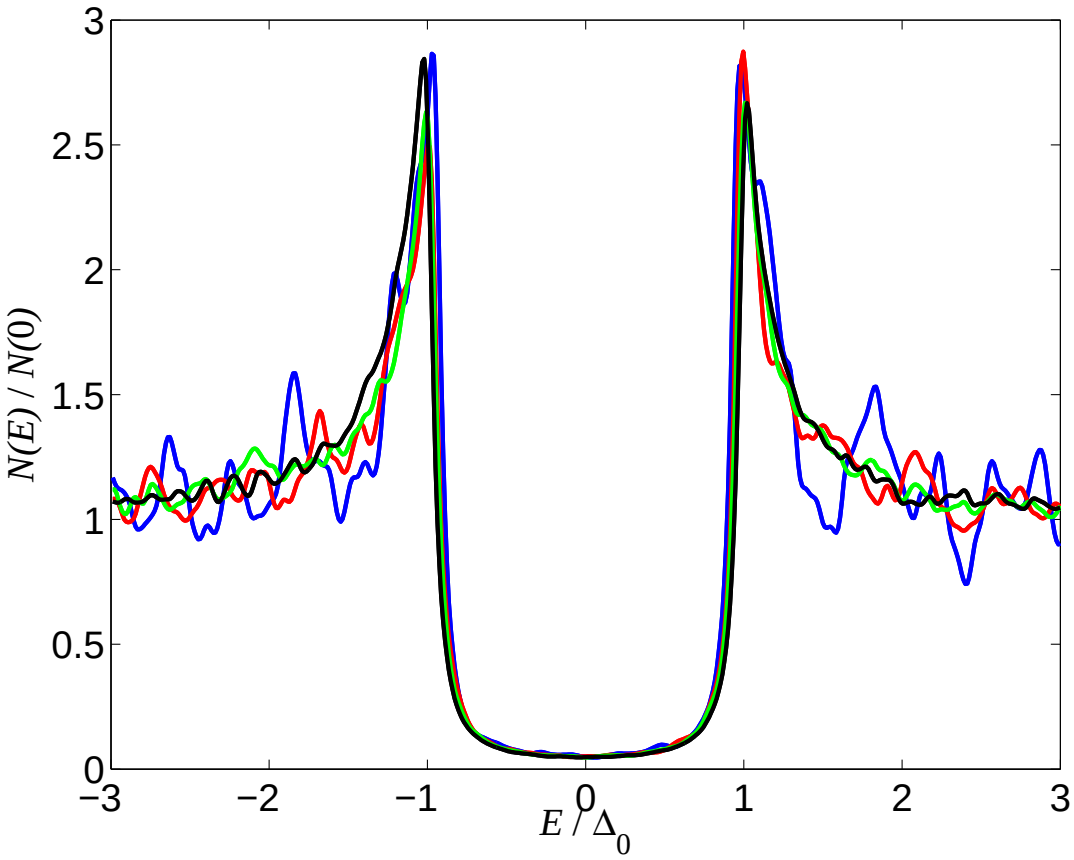

Figure 3.12: Density of states of a superfluid Fermi gas in a cylinder normalized to the normal state value $N(0)$. The gap and the coherence peaks at $E = \Delta_0$ are clearly visible. The energy delta functions were approximated by Lorentzians of width $\Gamma = 0.1\Delta_0$. The $k_{\mathrm{F}}|a|$ values are 0.43 (*blue*), 0.48 (*red*), 0.53 (*green*), and 0.59 (*black*).

Chapter 4

Superfluidity

> The existence of the superfluids and in particular the strange transfer mechanisms they exhibit are direct indications that they represent macroscopic systems for which the classical theory is incompetent and that presumably quantum mechanics is relevant to their constitution *as a whole*
>
> Fritz London in [115].

In the preceding chapter we derived the theory of a Fermi gas with pairing between particles. This chapter is devoted to showing how superfluidity arises in such a system. The strategy is to analyze superfluidity in the language of phase transitions, leading up to a definition and a direct calculation of the superfluid density of an inhomogeneous Fermi gas.

For a Fermi superfluid the velocity field associated with superflow is *defined* in terms of the gradient of the phase of the pairing field [14]. Writing $\Delta(\mathbf{r}) = |\Delta(\mathbf{r})|e^{i\theta(\mathbf{r})}$ we have

$$\mathbf{v}_s(\mathbf{r}) = \frac{\hbar}{2m_a}\nabla\theta(\mathbf{r}), \tag{4.1}$$

where the effective mass of $2m_a$ (compared with the equivalent definition for a superfluid Bose gas) reflects the fact that the atoms are joined in Cooper pairs, which are the fundamental entities responsible for the phase coherence of the system. One of the astounding consequences of the theory is that it is possible to have relative flow of the superfluid with respect to the walls of the container in *equilibrium* (even if it is inherently meta-stable, as we shall discuss below). Hence, we must interpret $\mathbf{v}_s$ (or equivalently $\theta(\mathbf{r})$) as an additional thermodynamic variable of a superfluid system [14, 116].

Since the dynamics of superfluid flow by virtue of (4.1) is radically different than that of a "normal" fluid, it has proven useful to describe the hydrodynamics of superfluids in terms of two interpenetrating liquids, the superfluid and the normal component, each with its own associated mass density distribution ρ_s and ρ_n, and velocity fields $\mathbf{v}_s$ and $\mathbf{v}_n$ [8, 10, 117]. This *two-fluid* model has proven to be tremendously successful in characterizing the hydrodynamics of liquid helium, and to some extend it has been applied to superconductors as well [9].

Superconductivity can be understood as superfluidity of electron pairs [55, 118]. The effect of the electric charge of the carriers is to modify the collective mode spectrum (the Bogoliubov-Anderson phonon becomes a plasmon mode, and is shifted to higher energies [71]). Additionally the paths of the particles are bent in the presence of magnetic fields, which acts equivalently to an external rotating perturbation on a neutral system. Aside from these few distinctions the underlying physics of superconductors is essentially identical to that of a neutral Fermi superfluid.

4.1 Macroscopic Rigidity From Microscopic Order

Phase transitions mark radical changes in the equilibrium properties of matter happening as one or more control parameters (most commonly the temperature) are changed. Familiar examples are the solidification of water at the freezing point, the change from a paramagnet to a ferromagnet, and the transition of a metal from a conductor with a finite resistivity to a zero resistance superconducting state. It is the purpose of the present section to introduce the concept of macroscopic rigidity, as an emergent property of matter that has undergone a phase transition. This concept can be thought of as the generalization of the rigidity of a solid against sheer stress deformations to a wider class of phase transitions. We wish to demonstrate how it arises from a microscopic ordering in the many-body system.

4.1.1 Broken Symmetry: The Birth of Order

In very general terms a phase transition is characterized by the transition of a many-body system from a disordered (high entropy) phase at high temperatures to a low temperature phase with long-ranged order (LRO) and correspondingly lower entropy. The transition occurs at a critical temperature T_c, the transition temperature. The ordered phase is distinguished from the disordered one by the non-vanishing thermal averages $\langle \hat{O} \rangle$ of operators $\hat{O}$, which are *not* invariant under the full symmetry group $\mathcal{G}$ of the Hamiltonian. The symmetry group of $\hat{H}$ is the group of transformations

$$\mathcal{U}^\dagger \hat{H} \mathcal{U} = \hat{H}, \tag{4.2}$$

which leave the Hamiltonian unchanged. We can represent any transformation by a unitary symmetry operator

$$\mathcal{U} = e^{-i\hat{G}\varepsilon/\hbar}, \tag{4.3}$$

where $\hat{G}$ is the Hermitian generator of the symmetry operation, and ε is a generalized displacement. An example is the rotation operator, where the generator is the projection of the angular momentum upon the rotation axis, and ε then represents the angle through which the system is rotated. The invariance of $\hat{H}$ under the transformation $\mathcal{U}$ is equivalent to $\hat{G}$ commuting with the Hamiltonian, $[\hat{G}, \hat{H}] = 0$, as can be seen from the Baker-Hausdorff lemma

$$e^{i\hat{G}\varepsilon/\hbar}\hat{O}e^{-i\hat{G}\varepsilon/\hbar} = \hat{O} + \frac{i\varepsilon}{\hbar}[\hat{G}, \hat{O}] + \frac{1}{2!}\left(\frac{i\varepsilon}{\hbar}\right)^2 [\hat{G}, [\hat{G}, \hat{O}]] + \cdots. \tag{4.4}$$

From the Heisenberg equation of motion it is then clear that $\hat{G}$ is a constant of the motion. If an operator $\hat{O}$ is invariant only under a subgroup of $\mathcal{G}$ it implies that there are symmetry operations in $\mathcal{G}$ under which

$$\hat{O}' = \mathcal{U}^\dagger \hat{O} \mathcal{U} = e^{i\varphi}\hat{O} \neq \hat{O}. \tag{4.5}$$

Denoting by $\hat{\rho}$ the density matrix of the system, the thermal average of $\hat{O}$ can be written as

$$\langle \hat{O} \rangle = \mathrm{Tr}[\hat{\rho}\,\hat{O}] = \mathrm{Tr}[\hat{\rho}'\hat{O}'] = \mathrm{Tr}[\hat{\rho}'\hat{O}]e^{i\varphi}. \tag{4.6}$$

Here we have defined the transformed density matrix $\hat{\rho}' = \mathcal{U}^\dagger \hat{\rho} \mathcal{U}$, and used the unitarity of the transformation operator, $\mathcal{U}^\dagger\mathcal{U} = \mathbf{1}$, as well as the cyclic property of the trace. In the ordered phase $\langle \hat{O} \rangle \neq 0$, and the only way to satisfy Eq. (4.6) is to have $\hat{\rho}' \neq \hat{\rho}$, or in other words, $[\hat{G}, \hat{\rho}] \neq 0$. The ordered phase therefore does not poses the full symmetry of the Hamiltonian, it is invariant only under a subgroup of $\mathcal{G}$, and represents a phase of *broken symmetry* [119]. This is to be

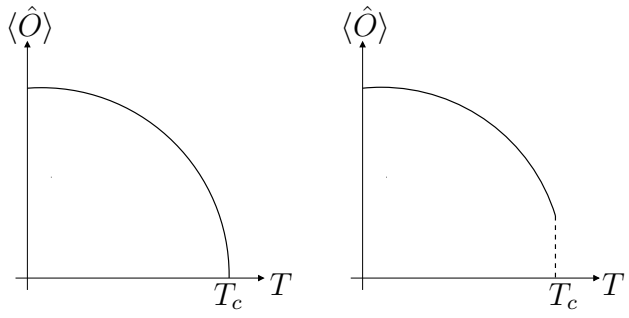

Figure 4.1: Schematic plot of the temperature variation of the order parameter $\langle\hat{O}\rangle$. Below the transition temperature it is finite, while it vanishes above T_c. Depending on the physical system the order parameter can either be continuous at the transition point (*left*), or jump to a finite value (*right*).

contrasted with the disordered phase where the density matrix commutes with all the generators of $\mathcal{G}$, and consequently $\langle\hat{O}\rangle$ vanishes. Since the ordered phase is characterized by a non-vanishing value of this thermal average, $\langle\hat{O}\rangle$ is called the order parameter of the system. A generic sketch showing the variation of the order parameter with temperature is shown in Fig.(4.1). Phase transitions are divided into two distinct classes. If $\langle\hat{O}\rangle$ descends continuously to zero, when T_c is approached from below, the transition is said to be of second order, whereas a first order transition is characterized by a finite jump of the order parameter at the transition point.

In the case of a ferromagnet the broken symmetry is rotation of the spin degrees of freedom, and the order parameter is the magnetization, whereas the transition from a gas to a solid breaks both the translational and rotational symmetry of the Hamiltonian, giving an order parameter which is the set of Fourier components of the density. For a Fermi superfluid the symmetry in

question is the *global* $U(1)$ symmetry associated with gauge transformations:

$$\mathcal{U} = e^{-i\hat{N}\varphi}, \tag{4.7}$$

where $\hat{N}$ is the number operator (3.27). Since the microscopic Hamiltonian (2.14) commutes with $\hat{N}$, it is indeed invariant under $\mathcal{U}$, as are all other physical observables since they are built from an equal number of creation and annihilation operators. The order parameter is given by the anomalous (pair) propagator

$$\Delta(\mathbf{r}) = -\tilde{g}(\mathbf{r})\langle\psi_\uparrow(\mathbf{r})\psi_\downarrow(\mathbf{r})\rangle = |\Delta(\mathbf{r})|e^{i\theta(\mathbf{r})}, \tag{4.8}$$

which is non-zero only below the transition temperature. Here we have defined the regularized interaction strength $\tilde{g}(\mathbf{r})$ as in Section 3.4. Using the commutator rules of the fermion field operators it is easy to prove the relations

$$\begin{aligned} [\hat{N}, \psi_\sigma(\mathbf{r})] &= -\psi_\sigma(\mathbf{r}), \\ [\hat{N}, \psi^\dagger_\sigma(\mathbf{r})] &= \psi^\dagger_\sigma(\mathbf{r}), \end{aligned} \tag{4.9}$$

from which it follows that

$$\begin{aligned} e^{i\hat{N}\varphi}\psi_\sigma(\mathbf{r})e^{-i\hat{N}\varphi} &= \psi_\sigma(\mathbf{r})e^{-i\varphi}, \\ e^{i\hat{N}\varphi}\psi^\dagger_\sigma(\mathbf{r})e^{-i\hat{N}\varphi} &= \psi^\dagger_\sigma(\mathbf{r})e^{i\varphi}. \end{aligned} \tag{4.10}$$

As expected we find that the order parameter is not gauge invariant

$$-\tilde{g}(\mathbf{r})\langle\mathcal{U}^\dagger\psi_\uparrow(\mathbf{r})\psi_\downarrow(\mathbf{r})\mathcal{U}\rangle = -\tilde{g}(\mathbf{r})\langle\psi_\uparrow(\mathbf{r})\psi_\downarrow(\mathbf{r})\rangle e^{-2i\varphi} = |\Delta(\mathbf{r})|e^{i[\theta(\mathbf{r})-2\varphi]}. \tag{4.11}$$

As a consequence of this broken symmetry the superfluid is a state where the particle number is ill defined. We denote it a coherent state in analogy with the generic states that have a non-vanishing average of the annihilation operator [66].

It is important to note that while $\Delta(\mathbf{r})$ is a macroscopic variable (it depends only on a single position coordinate), it encapsulates the underlying microscopic degrees of freedom. The existence of a non-vanishing order parameter with a definite phase $\theta(\mathbf{r})$ constitutes the establishment of a microscopic order in the system, which facilitates a reduced description of the condensed phase. In the following section we will see how this inevitably results in a propensity of the system to resist any changes in its phase.

We remark in passing that the order parameter can vanish in two ways: either the amplitude $|\Delta(\mathbf{r})|$ is zero everywhere, or the average of the phase over the sample vanishes [120, 121]. These situations are physically very different. The first describes the BCS limit, where Cooper pairs become immediately phase coherent as they form, *i.e.* $\Delta(\mathbf{r})$ is quenched uniformly in space as the transition is approached and the pairs dissociate. The second case exemplifies a scenario, where pairs form at a temperature $T^* > T_c$, but the phase fluctuates across the sample. It is only below T_c that the pairs form a macroscopic condensate with a global phase. For $T_c < T < T^*$ phase fluctuations destroy the long-range order in the system [122]. These fluctuations can be understood in terms of long wavelength excitations rotating the phase of the order parameter in the complex plane, as we will see below.

4.1.2 Free Energy Landscape: Rigidity in a Bottle

It is instructive to look at the shape of the free energy surface in the complex order parameter space, mapping the amplitude and phase onto the radial and angular polar coordinates, respectively. From simple heuristic arguments based on an expansion of the free energy $F = \langle \hat{H} \rangle - TS$ in terms of the order parameter

around the transition point, and by symmetry considerations [119], one can infer the general shape as depicted in Fig. 4.2 for a superfluid above and below the transition temperature. In the disordered phase the free energy is shaped like a paraboloid, and it has a single minimum corresponding to a vanishing order parameter. In the ordered phase, however, the free energy has the form of the bottom of a wine bottle as seen on the right in Fig. 4.2. It has a circular ring of minima at a fixed radius $|\Delta(\mathbf{r})|$. Both forms are rotationally invariant, since the Hamiltonian is invariant under gauge transformations as shown above. When the system condenses into the superfluid phase it has to choose one of the degenerate minima, that is to say, it has to adopt a particular global phase, thus breaking the symmetry of the Hamiltonian.

We can classify two distinct types of fluctuations in the system. *Size fluctuations* are modes in which the amplitude of the order parameter deviates from its mean value. As is seen from Fig. 4.2 these have a relatively high energy cost since they "climb" the hill of the free energy landscape. By an intuitive argument we can estimate the typical spatial scale ξ of these fluctuations: If the order parameter is suppressed over a spatial region of size ξ this results in a kinetic energy per particle of order $\hbar^2/2m_a\xi^2$. Equating this with the loss in condensation energy per particle $3\Delta_0^2/4\mu$, where Δ_0 is the bulk value of the order parameter, we find that around a point-like disturbance the order parameter will revert to its asymptotic value over a length

$$\xi \sim \frac{\hbar v_{\mathrm{F}}}{\Delta_0}, \tag{4.12}$$

which we recognize as essentially the BCS coherence length ($\xi_{\mathrm{BCS}} = \hbar v_{\mathrm{F}}/\pi\Delta_0$). Here v_{F} is the Fermi velocity $v_{\mathrm{F}} = \hbar k_{\mathrm{F}}/m_a$. The other category of excitations are *phase fluctuations*. These come in two flavors. The first is spatially uniform

changes in θ corresponding to a rotation from one minimum into another. This leaves the energy unchanged, as discussed above. If the fluctuation is spatially non-uniform, it will, however, be associated with a change in the free energy by an amount depending on the gradient of the phase variation through the system

$$F_{\rm phase} = \frac{1}{2}\int d^3r\, \Upsilon(\mathbf{r}, T, \mu)[\nabla\theta(\mathbf{r})]^2. \tag{4.13}$$

The quantity Υ, which in the general case will be a function of position, temperature and chemical potential, is called the helicity modulus or phase stiffness [123]. It will be calculated from microscopic considerations in Section 4.3. We can now understand how the appearance of a microscopic order, in our case a definite global phase of the superfluid order parameter, leads to a macroscopic rigidity: Imposing a twist on the phase costs a finite amount of strain energy, and the system will try to resist such phase variations. In the next section we shall see how this leads to persistent currents, or superfluid flow.

We close this section by commenting on the nature of the low energy excitations. Since only the phase gradient contributes to the excitation energy, phase fluctuations become zero energy modes in the long-wavelength limit. Such modes are often called soft modes. A general theorem due to Goldstone states that for each broken continuous symmetry there is a zero frequency mode at $\mathbf{q} \to 0$ [26, 72]. In a superfluid the Goldstone excitations are phonons, propagating at the speed of sound, which for the Fermi system is $c = v_{\rm F}/\sqrt{3}$ [27].

4.1.3 Quantization of Circulation

First discussed by London in his classic treatise on superfluids [115] the concept of flux quantization is now counted among the defining properties of supercon-

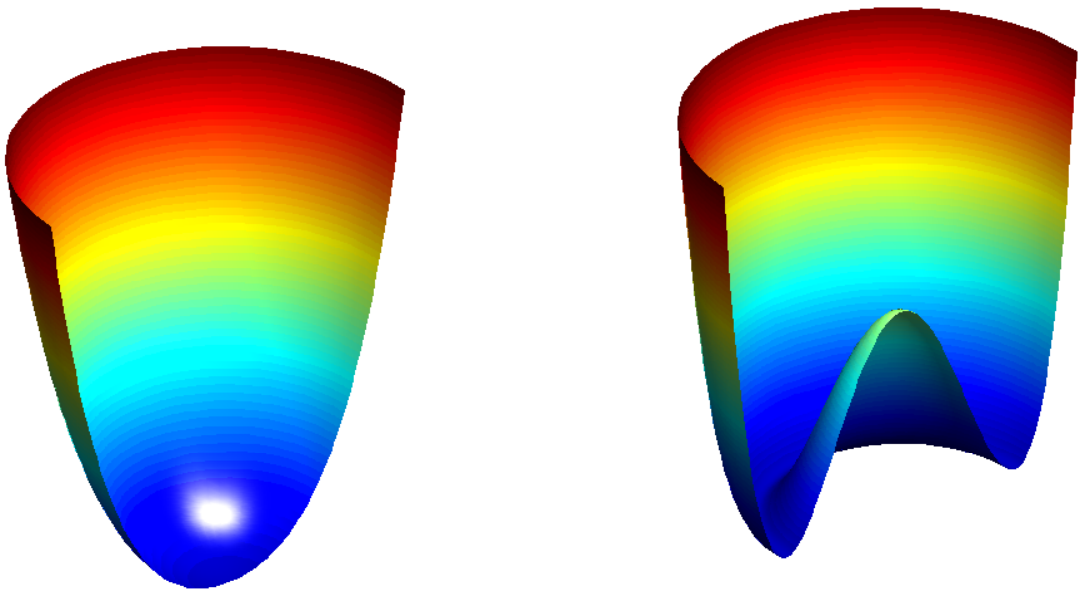

Figure 4.2: Schematic plot of the free energy surface as a function of the complex superfluid order parameter. The amplitude of $\Delta(\mathbf{r})$ is represented as the radial coordinate, while the phase is given by the azimuthal angle. In the disordered phase (*left*) the free energy is minimized when the order parameter vanishes. The ordered phase (*right*) has a degenerate, infinite set of minima at a fixed amplitude of $\Delta(\mathbf{r})$, but with varying phases.

ductivity, thanks in part to four remarkable papers appearing back-to-back in Physical Review Letters [124, 125, 126, 127]. For a neutral Fermi system the natural counterpart is the quantization of circulation around a closed loop, which we shall now discuss. The circulation Γ is given by the line integral of the superfluid velocity around a closed loop C lying entirely within the superfluid

$$\Gamma = \oint_C d\mathbf{l} \cdot \mathbf{v}_s = \frac{\hbar}{2m_a} \oint_C d\mathbf{l} \cdot \nabla\theta(\mathbf{r}). \tag{4.14}$$

Since the order parameter can be thought of as a macroscopic wavefunction it follows that it must necessarily be single-valued. Hence the phase must return

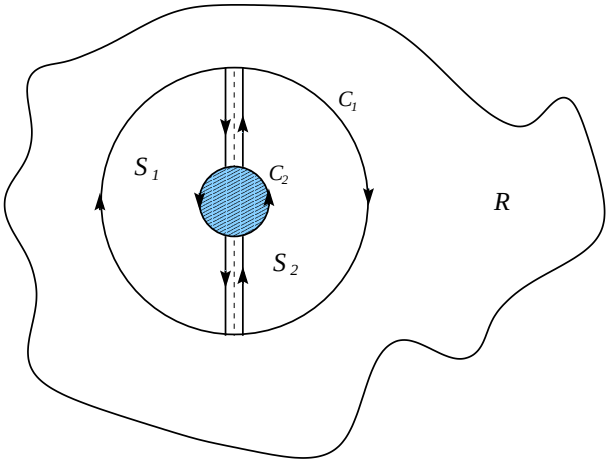

Figure 4.3: Schematic of a superfluid region R. If the hatched region is superfluid R is simply connected, and the circulation around C_1 vanishes. If the hatched region is in the normal phase R is multibly connected, and the gas can sustain a finite circulation (see text).

to the same value modulo 2π when going around the loop. This is exactly the quantization condition on the circulation

$$\Gamma = \kappa \frac{h}{2m_a} = \kappa\Gamma_0, \tag{4.15}$$

with $\kappa \in \mathbb{Z}$. While (4.14) is reminiscent of the Bohr-Sommerfeld quantization condition the pairing concept is needed to correctly predict the exact magnitude of Γ_0, the fundamental quantum of circulation for a superfluid Fermi gas, *cf.* [115]. At $h/2m_a$ it is half the value for a condensed Bose liquid. We stress that the quantization is a topological effect owing to the quantum mechanical nature of the macroscopic system. It is easy to see that a finite circulation about some point in the gas corresponds to a singularity in the order parameter phase at that point. If the superfluid region is simply connected one finds as a corollary to the quantization of circulation that only $\kappa = 0$ is allowed, *i.e.* no current can

flow around any closed loop inside the superfluid. The only currents allowed to flow are those that pass through the superfluid gas. To see this we consider as in Fig. 4.3 two concentric loops C_1 and C_2 lying entirely within a superfluid region R. From Stokes' theorem [128] we know that the surface integral of $\nabla \times \mathbf{v}_s$ over the area enclosed by the loops, which is the sum of the integrals over the surfaces S_1 and S_2, can be written as

$$\int_{S_1} d\mathbf{S} \cdot \nabla \times \mathbf{v}_s + \int_{S_2} d\mathbf{S} \cdot \nabla \times \mathbf{v}_s = \oint_{C_1} d\mathbf{l} \cdot \mathbf{v}_s + \oint_{C_2} d\mathbf{l} \cdot \mathbf{v}_s, \tag{4.16}$$

since the line integrals along the vertical dashed lines are equal and opposite. But $\nabla \times \mathbf{v}_s = 0$ everywhere inside the superfluid, and we therefore find that

$$\oint_{C_1} d\mathbf{l} \cdot \mathbf{v}_s + \oint_{C_2} d\mathbf{l} \cdot \mathbf{v}_s = 0. \tag{4.17}$$

If R is simply connected we can take the circumference of C_2 to zero, which proves that the circulation has to vanish for any closed path C_1. However, for a multiply connected region if both loops are enclosing a region of space where superfluidity is suppressed, and where the order parameter correspondingly vanishes, C_2 can not be made arbitrarily small, and the gas can sustain a finite circulation around the hole. One way to make a multiply connected superfluid is by enclosing the gas in an annulus, but a more interesting way of setting up rotational currents is if the gas is penetrated by vortex lines on which the order parameter is suppressed. A vortex is thus a topological defect in the order parameter field. From the discussion in the previous section we know that there is a finite energy cost associated with a configuration where the order parameter phase is not a constant in space. Accordingly the vortex represents an excited state of the system, and can only be created when the superfluid is rotated at a frequency, which exceeds a critical value Ω_c. If the rotation frequency is smaller than Ω_c the superfluid

remains in a state of zero angular momentum, while the normal component undergoes solid body rotation. As angular momentum is conserved, the rotation frequency of a rotating cylinder *increases* when it is cooled below the transition temperature, since only the normal component can participate in the rotation, effectively decreasing the moment of inertia. This rotational equivalent of the Meissner effect in superconductors was first demonstrated in liquid helium by Hess and Fairbank [129].

Each vortex line is characterized by the number of circulation quanta it carries, κ. This is known as the strength of the vortex or the winding number, as it signifies how many times the phase of the order parameter goes through 2π when the vortex line is circled once. Although the vortex is an excitation in the system it is extraordinarily stable owing to its topology. It is impossible to continuously distort the phase of the order parameter so as to remove the mathematical singularity in the phase on the vortex line. This *topological stability* results in an energy barrier making transitions from the current carrying state to the ground state where the phase is uniform highly unlikely [119, 130]. The reason for this is to be found in the phase coherence of the Fermi superfluid. It is not possible to bring the flow to a halt by changing the orbital states of the particles one by one. Only if the state of every particle is changed simultaneously can the gas be brought to rest. This results in an energy barrier, the height of which scales with the size of the system. Hence for a macroscopic system the time for quantized currents to decay through thermal or quantum fluctuations can become longer than the lifetime of the universe, and we talk about *persistent currents* or *superflow*.

Finally, we mention the work by Byers and Yang on superconductors [125],

and by Garrison *et al.* on superfluid helium [131], which derives the quantization of circulation (or magnetic flux for superconductor) in a way which differs slightly from the present discussion. On very general grounds they show from the irrotational character of superfluid flow (Meissner effect for superconductor) that the free energy is a periodic function of the circulation with local minima at integer multiples of the circulation quantum. Hence we should think of the quantization condition on the circulation in the sense of a condition on thermal stability. Non-quantized values of the circulation can occur, but these correspond to non-equilibrium states, and restoring currents will flow to return the system to an equilibrium state with an integer number of circulation quanta.

4.2 Local Superfluidity

Having discussed the *global* origin of superfluidity we now follow a slight intellectual sidetrack and focus on the origin of dissipationless flow in the system from a *local* perspective. Imagine a macroscopic object of mass M moving through a stationary superfluid at a velocity $\mathbf{v}$. The motion of the object through the gas is a local disturbance, which can potentially excite quasi-particles, and thus cause dissipation (alternatively, one can imagine a superfluid flowing at a uniform velocity in a hollow cylinder; in that case interaction with the walls is a source of friction in a boundary layer). Denoting by $\mathbf{P}$ the momentum of the moving object, and letting E be its energy we have

$$\mathbf{P} = M\mathbf{v}, \tag{4.18}$$

$$E = \frac{1}{2}M\mathbf{v}^2. \tag{4.19}$$

In case a quasi-particle with momentum $\mathbf{q}$ and energy $\epsilon(\mathbf{q})$ is excited the object will lose kinetic energy, and its new velocity will be determined by momentum conservation:

$$\mathbf{v}' = \mathbf{v} - \frac{\mathbf{q}}{M}, \tag{4.20}$$

resulting in a changed energy

$$E' = \frac{1}{2}\, M\mathbf{v}'^2 = E - \mathbf{q}\cdot\mathbf{v} + \frac{\mathbf{q}^2}{2M}. \tag{4.21}$$

The recoil energy $\mathbf{q}^2/2M$ can be safely neglected provided the mass M is large. However, due to energy conservation we must also have that

$$E' = E - \epsilon(\mathbf{q}). \tag{4.22}$$

Leading to the condition $\epsilon(\mathbf{q}) = \mathbf{q}\cdot\mathbf{v}$. From the our discussion of the paired state of the Fermi gas in Chapter 3 we know that there is a minimum energy associated with the creation of single-particle excitations, Δ_0. Hence quasi-particles can only be excited with energies $\epsilon(\mathbf{q}) \geq \Delta_0$. On the other hand the largest possible value of $\mathbf{q}\cdot\mathbf{v}$ is vq, which occurs when the momentum of the quasi-particle is aligned with the velocity of the object. Hence we conclude, that no excitations can be created by objects moving at speeds below a critical velocity

$$v_c = \frac{\Delta_0}{q}. \tag{4.23}$$

This is commonly referred to as the Landau criteria for superfluidity. While we have assumed a homogeneous system a similar condition can be derived locally if the pairing function varies in space. We note that the presence of an energy gap in the system is not a necessary condition for superfluidity. A phonon branch in the spctrum with linear dispersion also gives rise to a critical velocity, which will then equal the speed of sound. In reality the critical velocity is found to

be somewhat lower than the estimate given above, since the mechanism for the creation of low-energy excitations is the nucleation of vortex rings [132].

4.3 Microscopic Definition of Superfluid Density

Suppose that we were able to impose a spatial variation on the phase of the order parameter. Since this would correspond to a state with a finite superfluid velocity, it is clear that such an operation will impart kinetic energy to the gas. Denoting by Θ the accumulated phase twist over the length of the system, this kinetic energy of superflow, T_s, is given by the difference in ground state free energy for a twisted and non-twisted system

$$T_s = F_\Theta - F_0. \tag{4.24}$$

Here we implicitly assume that the twist angle is small. Otherwise we could not attribute the energy change entirely to the kinetic energy associated with the superfluid flow; there would also be a contribution due the the deformation of the amplitude of the order parameter. Additionally, for a sufficiently large phase twist T_s would exceed the gap in the non-twisted energy spectrum between the ground and first excited state. This would correspond to the generation of vortex rings, and occurs when $v_s = |\mathbf{v}_s|$ is larger than the critical velocity [132]. It will become clear below that the limit $\Theta \to 0$ is preferable for other reasons.

We take the phase twist to be arbitrarily along the $\hat{e}_x$ direction, where the system is taken to be periodic with a length L. Here x denotes a generic axis, not necessarily a cartesian coordinate (strictly speaking we do not need to require

periodicity. We could instead work with a linear system of length L, in which case the phase twist would correspond to the boundary conditions at the two ends being different). The many-body wavefunction of the untwisted system must obey periodic boundary conditions, or it would otherwise violate the single-valuedness criteria

$$\Psi^{(0)}(x_1, \ldots, x_i + L, \ldots, x_N) = \Psi^{(0)}(x_1, \ldots, x_i, \ldots, x_N). \tag{4.25}$$

The phase twist is accomplished by imposing twisted boundary conditions on Ψ [123, 133, 134, 135]

$$\Psi^{(\Theta)}(x_1, \ldots, x_i + L, \ldots, x_N) = e^{i\Theta}\Psi^{(\Theta)}(x_1, \ldots, x_i, \ldots, x_N). \tag{4.26}$$

The untwisted wavefunction is transformed into the twisted one under the action of a unitary transformation

$$\mathcal{U}_\Theta = \exp\left(i\sum_{i=1}^{N}\chi(\mathbf{r}_i)\right), \tag{4.27}$$

where χ is a scalar function, such that when integrated around a closed loop

$$\Delta\chi = \oint dx\, \nabla_x\chi(\mathbf{r}) = \Theta. \tag{4.28}$$

We note that we are imposing a phase variation on the wavefunction only along one spatial direction. In general, Θ can depend parametrically on the position coordinates along the two remaining directions.

We define as $E_\Theta(n)$ the energy eigenvalues of the system when subjected to the twisted boundary conditions. They are determined from

$$\hat{H}|\Psi_n^{(\Theta)}\rangle = E_\Theta(n)|\Psi_n^{(\Theta)}\rangle. \tag{4.29}$$

By acting on both sides with the reverse transformation we obtain

$$\hat{H}_\Theta|\Psi_n^{(0)}\rangle = \mathcal{U}_\Theta^\dagger\hat{H}\mathcal{U}_\Theta|\Psi_n^{(0)}\rangle = E_\Theta(n)|\Psi_n^{(0)}\rangle, \tag{4.30}$$

using the unitarity of $\mathcal{U}_\Theta$, and defining a twisted Hamiltonian $\hat{H}_\Theta$. To find $E_\Theta(n)$ we thus have to diagonalize $\hat{H}_\Theta$ subject to periodic boundary conditions [125, 131, 136]. It is important to caution that the eigenstates of $\hat{H}_\Theta$ will be different from those of the untwisted Hamiltonian. However, as we demonstrate below, the phase twist can be regarded as a perturbation on $\hat{H}$, when the twist angle Θ is small. In the language of gauge transformations the above discussion shows that the twisted boundary conditions are equivalent to a system with periodic boundary conditions threaded by an Aharonov-Bohm flux.

Assuming for the moment a linear phase variation along the $\hat{e}_x$ direction

$$\theta(\mathbf{r}) = \frac{2x\Theta}{L}, \tag{4.31}$$

is imposed on the order parameter (corresponding to a phase of $\exp(ix\Theta/L)$ on the field operators), the kinetic energy due to the superflow is given by

$$T_s = \int d^3r \, \frac{1}{2} m_a n_s(\mathbf{r}) v_s^2 = \int d^3r \, \frac{\hbar^2}{2m_a} \, n_s(\mathbf{r}) \left(\frac{\Theta}{L}\right)^2, \tag{4.32}$$

introducing the superfluid *particle* density $n_s(\mathbf{r})$. This defines the relation between the superfluid fraction $f_s = \int d^3r \, n_s(\mathbf{r})/N$ and the free energy difference $F_\Theta - F_0$

$$f_s = \frac{2m_a L^2}{\hbar^2 N} \frac{F_\Theta - F_0}{\Theta^2}. \tag{4.33}$$

This shows that the superfluid density is related to the phase stiffness of the order parameter, *i.e.* the rigidity of the system under an imposed phase twist. In terms of the helicity modulus the superfluid density is

$$n_s(\mathbf{r}) = \frac{4m_a}{\hbar^2} \Upsilon(\mathbf{r}, T, \mu). \tag{4.34}$$

The twisted Hamiltonian is

$$\hat{H}_\Theta = \hat{H}_0 + \hat{J} - \frac{1}{2}\hat{T}, \tag{4.35}$$

where the two parts of the perturbation are

$$\hat{J} = -\frac{i\hbar^2}{m_a}\sum_\sigma \int d^3r\, \frac{\Theta}{L}\,\psi_\sigma^\dagger(\mathbf{r})\nabla_x\psi_\sigma(\mathbf{r}), \tag{4.36}$$

$$\hat{T} = -\frac{\hbar^2}{m_a}\sum_\sigma \int d^3r\, \left(\frac{\Theta}{L}\right)^2 \psi_\sigma^\dagger(\mathbf{r})\psi_\sigma(\mathbf{r}). \tag{4.37}$$

The two terms are proportional to the current, and number operator of the system, respectively. Below we calculate $F_\Theta - F_0$ using perturbation theory to second order in Θ. Since we are interested in the limit $\Theta \to 0$ the perturbative treatment does not introduce any further approximations, as is evident from (4.33).

The superfluid density as defined here is equivalent to the so-called winding number which is used in the Monte Carlo community [135, 137]. It is also known as the Drude weight or charge stiffness in solid state physics, where it describes the real part of the DC conductivity [134, 138, 139]. We point out an important difference between the continuum definition we are employing and definitions of the superfluid density/Drude weight for a discrete Hubbard chain [134, 140, 141, 142, 143]. In the latter case the calculation of n_s is concerned only with the accumulation of phase differences *between* neighboring lattice sites. Any superfluid oscillations of the gas *within* the individual sites are neglected. On the other hand, the continuum model counts all contributions to the superfluid flow, whether they arise from inter-site flow or intra-site motion of the superfluid. Accordingly, the two definitions of n_s differ, which is most evident at zero temperature, where the continuum model predicts that the entire gas is superfluid regardless of the details of the external potential (see below). This is in contrast with the the discrete model in which the superfluid fraction is suppressed below one even at $T = 0$ whenever the translational symmetry of the

system is broken [142].

4.4 Perturbation Theory for Strain Energy

At zero temperature the perturbation expansion of the ground state energy of a single-particle quantum system is the well-known Rayleigh-Schödinger perturbation series [144]:

$$E_0 = E_0^{(0)} + \langle\phi_0|\mathcal{H}'|\phi_0\rangle + \sum_{n\neq 0} \frac{|\langle\phi_0|\mathcal{H}'|\phi_n\rangle|^2}{E_0^{(0)} - E_n^{(0)}} + \ldots, \tag{4.38}$$

where the unperturbed eigenstates and energies are given by $\mathcal{H}_0\phi_n = E_n^{(0)}\phi_n$. If the perturbation $\mathcal{H}'$ is sufficiently small the series will be convergent. For a general many-body system at a finite temperature the systematic way to develop a perturbation expansion of the energy shift is through the linked cluster (or cumulant) expansion. This gives a diagrammatic series for the grand canonical potential Ω defined as

$$e^{-\beta\Omega} = \mathrm{Tr}[e^{-\beta(\hat{H}-\mu\hat{N})}]. \tag{4.39}$$

If the Hamiltonian can be written as a sum of an unperturbed part $\hat{H}_0$ and a (small) perturbation $\hat{H}'$, $\hat{H} = \hat{H}_0 + \hat{H}'$, then the linked cluster expansion states that the shift in grand canonical potential under the perturbation is [46]

$$\Omega = \Omega_0 - \frac{1}{\beta}\sum_{n=1}^{\infty} \frac{(-1/\hbar)^n}{n} \int_0^{\beta\hbar} d\tau_1 \cdots \int_0^{\beta\hbar} d\tau_n \, \langle T_\tau \hat{H}'(\tau_1)\cdots\hat{H}'(\tau_n)\rangle_0 \tag{4.40}$$

where Ω_0 is the grand canonical potential in the absence of the perturbation ($\hat{H}' = 0$). The brackets $\langle\cdots\rangle_0 = \mathrm{Tr}[\exp(-\beta(\hat{H}_0 - \mu\hat{N}))\cdots]$ means the thermodynamic average evaluated in the equilibrium state of the unperturbed system at temperature T. We refer to Appendix C for a brief overview of the finite

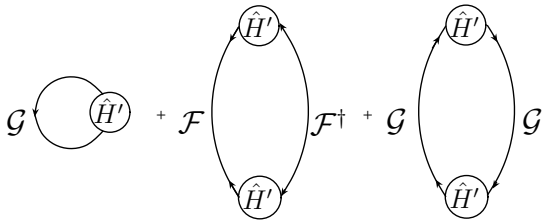

Figure 4.4: Lowest order distinct, connected diagrams contributing to the perturbation expansion of the grand canonical potential. The anomalous diagram (*middle*) is only non-vanishing below the superfluid transition temperature.

temperature many-body formalism. The name linked cluster expansion reflects the fact that the summation is over distinct, connected diagrams only. Since we are interested in the shift in the energy of a superfluid we must include diagrams in which both normal and anomalous propagators can occur. The three lowest order diagrams occurring in the series are shown in Fig. 4.4

We note that since the perturbation commutes with the number operator the states corresponding to Ω and Ω_0 will have the same number of particles. Hence the free energy difference will be exactly equal to the change in grand canonical potential $\Omega - \Omega_0$ as given by the linked cluster expansion. To second order we therefore find that

$$F_\Theta - F_0 = \Delta\Omega^{(1)} + \Delta\Omega^{(2)}. \tag{4.41}$$

If the phase twist is imposed on a state at rest, the average of the current operator vanishes, and only the term $\hat{T}$ in the Hamiltonian contributes in first order perturbation theory. We do get a non-vanishing contribution from $\hat{J}$ in second order, and these are the only two terms we need consider since we are interested only in the limit $\Theta \to 0$; terms of higher order than 2 in Θ will vanish.

We start by evaluating the first order shift (second order in Θ) of the grand

canonical potential:

$$\Delta\Omega^{(1)} = -\frac{1}{\beta\hbar}\frac{\hbar^2}{2m_a}\int_0^{\beta\hbar} d\tau\,\langle T_\tau\,\hat{T}(\tau)\rangle = \frac{\hbar^2}{2m_a}\int d^3r\,\left(\frac{\Theta}{L}\right)^2 n(\mathbf{r}). \tag{4.42}$$

We thus see that to first order the superfluid density is simply the total density of the system. Any depletion of the superfluid, be it due to finite temperature or interactions is hidden in the correction to the free energy from the $\hat{J}$ part of the perturbation. Treating this term in second order perturbation theory we get

$$\Delta\Omega^{(2)} = -\frac{1}{2\beta\hbar^2}\int_0^{\beta\hbar} d\tau_1\int_0^{\beta\hbar} d\tau'\,\langle T_\tau\,\hat{J}(\tau)\hat{J}(\tau')\rangle. \tag{4.43}$$

It is more convenient to write the current operator in a symmetric form using the fact the field operators must vanish at the system boundary; a simple integration by parts yields

$$\int d^3r\,\psi^\dagger_\sigma(\mathbf{r})\nabla\psi_\sigma(\mathbf{r}) = -\frac{1}{2}\int d^3r\,\left[\left(\nabla\psi^\dagger_\sigma(\mathbf{r})\right)\psi_\sigma(\mathbf{r}) - \psi^\dagger_\sigma(\mathbf{r})\nabla\psi_\sigma(\mathbf{r})\right]. \tag{4.44}$$

With this we can write the second order energy shift as

$$\begin{aligned}\Delta\Omega^{(2)} = -\frac{1}{2\beta\hbar^2}\left(\frac{i\hbar^2}{2m_a}\right)^2\sum_\sigma\sum_{\sigma'}\int d^3r\int d^3r'\,\left(\frac{\Theta}{L}\right)^2\int_0^{\beta\hbar}d\tau\int_0^{\beta\hbar}d\tau' \\ \times(\nabla_1-\nabla_2)_x\,(\nabla_{1'}-\nabla_{2'})_{x'}\,\langle T_\tau\,\psi^\dagger_\sigma(2)\psi_\sigma(1)\psi^\dagger_{\sigma'}(2')\psi_{\sigma'}(1')\rangle|_{2'=1'^+,2=1^+},\end{aligned} \tag{4.45}$$

adopting the shorthand notation $1 \equiv (\mathbf{r},\tau)$. To abbreviate our notation further we introduce the function $\mathcal{P}(\mathbf{r}\tau,\mathbf{r}'\tau')$ defined through

$$\Delta\Omega^{(2)} = -\frac{1}{2\beta\hbar^2}\left(\frac{i\hbar^2}{2m_a}\right)^2\int d^3r\int d^3r'\,\left(\frac{\Theta}{L}\right)^2\int_0^{\beta\hbar}d\tau\int_0^{\beta\hbar}d\tau'\,\mathcal{P}(\mathbf{r}\tau,\mathbf{r}'\tau'). \tag{4.46}$$

Using Wick's theorem (Appendix D), and neglecting magnetic terms, $\mathcal{P}$ can be expressed in terms of the single-particle Green's functions of the system:

$$\begin{aligned}\mathcal{P}(\mathbf{r}\tau,\mathbf{r}'\tau') &= (\nabla_1-\nabla_2)_x\,(\nabla_{1'}-\nabla_{2'})_{x'}\Big[4\mathcal{G}(12)\mathcal{G}(1'2') \\ &\quad -2\mathcal{G}(1'2)\mathcal{G}(12') + 2\mathcal{F}(11')\mathcal{F}^\dagger(2'2)\Big]_{2'=1'^+,2=1^+}.\end{aligned} \tag{4.47}$$

The first term does not contribute as it is proportional to $\langle \hat{J}(\mathbf{r})\rangle\langle \hat{J}(\mathbf{r}')\rangle$, which vanishes when the equilibrium state is current-free.

It is convenient to transform $\mathcal{P}$ to the frequency representation, and we thus write

$$\mathcal{P}(\mathbf{r}\tau,\mathbf{r}'\tau') = \frac{1}{\beta\hbar}\sum_{\omega_n} e^{-i\omega_n(\tau-\tau')}\,\mathcal{P}(\mathbf{r},\mathbf{r}';i\omega_n), \tag{4.48}$$

where it is important to note that ω_n is a *bosonic* Matsubara frequency (see Appendix C), as it is the difference between two fermionic frequencies. The Fourier transform is expressed as a sum over fermionic Matsubara frequencies

$$\begin{aligned}\mathcal{P}(\mathbf{r},\mathbf{r}';i\omega_n) &= \frac{2}{\beta\hbar}\sum_{\omega_1}(\nabla_1-\nabla_2)_x\,(\nabla_{1'}-\nabla_{2'})_{x'} \\ &\Big[\mathcal{F}(r_1,r_1';i\omega_n+i\omega_1)\mathcal{F}^\dagger(r_2',r_2;i\omega_1) \\ &-\mathcal{G}(r_1,r_2';i\omega_1+\omega_n)\mathcal{G}(r_1,r_2;i\omega_1)\Big]_{2'=1'^+,2=1^+}. \end{aligned}\tag{4.49}$$

Inserting the expansions of the Green's functions on the quasi-particle basis of the superfluid ground state (Appendix C) we get

$$\begin{aligned}\mathcal{P}(\mathbf{r},\mathbf{r}';i\omega_n) &= \frac{2}{\beta\hbar}\sum_{\omega_1}\sum_{\eta}\sum_{\nu}\Big[\frac{A_{\eta\nu}(\mathbf{r},\mathbf{r}')}{i\omega_1+i\omega_n-E_\eta/\hbar}\,\frac{1}{i\omega_1-E_\nu/\hbar} \\ &+\frac{B_{\eta\nu}(\mathbf{r},\mathbf{r}')}{i\omega_1+i\omega_n-E_\eta/\hbar}\,\frac{1}{i\omega_1+E_\nu/\hbar} \\ &+\frac{C_{\eta\nu}(\mathbf{r},\mathbf{r}')}{i\omega_1+i\omega_n+E_\eta/\hbar}\,\frac{1}{i\omega_1-E_\nu/\hbar} \\ &+\frac{D_{\eta\nu}(\mathbf{r},\mathbf{r}')}{i\omega_1+i\omega_n+E_\eta/\hbar}\,\frac{1}{i\omega_1+E_\nu/\hbar}\Big]. \end{aligned}\tag{4.50}$$

The four functions A, B, C, D are generally very complicated, but for completeness we reproduce them here using a prime to denote the gradient along x of u or v

$$A_{\eta\nu}(\mathbf{r},\mathbf{r}') = u_\eta'(\mathbf{r})v_\eta^{*\prime}(\mathbf{r}')u_\nu^*(\mathbf{r})v_\nu(\mathbf{r}') + u_\eta(\mathbf{r})v_\eta^*(\mathbf{r}')u_\nu^{*\prime}(\mathbf{r})v_\nu'(\mathbf{r}')$$

$$
\begin{aligned}
&-u_\eta(\mathbf{r})v^{*\prime}_\eta(\mathbf{r}')u^{*\prime}_\nu(\mathbf{r})v_\nu(\mathbf{r}') - u'_\eta(\mathbf{r})v^*_\eta(\mathbf{r}')u^*_\nu(\mathbf{r})v'_\nu(\mathbf{r}') \\
&+u'_\eta(\mathbf{r})u^{*\prime}_\eta(\mathbf{r}')u_\nu(\mathbf{r}')u^*_\nu(\mathbf{r}) + u_\eta(\mathbf{r})u^*_\eta(\mathbf{r}')u'_\nu(\mathbf{r}')u^{*\prime}_\nu(\mathbf{r}) \\
&-u'_\eta(\mathbf{r})u^*_\eta(\mathbf{r}')u'_\nu(\mathbf{r}')u^*_\nu(\mathbf{r}) - u_\eta(\mathbf{r})u^{*\prime}_\eta(\mathbf{r}')u_\nu(\mathbf{r}')u^{*\prime}_\nu(\mathbf{r}), \quad (4.51)
\end{aligned}
$$

$$
\begin{aligned}
B_{\eta\nu}(\mathbf{r},\mathbf{r}') &= -u'_\eta(\mathbf{r})v^{*\prime}_\eta(\mathbf{r}')u^*_\nu(\mathbf{r}')v_\nu(\mathbf{r}) - u_\eta(\mathbf{r})v^*_\eta(\mathbf{r}')u^{*\prime}_\nu(\mathbf{r}')v'_\nu(\mathbf{r}) \\
&+u'_\eta(\mathbf{r})v^*_\eta(\mathbf{r}')u^{*\prime}_\nu(\mathbf{r}')v_\nu(\mathbf{r}) + u_\eta(\mathbf{r})v^{*\prime}_\eta(\mathbf{r}')u^*_\nu(\mathbf{r}')v'_\nu(\mathbf{r}) \\
&+u'_\eta(\mathbf{r})u^{*\prime}_\eta(\mathbf{r}')v_\nu(\mathbf{r})v^*_\nu(\mathbf{r}') + u_\eta(\mathbf{r})u^*_\eta(\mathbf{r}')v'_\nu(\mathbf{r})v^{*\prime}_\nu(\mathbf{r}') \\
&-u'_\eta(\mathbf{r})u^*_\eta(\mathbf{r}')v_\nu(\mathbf{r})v^{*\prime}_\nu(\mathbf{r}') - u_\eta(\mathbf{r})u^{*\prime}_\eta(\mathbf{r}')v'_\nu(\mathbf{r})v^*_\nu(\mathbf{r}'), \quad (4.52)
\end{aligned}
$$

$$
\begin{aligned}
C_{\eta\nu}(\mathbf{r},\mathbf{r}') &= -u'_\eta(\mathbf{r}')v^{*\prime}_\eta(\mathbf{r})u^*_\nu(\mathbf{r})v_\nu(\mathbf{r}') - u_\eta(\mathbf{r}')v^*_\eta(\mathbf{r})u^{*\prime}_\nu(\mathbf{r})v'_\nu(\mathbf{r}') \\
&+u'_\eta(\mathbf{r}')v^*_\eta(\mathbf{r})u^{*\prime}_\nu(\mathbf{r})v_\nu(\mathbf{r}') + u_\eta(\mathbf{r}')v^{*\prime}_\eta(\mathbf{r})u^*_\nu(\mathbf{r})v'_\nu(\mathbf{r}') \\
&+v'_\eta(\mathbf{r}')v^{*\prime}_\eta(\mathbf{r})u_\nu(\mathbf{r}')u^*_\nu(\mathbf{r}) + v_\eta(\mathbf{r}')v^*_\eta(\mathbf{r})u'_\nu(\mathbf{r}')u^{*\prime}_\nu(\mathbf{r}) \\
&-v_\eta(\mathbf{r}')v^{*\prime}_\eta(\mathbf{r})u'_\nu(\mathbf{r}')u^*_\nu(\mathbf{r}) - v'_\eta(\mathbf{r}')v^*_\eta(\mathbf{r})u_\nu(\mathbf{r}')u^{*\prime}_\nu(\mathbf{r}), \quad (4.53)
\end{aligned}
$$

$$
\begin{aligned}
D_{\eta\nu}(\mathbf{r},\mathbf{r}') &= u'_\eta(\mathbf{r}')v^{*\prime}_\eta(\mathbf{r})u^*_\nu(\mathbf{r}')v_\nu(\mathbf{r}) + u_\eta(\mathbf{r}')v^*_\eta(\mathbf{r})u^{*\prime}_\nu(\mathbf{r}')v'_\nu(\mathbf{r}) \\
&-u'_\eta(\mathbf{r}')v^*_\eta(\mathbf{r})u^*_\nu(\mathbf{r}')v'_\nu(\mathbf{r}) - u_\eta(\mathbf{r}')v^{*\prime}_\eta(\mathbf{r})u^{*\prime}_\nu(\mathbf{r}')v_\nu(\mathbf{r}) \\
&+v'_\eta(\mathbf{r}')v^{*\prime}_\eta(\mathbf{r})v_\nu(\mathbf{r})v^*_\nu(\mathbf{r}') + v_\eta(\mathbf{r}')v^*_\eta(\mathbf{r})v'_\nu(\mathbf{r})v^{*\prime}_\nu(\mathbf{r}') \\
&-v'_\eta(\mathbf{r}')v^*_\eta(\mathbf{r})v'_\nu(\mathbf{r})v^*_\nu(\mathbf{r}') - v_\eta(\mathbf{r}')v^{*\prime}_\eta(\mathbf{r})v_\nu(\mathbf{r})v^{*\prime}_\nu(\mathbf{r}'). \quad (4.54)
\end{aligned}
$$

The sum over Matsubara frequencies ω_1 is easily performed, and we are left with

$$
\begin{aligned}
\mathcal{P}(\mathbf{r},\mathbf{r}';i\omega_n) &= 2\sum_\eta\sum_\nu \Big[\Big(\frac{A_{\eta\nu}(\mathbf{r},\mathbf{r}')}{E_\eta/\hbar - E_\nu/\hbar - i\omega_n} + \frac{D_{\eta\nu}(\mathbf{r},\mathbf{r}')}{E_\eta/\hbar - E_\nu/\hbar + i\omega_n}\Big) \\
&\times(f(E_\eta) - f(E_\nu)) \\
&- \Big(\frac{B_{\eta\nu}(\mathbf{r},\mathbf{r}')}{E_\eta/\hbar + E_\nu/\hbar - i\omega_n} + \frac{C_{\eta\nu}(\mathbf{r},\mathbf{r}')}{E_\eta/\hbar + E_\nu/\hbar + i\omega_n}\Big)
\end{aligned}
$$

$$\times(1 - f(E_\eta) - f(E_\nu))\Big]. \tag{4.55}$$

Here we have used explicitly that ω_n is a bosonic Matsubara frequency. To get any further in evaluating the second order contribution to the energy shift we must assume a simplifying form for the quasi-particle wavefunctions. As a first example we will focus on the case of a translationally invariant system.

4.5 Homogeneous System

In a spatially uniform gas the quasi-particle amplitudes are plane wave states:

$$\begin{aligned} u_{\mathbf{k}}(\mathbf{r}) &= \frac{1}{\sqrt{V}} u_{\mathbf{k}} e^{i\mathbf{k}\cdot\mathbf{r}}, \\ v_{\mathbf{k}}(\mathbf{r}) &= \frac{1}{\sqrt{V}} v_{\mathbf{k}} e^{i\mathbf{k}\cdot\mathbf{r}}, \end{aligned} \tag{4.56}$$

taking the system volume to be V. The mode functions $u_{\mathbf{k}}$, $v_{\mathbf{k}}$ are the solutions to the BdG equations with a constant pairing field (3.46). The expressions for A, B, C, and D are now simplified:

$$A_{\mathbf{k}\mathbf{k}'}(\mathbf{r},\mathbf{r}') = \frac{(k_x + k'_x)^2}{V^2} u_{\mathbf{k}} u^*_{\mathbf{k}'} \left[v^*_{\mathbf{k}} v_{\mathbf{k}'} + u^*_{\mathbf{k}} u_{\mathbf{k}'}\right] e^{i(\mathbf{k}-\mathbf{k}')\cdot(\mathbf{r}-\mathbf{r}')}, \tag{4.57}$$

$$B_{\mathbf{k}\mathbf{k}'}(\mathbf{r},\mathbf{r}') = -\frac{(k_x - k'_x)^2}{V^2} u_{\mathbf{k}} v_{\mathbf{k}'} \left[v^*_{\mathbf{k}} u^*_{\mathbf{k}'} - u^*_{\mathbf{k}} v^*_{\mathbf{k}'}\right] e^{i(\mathbf{k}+\mathbf{k}')\cdot(\mathbf{r}-\mathbf{r}')}, \tag{4.58}$$

$$C_{\mathbf{k}\mathbf{k}'}(\mathbf{r},\mathbf{r}') = -\frac{(k_x - k'_x)^2}{V^2} u^*_{\mathbf{k}'} v^*_{\mathbf{k}} \left[u_{\mathbf{k}} v_{\mathbf{k}'} - v_{\mathbf{k}} u_{\mathbf{k}'}\right] e^{-i(\mathbf{k}+\mathbf{k}')\cdot(\mathbf{r}-\mathbf{r}')}, \tag{4.59}$$

$$D_{\mathbf{k}\mathbf{k}'}(\mathbf{r},\mathbf{r}') = \frac{(k_x + k'_x)^2}{V^2} v^*_{\mathbf{k}} v_{\mathbf{k}'} \left[u_{\mathbf{k}} u^*_{\mathbf{k}'} + v_{\mathbf{k}} v^*_{\mathbf{k}'}\right] e^{-i(\mathbf{k}-\mathbf{k}')\cdot(\mathbf{r}-\mathbf{r}')}. \tag{4.60}$$

Integrating out the spatial part of $\mathcal{P}$ results in

$$\begin{aligned} \int d^3r \int d^3r' \, \mathcal{P}(\mathbf{r},\mathbf{r}';i\omega_n) = 2 \sum_{\mathbf{k}} \sum_{\mathbf{k}'} (k_x + k'_x)^2 \left(f(E_{\mathbf{k}}) - f(E_{\mathbf{k}'})\right) \delta_{\mathbf{k}\mathbf{k}'} \\ \times \left(\frac{|u_{\mathbf{k}}|^2}{E_{\mathbf{k}}/\hbar - E_{\mathbf{k}'}/\hbar - i\omega_n} + \frac{|v_{\mathbf{k}}|^2}{E_{\mathbf{k}}/\hbar - E_{\mathbf{k}'}/\hbar + i\omega_n} \right), \end{aligned} \tag{4.61}$$

as can be seen by using the identity $\int d^3r \exp(\mathbf{q}\cdot\mathbf{r})/V = \delta_{\mathbf{q}0}$, and the symmetry of $u_{\mathbf{k}}$ and $v_{\mathbf{k}}$ under $\mathbf{k} \to -\mathbf{k}$, as well as the normalization condition $|u_{\mathbf{k}}|^2 + |v_{\mathbf{k}}|^2 = 1$. We are now in a position to put together all the pieces, and finalize the expression for the second order energy shift

$$\Delta\Omega^{(2)} = \frac{\hbar}{4m_a^2\beta^2}\left(\frac{\Theta}{L}\right)^2 \int_0^{\beta\hbar} d\tau \int_0^{\beta\hbar} d\tau' \sum_{\mathbf{k}} \sum_{\mathbf{k}'} \sum_{\omega_n} e^{-i\omega_n(\tau-\tau')}$$
$$\times \left(f(E_{\mathbf{k}}) - f(E_{\mathbf{k}'})\right)\left(\frac{|u_{\mathbf{k}}|^2(k_x+k_x')^2}{E_{\mathbf{k}}/\hbar - E_{\mathbf{k}'}/\hbar - i\omega_n} + \frac{|v_{\mathbf{k}}|^2(k_x+k_x')^2}{E_{\mathbf{k}}/\hbar - E_{\mathbf{k}'}/\hbar + i\omega_n}\right). \quad (4.62)$$

The integration over τ' yields $\beta\hbar\delta_{\omega_n 0}$, and the τ integral gives simply an extra factor of $\beta\hbar$. Hence

$$\Delta\Omega^{(2)} = 4\left(\frac{\hbar^2}{2m_a}\right)^2\left(\frac{\Theta}{L}\right)^2 \sum_{\mathbf{k}} k_x^2 \lim_{\mathbf{k}'\to\mathbf{k}}\left(\frac{f(E_{\mathbf{k}}) - f(E_{\mathbf{k}'})}{E_{\mathbf{k}} - E_{\mathbf{k}'}}\right). \quad (4.63)$$

For a sufficiently large system the sum can be converted into an integral, $\sum_{\mathbf{k}} \to (V/2\pi)\int d^3k$, and the limit can be taken by means of l'Hôpital's rule

$$\Delta\Omega^{(2)} = \frac{4}{3}\left(\frac{\hbar^2}{2m_a}\right)^2\left(\frac{\Theta}{L}\right)^2 \frac{V}{2\pi^2}\int_0^{\infty} dk\, k^4 \frac{\partial f(E_{\mathbf{k}})}{\partial E_{\mathbf{k}}}, \quad (4.64)$$

where the factor of $1/3$ is from the isotropy of space. Combining this result with (4.33), (4.41), and (4.42) we find for the superfluid density of a homogeneous Fermi gas

$$n_s = n + \frac{\hbar^2}{3m_a\pi^2}\int_0^{\infty} dk\, k^4 \frac{\partial f(E_{\mathbf{k}})}{\partial E_{\mathbf{k}}}, \quad (4.65)$$

where $n = n_\uparrow + n_\downarrow$ is the total density. This is exactly the standard result as obtained from a linear response calculation [27], and we note that the integral is always negative and vanishes at $T = 0$, ensuring that the superfluid density is smaller than or equal to the particle density, as one would expect.

4.6 Cylindrically Symmetric System

Encouraged by the demonstration of equivalence between the phase twist method and the standard linear response analysis in the trivial case of a homogeneous system, we now move to tackle the more interesting situation where the superfluid is not spatially uniform, for example as a result of confinement. However, we assume that there exists an axis of symmetry, such that rotations about this leave the system unchanged. In this case the natural set of coordinates are (ρ, ϕ, z), where ρ measures the perpendicular distance from the symmetry axis, z is the axial coordinate, and ϕ is the azimuthal angle around $\hat{e}_z$. While the radial and longitudinal variation of the quasi-particle wavefunctions are in general non-trivial, and have to be obtained from a self-consistent solution of the BdG equations, the angular part is simplified by the states being eigenstates of the axial angular momentum operator L_z with eigenvalues $\hbar m$, where $m \in \mathbb{Z}$. Hence we write the solutions of the BdG equations in the form

$$u_\eta(\mathbf{r}) = u_\eta(\rho, z)\,\frac{e^{im\phi}}{\sqrt{2\pi}}, \tag{4.66}$$

$$v_\eta(\mathbf{r}) = v_\eta(\rho, z)\,\frac{e^{im\phi}}{\sqrt{2\pi}}. \tag{4.67}$$

An important question is how to impose the phase twist on the system in a closed geometry. We envision applying a rotation of frequency Ω to the gas. Practically, this can be achieved in one of two ways: the first is by rotating the confining potential in an analog of the rotating bucket experiment (though this requires a small anisotropy, which breaks the symmetry, since a perfectly symmetric rotating potential is equivalent to a stationary one). The second way is to "stir" the cloud with a rotating force pushing the atoms, *e.g* a blue detuned laser beam. Assuming that the rotation is sufficiently slow that vortices do not

nucleate, the superfluid will remain stationary in the laboratory frame, such that the moment of inertia is entirely due to the normal component. Going to the rotating frame, where the potential is stationary, the situation is reversed, and the normal fluid is at rest with the walls, while the superfluid undergoes solid body rotation with a velocity

$$\mathbf{v}_s^{\mathrm{rot}}(\rho) = \Omega\rho\hat{e}_\phi, \tag{4.68}$$

where the superscript indicates that this is the velocity of superfluid flow as measured in the rotating frame. This implies that the phase twist operator for a fixed distance ρ from the rotation axis is

$$\mathcal{U}_\Theta = \exp\left(i\sum_{i=1}^{N}\frac{m_a\rho^2\Omega\phi_i}{\hbar}\right) = \exp\left(i\sum_{i=1}^{N}\frac{\Theta(\rho)\phi_i}{2\pi}\right), \tag{4.69}$$

which defines a (ρ dependent) phase twist angle $\Theta(\rho) = 2\pi m_a\rho^2\Omega/\hbar$. Since the system is now periodic, the length L is replaced by the period 2π of the angular degree of freedom. In terms of Θ the velocity of the superfluid is $\mathbf{v}_s = \hbar\Theta\hat{e}_\phi/2\pi m_a\rho$. Hence the change in kinetic energy due to the phase twist is in this case

$$T_s = \int d^3r\frac{1}{2}m_a n_s(\mathbf{r})\Omega^2\rho^2. \tag{4.70}$$

The superfluid density at any given point in space can thus be found by equating the integrand in (4.70) with that of the perturbation expression for the free energy difference $F_\Theta - F_0$.

Since the system is invariant under rotations about $\hat{e}_z$ the energy density must be independent of ϕ. This means that when finding the transformed Hamiltonian $\hat{H}_\Theta$ we must keep ρ fixed. This is equivalent to dividing the gas up into a series of concentric annuli, and considering the phase twist to be applied to the

wavefunction within each annulus separately. This requires the thickness of the annuli to be small compared to their radius, such that centrifugal effects can be neglected. With these considerations we find for the first order contribution to $\Delta\Omega$

$$\Delta\Omega^{(1)} = \sum_{\sigma} \int d^3r \, \frac{1}{2} m_a n_\sigma(\mathbf{r}) \Omega^2 \rho^2. \tag{4.71}$$

The second order contribution can again be simplified by carrying out the derivatives in A, B, C, and D, and performing the τ integrals

$$\begin{aligned}
\Delta\Omega^{(2)} &= \frac{\hbar^2\Omega^2}{4} \int d^3r \int d^3r' \sum_{\eta} \sum_{\nu} \Big[\frac{f(E_\eta) - f(E_\nu)}{E_\eta - E_\nu} (m + m')^2 \\
&\times \Big\{ u_\eta(\mathbf{r}) u_\nu^*(\mathbf{r}) (u_\eta^*(\mathbf{r}') u_\nu(\mathbf{r}') + v_\eta^*(\mathbf{r}') v_\nu(\mathbf{r}')) \\
&+ v_\eta^*(\mathbf{r}) v_\nu(\mathbf{r}) (u_\eta(\mathbf{r}') u_\nu^*(\mathbf{r}') + v_\eta(\mathbf{r}') v_\nu^*(\mathbf{r}')) \Big\} \\
&+ \frac{1 - f(E_\eta) - f(E_\nu)}{E_\eta + E_\nu} (m - m')^2 \Big\{ u_\eta(\mathbf{r}) v_\nu(\mathbf{r}) \\
&\times (v_\eta^*(\mathbf{r}') u_\nu^*(\mathbf{r}') - u_\eta^*(\mathbf{r}') v_\nu^*(\mathbf{r}')) + u_\nu^*(\mathbf{r}) v_\eta^*(\mathbf{r}) \\
&\times (u_\eta(\mathbf{r}') v_\nu(\mathbf{r}') - v_\eta(\mathbf{r}') u_\nu(\mathbf{r}')) \Big\} \Big],
\end{aligned} \tag{4.72}$$

assigning the quantum numbers $\eta = (n, m, k)$ and $\nu = (n', m', k')$. Using the orthonormality and completeness relations of the quasi-particle wavefunctions

$$\int d^3r \, [u_\eta(\mathbf{r}) u_\nu^*(\mathbf{r}) + v_\eta(\mathbf{r}) v_\nu^*(\mathbf{r})] = \delta_{\eta\nu} \tag{4.73}$$

$$\int d^3r \, [u_\eta(\mathbf{r}) v_\nu(\mathbf{r}) - u_\nu(\mathbf{r}) v_\eta(\mathbf{r})] = 0, \tag{4.74}$$

the integral over $\mathbf{r}'$ can be done, and we are left with

$$\Delta\Omega^{(2)} = (\hbar\Omega)^2 \sum_{\eta} \frac{\partial f(E_\eta)}{\partial E_\eta} m^2 \int d^3r \left(|u_\eta(\mathbf{r})|^2 + |v_\eta(\mathbf{r})|^2 \right). \tag{4.75}$$

Thus the expression for the superfluid density for a cylindrically symmetric system is

$$n_s(\mathbf{r}) = n(\mathbf{r}) + \frac{2\hbar^2}{m_a \rho^2} \sum_{\eta} \frac{\partial f(E_\eta)}{\partial E_\eta} m^2 \left(|u_\eta(\mathbf{r})|^2 + |v_\eta(\mathbf{r})|^2 \right). \tag{4.76}$$

One might worry about the appearance of ρ^2 in the denominator of the second term. However, it is easy to see that the only quasi-particle wavefunctions with a finite amplitude at the origin are those corresponding to $m = 0$. Hence the superfluid density is indeed regular at $\rho = 0$. For large radii ρ we can make the substitution $k = m/\rho$, and treat this as a continuous variable. In that case we recover, as expected, for a homogeneous system the expression we found in the previous section.

Chapter 5

A Descent into the Fermi Maelstrom

Vortex structures occur in an extremely wide variety of natural phenomena, from vortex shedding on wings, to tornadoes, and Jupiter's Great Red Spot. Vortices are encountered on all length scales, ranging from atomic systems to cosmic strings, which are vortices in the structure of space time [62].

As we saw in Chapter 4, superfluids unlike their classical counterparts are restricted to potential flow ($\nabla \times \mathbf{v}_s = 0$). Consequently, a superfluid can only support rotational flow around vortices, which are nodal lines in the order parameter field. The presence of such line defects makes the system multiply connected. The quantum nature of the order parameter enforces a quantization of the circulation around such a line in units of Γ_0, where $\Gamma_0 = \pi h/2m_a$ for a gas of superfluid Cooper pairs. A quantized vortex consists of a cylindrical core around which the phase of the order parameter winds by an integer multiple of 2π, while within the core the amplitude of $\Delta(\mathbf{r})$ is suppressed from its bulk value, vanishing on the vortex line.

Quantization of vorticity is a generic feature of all superfluids be it (type II) superconductors [145], superfluid ^{4}He [146], or ^{3}He [147], and vortex lines are

speculated to penetrate the superfluid interior of fast rotating neutron stars [148, 149, 150, 151, 152]. For trapped, gaseous Bose-Einstein condensates vortices have been observed experimentally [153, 154, 155], and a large body of work exists on the theory (see for instance [156]). A superfluid Fermi gas would be no exception, and this chapter describes the physics of an isolated vortex line in such a system.

With an eye on future experiments it is important to have an unambiguous experimental signature of superfluidity in a dilute Fermi gas. As we have discussed in Chapter 3, the bulk properties of the gas are essentially unaffected when going through the BCS transition. But since quantized circulation is one of the hallmarks of superfluidity, the creation and subsequent detection of a quantized vortex in an atomic Fermi gas would be a "smoking gun" for superfluidity in the system.

5.1 Vortex Physics 101

A vortex line is a familiar concept in classical hydrodynamics, where it has been studied for more than a century [157, 158]. We can define it as a curve directed along the *vorticity vector* $\boldsymbol{\omega} = \nabla \times \mathbf{v}$ of the fluid. The vorticity is equal to the circulation per unit area. Since the vorticity field is divergence free, it follows that vortex lines can not terminate in the fluid, they must either be closed in vortex rings or terminate at the boundaries of the system.

For a superfluid system the velocity field is given by the gradient of a velocity potential $\theta(\mathbf{r})$, which is the phase of the order parameter

$$\mathbf{v}_s = \frac{\hbar}{2m_a}\nabla\theta(\mathbf{r}), \tag{5.1}$$

where $2m_a$ is the mass of a Cooper pair. Such potential flow is necessarily

irrotational. Furthermore, bulk superfluids are incompressible; due to the energy gap an infinitesimal change in the density is associated with a finite change in the energy of the system. The density is therefore a constant of the motion, and from the continuity equation

$$\frac{\partial n_s}{\partial t} + \nabla \cdot \mathbf{j}_s = 0, \tag{5.2}$$

if follows that the velocity field is divergence free in the bulk where the density does not vary spatially. Thus the superfluid velocity satisfies the conditions

$$\nabla \cdot \mathbf{v}_s = 0, \qquad \nabla \times \mathbf{v}_s = 0, \tag{5.3}$$

resembling the Maxwell equations for a magnetic field in a source free vacuum. Since the vortex line is a singular region where the vorticity is non-vanishing the electromagnetic equivalent is a wire carrying an electrical current $\mathbf{j}$. The magnetic field on the wire satisfies the equation $\nabla \times \mathbf{B} = 4\pi\mathbf{j}/c$, where c is the speed of light in vacuum. The magnetic field away from the wire is given by the Biot-Savart law [159], and by analogy the superfluid velocity field at the point $\mathbf{r}$ due to a vortex of circulation Γ is therefore given by

$$\mathbf{v}_s(\mathbf{r}) = \frac{\Gamma}{4\pi} \int d\mathbf{r}' \times \frac{\mathbf{r} - \mathbf{r}'}{|\mathbf{r} - \mathbf{r}'|^3}, \tag{5.4}$$

where the integral is along the entire length of the vortex line. The circulation Γ is equivalent to the magnetic flux $4\pi I/c$ through a contour surrounding a wire carrying current I. The streamlines described by this velocity field are circles.

Taking the electromagnetic analogy further a "Lorentz force picture" shows that two vortices exert a force on each other, the sign of which depends on their relative circulation: vortices with an opposite sense of circulation attract, while vortices with the same sense of circulation repel each other. Accordingly, when a

system contains multiple vortex lines, all carrying rotational currents in the same direction, they organize themselves in a regular lattice structure to minimize the energy [160]. In trapped atomic BECs lattices containing more than 100 vortex lines have been generated [155, 161]. Recently, the fundamental oscillations of such vortex lattices were observed. [162]. For the theory of these modes see the review article by Sonin, which also discusses similar experimental results for liquid helium [163].

We are interested in a straight, isolated vortex line of length L situated on the symmetry axis of a cylindrically symmetric potential. It is then natural to work in cylindrical coordinates (ρ, z, φ). For historical reasons we choose the gauge such that the pairing field is written as

$$\Delta(\mathbf{r}) = |\Delta(\mathbf{r})| e^{-i\kappa\varphi}, \tag{5.5}$$

corresponding to Cooper pairs with angular momentum $-\kappa\hbar$ [70]. Note that the flow pattern of the vortex is such that the angular momentum is the same everywhere. All Cooper pairs carry exactly κ units of angular momentum regardless of their position in the gas.

The quasi-particle wavefunctions consistent with an order parameter of the form (5.5) are

$$\begin{aligned} u_\eta(\mathbf{r}) &= \rho^{-1/2} u_{nmk_z}(\rho) \frac{e^{im\varphi}}{\sqrt{2\pi}} \frac{e^{ik_z z}}{\sqrt{L}} \\ v_\eta(\mathbf{r}) &= \rho^{-1/2} v_{nmk_z}(\rho) \frac{e^{i(m+\kappa)\varphi}}{\sqrt{2\pi}} \frac{e^{ik_z z}}{\sqrt{L}}. \end{aligned} \tag{5.6}$$

We are assuming free motion along the vortex axis, and imposing periodic boundary conditions at $z = \pm L/2$. The allowed values of the angular momentum quantum number are $\{m = 0, \pm 1, \pm 2, \ldots\}$, and the axial momentum is given

by $k_z = 2\pi\ell/L$, with $\{\ell = 0, \pm 1, \pm 2, \ldots\}$. The radial functions (u_{nmk_z}, v_{nmk_z}) are taken to be real. Note that u_η and v_η differ by exactly κ units of angular momentum, indicating that Cooper pairs form between particles with angular momentum $\hbar m$ and $-\hbar(m+\kappa)$ around the symmetry axis, yielding a vortex with circulation $-\kappa\Gamma_0$. This should be contrasted with the situation in the absence of vorticity, where the cylindrical symmetry dictates that pair constituents have angular momentum $\hbar m$ and $-\hbar m$, *i.e.* Cooper pairs form in time-reversed states [164].

The flow velocity of the superfluid decreases away from the center of rotation, but diverges as $\rho \to 0$:

$$\mathbf{v}_s = -\frac{\kappa\hbar}{2m_a\rho}\hat{\mathrm{e}}_\varphi. \tag{5.7}$$

This implies the existence of a region close to the vortex axis where the kinetic energy is large enough to break the Cooper pairs. Hence the order parameter will be suppressed in the vortex core and will heal to its bulk value over a length scale governed by the coherence length $\xi_{\rm BCS} = \hbar v_{\rm F}/\pi\Delta_0$, with $v_{\rm F} = \hbar k_{\rm F}/m_a$ being the Fermi velocity. We can estimate the radius of the cylinder in which interior superfluidity will be suppressed by equating the kinetic energy $\frac{1}{2}m\mathbf{v}_s^2$ with the condensation energy per particle $3\Delta_0^2/4\mu$. This gives just $\sim \xi_{\rm BCS}$.

5.2 Rotating Bucket

Vortices can be generated in a fluid in two different ways. The first is by draining the liquid through a small hole in the base of the container. Such a "bathtub vortex" was recently studied in detail in an elegant tabletop experiment [165]. Vortices can also be produced when the system is exposed to a rotating potential.

If the potential is anisotropic a torque is applied to the system, thereby imparting an angular momentum on the particles. For an atomic gas such a stirring potential can be applied in several different ways. One can use the optical dipole force of a blue-detuned laser beam rotated at the desired frequency [154, 155]. Alternatively, the trap potential can be elliptically deformed in the plane perpendicular to the rotation axis $\hat{e}_\Omega$. Rotating the deformation about $\hat{e}_\Omega$ then stirs the trapped cloud [161]. A third method involves imprinting directly on the many-body wavefunction a phase consistent with a rotating cloud [153, 166].

When a vessel of radius containing a superfluid liquid at zero temperature is rotated at a low uniform frequency Ω the inability of the fluid to participate in non-potential flow means that it will remain at rest, seemingly oblivious to the rotation of the walls of the container (see Fig. 5.1). At larger rotation frequencies a parabolic meniscus forms on the liquid surface, indicating that the fluid is rotating as a whole. Such solid body rotation is characterized by each particle maintaining its relative position with respect to the bucket. The formation of the meniscus is due to the balance between centripetal and gravitational forces [167, 168]. In a classical fluid rotating at the uniform frequency Ω the surface profile is [169]

$$z(\rho) = \frac{\Omega^2}{2g}\left(\rho^2 - R^2\right), \tag{5.8}$$

where g is the acceleration due to gravity, and we have defined the zero of the coordinate such that $z(R) = 0$, where R is the radius of the cylinder. In a rotating superfluid this drastic change in behavior is associated with the appearance of vortex lines parallel to the rotation axis threading the fluid at angular velocities exceeding Ω_c, the critical frequency where the first vortex is formed. As Ω is further increased more and more vortices enter the system, forming a regular

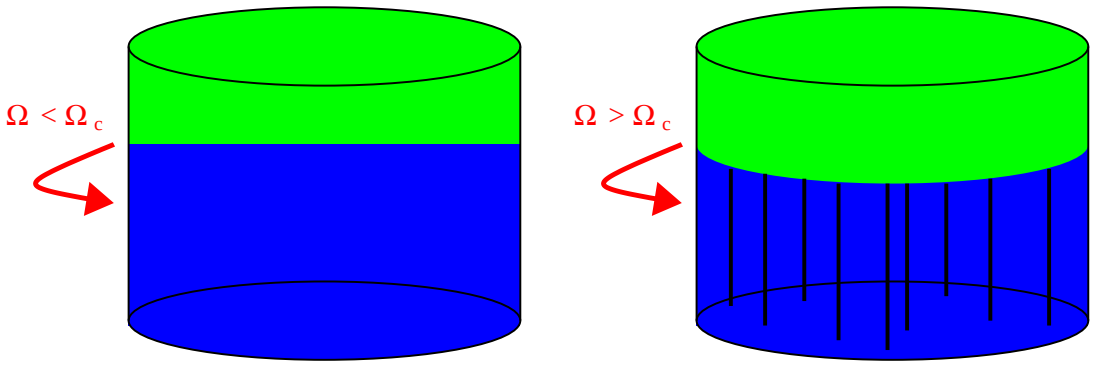

Figure 5.1: The rotating bucket experiment. A bucket containing a superfluid liquid at zero temperature (*blue*) is rotated at a frequency Ω. If Ω is smaller than a critical frequency Ω_c the fluid remains at rest (*left*). At frequencies higher than Ω_c vortex lines penetrate the fluid and form a lattice. The vortex lattice undergoes solid body rotation, and a meniscus forms at the fluid surface (*right*).

lattice. Since the vortex cores are in the normal (non-superfluid) state the lattice structure as a whole undergoes solid body rotation. As the number of vortices grows the velocity profile of the fluid tends to the solid body value, increasing linearly with the distance from the rotation axis. This can be viewed as a correspondence principle: on a scale larger than the distance between the vortices, the coarse grained average of the quantum velocity field becomes identical to that of a classical, rotating rigid body.

Early experiments on rotating samples of liquid helium were performed at angular velocities far exceeding the critical value, which is very small for this system ($\Omega_c \sim 10^{-3}\ s^{-1}$ for a cylinder with a radius of 1 cm), and correspondingly the liquid was found to rotate like a solid body. As other experiments demonstrated the persistence of superfluid phenomena (like the fountain effect) under rotation, this presented a problem for the Landau theory, according to

which only potential flow is allowed [167]. Onsager and Feynman qualified this statement by showing that $\nabla \times \mathbf{v}_s \neq 0$ is allowed on a singular vortex line, thereby explaining the experimental findings.

5.2.1 Critical Frequency

In the absence of rotation the vortex is an excited state of the system, corresponding to a nodal line in the macroscopic wavefunction $\Delta(\mathbf{r})$. In the ground state the superfluid is at rest, and it takes a finite amount of energy to excite the vortex mode. We define $\Delta E = E_v - E_0$ as the energy difference between the superfluid state with the vortex present and without. For a system in a rotating potential the appropriate frame for minimizing the free energy to determine the thermodynamic ground state is the co-rotating frame, where the Hamiltonian is time-independent. If the time-dependent part of the Hamiltonian is periodic with a frequency Ω we can use a unitary transformation

$$|\Psi(\mathbf{r}', t)\rangle_{\text{rot}} = \mathcal{U}_\Omega |\Psi(\mathbf{r}, t)\rangle_{\text{lab}}, \tag{5.9}$$

where $\mathcal{U}_\Omega = \exp(-i\Omega t L_z/\hbar)$, to rotate the state vector to the frame where the Hamiltonian is stationary. Here and in the following we take the z-axis to coincide with the rotation axis. The correspondence between the total energy in the two frames is given by a Legendre transformation

$$E_{\text{rot}} = E_{\text{lab}} - \Omega \langle L_z \rangle . \tag{5.10}$$

Therefore the energy in the rotating frame is a decreasing function of the rotation frequency for any state with a non-vanishing angular momentum, provided the flow is in the direction of the external rotation, such that Ω and $\langle L_z \rangle$ have

the same sign. On the other hand if the superfluid is at rest its energy in the laboratory and rotating frames are identical. As illustrated in Fig. 5.2 this implies the existence of a critical rotation frequency Ω_c above which the vortex state becomes the energetic ground state of the system. Due to the simple linear relation between $E_{\rm rot}$ and the rotation frequency, the critical frequency is simply given by

$$\Omega_c = \frac{\Delta E}{\langle L_z \rangle}, \tag{5.11}$$

i.e. it is determined by the excitation energy at $\Omega = 0$ and the angular momentum of the vortex state. While ΔE can be calculated in our mean-field theory by solving the BdG equations with the constraint that $\Delta(\mathbf{r})$ corresponds to a vortex state, the expectation value of the angular momentum at $T = 0$ is $\langle L_z \rangle = -\kappa N_\sigma \hbar$ by construction (see the discussion following (5.6)). Below we present a detailed calculation of the vortex energy ΔE.

It is important to stress that while Ω_c (sometimes also referred to as Ω_{c1}) denotes the frequency at which a vortex along the rotation axis becomes thermodynamically stable, there is a different frequency $\Omega_{\rm dyn}$ associated with the dynamical stability of the vortex. For a trapped atomic gas this frequency marks the point where surface modes first become unstable. For sufficiently fast rotation of the cloud the breaking of such waves causes vortices to nucleate at the surface [170, 171, 172]. If the rotation frequency exceeds Ω_c these vortex lines are energetically stable features, and settle down in an equilibrium configuration. In most experiments on atomic BECs it is found that $\Omega_{\rm dyn} > \Omega_c$, implying hysteretic effects as the frequency of the rotating drive is ramped up and down.

As stated above, further increasing the rotation frequency beyond Ω_c causes more and more vortices to enter the system, leading to the formation of a vortex

lattice. As the lattice grows the spacing between the vortex lines decreases. When the vortices begin to overlap the system collectively undergoes a transition to the normal state, destroying superfluidity. This happens at the so-called upper critical frequency Ω_{c2} [173]. The transition is not expected to be sharp, but rather a gradual melting of the lattice, leading to a vortex fluid, in which the random thermal motion of the vortices quench the phase coherence thus suppressing superfluidity in the system [174].

It is rather surprising that despite the large amount of work concerned with the structure of a vortex for a fermionic system, there is no clear result regarding the vortex energy. This is in contrast with the case of a dilute bosonic superfluid, where the Gross-Pitaevskii equation allows an analytical calculation of the vortex energy for $T = 0$ if quantum fluctuations are neglected [13]. The equivalent theory relevant for fermions, Ginzburg-Landau (GL) theory, is unfortunately only valid for $|T - T_c|/T_c \ll 1$ making an analytical calculation of the energy for $T = 0$ more complicated.

To find the energy per unit length associated with the vortex we invoke a simplified model of its microscopic structure. Since the order parameter is suppressed in the core region, and vanishes on the vortex line, we adopt a *cylinder model*, where the pairing field is replaced by a step function. It is taken to be zero inside a cylindrical volume of radius r_0, and equal to its bulk value Δ_0 for $r_0 < \rho < R$. The superfluid velocity flow then extends from $\rho = r_0$ to $\rho = R$, but vanishes at shorter distances from the vortex line, implying that the core is filled with atoms in the normal state at rest. From the arguments presented in Section 3.6 we expect the variation in the particle density to be negligible near the vortex line. We consequently suppose it to be constant throughout the gas.

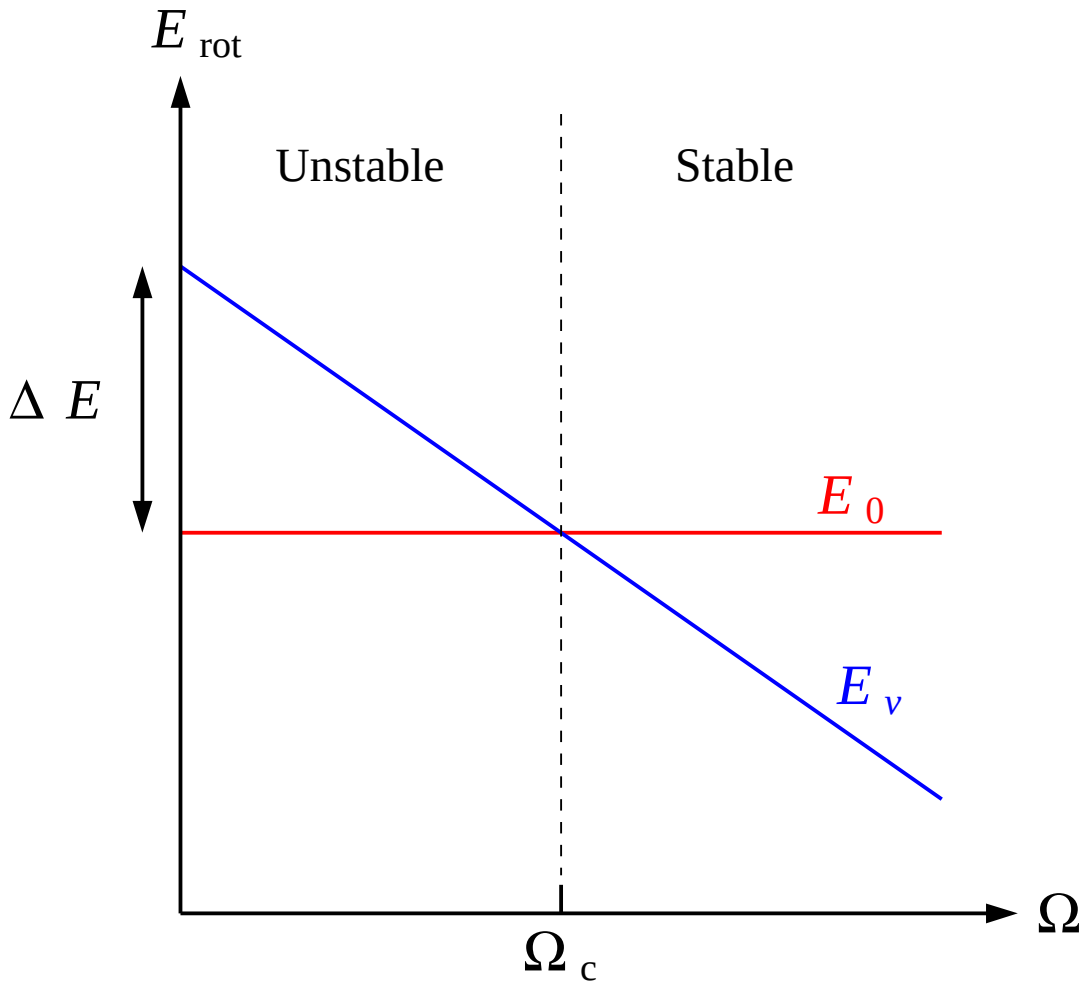

Figure 5.2: Schematic graph of the evolution of the rotating frame energy of the vortex and non-vortex state as a function of the rotation frequency. For frequencies larger than Ω_c the vortex state is the thermodynamic ground state of the system. For $\Omega < \Omega_c$ it is energetically unstable. The sense of the fluid motion around the vortex line is assumed to be in the direction of the applied rotation, otherwise the energy would be shifted in the opposite direction.

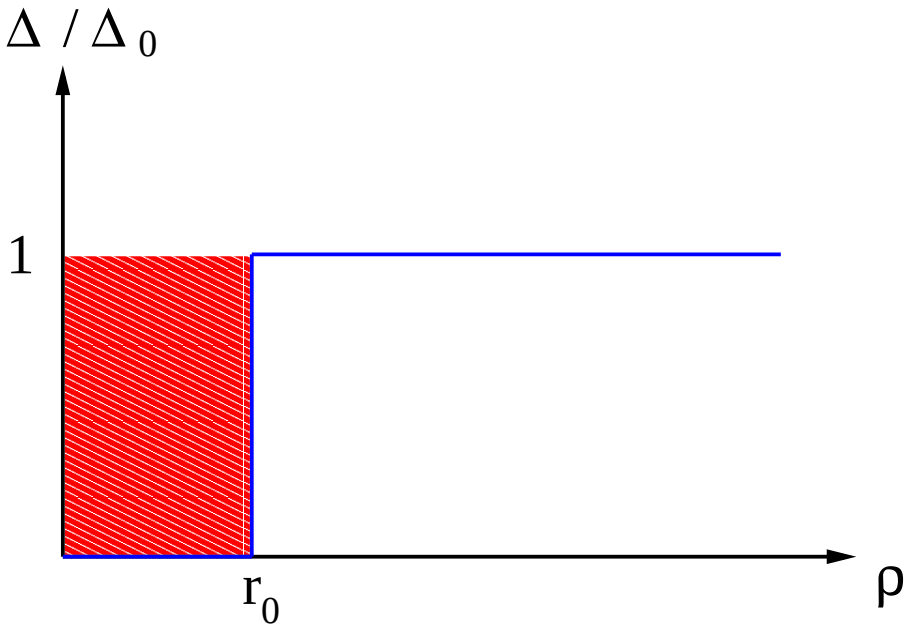

Figure 5.3: Illustration of the cylinder model. The order parameter (*blue*) is taken to zero inside the vortex core, which is a cylinder of radius r_0. The core (*hatched red*) consists of atoms in the normal state. For $\rho > r_0$ the order parameter assumes its bulk value Δ_0.

Conversely, the superfluid density must vanish in the core, whereas it is is equal to $2n_\sigma$ in the exterior region.

The energy per unit length of the vortex, $\mathcal{E}_v = \Delta E/L$, is then given by the sum of two contributions. One is the kinetic energy associated with the superfluid flow in the region outside the core

$$\mathcal{E}_{\rm kin} = \int_{r_0}^{R} d^2r\, \frac{1}{2} m_a n_s \mathbf{v}_s^2 = 2\pi \int_{r_0}^{R} d\rho\rho\, m_a n_\sigma \left(\frac{\kappa\hbar}{2m_a\rho}\right)^2 = \frac{\pi\kappa^2\hbar^2 n_\sigma}{2m_a} \ln\frac{R}{r_0}, \quad (5.12)$$

and the other constitutes the loss in condensation energy in the core

$$\mathcal{E}_{\rm cond} \simeq \frac{\pi r_0^2 E_{\rm cond}}{V} = \frac{\pi\hbar^2 n_\sigma}{2m_a}\frac{3}{\pi^2}\left(\frac{r_0}{\xi_{\rm BCS}}\right)^2, \quad (5.13)$$

using the definition of the BCS coherence length. Hence the vortex energy per

unit length in the cylinder model is given by

$$\mathcal{E}_v = \mathcal{E}_{\rm kin} + \mathcal{E}_{\rm cond} \simeq \frac{\pi\kappa^2\hbar^2 n_\sigma}{2m_a} \ln\left(\frac{R\, e^{3r_0^2/\pi^2\kappa^2\xi_{\rm BCS}^2}}{r_0}\right). \tag{5.14}$$

This expression is minimized for $r_0 = \pi\kappa\xi_{\rm BCS}/\sqrt{6}$, which leads us to anticipate that the extent of the vortex core is on the order of the coherence length. However, due to the simplicity of the cylinder model we can not rely on it to directly infer the relationship between r_0 and $\xi_{\rm BCS}$. To do this we must determine the vortex energy from a numerical solution of the BdG equations. The results of such a calculation are presented in Section 5.2.3. For now we instead write the vortex energy as

$$\mathcal{E}_v \simeq \frac{\pi\kappa^2\hbar^2 n_\sigma}{2m_a} \ln\left(D\frac{R}{\kappa\xi_{\rm BCS}}\right), \tag{5.15}$$

defining the parameter $D = (\kappa\xi_{\rm BCS}/r_0)\exp(3r_0^2/\pi^2\kappa^2\xi_{\rm BCS}^2)$. From this expression it is clear that vortices with multiple circulation quanta, $\kappa > 1$, must be energetically unstable for a homogeneous gas, inasmuch as two lines with $\kappa = 1$ have a smaller energy than a single vortex with $\kappa = 2$ [12, 175, 176]. We therefore expect vortices with $\kappa > 1$ to break up into κ single-quantized vortices. For harmonically trapped Bose-Einstein condensates the instability of multiple circulation vortices is known to remain valid [177], and we speculate that the same holds true for trapped Fermi superfluids. For studies on the dynamics of the disintegration of doubly quantized vortices in a Bose superfluid we refer to Refs. [178, 179]. These authors identify complex eigenvalues in the Bogoliubov spectrum associated with exponentially growing modes. A similar analysis is not possible within our theory, since the BdG equations for a superfluid Fermi gas are hermitian, as we saw in Chapter 3. A treatment of the collective modes (*i.e.* RPA theory) is needed in order to address these issues for a gas of fermions.

Multiquantum vortices are allowed in superfluid ^{3}He, where they have been observed experimentally [180]. Their existence is tied to the complicated topology of the order parameter in the spin triplet superfluid state. The observation of vortex lines with winding numbers larger than one in thin films of ^{4}He is due to the dynamical stability of these in 2 dimensions, since no mechanism exists for them to decay into singly quantized lines [181]. We also point attention to the experiment by P. Engels *et al.*, where a focused, resonant laser was used to evaporate atoms from the center of a spinning Bose-Einstein condensate containing a vortex lattice. The result was the transient formation of a 'giant vortex' containing up to 60 phase singularities [182]. From this point onward though we will focus on $\kappa = 1$ vortices.

The energy of the vortex depends on the background density. Hence vortices in an inhomogeneous potential will dissipate into areas where the density is lower. In a harmonic trap this means the vortices will spiral toward the edge of the cloud, eventually slipping off. In experiments with trapped Bose gases vortex lifetimes of several seconds have been reported [155].

Recently, two papers have calculated the $T = 0$ vortex energy for a Fermi superfluid using the phenomenological model presented above. It was argued in Ref. [183] that a microscopic calculation for $T = 0$ would yield D to be a *constant* $\sim \mathcal{O}(1)$ independent of $k_{\rm F}$ and $|a|$ since the characteristic length-scale of a vortex must be expected to be $\mathcal{O}(\xi_{\rm BCS})$. If the vortex is modeled as a cylinder of radius $r_0 = \xi_{\rm BCS}$ containing a normal stationary fluid, surrounded by a rotating superfluid one obtains $D = 1.36$. A different calculation using GL theory was shown in [183] to give $D = 1.65$. We cite this result, since the GL method provides a more detailed treatment of the core structure than

the cylinder model. Even though the GL equation is only strictly valid for $|T - T_c|/T_c \ll 1$, the method gives a qualitative estimate of the vortex energy.

These conclusions were however disputed in the work of Ref. [184]. Here it was argued that the characteristic length scale of the vortex is much smaller than $\xi_{\rm BCS}$ and the energy correspondingly higher. This is because the structure of the vortex core is determined by the lowest lying vortex states. These states are formed out of excitations around the Fermi level with typical wavelengths $\sim k_{\rm F}^{-1}$ (see below), and following the conclusions based on the analytical and numerical solutions of the Bogoliubov-de Gennes (BdG) equations [185, 186] it was argued that the important length scale of the core region is $\xi_1 = 4/\pi k_{\rm F}^2|a| \ll \xi_{\rm BCS}$ in the dilute regime [184]. Using ξ_1 as the size of the vortex core leads to a vortex energy given by Eq. (5.15) but with $D \simeq \xi_{\rm BCS}/\xi_1 \gg 1$ in the dilute regime. Thus, the energy was predicted to be significantly higher than what was estimated in Ref. [183]. Note that D is now not a constant but depends on $k_{\rm F}$ and $|a|$.

It is presently not evident a priori which of the two quite different predictions is correct and thus what the energy of the vortex actually is. In order to settle this question, we have performed the first *microscopic* calculation of the vortex energy [187].

5.2.2 To Fix N or Not to Fix N, That is the Question

The energy cost of creating a single vortex line can be calculated numerically as the difference in energy of the superfluid state with the vortex present and without. This energy difference must be evaluated at a fixed particle number, *i.e.* we require the vortex state and the superfluid state with no vortex to have the same number of atoms. Otherwise comparing their energies is meaningless.

However, fixing N in the calculation involves a root-finding procedure, where the chemical potential is adjusted to give the desired number of particles (see Chapter B). This introduces an undesired computational overhead, relative to solving the BdG equations for a fixed value of μ. However, as we shall now show the *energy* difference between the two states at fixed $N = N_v(\mu_v) = N_0(\mu_0)$, denoted by $E_v(N) - E_0(N)$, is to excellent approximation equal to their *grand canonical potential* difference, $\Omega_v(\mu_v) - \Omega_0(\mu_v)$, at fixed μ. Here the parameters in parenthesis are taken to be held fixed in the calculation. Additionally, μ_v (μ_0) is the chemical potential which corresponds to a state with N_v (N_0) atoms. To demonstrate this relation we note that $\Omega(\mu) = E(N) - \mu N$ at zero temperature, such that the energy difference can be written as

$$\Delta E \equiv E_v(N) - E_0(N) = \Omega_v(\mu_v) + \mu_v N - \Omega_0(\mu_0) - \mu_0 N. \tag{5.16}$$

The grand canonical potential of the non-vortex state can be expanded in a Taylor series around $\mu = \mu_v$

$$\Delta E = \Omega_v(\mu_v) + \mu_v N - \mu_0 N - \Omega_0(\mu_v) - (\mu_0 - \mu_v) \left(\frac{\partial \Omega_0}{\partial \mu} \right)_{\mu=\mu_v} + \mathcal{O}(\delta^2), \tag{5.17}$$

introducing the dimensionless difference in chemical potential $\delta = (\mu_0 - \mu_v)/\mu_v$. We then use the thermodynamic identity [27]

$$\left(\frac{\partial \Omega}{\partial \mu} \right)_{TV} = -N, \tag{5.18}$$

to obtain the relation we are looking for

$$\begin{aligned} \Delta E &= \Omega_v(\mu_v) - \Omega_0(\mu_v) + (\mu_v - \mu_0) \left[N_0(\mu_0) - N_0(\mu_v) \right] + \mathcal{O}(\delta^2) \\ &= \Omega_v(\mu_v) - \Omega_0(\mu_v) + \Delta\mu \Delta N_0 + \mathcal{O}(\delta^2). \end{aligned} \tag{5.19}$$

Since δ is small we can safely omit the δ^2 correction term, and the error in using $\Delta\Omega$ instead of ΔE is negligible, provided $|\Delta\mu\Delta N_0|/\Delta E \ll 1$. This is indeed the

case for the situations we have investigated. Fig. 5.4 compares the actual particle number found from the self-consistent solution of the BdG equations with the thermodynamic relation (5.18). The line is the derivative of the grand canonical potential for the vortex-free case calculated at fixed μ, and the points are the atom numbers from the same calculation. The agreement confirms that the the substitution (5.18) in the Taylor expansion of the energy difference remains valid in a finite system. The vortex energy is plotted in Fig. 5.5 calculated both for fixed N and fixed μ (*i.e.* $\Delta E \simeq \Omega_v(\mu_v) - \Omega_0(\mu_v)$). As expected the difference is negligible. In the next section we will therefore present results found by fixing the chemical potential. It is important to stress that $E(N) \neq \Omega(\mu)$, since μN is comparable to $E(N)$. Hence the replacement is only valid when evaluating energy differences.

5.2.3 The Vortex Energy

In Fig. 5.6, we plot the value of D found by inverting Eq. (5.15), using the numerically calculated vortex energy $\mathcal{E}_v$ for cylinders with two different radii. Note that we are at the limit of the weak coupling regime $k_{\rm F}|a| \ll 1$, appropriate for dilute gases. For the purposes of comparison with analytical results, however, it is important to calculate properties for the widest possible range of $\xi_{\rm BCS}$, subject to the condition $\xi_{\rm BCS} \ll R$ which ensures that the gap function can heal to its bulk value before becoming suppressed at the cylinder surface. The cylinder length was taken to be 11.4μm, and the atomic properties (mass and scattering length) to be those of ^{6}Li as usual. The dashed line corresponds to the prediction $D = 1.36$ [183] and the solid line to $D = \xi_{\rm BCS}/\xi_1$ [184]. We see that the two predictions for D have a completely different dependence on

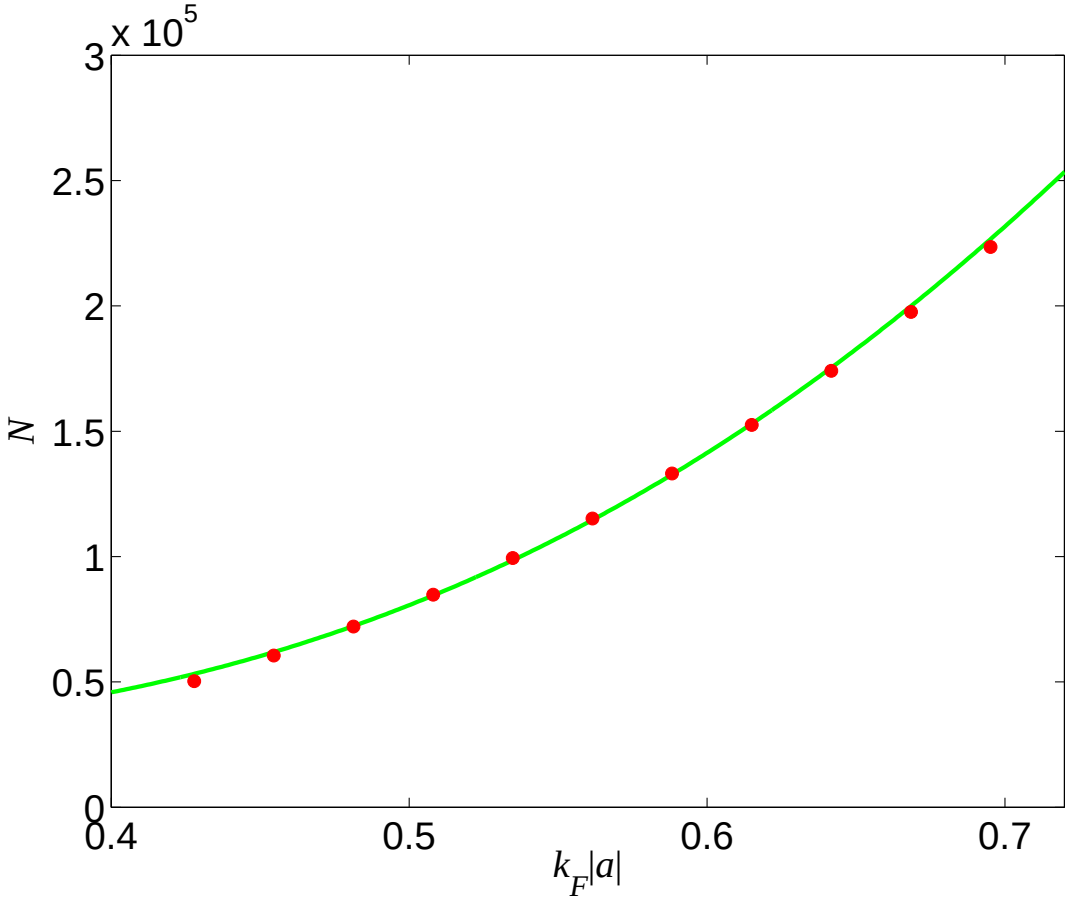

Figure 5.4: Total number of particles as a function of $k_{\rm F}|a|$ for the vortex-free case in a cylinder of radius $R = 28.5$ μm. The atom number as obtained from a fixed μ calculation (•) are compared with the thermodynamic identity (5.18) shown by a green line.

$k_{\rm F}|a|$. The important conclusion is that the numerical results confirm $D \sim \mathcal{O}(1)$ being a *constant* independent of $k_{\rm F}|a|$ in agreement with Ref. [183]. On the other hand, the prediction $D = \xi_{\rm BCS}/\xi_1$ yields a qualitatively incorrect result. We note that the kink in $\mathcal{E}_v$ (see inset) is due to $R/\xi_{\rm BCS}$ being different for the two cylinder sizes, whereas the spread in D at $k_{\rm F}|a| = 0.43$ is indicative

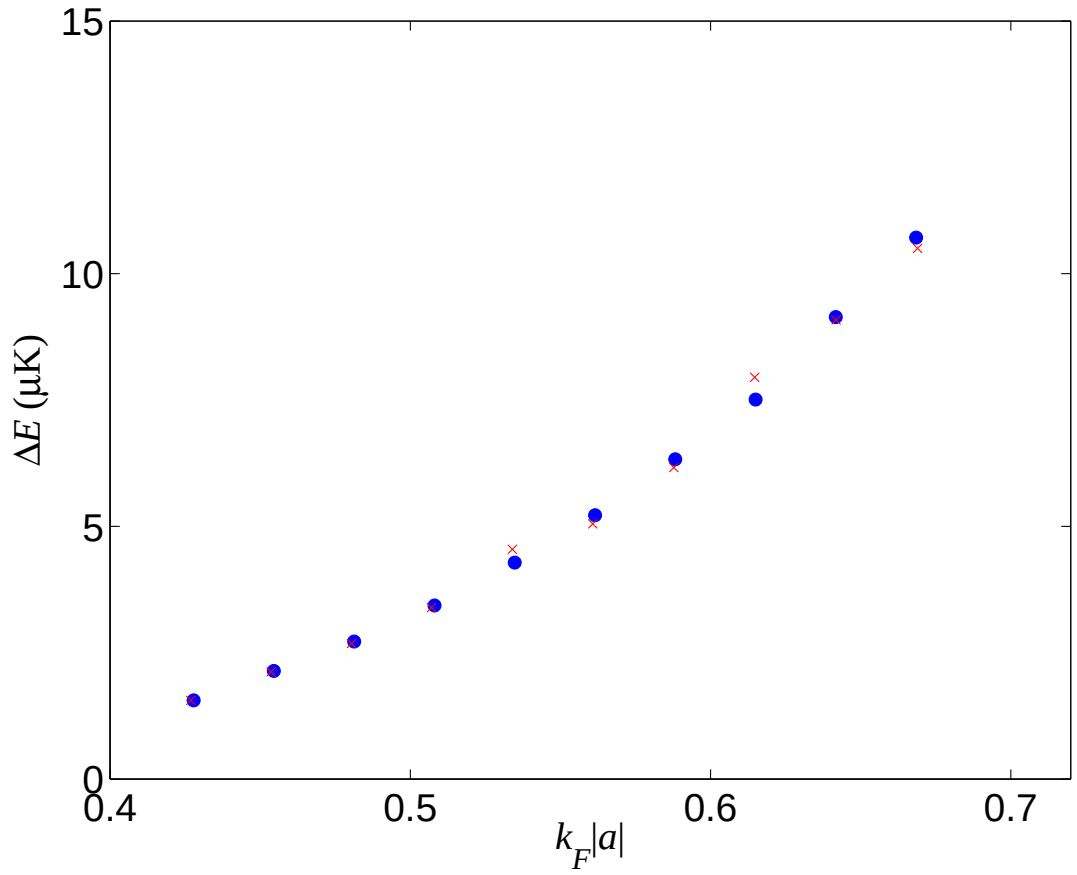

Figure 5.5: Energy of a vortex line calculated using the fixed μ method (•'s) and fixed N method (×'s).

of our numerical accuracy. The numerical value $D \simeq 2.5$ is higher than the prediction of phenomenological models in Ref. [183]. This is as expected since these models only can yield the correct order of magnitude of the constant inside the logarithm. Thus, the length scale determining the energy of the vortex is $\sim \xi_{\rm BCS}$ and not ξ_1.

To examine this in more detail, we plot in Fig. 5.7 the numerically calculated profile of a vortex for two representative values of $k_{\rm F}|a|$. As is evident the order parameter varies on two distinct length scales: close to the vortex core, only the

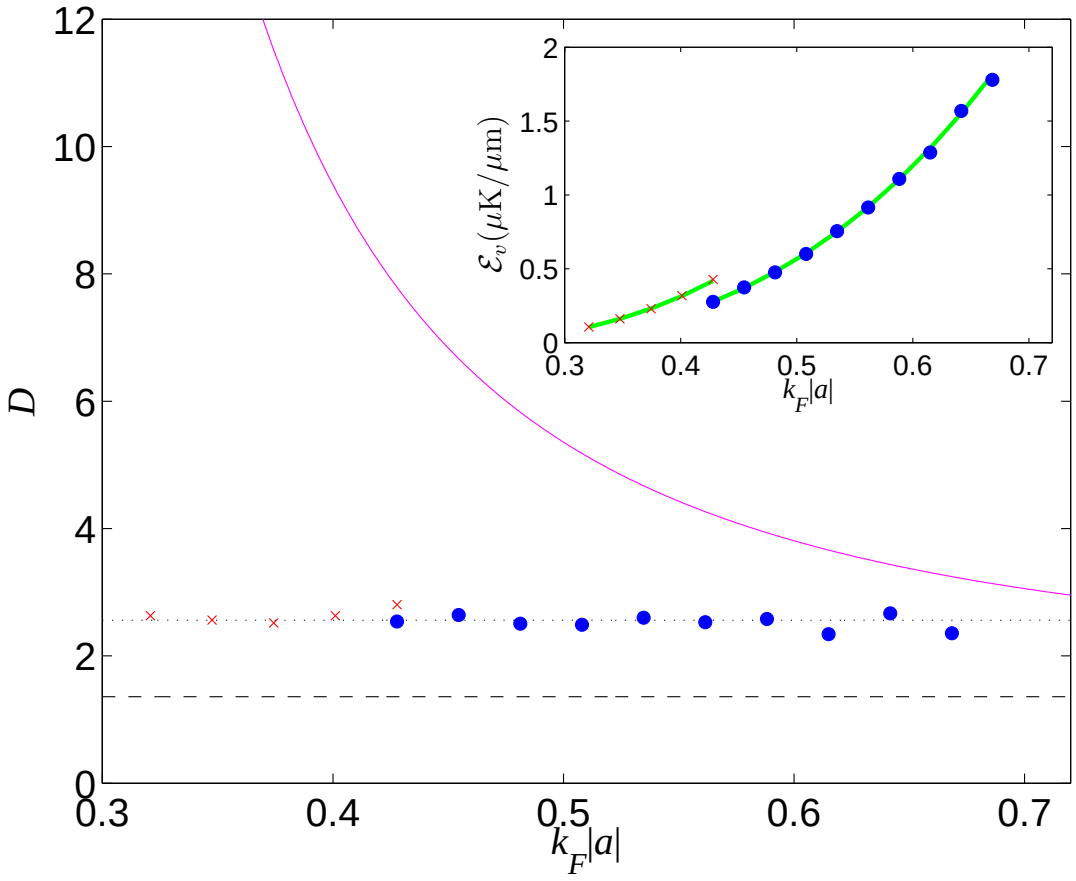

Figure 5.6: The energy of the vortex in terms of the parameter D. The dashed and solid lines correspond to the analytical predictions of Ref. [183] and [184], respectively, and the numerical results are indicated with •'s ($R = 28.5\ \mu$m) and ×'s ($R = 99.7\ \mu$m) with the average $\bar{D}$ represented by the dotted line. The inset depicts $\mathcal{E}_v$ with lines giving the analytical prediction of Eq. 5.15 using $D = \bar{D}$.

lowest-energy (bound) states contribute to the order parameter; these give rise to the observed Friedel oscillations, which have a wavelength on the order of k_{F}^{-1}. We see that the length scale defined as $\xi_1 = \lim_{\rho\to 0}[\Delta(\rho, z)/\rho\Delta_\infty]^{-1}$ giving the slope of $\Delta(\mathbf{r})$ at the vortex core actually is much smaller than ξ_{BCS} as predicted in Ref. [184, 185]. Here, Δ_∞ is the value of $|\Delta(\mathbf{r})|$ far away from the vortex core

with $\Delta_\infty \simeq \Delta_0$ as expected. However, as the distance ρ from the vortex core increases, the slope decreases and $\Delta(\mathbf{r})$ reaches the value Δ_∞ on a length scale $\sim \xi_{\rm BCS}$ and not ξ_1. To quantify this, we use the cylinder model of the vortex with a vortex radius $r_0 = x\xi_{\rm BCS}$ to calculate $\mathcal{E}_v$. This yields Eq. (5.15) but now with $D = (1.36)^{x^2}/x$. The equation $D = 2.5$ then gives $x = 0.42$. Thus $r_0 = 0.42\xi_{\rm BCS}$ is the length scale determining the energy of the vortex. Again, it should be emphasized that $x \simeq 0.42$ is a *constant* over the large range of $\xi_{\rm BCS}$ used in the calculations thereby verifying that indeed $\xi_{\rm BCS}$ determines the length-scale relevant for the energy as discussed in [183]. The cylinder model of $\Delta(\rho)$ with the correct radius $r_0 = 0.42\xi_{\rm BCS}$ is also indicated in Fig. 5.7.

5.3 Microscopic Vortex Structure

While the topic of the previous section was the global stability of a Fermi vortex, the present section will examine the microscopic structure of the vortex line. All of this discussion will pertain to a superfluid in a cylindrical box, but later in Section 5.6 a few key results will be presented for a vortex line in a gas with harmonic radial confinement.

5.3.1 Core Bound States

In Section 3.6 we saw that in the case of a trapped Fermi superfluid the spatial inhomogeneity of the pairing field gave rise to a branch of low energy excitations, or in-gap states. These bound states were confined to a small region at the edge of the cloud, where the pairing field and trap formed an effective potential well for the quasi-particles. The suppression of the gap function in the vortex core

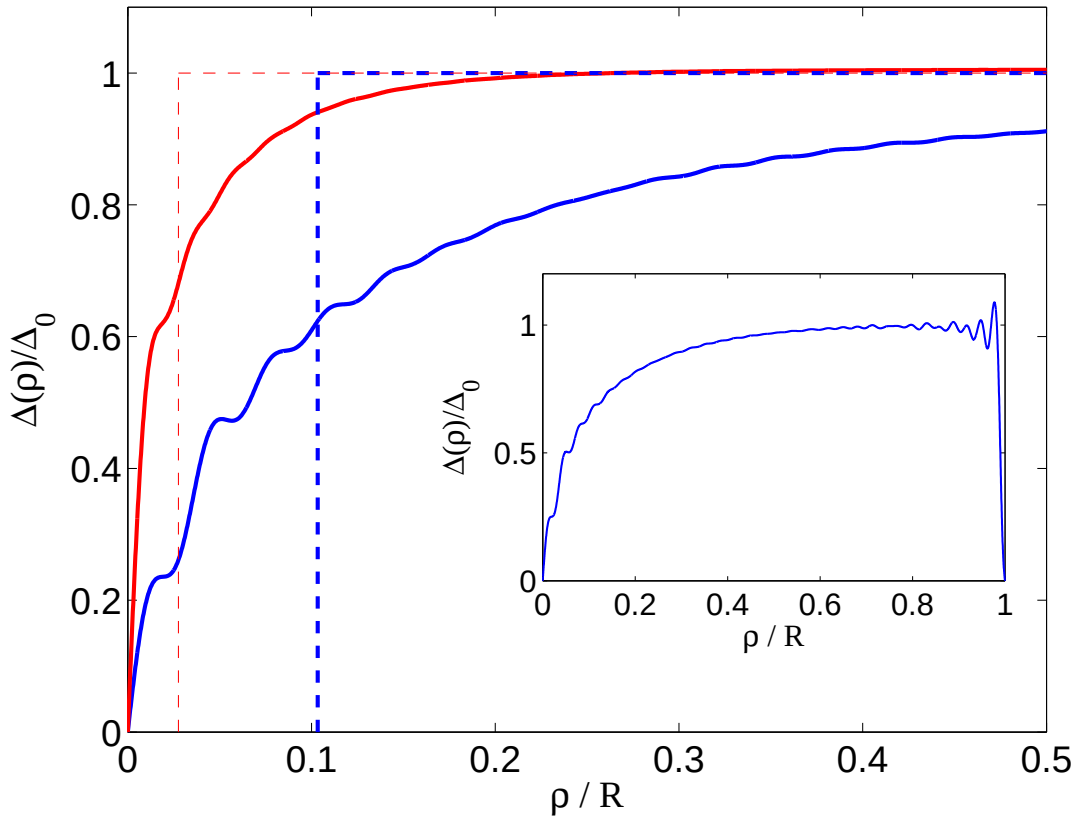

Figure 5.7: Pairing field vs. ρ at $T = 0$ for two different values of $k_{\mathrm{F}}|a|$: 0.43 (*blue line*) and 0.59 (*red line*). The dashed lines indicate the profile of the order parameter in the cylinder model with $r_0 = 0.42\xi_{\mathrm{BCS}}$. Inset: The full solution for $k_{\mathrm{F}}|a| = 0.43$.

creates a similar situation allowing for the existence of bound states localized inside the core region with energies well below the bulk value of the gap Δ_0. Since these *core bound states* are localized in the center of the vortex structure, where the centrifugal potential is largest, their energies have a strong angular momentum dependence. Most strikingly, the in-gap excitations exist only for angular momentum quantum numbers $m \geq 0$ [188, 189] (for $m < 0$ the spectrum has no single-particle excitations with energies less than Δ_0). Conversely, only in-gap

states with negative angular momentum exist for $E_\eta < 0$. Since they have positive angular momentum the occupation of the the core bound states corresponds to a quasi-particle current around the vortex core in opposite direction to that of the vortex current. We can think of this in terms of a Doppler shift: for a superfluid moving at a uniform velocity $\hbar\mathbf{q}/m_a$ a Galilean transformation shows that in the laboratory frame the energy of an excitation with momentum $\hbar\mathbf{k}$ is shifted from its value, $E^0_{\mathbf{k}}$, in the frame where the superfluid is at rest:

$$E^{\mathbf{q}}_{\mathbf{k}} = E^0_{\mathbf{k}} + \frac{\hbar\mathbf{k}\cdot\mathbf{q}}{m_a}. \tag{5.20}$$

This simple boost of the energies applies even if the velocity is varying in space as is the case for the vortex, as long as the local velocity does not exceed the local Fermi velocity [70]. For rotational currents we can divide the system into concentric annuli of infinitesimal width, and replace $\hbar\mathbf{k}\cdot\mathbf{q}/m_a$ in each with $m\Omega(\rho)$, where the local rotation frequency is $\Omega(\rho) = \rho v_s(\rho)$. Hence the counter-propagating modes with $m > 0$ are shifted to lower energies, some below the bulk gap, making them core bound states, while the energies of the modes propagating in the direction of the vortex current are increased.

In a detailed analysis it was found that the energy spectrum of the lowest core bound states with $0 \leq m \ll k_{\mathrm{F}}\xi_{\mathrm{BCS}}$ for $T = 0$ is given by

$$E_{mk_z} \sim (m + 1/2)\frac{\Delta_0^2}{E_{\mathrm{F}}}\frac{h(\theta)}{\sin\theta} \tag{5.21}$$

where $k_z = k_{\mathrm{F}}\cos\theta$ and $h(\theta)$ is a function of order unity [188]. Since $\Delta_0^2/E_{\mathrm{F}} \ll 1$ in the weak-coupling limit, the spectrum is essentially gapless. In Fig. 5.8, we plot the lowest quasi-particle energies as a function of m for $m \geq 0$ obtained from a numerical solution of the BdG equations. For clarity we have plotted only the states with $k_z = 0$. The gapless branch associated with the core states with

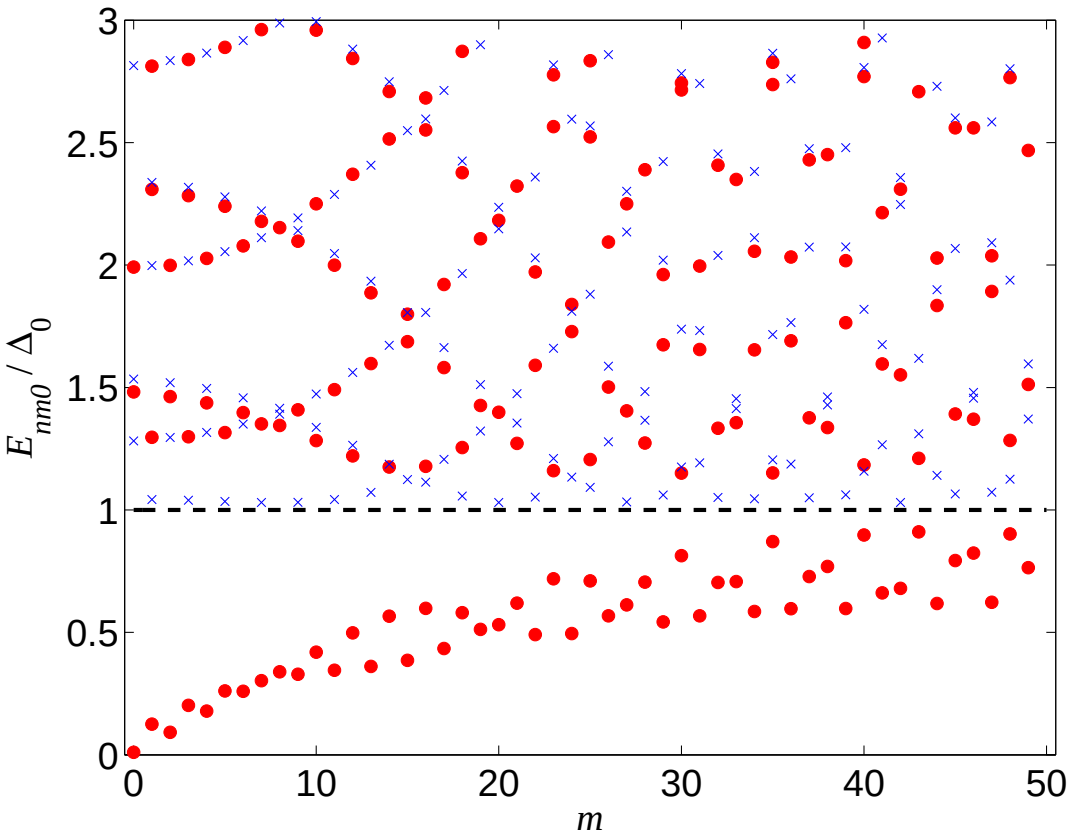

Figure 5.8: Energy spectrum for the lowest quasi-particle states in a superfluid with a vortex (•'s) and the vortex free state (×'s) at $T = 0$. For clarity only the energies of states with $k_z = 0$ have been plotted. There are branches of bound states for several values of k_z. The part of the spectrum with $m < 0$ is not shown, it has no in-gap excitations.

energies less than Δ_0 is clearly visible, and as expected from (5.21) it is linear in m for small angular momenta. There is a bound state branch associated with several values of k_z, together they form a band of in-gap energy states.

The core bound states are prominently displayed in the LDOS, where they give rise to a peak structure at energies $E < |\Delta_0|$ for small values of ρ, *i.e.* inside the vortex core. This is shown in Fig. 5.9. The local density of states

was calculated using (3.82), and as before the delta functions are replaced with smooth Lorentzians. This results in finite width of the modes, which along with the the band structure from different k_z-values causes the bound state peaks to appear largely unresolved. Some features are visible though: the bound state peak at $\rho = 0$ is displaced slightly from $E = 0$ to positive energies. This reflects the underlying particle-hole asymmetry of the vortex state. Close to the vortex line the lowest energy quasi-particle wavefunctions for a state with angular momentum quantum number m are $u_{nm}(\rho) \propto J_m(k_{nm}\rho)$ and $v_{nm}(\rho) \propto J_{m+1}(k_{nm+1}\rho)$, neglecting the axial part of the wavefunctions for the moment. Here J_m is the Bessel function of order m. A bound state peak corresponding to an energy $E = E_{nm}$ comes from quasi-particle wavefunctions $u_{nm}(\rho)$ and $v_{n-m-1}(\rho)$ as is seen from (3.82), since $-E_{nm} = E_{n-m-1}$ for the vortex (see Appendix E). Only the states u_{10} and v_{1-1} contribute to the peak at $\rho = 0$ in the LDOS, since only J_0 is finite at the origin. The peak corresponding to the energy state $E_{1-1} = -E_{10}$ is offset to finite ρ, as the wavefunctions for this state u_{1-1} and v_{10} both vanish on the vortex line.

The entire branch of core bound states gives rise to a fork-like ridge structure with energies approaching the bulk value of the gap as one moves further away from the vortex line. This is a spatial image of the spectrum in Fig. 5.8 since the localization of the bound states are correlated with their angular momentum; the states with higher angular momentum are peaked further from the origin. This is clearly displayed in Fig. 5.10, which is a contour plot of the LDOS. The plot also shows how the coherence peaks at $E = \pm\Delta_0$ grows as the bound state ridges approach the bulk value of the gap, and the spectral weight of the in-gap modes is depleted.

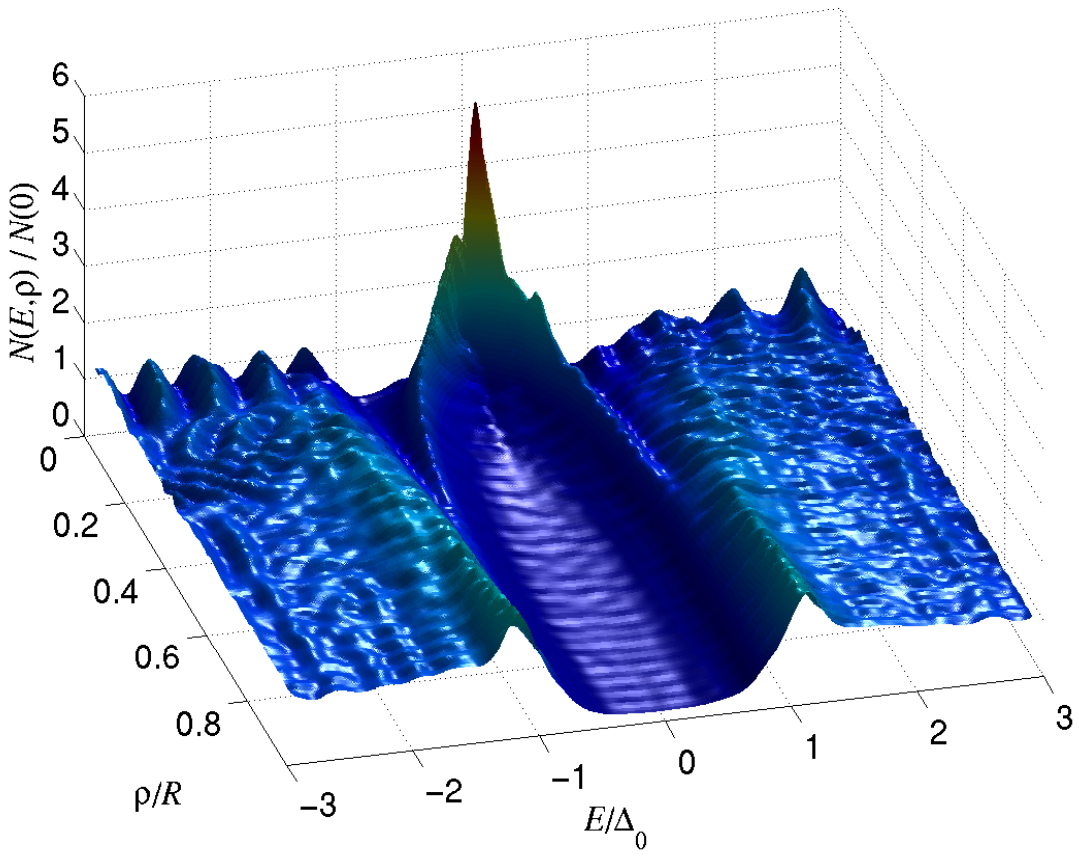

Figure 5.9: The local density of states around a vortex line normalized to the DOS in the normal state. The bound states in the vortex core are clearly visible as a largely unresolved peak structure at small ρ at energies inside the bulk gap. Further away from the vortex line the spectral structure reverts to that of a bulk Fermi superfluid.

The core bound states have been directly observed for vortices in superconductors using a Scanning-Tunneling Microscope (STM) with a spatial resolution smaller than the size of the vortex core [190, 191]. A number of theoretical papers using either a full, self-consistent solution of the BdG equations [192, 186], or more approximate methods [193, 194, 195] have found good agreement with

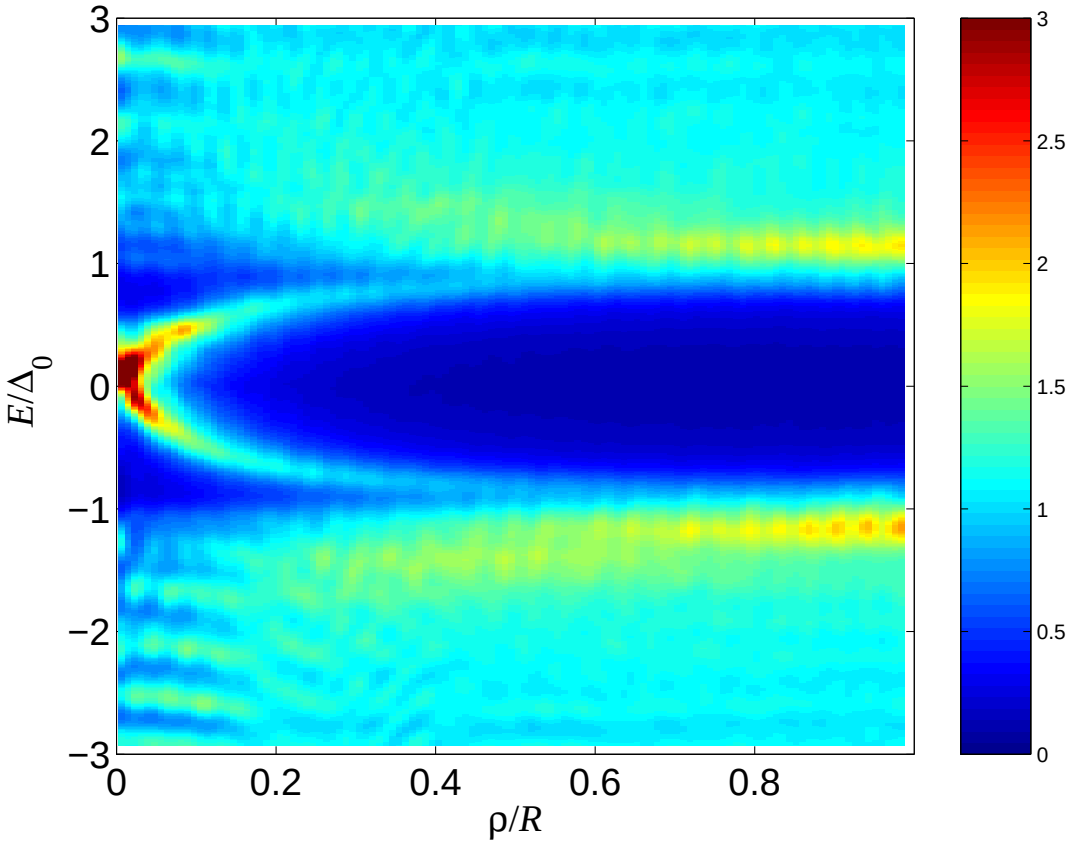

Figure 5.10: Contour plot of the LDOS. The bound state branches appear as a fork-like structure, and the evolution of the spectral gap and the coherence peaks with distance from the vortex line are evident.

the experiments. In Section 5.5 we discuss how these modes can be detected in an atomic gas sample using laser spectroscopy.

5.3.2 The Supercurrent

The vortex is of course characterized by a rotational mass current. In the absence of vorticity there is no net circular flow in the system. In this section we present a calculation of the current profile from a self-consistent solution of the BdG

equations for a vortex state. The current density is defined as

$$\mathbf{j}(\mathbf{r}) = \frac{i\hbar}{2m_a} \sum_{\sigma} \left\langle \hat{\psi}^{\dagger}_{\sigma}(\mathbf{r}) \nabla \hat{\psi}_{\sigma}(\mathbf{r}) - (\nabla \hat{\psi}^{\dagger}_{\sigma}(\mathbf{r})) \hat{\psi}_{\sigma}(\mathbf{r}) \right\rangle . \tag{5.22}$$

Because the superflow is rotational, only the tangential contribution is non-vanishing. By using the Bogoliubov-Valatin transformation (3.28) it can be written as

$$j_{\varphi}(\rho) = \frac{2\hbar}{m_a} \sum_{\eta} \left[\frac{m}{\rho} |u_{\eta}(\rho)|^2 f(E_{\eta}) - \frac{m+1}{\rho} |v_{\eta}(\rho)|^2 (1 - f(E_{\eta})) \right], \tag{5.23}$$

where the quasi-particle states are specified by $\eta = (n, m, k_z)$. Because of the suppression of superfluidity in the vortex core the current density must vanish there. As seen in Fig. 5.11 the current increases linearly towards a maximum located roughly at the edge of the vortex core. However there is no simple relationship between the location of the peak current density and the size of the vortex core (as determined by r_0).

The contributions to j_{φ} close to the vortex line comes almost entirely from the in-gap states. This explains the linear rise of the current density in that region: since single-particle wavefunctions proportional to J_0 do not contribute to the current (as seen from Eq. (5.23)), the behavior of $j_{\varphi}(\rho)$ for very small ρ is determined by core bound states with angular momentum $m \neq 1$. Due to the centrifugal barrier these must vanish like $\rho^{|m|}$ close to the vortex axis, giving rise to the linear current profile as $\rho \to 0$ [196].

Far away the vortex line where the superfluid density has healed to its bulk value the current is ($T = 0$):

$$j_{\varphi} \overset{\rho \to \infty}{\longrightarrow} -2n_{\sigma} v_s(\rho) = -\frac{\hbar n_{\sigma}}{m_a \rho} \tag{5.24}$$

reflecting the superfluid flow around the vortex.

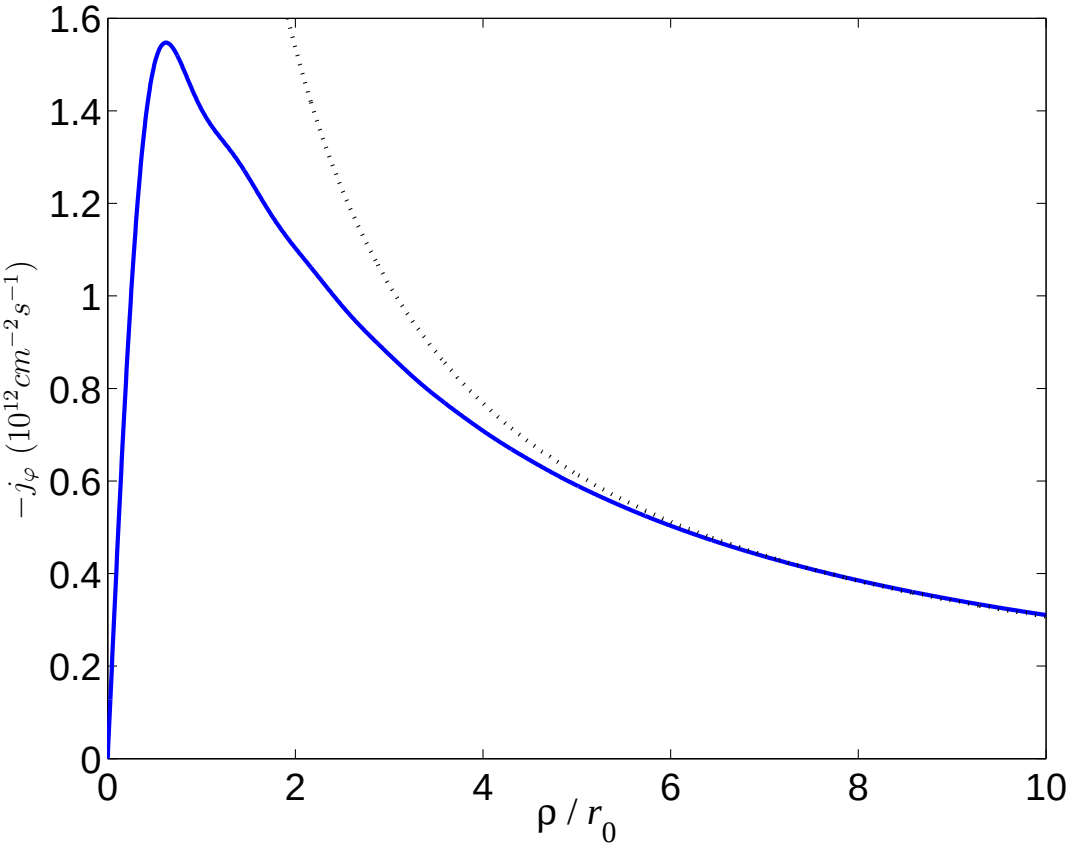

Figure 5.11: Current density near the vortex core (*blue line*) for $k_{\mathrm{F}}|a| = 0.59$ and $T = 0$. The dotted line is the asymptotic expression for the current (5.24). The distance from the vortex line is given in units of $r_0 = 0.42\xi_{\mathrm{BCS}}$, the characteristic length scale of the vortex core.

5.4 Thermodynamics

In this section, we present results for various thermodynamic quantities of the vortex phase obtained by solving the BdG equations numerically. All calculations were done for a fixed average particle number $N_\sigma = 28\,000$. It is necessary to keep N_σ fixed in the calculations in order to compare the thermodynamic quantities at different temperatures in a meaningful way. This is in contrast

with the calculation of the vortex energy presented above, where we sought an energy difference. In all runs the chemical potential was adjusted, such that relative deviation of N_σ from the desired value was less than 10^{-6}. The radius and length of the box were taken to be 28.5μm and 11.4μm, respectively. Using the ^{6}Li parameters, this gives a bulk value of the transition temperature $T_{c0} = 8e^{-2}\mu e^{-\pi/2k_{\rm F}|a|} = 0.01\mu$K, and a Fermi temperature of $T_F = 0.70\mu$K for the chosen density. Below we present results for the temperature variation of several thermodynamic quantities, comparing the case of a superfluid with a vortex (●'s) with those of a non-rotating superfluid (×'s), and a gas in the normal phase (♦'s).

A couple of things are worth noting. First there is no data point at $T = 0$ for the case of the Fermi gas in the normal state, since we have difficulty converging to a specific atom number for very low temperatures. This is a manifestation of shell structure in the system, due to the finite size of the container, which results in a discrete energy spectrum. The effect of this is the appearance of step-like features in $\mu(N)$, the chemical potential as a function of particle number [44, 48]. These steps are smoothed out by the pairing field, and by increasing the temperature. Secondly, the convergence of the numerical procedure for a superfluid state gets extremely slow when we approach the transition point T_c. The reason for this is the rapid variation with temperature of the pairing field (see Fig. 5.12). In this set of calculations we were able to reach a self-consistent superfluid solution for temperatures up to roughly $0.95T_c$. In order to push the upper temperature closer to T_c we would need to implement a more sophisticated convergence scheme. At temperatures above the transition point the self-consistent solution converges to $\Delta(\mathbf{r}) = 0$. The variation of the order parameter with temperature is illustrated in Fig. 5.12, where the vortex case is compared with that of a sta-

tionary superfluid in a cylinder. In both cases the plotted value of the pairing field is $\Delta(\rho = 0.8R)$. This ensures that in the vortex case the gap function has healed to its asymptotic value, while minimizing the effects due to the hard wall at $\rho = R$. For comparison we also plot the behavior of $\Delta_0(T)$ for a bulk superfluid. In this case the gap at a given temperature is found by solving (3.73) subject to the constraint that the particle number is fixed. This yields a universal curve for $\Delta_0(T)/\Delta_0$. In Fig. 5.12 all three curves have been normalized to their respective zero temperature values, and it is clear that at low temperatures the gap for the finite systems follow the universal curve nicely. However at larger temperature we do see deviations. These are largest for the vortex case, where the gap at $\rho = 0.8R$ is smaller then expected for a bulk system. We interpret in terms of the coherence length growing with increasing temperature (diverging as $T \to T_c$), hence at large temperatures the asymptotic value of the pairing field gets limited by the finite box size. As we shall see in Chapter 6 this leads to a shift of the transition temperature for the vortex case relative to that of the superfluid at rest.

The above-mentioned shell effects are visible in the low temperature behavior of the chemical potential in the normal state as shown in Fig. 5.13. Instead of the usual Sommerfeld form, according to which μ decreases like T^2 [197], the chemical potential increases at very small T. Such a behavior is characteristic of a system with a particle number just below one of the "magic numbers" needed to close a shell [44]. At higher temperatures $\mu(T)$ is well described by the Sommerfeld formula. As the chemical potential for the normal and superfluid states are identical at $T = T_c$, we expect on the basis of this plot a shift of the transition temperature due to the presence of the vortex. A detailed calculation

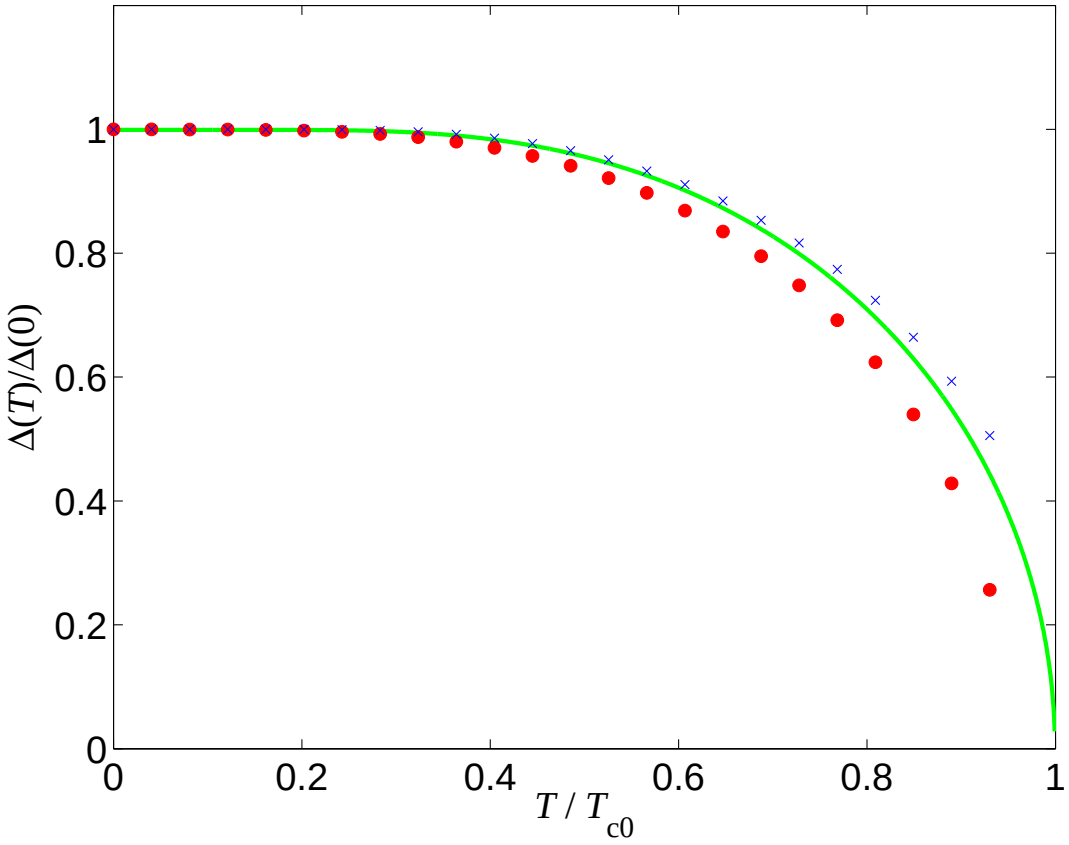

Figure 5.12: Plot of the temperature dependence of the order parameter for a superfluid Fermi gas with vortex (•'s) and with no vortex (×'s), compared with that of a bulk system (*green line*). All are normalized to their respective zero temperature values.

of this shift will be performed in Chapter 6, using a linearized version of the gap equation.

In figure 5.14 we plot the free energy $F = \langle \hat{H} \rangle - TS$ per particle as a function of the temperature T. Again, we have calculated this quantity for the vortex phase, the superfluid phase without a vortex, and for the normal phase. Both the condensation energy $F_n - F_s$, and the vortex energy $F_{s,v} - F_s$ are visible on

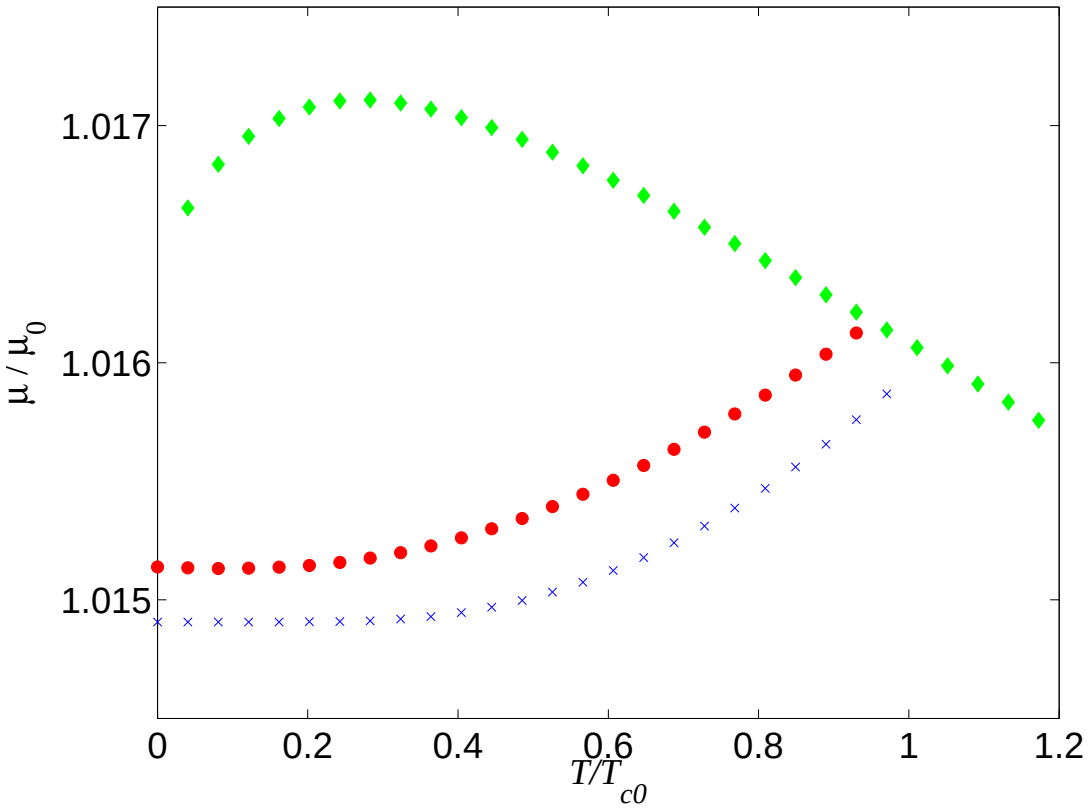

Figure 5.13: Chemical potential in the normal (♦'s), and superfluid phase with a vortex (•'s), and without (×'s) as determined by the constraint that $N_\sigma = 28000$. We attribute the low temperature behavior of the normal phase chemical potential to shell effects due to the finite volume [44]. For the vortex state the transition temperature is shifted downwards.

this scale. Both decrease as the temperature is increased towards T_{c0}, the bulk value of the phase transition temperature.

The temperature variation of the entropy is displayed in Fig. 5.15. The expression for the entropy in terms of the quasi-particle energies was given earlier in Eq. (3.42). Due to the energy gap the number of accessible states is suppressed for $T < T_c$, and correspondingly the entropy in the superfluid state

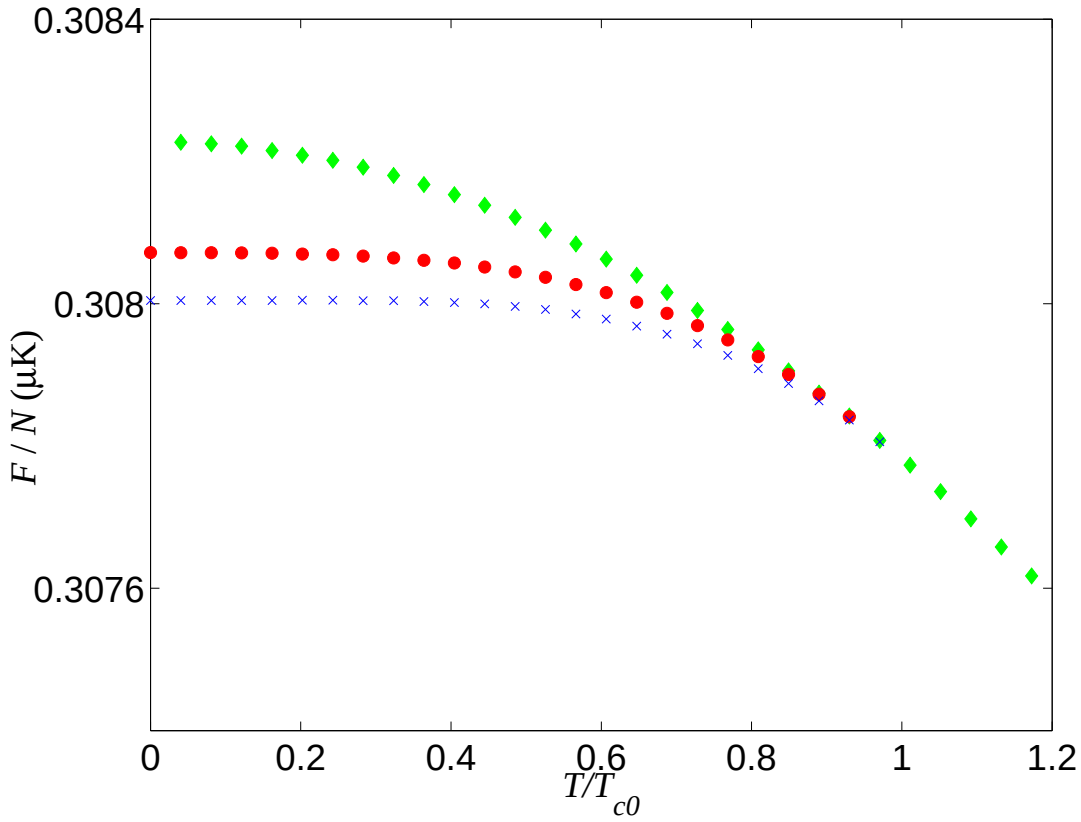

Figure 5.14: Plot of the free energy per particle in the normal, and superfluid phase with and without a vortex as a function of temperature.

(with and without a vortex) is lower than in the normal state. We have defined the quantity $\gamma = 2\pi^2 N(0) k_B^2/3$, which is the coefficient of the linear term in the low temperature heat capacity of a two-component gas in the normal phase: $c_{\rm V}^n = \gamma T$ for $T \to 0$.

The heat capacity per (fixed) unit volume is given by

$$c_{\rm V} = \frac{T}{V}\left(\frac{\partial S}{\partial T}\right)_V . \tag{5.25}$$

In Fig. 5.16 we plot this as a function of temperature. Again, we show for comparison results both for the system in the normal phase, in the superfluid phase

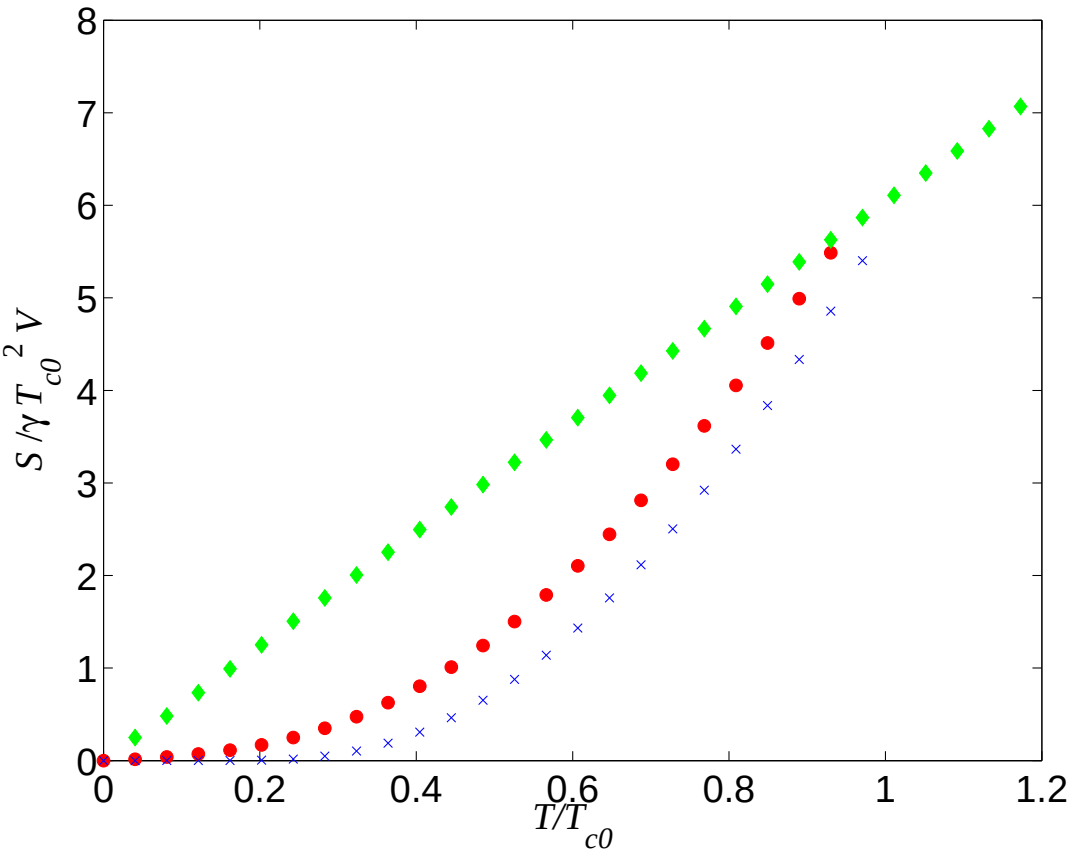

Figure 5.15: Temperature variation of the entropy per unit volume. The entropy in the superfluid state (with or without a vortex) is suppressed relative to the entropy in the normal state, reflecting the influence of pairing on the spectrum. Due to the low energy states in the core the vortex entropy is slightly higher than the that of the non-rotating superfluid.

without a vortex, and in the vortex phase. The heat capacity for the superfluid phase without the vortex is exponentially damped by a factor $\exp(-\beta\Delta_0)$ for $T \ll T_c$ due to the gap in the energy spectrum [27]. Figure 5.16 on the other hand shows that the heat capacity in vortex phase $c_{\rm V}^v$ depends linearly on T at low temperatures. This linear T-dependence is due to the presence of the bound

core modes in the vortex phase. The $T = 0$ density of vortex states per unit volume is calculated by integrating Eq. (5.21) over k_z which yields

$$N_v(\epsilon) = N(0)\alpha_1 \frac{\xi_{\rm BCS}^2}{R^2} \tag{5.26}$$

for $0 \ll \epsilon \ll \Delta_0$ where $\alpha_1 \sim \mathcal{O}(1)$ [145]. Thus, the density of bound core states per unit volume is the same, apart from a factor α_1, as that of a cylindrical region of a single component gas in the normal phase with radius $\xi_{\rm BCS}$ and length L. From this we conclude that the low T heat capacity per unit volume of the gas in vortex phase $c_{\rm V}^v$ associated with the core states is

$$c_{\rm V}^v \sim c_{\rm V}^n \alpha_1 \frac{\xi_{\rm BCS}^2}{R^2} \tag{5.27}$$

explaining the linear T-dependence of $c_{\rm V}^v$ observed in Fig. 5.16. A fit to the numerical data yields $\alpha_1 \simeq 2$. We remark that a linear contribution to the heat capacity has been observed for a superconductor in the mixed state [198]. The jump in the heat capacity at the transition temperature is characteristic of a second order phase transition.

We finally turn to the determination of the critical rotation frequency for thermodynamic stabilization of the vortex state. At finite temperature this is defined as

$$\Omega_c(T) = \frac{F_{sn} - F_s}{\langle L_z \rangle (T)}. \tag{5.28}$$

As we saw in Fig. 5.14 the free energy of the vortex state approach F_s as the the temperature is increased. However, as we raise T we are creating excitations out of the Cooper pair condensate, and these do not participate in the superfluid flow. Hence the angular momentum of the vortex state is also reduced with temperature. This is illustrated in Fig. 5.17, where the expectation value of L_z

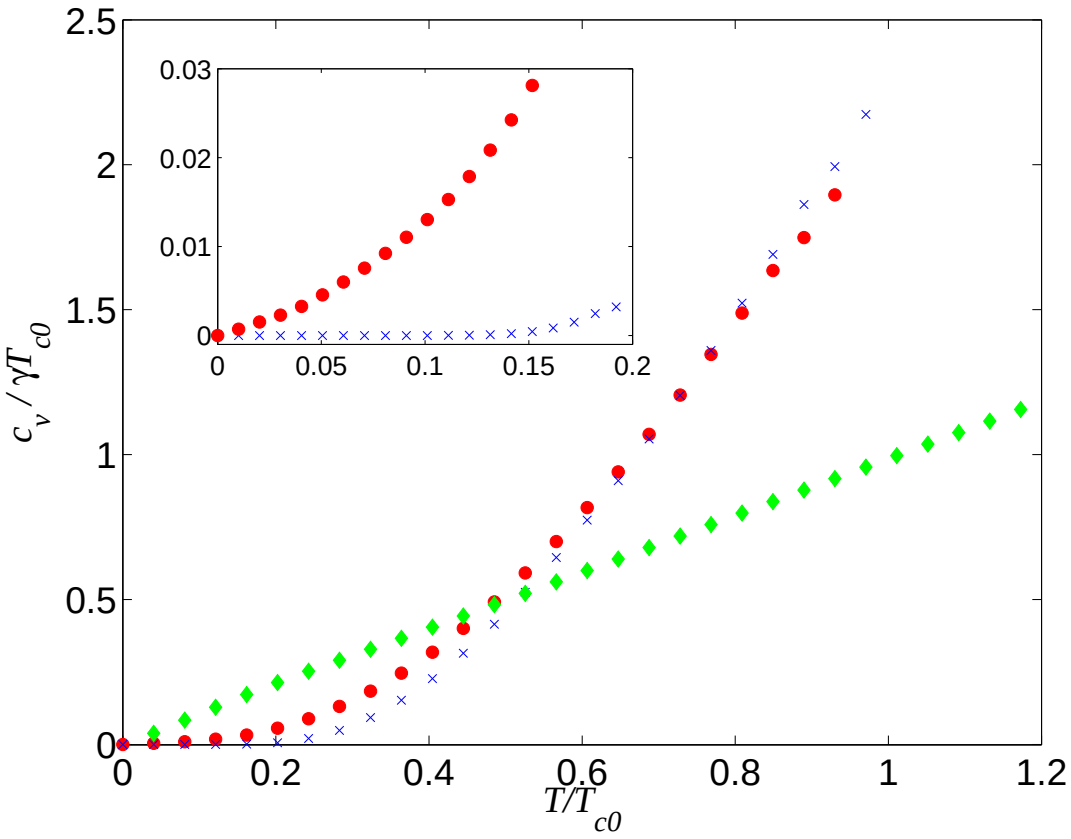

Figure 5.16: Plot of the specific heat in the normal, and superfluid phase with and without a vortex. The inset shows the low temperature behavior for the vortex state and the superfluid state without a vortex.

as calculated from our solution of the BdG equations is plotted as a function of temperature. Notice that the vortex angular momentum vanishes at a temperature lower than the bulk value of T_c, again indicating a shift in the transition temperature for the vortex state.

Fig. 5.18 shows the resulting temperature variation of Ω_c. We find that at temperatures close to the transition point the critical frequency strongly deviates from its zero temperature value. A similar behavior was found in theoretical studies of a trapped Bose gas [199, 172].

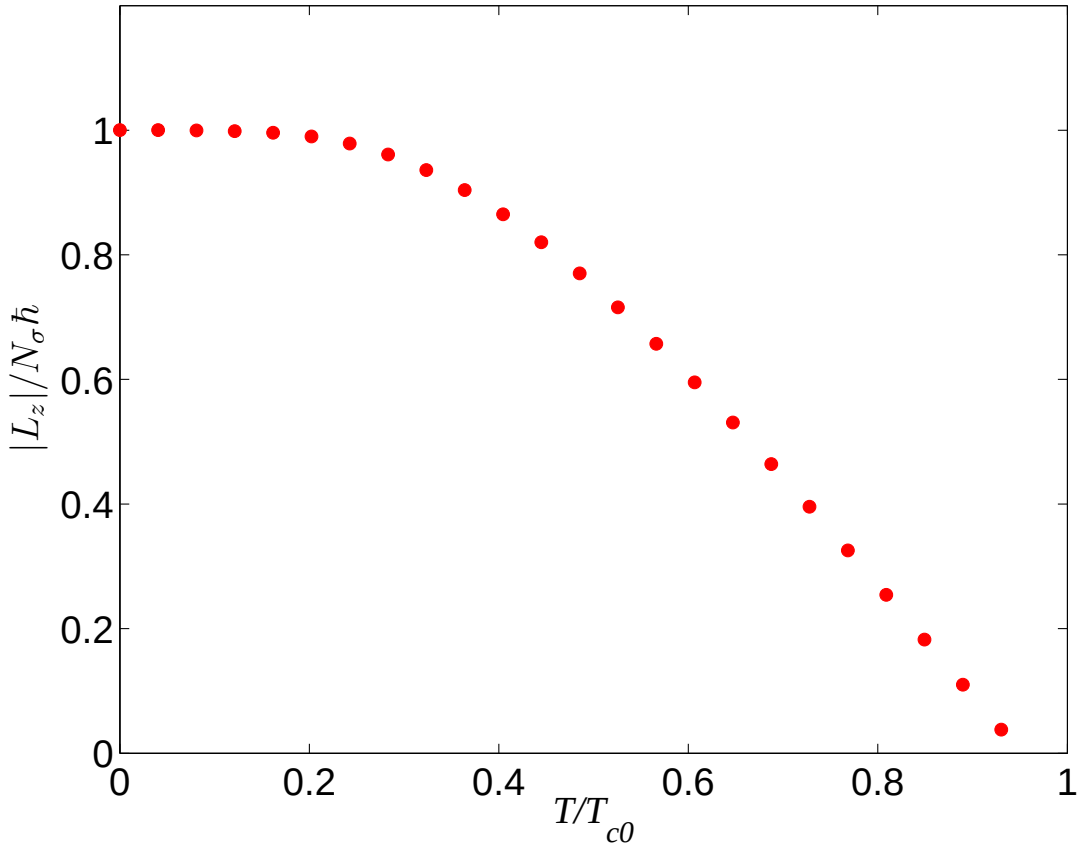

Figure 5.17: Angular momentum per particle of the vortex state as a function of temperature. The depletion of the superfluid condensate decreases $\langle L_z \rangle$, which vanishes at a temperature lower than the transition temperature for a bulk Fermi superfluid.

5.5 Imaging the Vortex

In superconductors the supercurrent carries charge, thus giving rise to a magnetic field associated with each vortex line. For this reason superconducting vortices are often referred to as magnetic flux tubes. The magnetic field can be measured using a Hall probe or a superconducting quantum interference device (SQUID) [77]. For an interesting application of these techniques see [200]. In

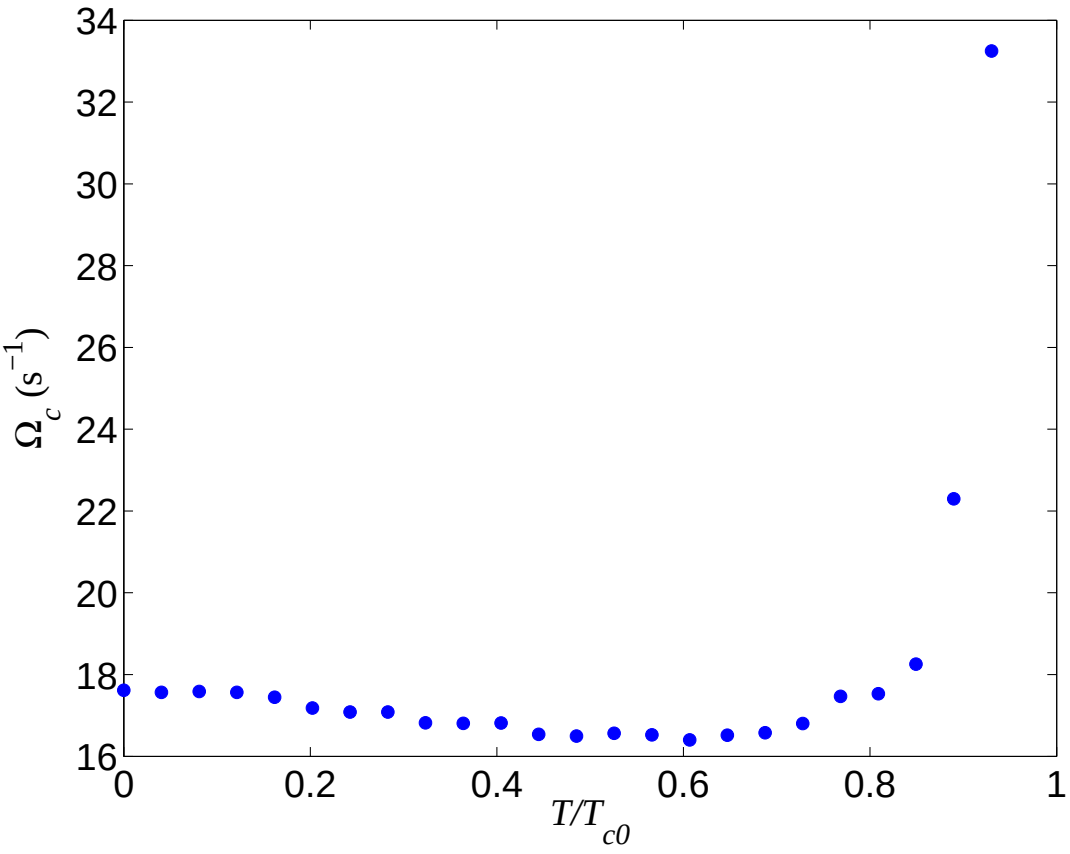

Figure 5.18: Temperature variation of the thermodynamic critical frequency for the vortex state in a cylinder.

liquid helium vortices have been photographed by exploiting their ability to trap ions in their cores [201]. The vortex cores in spinning Bose condensed gases can be directly viewed by photographing the atomic density distribution, where they show up as "holes". When the cloud is held in the trap the cores are too small to be detected, but if the gas is released from the trap and allowed to expand, the size of the cores increase, eventually exceeding the resolution limit of the imaging system [153, 154]. As is seen in Fig. 5.19 a similar direct imaging of the vortex cores may not be possible for a bulk superfluid Fermi gas. The figure illustrates

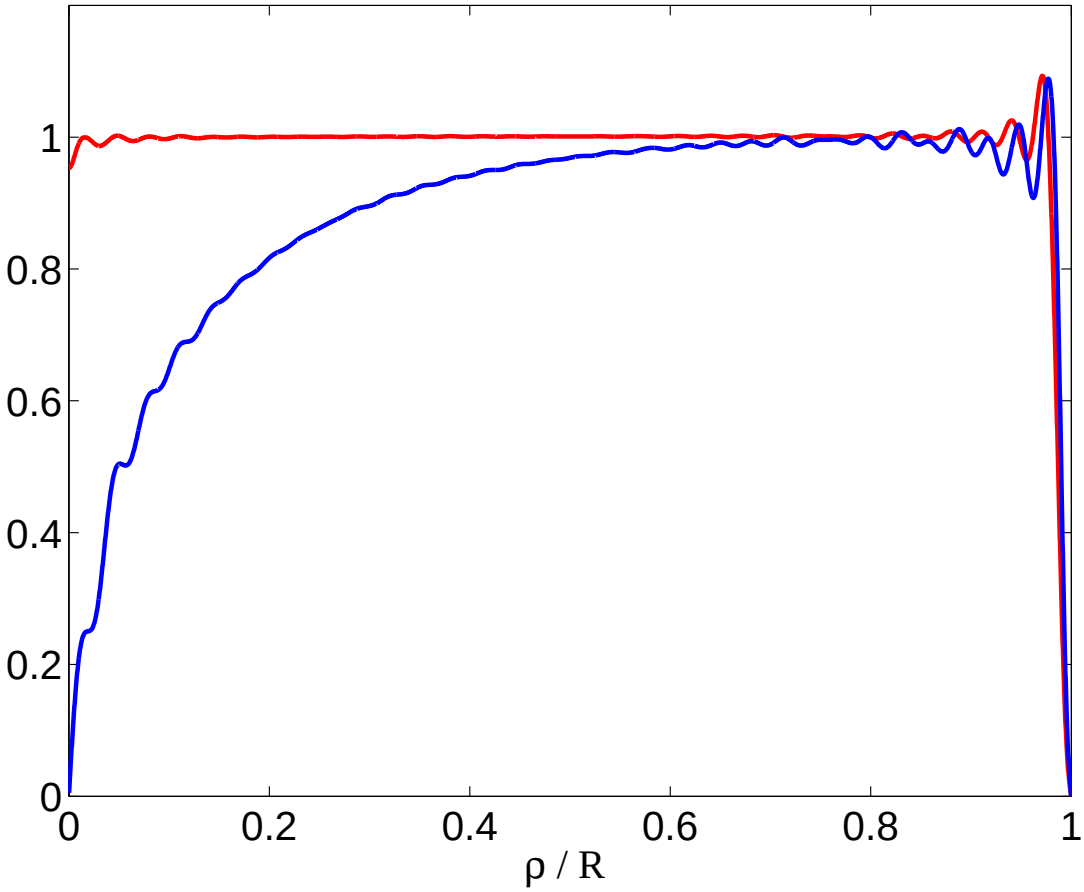

Figure 5.19: The atomic density (*red line*) and the pairing field (*blue line*) for a vortex, both normalized to their respective bulk values. The density distribution is almost unaffected by the vanishing of the order parameter in the core.

that the vortex line has virtually no effect on the particle density for a system in a cylindrical box. We thus conclude that in this system the presence of a vortex can not be inferred directly from probing the atomic density distribution. In the following we will describe alternative ways of probing the vortex state.

5.5.1 Laser Probing

In the present section, we investigate the feasibility of detecting the bound quasiparticle states in the vortex core through a recently proposed laser probing scheme [202, 203]. The laser probing scheme is similar to a STM measurement on a superconductor in that it relies on induced tunneling between a superfluid and a normal phase. Whereas a STM probe uses a bias voltage to transfer population across a superconducting-normal interface existing between the normal microscope tip and the superconducting substrate, the laser probe instead creates an effective interface by coupling different internal states of the atoms by laser fields. The presence of bound pair states in the superfluid can be detected as a shift of the resonance condition since the laser needs to break a pair to excite an atom. Specifically, a spin state $|\uparrow\rangle$, which is Cooper paired with the state $|\downarrow\rangle$ is coupled via a laser field to a third state $|e\rangle$ that has been chosen such that it does not participate in the pairing (either it does not have strong attractive interactions with the two other states or the disparity in chemical potentials is too large). This setup is shown schematically in Fig. 5.20. Hence, the $|e\rangle$ atoms define the normal part of the interface. If the detuning of the laser from the atomic transition is $\delta = \hbar(\omega_{\rm hf} - \omega_L)$, where ω_L is the laser frequency and $\omega_{\rm hf}$ the hyperfine splitting between the level $|\uparrow\rangle$ and $|e\rangle$, the Hamiltonian reads in the rotating-wave approximation

$$\hat{H} = \hat{H}_e + \hat{H}_{\uparrow\downarrow} + \frac{\delta}{2}\int d^3r\,\left[\hat{\psi}_e^\dagger(\mathbf{r})\hat{\psi}_e(\mathbf{r}) - \hat{\psi}_\uparrow^\dagger(\mathbf{r})\hat{\psi}_\uparrow(\mathbf{r})\right] + \hat{H}_T, \tag{5.29}$$

with the tunneling part of the Hamiltonian given by

$$\hat{H}_T = \int d^3r\,\left[\Omega(\mathbf{r})\hat{\psi}_e^\dagger\hat{\psi}_\uparrow + \Omega^*(\mathbf{r})\hat{\psi}_\uparrow^\dagger(\mathbf{r})\hat{\psi}_e(\mathbf{r})\right]. \tag{5.30}$$

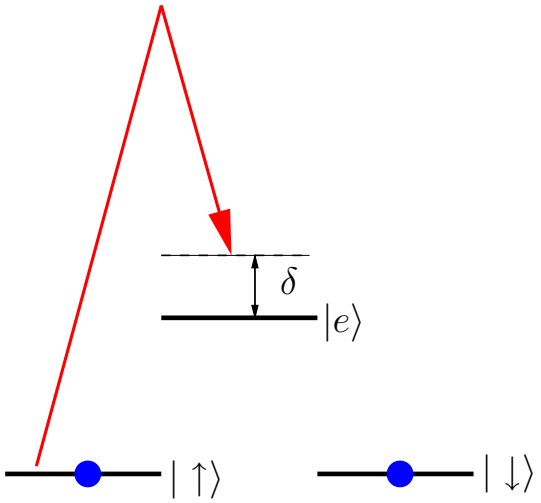

Figure 5.20: Laser probing of the pairing gap. Atoms in one of the Cooper paired states $|\uparrow\rangle$ and $|\downarrow\rangle$ are coupled to a third state $|e\rangle$ by a laser field with Rabi frequency Ω (*red*) detuned by δ from the atomic transition. The resonance condition is shifted due to the energy needed to break a pair.

Here the spatial profile and intensity of the laser field are contained in the Rabi frequency $\Omega(\mathbf{r})$, which has units of energy. For the ensuing analysis it does not matter if the population is transfered by a direct transition or through a Raman process, in which case the laser parameters should be considered as effective quantities. The mean-field Hamiltonian of the Cooper paired atoms in the BCS approximation is $\hat{H}_{\uparrow,\downarrow}$, and the dynamics of the atoms in the $|e\rangle$ state is described by $\hat{H}_e$

$$\hat{H}_e = \int d^3r\, \hat{\psi}_e^\dagger(\mathbf{r}) \mathcal{H}_e \hat{\psi}_e(\mathbf{r}). \tag{5.31}$$

The appropriate single-particle states for the state $|e\rangle$ are the eigenstates ϕ_n of the mean-field Hamiltonian

$$\mathcal{H}_e = -\frac{\hbar^2}{2m_a}\nabla^2 + V_{\mathrm{ext},e}(\mathbf{r}) + \sum_{\sigma=\uparrow,\downarrow} g_{e\sigma} n_\sigma(\mathbf{r}), \tag{5.32}$$

with energies given by $(\mathcal{H}_e - \mu_e)\phi_n = \xi_n \phi_n$. The chemical potential μ_e is determined from the constraint on the number of particles in $|e\rangle$:

$$N_e = \langle \hat{N}_e \rangle = \int d^3r \left\langle \hat{\psi}_e^\dagger(\mathbf{r}) \hat{\psi}_e(\mathbf{r}) \right\rangle . \tag{5.33}$$

We continue to take $\mu_\uparrow = \mu_\downarrow = \mu$. In the following we will neglect the influence of the Cooper paired states on the particles in the excited state and vice versa. That is we take $g_{e\uparrow} = g_{e\downarrow} = 0$. To go beyond this approximation we must solve self-consistently a set of three coupled equations; the BdG equations for the $|\uparrow\rangle$ and $|\downarrow\rangle$ atoms and a HF equation for the $|e\rangle$ state atoms.

We are interested in calculating the tunneling current, defined as the rate of change in the population of the $|e\rangle$ state. The current operator is defined such that the current is positive if there is a net flow of population from $|e\rangle$ to $|\uparrow\rangle$:

$$\hat{I} = -\dot{\hat{N}}_e = -\frac{1}{i\hbar}[\hat{N}_e, \hat{H}] = -\frac{1}{i\hbar}[\hat{N}_e, \hat{H}_T], \tag{5.34}$$

where the last equality arises because $\hat{H} - \hat{H}_T$ conserves the number of $|e\rangle$ atoms. The current is then given by

$$I(t) = -\langle \dot{\hat{N}}_e \rangle(t) = \frac{i}{\hbar} \int_0^t dt' \, \theta(t - t') \langle [\hat{H}_T(t'), \hat{I}(t)] \rangle. \tag{5.35}$$

This is is the observable of the proposed experiment. The population transfer can be measured either directly by resonance fluorescence, *i.e.* counting the number of atoms in state $|e\rangle$, or indirectly from the intensity difference between two Raman beams.

Provided the laser intensity is small a calculation treating the tunneling terms in the Hamiltonian perturbatively yields the current I as the linear response of the system to the laser coupling probe. The detail of this calculation were

given in [202, 203], and we shall not repeat them here. The result for a general inhomogeneous system is

$$\begin{aligned} I(\delta) = \; - \; & \frac{2\pi}{\hbar} \sum_{\eta,n} \Big\{ \left| \int d^3r \, \Omega(\mathbf{r}) u_\eta(\mathbf{r}) \phi_n^*(\mathbf{r}) \right|^2 [f(E_\eta) - f(\xi_n)] \, \delta(E_\eta - \xi_n - \tilde{\delta}) \\ + \; & \left| \int d^3r \, \Omega(\mathbf{r}) v_\eta^*(\mathbf{r}) \phi_n^*(\mathbf{r}) \right|^2 [1 - f(E_\eta) - f(\xi_n)] \\ & \times \delta(E_\eta + \xi_n + \tilde{\delta}) \Big\}. \end{aligned} \tag{5.36}$$

Here $\tilde{\delta} = \mu_e - \mu + \delta \equiv \Delta\mu + \delta$ is the effective detuning. In practical calculations the energy delta functions are replaced by Lorentzians of a finite width Γ as in Section 3.7. The first term corresponds to a current from the excited state into the condensate, it is proportional to $|u_\eta|^2$, the amplitude that a given Cooper pair state is unoccupied. The second term describes the current into $|e\rangle$, thus creating an unpaired quasi-particle excitation.

In the present analysis, we assume for simplicity that the $|e\rangle$ atoms are non-interacting such that their wavefunctions ϕ_n are the eigenstates of the confining cylindrical box. Furthermore, we consider the case of a constant laser profile $\Omega(\mathbf{r}) = \Omega$. Since, as we have seen, the system is quasi-homogeneous it makes sense to compare the numerical result for the current with that of a homogeneous gas. In that case we have the selection rule $\mathbf{k}_\uparrow = \mathbf{k}_e$ where $\mathbf{k}_\uparrow$ is the momentum of an $|\uparrow\rangle$ atom coupled by the laser beam to an $|e\rangle$ atom with momentum $\mathbf{k}_e$. If all the single-particle states are plane waves, the current given by Eq. (5.36) can be shown to be (at zero temperature) [202, 203]

$$I_0(\delta) = \pm \pi \Omega^2 N(\xi_{\mathbf{k}_0}) \, \Theta(\delta^2 - \Delta_0^2) \frac{\Delta_0^2}{\delta^2}, \tag{5.37}$$

where $\pm$ corresponds to $\delta > 0$ and $\delta < 0$ respectively and $N(\xi_{k_0})$ is the density of states of the $|e\rangle$ atoms at the energy which satisfies the energy conservation

condition $E_{\mathbf{k}_0} \pm \xi_{\mathbf{k}_0} \pm \tilde{\delta} = 0$:

$$N(\xi_{\mathbf{k}_0}) = \frac{V m_a k_0}{2\pi^2 \hbar^2} = \frac{V}{2\pi^2} \left(\frac{m_a}{\hbar^2}\right)^{3/2} \sqrt{\frac{\Delta_0^2 - \delta^2}{\delta} + 2\mu}. \tag{5.38}$$

It is instructive to analyze (5.37) in the limit where the chemical potentials are equal $\mu_e = \mu$. In that case one obtains for the current

$$I_0(\delta) = -\frac{\pi\Omega^2}{\hbar} \left(\frac{\Delta_0}{\delta}\right)^2 N(\xi_{\mathbf{k}_0}) \left[\Theta(-\delta - \Delta_0) - \Theta(\delta - \Delta_0)\right]. \tag{5.39}$$

Here the first step function corresponds to tunneling from the state $|\uparrow\rangle$ to $|e\rangle$ ($\delta < 0$). Since the atoms in $|\uparrow\rangle$ are Cooper paired this process requires an additional energy Δ_0 to break a pair. Hence the laser must provide an energy $\hbar\omega_L = \hbar\omega + \Delta_0$, or $\delta = -\Delta_0$. The reverse process, tunneling into the condensate, also has a sharp energy onset at $\delta = \Delta_0$, since a single atom entering the superfluid becomes a quasi-particle excitation with a minimum energy of Δ_0. This is embodied in the second step function. When $|\delta|$ is increased beyond Δ_0 one is probing states away from the Fermi surface, where the density of Cooper pairs is reduced, correspondingly this decreases the tunneling current.

Let us now consider how the laser probing method can be used to probe the presence of the core states. We examine two opposite cases of interest (see Fig. 5.21): The case when there are initially no $|e\rangle$ atoms present ($N_e = 0$) and the case where there initially are an equal number of $|\uparrow\rangle$ and $|e\rangle$ atoms present ($N_\uparrow = N_e$, *i.e.* $\mu_e = \mu$). The response to the laser probe when the $|\uparrow\rangle$ atoms are in the normal state differs dramatically in these two different situations. If the state $|e\rangle$ is initially empty the current is simply a Lorentzian of width Γ centered at zero detuning, *i.e.* the current flows when the laser is tuned on the atomic resonance. The peak height is determined by the number of atoms in state $|\uparrow\rangle$. In contrast, when $N_e = N_\uparrow$ and both are in the normal state the selection rule

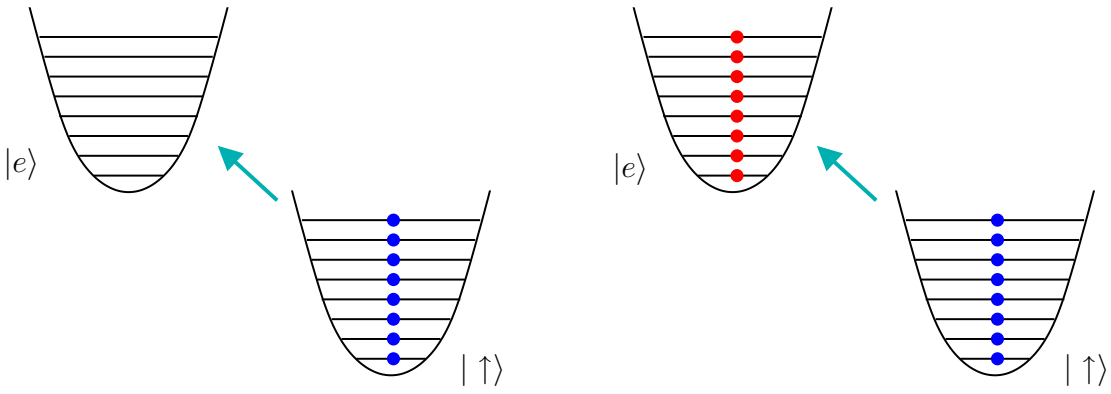

Figure 5.21: We consider a laser probing experiment under two different conditions: either the excited state contain no atoms initially, $\mu_e = 0$ (*left*), or it has a filled Fermi sea with $\mu_e = \mu$ (*right*).

along with the filled Fermi sea means that all low-lying transitions are Pauli blocked, causing a substantial reduction of the current.

From Eq. (5.36) it is straightforward to show that for the total current we have $\int d\delta I(\delta) \propto N_e - N_\uparrow$. We demonstrate this explicitly in Appendix F. That is, the net current from the $|e\rangle$ atoms to the $|\uparrow\rangle$ atoms is proportional to the difference of initial populations between the two spin states. This sum rule states that the area under the current curve is conserved, regardless of the state of the atoms in $|\uparrow\rangle$. Likewise, the total current from the core states trapped inside the vortex is clearly proportional to the total number of core states $N_{\rm cs}$. Thus, when there initially are no $|e\rangle$ atoms present ($N_e = 0$) the spectral weight of the current due the core states as compared to the total current observed scales as $N_{\rm cs}/N_\uparrow$. Using $N_{\rm cs} \sim N_v \Delta_0 \pi R^2 L$ with N_v given by Eq. (5.26), one obtains that the current from the core states divided by the total current scales as $\Delta_0 E_{\rm F}^{-1} \xi_{\rm BCS}^2 R^{-2} \ll 1$. Thus, the signal from the core states is completely overwhelmed by the bulk signal coming from the current out of the whole Fermi

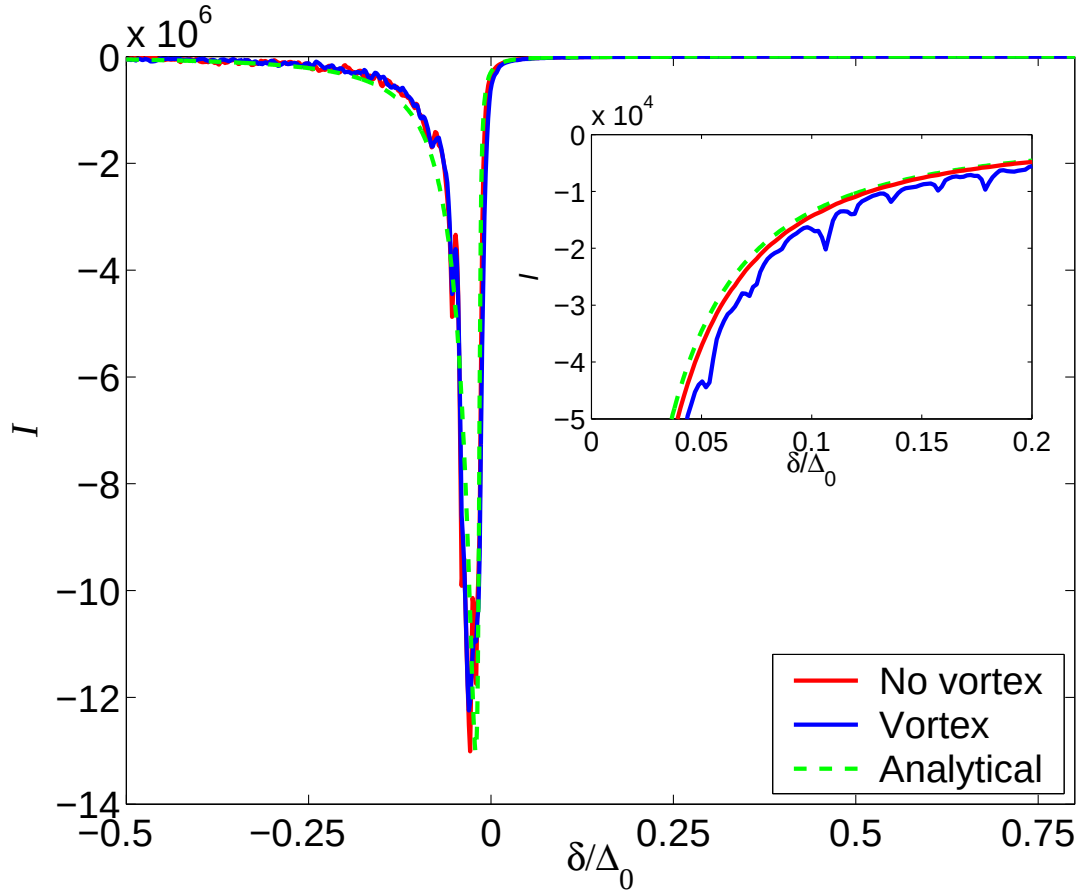

Figure 5.22: The zero temperature current when tunneling into an empty state ($N_e = 0$). The vortex signal (*blue*) is virtually indistinguishable from that of the superfluid with no vortex (*red*), except for very small deviations at small detunings (see inset). The dashed green line gives the analytical expression for the current in a homogeneous system with no vortex (5.37).

sea of $|\uparrow\rangle$ atoms. We therefore conclude that it is most likely not possible to probe the core states starting with initially no $|e\rangle$ present. This conclusion is supported by numerical simulations, as shown in Fig. 5.22. We note that the superfluidity of the system does show up clearly though, as an asymmetry in the peak, which is also displaced to negative detunings.

Let us therefore consider the case when there initially are an equal number of $|\uparrow\rangle$ and $|e\rangle$ atoms present ($N_\uparrow = N_e$). In that way, the bulk signal of transitions of $|\uparrow\rangle$ atoms deep within the Fermi sea is Pauli blocked due to the presence of the $|e\rangle$ atoms since we have the selection rule $\mathbf{k}_\uparrow = \mathbf{k}_e$. One can then show from Eq. (5.36) that the total signal scales as $\int d\delta |I(\delta)| \propto N_\uparrow \Delta_0 / E_\mathrm{F}$, i.e. the current is proportional to the total number of Cooper pairs. Thus, the bulk signal is suppressed by a factor Δ_0/E_F compared to the case when there are no $|e\rangle$ atoms present simply due to the Fermi blocking effect. The current due to the vortex core states should therefore be easier to observe as it is not overwhelmed by a huge background signal. In Fig. 5.23 we plot the $T = 0$ laser probing current $I(\delta)$ for the case when $N_e = N_\uparrow$. The effect of the Hartree field gn_σ is primarily to shift the entire profile to lower detunings δ since it shifts the energies of the $|\uparrow\rangle$ atoms by the amount gn_σ whereas the $|e\rangle$ atoms are assumed non-interacting. In the plot we have explicitly eliminated this overall shift for reasons of clarity. We plot the current both when there is no vortex present and when there is a vortex.

Equation (5.37) is also shown on Fig. 5.23 and we see good agreement with the numerical result when there is no vortex present. Note that since the numerical calculations use a Lorentzian of width $\Gamma = 0.01\Delta_0$ instead of $\delta(x)$ functions in Eq. (5.36), we have convoluted Eq. (5.37) accordingly

$$I_0^\mathrm{conv}(\delta) = \int_{-\infty}^{\infty} dy\, I_0(y) \frac{\Gamma/2}{(\delta - y)^2 + \Gamma^2/4}. \tag{5.40}$$

We see that the signal when there is a vortex present is markedly different from the case with no vortex. In particular, there is a significant current for $|\delta| < \Delta_0$. This current is directly due to the presence of the core states which have a pairing energy less than Δ_0. The signal from the vortex phase is finite for $\delta \sim 0$

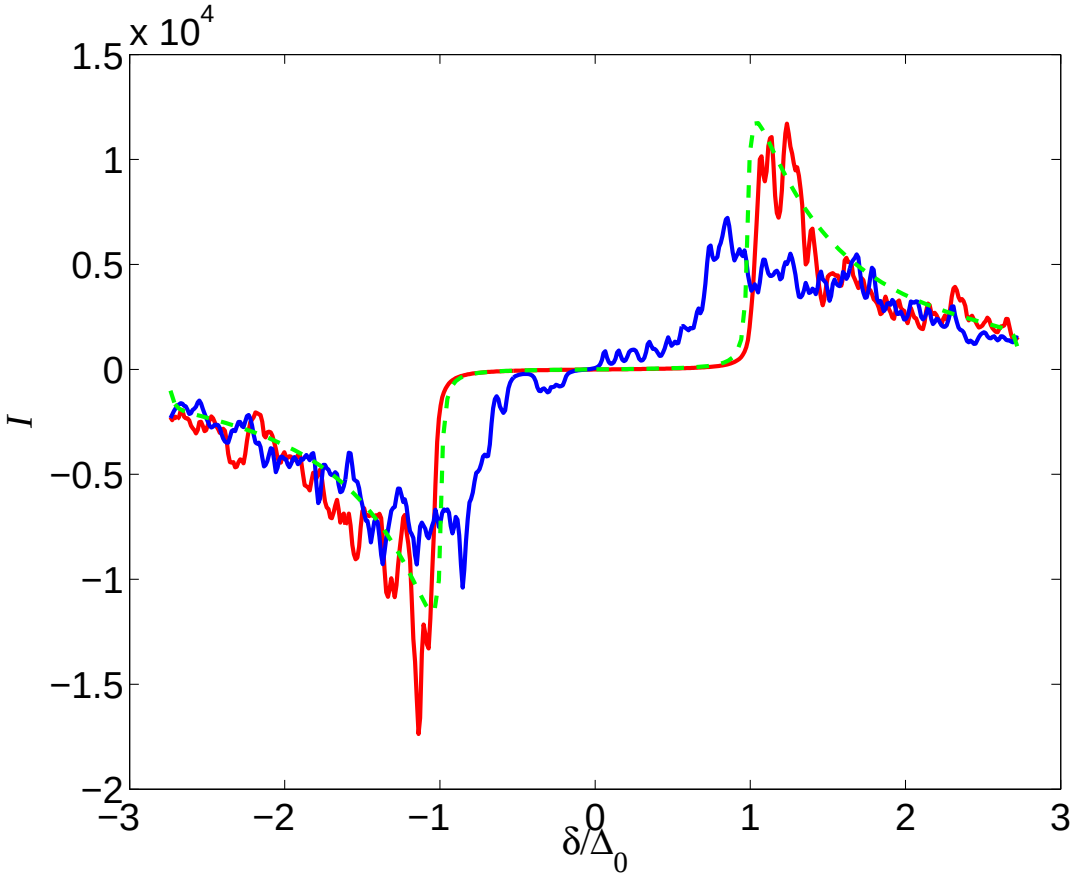

Figure 5.23: The tunneling current as a function of detuning (in units of the bulk value of the gap) for tunneling into filled state from both a vortex state (*blue line*) and a superfluid without a vortex (*red line*). For comparison Eq. (5.40) is also plotted (*dashed green line*). The profiles have been shifted to compensate for the Hartree mean field shift gn_σ of the energies of the $|\uparrow\rangle$ atoms. If the $|\uparrow\rangle$ atoms are in the normal state no current flows due to Pauli blocking.

reflecting the fact that the energy spectrum of the core states approximately given by Eq. (5.21) is gapless. Thus, the existence of core states bound in the vortex is reflected in the current profile $I(\delta)$. From the area under the current curve in the detuning interval $[-\Delta_0, 0]$ we conclude that the vortex core contains ≈ 500 particles for the parameters chosen here.

We conclude that the laser probing scheme experimentally gives the possibility of probing the core states directly. This is a very appealing prospect as the precise interpretation of analogous STM experiments in solid state superconductors probing the core states [190, 191] is complicated by the fact that the underlying microscopic interaction between the electrons forming the Cooper pairs is less straightforward [186, 204]. The atomic gas systems therefore in principle give the possibility of measuring in a cleaner way the predicted presence of vortex core excitations - a prediction which is an important piece in the microscopic theory of superfluid vortices.

In the present context we have not discussed the effect of focusing the laser probe on different regions of the cloud. If experimentally feasible this would allow a direct mapping of the spatial profile of the gap function, in essence probing the structure of LDOS.

5.5.2 Other Probes

The quantized currents, and therefore the presence of superfluidity, can possibly be detected using at least three alternative approaches. One of these is the collective mode spectrum. When no vortex is present, excitations carrying equal and opposite angular momentum along the z-axis are degenerate in energy. The vortex currents lift this degeneracy since the rotational symmetry is removed.

The resultant splitting of the surface modes is proportional to the angular momentum of the gas [183, 205, 206, 207, 208]. This technique has been used to infer the presence of a vortex in a trapped BEC [209]. A second approach was demonstrated in a recent experiment where the precession rate of the scissors oscillation mode was used to measure the quantized angular momentum per particle with great accuracy [210, 211]. A third method is spatially selective Bragg scattering; the superfluid currents modify the Bragg momentum conservation conditions, giving rise to a strongly anisotropic outcoupled atomic beam [212].

5.6 Vortex Structure in a Harmonic Trap

Most experiments on quantum gases are conducted in traps with harmonic confinement in all directions. While we have modeled a superfluid Fermi gas in an isotropic harmonic oscillator potential in Chapter 3, studying the microscopic structure of a vortex in such a trap configuration using the BdG equations would require solving the self-consistent eigenvalue problem in effectively two dimensions, since the vortex breaks the rotational symmetry. This is much more demanding than the effectively one dimensional numerical problem we are tackling in this thesis. However, Randall Hulet's group at Rice University conducts experiments on ultracold fermions using an optical trap with a unique geometry. A focused red-detuned laser beam confines the cloud radially in a potential, which is approximately harmonic, with a frequency of $\omega \sim 2\pi \times 800$ Hz. The axial confinement is provided by a pair of blue-detuned capping lasers. These give rise to an extremely elongated box-like potential in the axial direction, with a length of 480 μm, compared with the radial oscillator length $d_{\rm osc} = 1.4$ μm [213, 96].

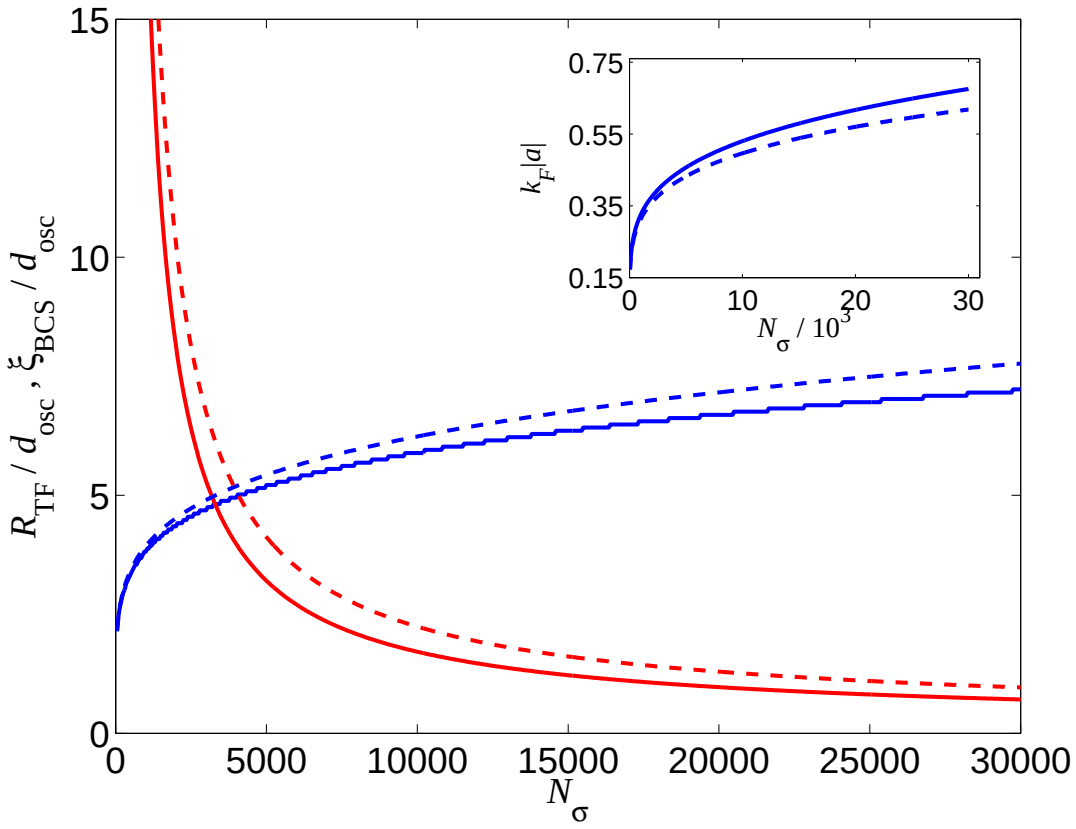

Figure 5.24: Thomas-Fermi radius (*blue line*) and BCS coherence length (*red line*) of as a function of atom number for a Fermi gas in a harmonic trap with an axial box potential. The boxlength is $L = 50\ d_{\rm osc}$. The dashed lines give the same quantities, when the Hartree field is neglected. The inset shows the value of $k_{\rm F}|a|$ on the symmetry axis.

Should a vortex be created along the symmetry axis of this potential it would correspond exactly to the situation described here. The only difference is that we use periodic boundary conditions along the vortex axis, but for a sufficiently long cylinder this should be of no consequence. In the calculations presented here we take the length of the cylinder to be $L = 50\ d_{\rm osc}$, and the coupling strength to be $g = -1\ \hbar\omega d_{\rm osc}^3$.

As we have seen the size of the core of a singly quantized vortex in a bulk Fermi superfluid is determined by the BCS coherence length ξ_{BCS}. A necessary condition for the stability of the vortex is that this length scale is much smaller than the spatial extent of the cloud in the radial direction. The latter can be estimated in a LDA calculation as the point where the density vanishes, this is known as the Thomas-Fermi radius of the cloud R_{TF}. We plot in Fig. 5.24 the coherence length in the center of the trap and R_{TF} as determined in the LDA as a function of the particle number N_σ. For comparison the same quantities calculated when neglecting the Hartree field are also shown. We see that the vortex is only stable, when the number of atoms is large. In numerical calculations this is manifested by the failure to achieve a converged vortex solution with a non-vanishing order parameter for small N_σ. As is seen from the inset in Fig. 5.24 this means that we are necessarily at the limit of the dilute gas regime for which $k_{\mathrm{F}}|a| \ll 1$. Hence the results presented here should in some sense only be considered qualitative. As $k_{\mathrm{F}}|a|$ approaches one, a more sophisticated theory to account for effects beyond our mean-field picture is needed to produce quantitative predictions. However, we expect the main conclusions of this section to remain valid when strong coupling effects are treated properly.

Our calculation of the gap function corresponding to a self-consistent numerical solution of the BdG equations is plotted in Fig. 5.25 for 50 000 atoms in each spin state, corresponding to a chemical potential of $\mu = 30.8\ \hbar\omega$. The profile of the pairing field for a vortex state is compared with that of a superfluid in the ground state. We observe that as the the case of a Fermi superfluid in a cylindrical box the vortex order parameter is suppressed in a core region with a size on the order of the BCS coherence length (for this system $\xi_{\mathrm{BCS}} = 0.5\ d_{\mathrm{osc}}$).

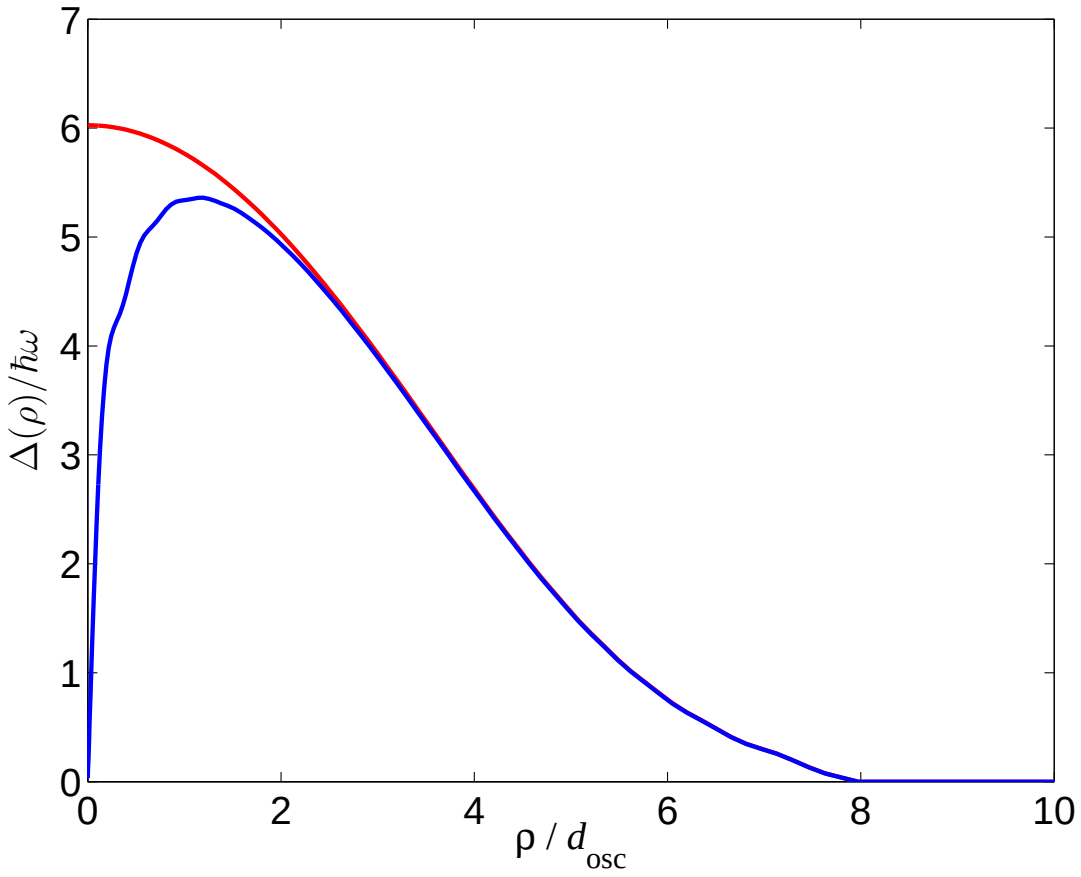

Figure 5.25: Gap function in cylinder with radial confinement. The particle number is $N_\sigma = 50\,000$, and the length of the axial box is $L = 50\ d_{\rm osc}$, with $d_{\rm osc} = 1.4\ \mu$m. The blue line gives $\Delta(\mathbf{r})$ for the vortex state, while the red line shows the order parameter when no vortex is present.

Far away from the vortex core the order parameter coincides with that of a system with no vortex. The the shape of the pairing field profile from this microscopic calculation at zero temperature closely resembles that of the solution of the Ginzburg-Landau equations at temperatures $T \sim T_c$, as presented in [214].

The density distribution is portrayed in Fig. 5.26 for both the vortex state and the superfluid in the ground state. For the parameters chosen here the

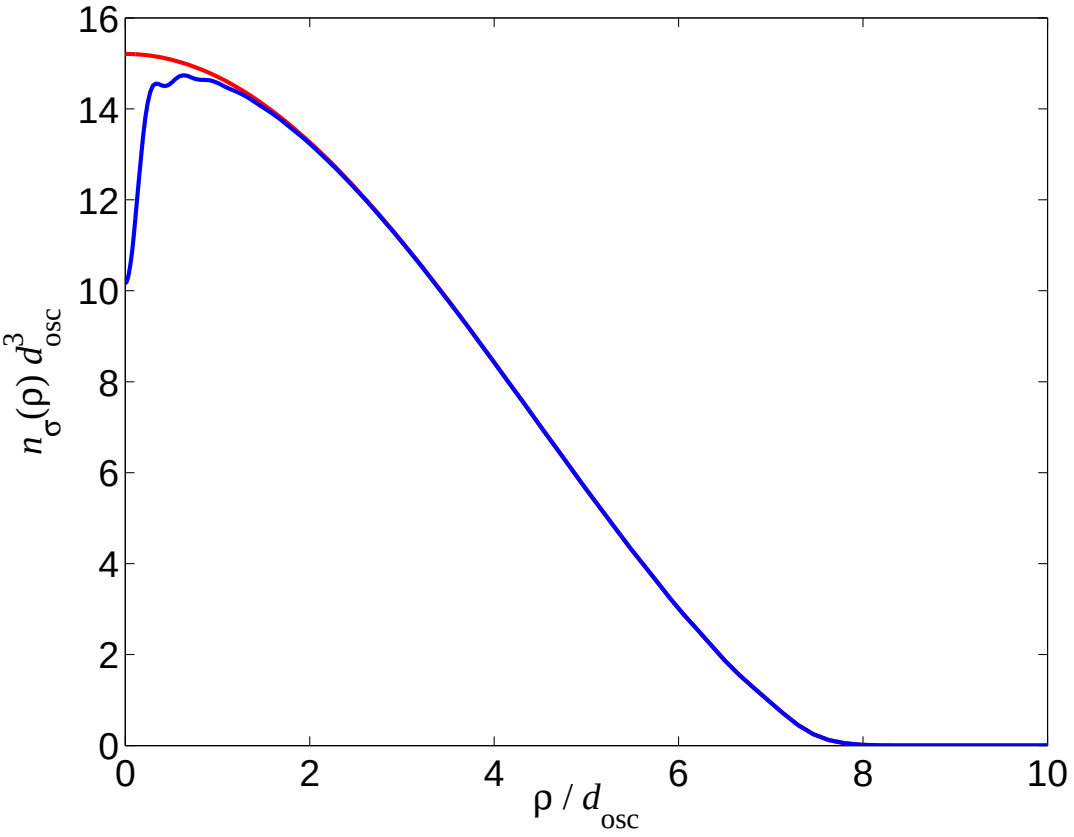

Figure 5.26: Density profile in a cylinder with radial confinement. The parameters are the same as in Fig. 5.25. Again the vortex state is indicated by the blue line, and the density of the superfluid with no vortex is shown by the red line. For the chosen parameters we see a significant (observable) reduction of the atomic density in the core region.

density in the vortex core is reduced by $\sim 30\%$ from the peak density without a vortex. This large reduction is due to the high value of $k_{\rm F}|a| = 0.76$ at $\rho = 0$. If the particle number is reduced the contrast of the density depression in the core is reduced as shown in Fig. 5.27. Furthermore, the dip fills in as the temperature is increased, eventually vanishing completely at $T = T_c$.

However, we conclude from the present analysis (with the caveat discussed

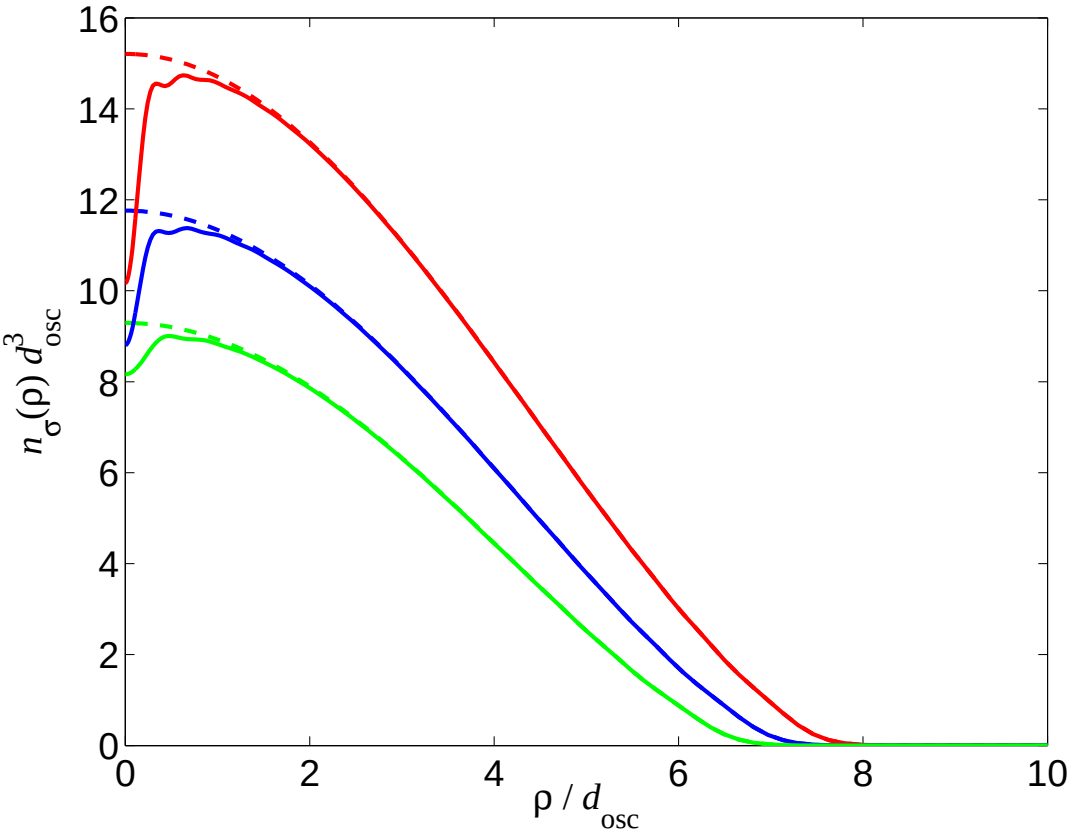

Figure 5.27: Variation of the density distribution for a Fermi superfluid with particle number. The solid lines give the atomic density for a vortex state, whereas as the dashed curves are the densities of a Fermi superfluid with no vortex, but with the same number of particles. The particle number are: $N_\sigma \simeq$ 51 000 (*red*), 35 000 (*blue*), and 25 000 (*green*). As the number of particles is reduced the suppression of the vortex core atomic density gradually vanishes.

above) that direct observation of the core of a vortex in a Fermi superfluid *may* be possible in the limit of a large condensate.

Chapter 6

Transition Temperature

In Chapter 3 we derived the gap equation for a superfluid Fermi gas. In the special case of a homogeneous system, or within a LDA calculation, the temperature at which the pairing field vanishes everywhere was determined analytically. However, the solution of the full set of self-consistent equations in the vicinity of T_c is impaired by the slow convergence of the numerical scheme near the transition point. In this chapter we use a different strategy to determine the transition temperature of the gas, exploiting that close to T_c the gap function is small, and therefore may be treated as a perturbation on the normal state wavefunctions. This approach results in a linearization of the non-linear set of BdG equations, and the resulting integral gap equation can be solved effectively to find the transition temperature.

6.1 Linearizing the Gap Equation

Our starting point is the BdG equations for the quasi-particle amplitudes $u_\eta(\mathbf{r})$ and $v_\eta(\mathbf{r})$ (3.36), and the self-consistency relations for the atomic density (3.38), and the pairing field (3.39). We assume that the system is close to the transition

point such that $\Delta(\mathbf{r})$ is small and can be treated as a perturbation. That is we write the quasi-particle amplitudes in terms of a perturbation expansion

$$\begin{aligned} u_\eta(\mathbf{r}) &= u_\eta^0(\mathbf{r}) + u_\eta^1(\mathbf{r}) + \dots \\ v_\eta(\mathbf{r}) &= v_\eta^0(\mathbf{r}) + v_\eta^1(\mathbf{r}) + \dots \end{aligned} \tag{6.1}$$

where the zeroth order terms correspond to a state where $\Delta(\mathbf{r}) = 0$. In this normal (non-superfluid) state the quasi-particle states correspond to either particle or hole states

$$\begin{aligned} u_\eta^0(\mathbf{r}) &= \phi_\eta(\mathbf{r}), \quad v_\eta^0(\mathbf{r}) = 0 \quad (\xi_\eta > 0) \\ u_\eta^0(\mathbf{r}) &= 0, \quad v_\eta^0(\mathbf{r}) = \phi_\eta^*(\mathbf{r}) \quad (\xi_\eta < 0), \end{aligned} \tag{6.2}$$

which are solutions of a single-particle mean-field equation

$$\mathcal{L}(\mathbf{r})\phi_\eta(\mathbf{r}) = \left[-\frac{\hbar^2}{2m_a}\nabla^2 + V_{\text{ext}}(\mathbf{r}) + g n_\sigma(\mathbf{r}) - \mu \right] \phi_\eta(\mathbf{r}) = \xi_\eta \phi_\eta(\mathbf{r}). \tag{6.3}$$

As usual we are assuming equal population of both spin states. We point out that since the eigenvalues of the BdG equations are manifestly positive, we must have $E_\eta^0 = |\xi_\eta|$ (*c.f.* the discussion in Section 3.3). As u_η^0 and v_η^0 are never finite simultaneously we find that $\Delta^0 = 0$ as expected. To get the first order expression for $\Delta(\mathbf{r})$ we write the quasi-particle amplitudes to first order as

$$\begin{aligned} u_\eta^1(\mathbf{r}) &= \sum_\nu a_{\eta\nu}\phi_\nu(\mathbf{r}), \\ v_\eta^1(\mathbf{r}) &= \sum_\nu b_{\eta\nu}\phi_\nu^*(\mathbf{r}). \end{aligned} \tag{6.4}$$

To first order the BdG equations become

$$\mathcal{L}u_\eta^1(\mathbf{r}) + \Delta^1(\mathbf{r})v_\eta^0(\mathbf{r}) = E_\eta^0 u_\eta^1(\mathbf{r}), \tag{6.5}$$

$$-\mathcal{L}v_\eta^1(\mathbf{r}) + \Delta^{1*}(\mathbf{r})u_\eta^0(\mathbf{r}) = E_\eta^0 v_\eta^1(\mathbf{r}). \tag{6.6}$$

Multiplying (6.5) by $\phi_\nu^*(\mathbf{r})$, and (6.6) by $\phi_\nu(\mathbf{r})$ and integrating over $d^3\mathbf{r}$ we obtain the equations determining the expansion coefficients:

$$\begin{aligned}(E_\eta^0 - \xi_\nu)a_{\eta\nu} &= \int d^3r'\,\Delta(\mathbf{r}')\phi_\nu^*(\mathbf{r}')v_\eta^0(\mathbf{r}'),\\ (E_\eta^0 + \xi_\nu)b_{\eta\nu} &= \int d^3r'\,\Delta^*(\mathbf{r}')\phi_\nu(\mathbf{r}')u_\eta^0(\mathbf{r}').\end{aligned} \tag{6.7}$$

To leading order the order parameter is

$$\Delta(\mathbf{r}) = -\tilde{g}\sum_\eta \left[u_\eta^0(\mathbf{r})v_\eta^{1*}(\mathbf{r}) + u_\eta^1(\mathbf{r})v_\eta^{0*}(\mathbf{r})\right](1 - 2f(E_\eta^0)). \tag{6.8}$$

Here the coupling constant has been regularized from its bare value to avoid unphysical ultra-violet divergences in the theory (see below). By inserting the expressions for the first order quasi-particle amplitudes we arrive at an integral gap equation to be solved for the order parameter near T_c [70]

$$\Delta(\mathbf{r}) = \int d^3r'\,K(\mathbf{r},\mathbf{r}')\Delta(\mathbf{r}'), \tag{6.9}$$

The kernel is defined as

$$K(\mathbf{r},\mathbf{r}') \equiv -\tilde{g}\sum_{\eta\nu}(1 - 2f(|\xi_\eta|))\left[\frac{u_\eta^{0*}(\mathbf{r}')u_\eta^0(\mathbf{r})}{|\xi_\eta| + \xi_\nu} + \frac{v_\eta^{0*}(\mathbf{r})v_\eta^0(\mathbf{r}')}{|\xi_\eta| - \xi_\nu}\right]\phi_\nu(\mathbf{r})\phi_\nu^*(\mathbf{r}'), \tag{6.10}$$

where we have used that $E_\eta^0 = |\xi_\eta|$. Using (6.2) and symmetrizing in the indices we get for the kernel

$$K(\mathbf{r},\mathbf{r}') = -\frac{\tilde{g}}{2}\sum_{\eta\nu}\left[\frac{\tanh(\frac{\beta\xi_\eta}{2}) + \tanh(\frac{\beta\xi_\nu}{2})}{\xi_\eta + \xi_\nu}\right]\phi_\nu(\mathbf{r})\phi_\nu^*(\mathbf{r}')\phi_\eta^*(\mathbf{r}')\phi_\eta(\mathbf{r}). \tag{6.11}$$

The transition temperature is determined as the temperature at which the largest eigenvalue $\lambda_{\max}$ of $K(\mathbf{r},\mathbf{r}')$ crosses 1, such that (6.9) has a solution.

It is not difficult to see that the sums over quasi-particle states in $K(\mathbf{r},\mathbf{r}')$ is divergent when $\mathbf{r} = \mathbf{r}'$. At high energies $\tanh(\beta\xi_\nu/2) \to 1$, whereas $\phi_\eta(\mathbf{r})$ may be

taken to be a plane-wave state. Hence the diagonal part of the kernel becomes proportional to

$$\int\int dkdk' \frac{k^2 k'^2}{k^2 + k'^2}, \tag{6.12}$$

when the the integral limits of the sums are taken. Both integrals are divergent in the upper limit. The off-diagonal parts of $K(\mathbf{r}, \mathbf{r}')$ on the other hand are regular, as the high energy terms are killed by fast oscillating exponentials. To regularize the diagonal terms we need to find the nature of the divergence.

6.2 Regularizing the Gap Equation

In order to get rid of the ultraviolet divergence we need to be a little more cautious. We recall that the properly regularized definition of the order parameter is

$$\Delta(\mathbf{r}) \equiv -g \lim_{\tilde{r}\to 0} \partial_{\tilde{r}} \left[\tilde{r} \left\langle \hat{\psi}_\uparrow(\mathbf{R} + \frac{\tilde{\mathbf{r}}}{2}) \hat{\psi}_\downarrow(\mathbf{R} - \frac{\tilde{\mathbf{r}}}{2}) \right\rangle \right], \tag{6.13}$$

which takes the correct scattering physics into account. The coordinates of the paired particles are $\mathbf{r} = \mathbf{R} + \frac{\tilde{\mathbf{r}}}{2}$ and $\mathbf{r}'' = \mathbf{R} - \frac{\tilde{\mathbf{r}}}{2}$. By using the Bogoliubov-Valatin transformation we can express $\Delta(\mathbf{r})$ to first order in the quasi-particle basis:

$$\begin{aligned} \Delta(\mathbf{r}) \;=\; & -g \lim_{\tilde{r}\to 0} \partial_{\tilde{r}} \sum_\eta \tilde{r} \Big[u_\eta^0(\mathbf{R} + \frac{\tilde{\mathbf{r}}}{2}) v_\eta^{1*}(\mathbf{R} - \frac{\tilde{\mathbf{r}}}{2})(1 - f(E_\eta^0)) \\ & + u_\eta^1(\mathbf{R} + \frac{\tilde{\mathbf{r}}}{2}) v_\eta^{0*}(\mathbf{R} - \frac{\tilde{\mathbf{r}}}{2})(1 - f(E_\eta^0)) - v_\eta^{0*}(\mathbf{R} + \frac{\tilde{\mathbf{r}}}{2}) u_\eta^1(\mathbf{R} - \frac{\tilde{\mathbf{r}}}{2}) f(E_\eta^0) \\ & - v_\eta^{1*}(\mathbf{R} + \frac{\tilde{\mathbf{r}}}{2}) u_\eta^0(\mathbf{R} - \frac{\tilde{\mathbf{r}}}{2}) f(E_\eta^0) \Big]. \end{aligned} \tag{6.14}$$

Inserting now the expansions of the first order quasi-particle amplitudes we obtain an integral equation for Δ:

$$\Delta(\mathbf{r}) = \int d^3 r' \, K(\mathbf{r}, \mathbf{r}') \Delta(\mathbf{r}'), \tag{6.15}$$

where the regularized kernel is given by the complicated expression

$$\begin{aligned} K(\mathbf{r},\mathbf{r}') &\equiv -g\lim_{r\to 0}\partial_r r\left[\sum_\nu\sum_{\xi_\eta>0}\frac{1-f(E^0_\eta)}{|\xi_\eta|+\xi_\nu}\,\phi_\eta(\mathbf{R}+\frac{\tilde{\mathbf{r}}}{2})\phi^*_\nu(\mathbf{r}')\phi^*_\eta(\mathbf{r}')\phi_\nu(\mathbf{R}-\frac{\tilde{\mathbf{r}}}{2})\right. \\ &+\sum_\nu\sum_{\xi_\eta<0}\frac{1-f^0_\eta}{|\xi_\eta|-\xi_\nu}\,\phi_\nu(\mathbf{R}+\frac{\tilde{\mathbf{r}}}{2})\phi^*_\nu(\mathbf{r}')\phi^*_\eta(\mathbf{r}')\phi_\eta(\mathbf{R}-\frac{\tilde{\mathbf{r}}}{2}) \\ &-\sum_\nu\sum_{\xi_\eta<0}\frac{f^0_\eta}{|\xi_\eta|-\xi_\nu}\,\phi_\eta(\mathbf{R}+\frac{\tilde{\mathbf{r}}}{2})\phi^*_\nu(\mathbf{r}')\phi^*_\eta(\mathbf{r}')\phi_\nu(\mathbf{R}-\frac{\tilde{\mathbf{r}}}{2}) \\ &\left.-\sum_\nu\sum_{\xi_\eta>0}\frac{f^0_\eta}{|\xi_\eta|+\xi_\nu}\,\phi_\nu(\mathbf{R}+\frac{\tilde{\mathbf{r}}}{2})\phi^*_\nu(\mathbf{r}')\phi^*_\eta(\mathbf{r}')\phi_\eta(\mathbf{R}-\frac{\tilde{\mathbf{r}}}{2})\right]. \end{aligned} \tag{6.16}$$

Since $\lim_{\tilde{r}\to 0}[\phi_\eta(\mathbf{R}+\frac{\tilde{\mathbf{r}}}{2})\phi_\nu(\mathbf{R}-\frac{\tilde{\mathbf{r}}}{2})]=\lim_{\tilde{r}\to 0}[\phi_\nu(\mathbf{R}+\frac{\tilde{\mathbf{r}}}{2})\phi_\eta(\mathbf{R}-\frac{\tilde{\mathbf{r}}}{2})]$ we can write the regular part of the kernel in the more compact form

$$\begin{aligned} K(\mathbf{r},\mathbf{r}') &= -g\lim_{\tilde{r}\to 0}\partial_{\tilde{r}}\tilde{r}\left[\sum_\nu\sum_{\xi_\eta>0}\frac{\tanh\left(\frac{\beta|\xi_\eta|}{2}\right)}{|\xi_\eta|+\xi_\nu}\,\phi_\eta(\mathbf{R}+\frac{\tilde{\mathbf{r}}}{2})\phi^*_\nu(\mathbf{r}')\phi^*_\eta(\mathbf{r}')\phi_\nu(\mathbf{R}-\frac{\tilde{\mathbf{r}}}{2})\right. \\ &\left.+\sum_\nu\sum_{\xi_\eta<0}\frac{\tanh\left(\frac{\beta|\xi_\eta|}{2}\right)}{|\xi_\eta|-\xi_\nu}\,\phi_\eta(\mathbf{R}+\frac{\tilde{\mathbf{r}}}{2})\phi^*_\nu(\mathbf{r}')\phi^*_\eta(\mathbf{r}')\phi_\nu(\mathbf{R}-\frac{\tilde{\mathbf{r}}}{2})\right], \end{aligned} \tag{6.17}$$

where we have used that $1-2f(x)=\tanh(\beta x/2)$. Using the fact that $\tanh(x)$ is an odd function we then have

$$\begin{aligned} K(\mathbf{r},\mathbf{r}') &= -g\lim_{\tilde{r}\to 0}\partial_{\tilde{r}}\tilde{r}\Big[\sum_{\eta\nu}\frac{\tanh\left(\frac{\beta\xi_\eta}{2}\right)}{\xi_\eta+\xi_\nu} \\ &\quad\times\phi_\eta(\mathbf{R}+\frac{\tilde{\mathbf{r}}}{2})\phi^*_\nu(\mathbf{r}')\phi^*_\eta(\mathbf{r}')\phi_\nu(\mathbf{R}-\frac{\tilde{\mathbf{r}}}{2})\Big], \end{aligned} \tag{6.18}$$

where both sums extend over all quasi-particle states.

Even though the expression for $K(\mathbf{r},\mathbf{r}')$ is formally divergence free, we have yet to resolve how to implement the regularization operator $\partial_{\tilde{r}}\tilde{r}$ when evaluating the kernel numerically. To do this we first write the regularized kernel as

$$K(\mathbf{r},\mathbf{r}')=-g\lim_{\tilde{r}\to 0}\partial_{\tilde{r}}\tilde{r}M(\mathbf{r},\mathbf{r}',\tilde{\mathbf{r}}), \tag{6.19}$$

defining the auxiliary kernel $M(\mathbf{r},\mathbf{r}',\tilde{\mathbf{r}})$, which diverges in the limit of vanishing $\tilde{r}$

$$M(\mathbf{r},\mathbf{r}',\tilde{\mathbf{r}}) \equiv \sum_{\eta\nu} \frac{\tanh\left(\frac{\beta\xi_\eta}{2}\right)}{\xi_\eta+\xi_\nu}\,\phi_\eta(\mathbf{R}+\frac{\tilde{\mathbf{r}}}{2})\phi^*_\nu(\mathbf{r}')\phi^*_\eta(\mathbf{r}')\phi_\nu(\mathbf{R}-\frac{\tilde{\mathbf{r}}}{2}). \tag{6.20}$$

We then proceed to identify the exact nature of the divergence of $M(\mathbf{r},\mathbf{r}',\tilde{\mathbf{r}})$. To do this, we operate on $M(\mathbf{r},\mathbf{r}',\tilde{\mathbf{r}})$ with $\mathcal{L}(\mathbf{r})+\mathcal{L}(\mathbf{r}'')$. Since $\phi_\eta(\mathbf{r})$ is an eigenstate of $\mathcal{L}(\mathbf{r})$ with eigenvalue ξ_η we have

$$\begin{aligned}\left(\mathcal{L}(\mathbf{r})+\mathcal{L}(\mathbf{r}'')\right) M(\mathbf{r},\mathbf{r}',\tilde{\mathbf{r}}) &= \sum_{\eta\nu}\tanh\left(\frac{\beta\xi_\eta}{2}\right)\\ &\quad\times\phi_\eta(\mathbf{R}+\frac{\tilde{\mathbf{r}}}{2})\phi^*_\nu(\mathbf{r}')\phi^*_\eta(\mathbf{r}')\phi_\nu(\mathbf{R}-\frac{\tilde{\mathbf{r}}}{2}).\end{aligned} \tag{6.21}$$

However, since the divergence is arising due to the high energy parts of the sums we can take $\tanh(\beta\xi_\eta/2)\sim 1$ and exploiting the completeness of the single-particle eigenstates ϕ_η $\sum_\eta \phi^*(\mathbf{r})\phi_\eta(\mathbf{r}')=\delta(\mathbf{r}-\mathbf{r}')$ we get

$$\begin{aligned}\left(\mathcal{L}(\mathbf{r})+\mathcal{L}(\mathbf{r}'')\right) M(\mathbf{r},\mathbf{r}',\tilde{\mathbf{r}}) &= \delta(\mathbf{R}+\frac{\tilde{\mathbf{r}}}{2}-\mathbf{r}')\,\delta(\mathbf{R}-\frac{\tilde{\mathbf{r}}}{2}-\mathbf{r}')\\ &\quad+\text{regular terms.}\end{aligned} \tag{6.22}$$

The product of delta functions can be written as

$$\delta(\mathbf{R}+\frac{\tilde{\mathbf{r}}}{2}-\mathbf{r}')\,\delta(\mathbf{R}-\frac{\tilde{\mathbf{r}}}{2}-\mathbf{r}')=\delta(\mathbf{r}-\mathbf{r}')\,\delta(\mathbf{r}-\mathbf{r}'')=\delta(\mathbf{r}-\mathbf{r}')\,\delta(\tilde{\mathbf{r}}). \tag{6.23}$$

Hence we have for the auxiliary kernel

$$\left(\mathcal{L}(\mathbf{r})+\mathcal{L}(\mathbf{r}'')\right) M(\mathbf{r},\mathbf{r}',\tilde{\mathbf{r}})=\delta(\tilde{\mathbf{r}})\delta(\mathbf{r}-\mathbf{r}')+\text{regular terms.} \tag{6.24}$$

We finally use the fact that $\mathcal{L}(\mathbf{r})+\mathcal{L}(\mathbf{r}'')$ contains the differential operator $-\hbar^2(\nabla^2_{\mathbf{r}}+\nabla^2_{\mathbf{r}''})/2m_a=-\hbar^2(\nabla^2_{\tilde{\mathbf{r}}}+\nabla^2_{\mathbf{R}}/4)/m_a$ and the identity $\nabla^2_{\mathbf{r}}(1/r)=-4\pi\delta(\mathbf{r})$ to write the auxiliary kernel in the form

$$M(\mathbf{r},\mathbf{r}',\tilde{r})=\delta(\mathbf{r}-\mathbf{r}')\frac{gm_a}{4\pi\hbar^2\tilde{r}}+M^{\text{reg}}(\mathbf{r},\mathbf{r}'), \tag{6.25}$$

which explicitly shows that the divergence behaves as $1/\tilde{r}$. This is the same divergence we encountered in regularizing the gap function in Section 3.4, and we shall proceed in the same manner by adding and subtracting the single-particle Green's function, which we evaluate in a local density approximation (LDA). Specifically, since

$$G_\mu(\mathbf{r},\mathbf{r}'') = \frac{m_a}{2\pi\hbar^2\tilde{r}} + G_\mu^{\rm reg}(\mathbf{r}) + \mathcal{O}(\tilde{r}), \tag{6.26}$$

we see that the divergence free kernel for the linearized gap equation can be evaluated as

$$\begin{aligned} K(\mathbf{r},\mathbf{r}') = & - g\lim_{r\to 0}\left[M(\mathbf{r},\mathbf{r}',\tilde{\mathbf{r}}) - \delta(\mathbf{r}-\mathbf{r}')\frac{1}{2}G_\mu(\mathbf{r},\mathbf{r}'')\right] \\ & - \delta(\mathbf{r}-\mathbf{r}')\frac{g}{2}G_\mu^{\rm reg}(\mathbf{r}). \end{aligned} \tag{6.27}$$

In this expression the bracketed terms are divergence free, and the remaining tasks are to evaluate the Green's function and its regular part using LDA. This calculation was detailed in Section 3.4, and we shall not repeat it here. Instead we just state the result:

$$\begin{aligned} K(\mathbf{r},\mathbf{r}') = & - \frac{g}{2}\sum_{\xi_\eta<E_c}\sum_{\xi_\nu<E_c}\frac{\tanh\left(\frac{\beta\xi_\eta}{2}\right)+\tanh\left(\frac{\beta\xi_\nu}{2}\right)}{\xi_\eta+\xi_\nu}\,\phi_\eta(\mathbf{r})\phi_\nu^*(\mathbf{r}')\phi_\eta^*(\mathbf{r}')\phi_\nu(\mathbf{r}) \\ & + \delta(\mathbf{r}-\mathbf{r}')\frac{gm_a}{2\pi^2\hbar^2}\left(k_c(\mathbf{r}) - \frac{k_{\rm F}(\mathbf{r})}{2}\ln\frac{k_c(\mathbf{r})+k_{\rm F}(\mathbf{r})}{k_c(\mathbf{r})-k_{\rm F}(\mathbf{r})}\right), \end{aligned} \tag{6.28}$$

where E_c, $k_c(\mathbf{r})$ and $k_{\rm F}(\mathbf{r})$ are defined in Section 3.4, and we have symmetrized the first term in the summation indices.

To check that the derived linear gap equation makes sense, we analyze it for the case of a homogeneous system where the normal state wavefunctions are plane waves, $\phi_{\mathbf{k}} = e^{i\mathbf{k}\cdot\mathbf{r}}/\sqrt{V}$, and the pairing field is constant in space $\Delta(\mathbf{r}) = \Delta_0$.

The integral in (6.15) is then easily performed, and we find

$$\begin{aligned}\Delta_0 &= -\frac{g\Delta_0}{2V}\sum_{\xi_{\mathbf{k}}<E_c}\sum_{\xi_{\mathbf{k}'}<E_c}\frac{\tanh\left(\frac{\beta\xi_{\mathbf{k}}}{2}\right)+\tanh\left(\frac{\beta\xi_{\mathbf{k}'}}{2}\right)}{\xi_{\mathbf{k}}+\xi_{\mathbf{k}'}}\delta_{\mathbf{k}+\mathbf{k}',0} \\ &\quad +\frac{gm_a\Delta_0}{2\pi^2\hbar^2}\left(k_c-\frac{k_{\mathrm{F}}}{2}\ln\frac{k_c+k_{\mathrm{F}}}{k_c-k_{\mathrm{F}}}\right). \qquad (6.29)\end{aligned}$$

The energy is an even function of $\mathbf{k}$, $\xi_{\mathbf{k}}=\xi_{-\mathbf{k}}$, and consequently we find for the gap

$$\Delta_0=-\frac{\tilde{g}\Delta_0}{V}\sum_{\xi_{\mathbf{k}}<E_c}\frac{\tanh\left(\frac{\beta\xi_{\mathbf{k}}}{2}\right)}{2\xi_{\mathbf{k}}}, \qquad (6.30)$$

which is the usual gap equation for a bulk gas (*c.f.* (3.73)), as expected.

6.3 Symmetry Requirements on the Kernel

As we will demonstrate in this section any symmetry in the problem can significantly reduce the number of non-vanishing terms in the double sum in (6.28). To analyze the symmetry requirements on the kernel of the integral gap equation we write it in the form

$$K(\mathbf{r},\mathbf{r}')=\sum_{\eta\eta'}F_{\eta\eta'}\phi_{\eta'}(\mathbf{r})\phi^*_{\eta'}(\mathbf{r}')\phi^*_{\eta}(\mathbf{r}')\phi_{\eta}(\mathbf{r})+A(\mathbf{r})\delta(\mathbf{r}-\mathbf{r}'). \qquad (6.31)$$

The function $F_{\eta\eta'}$ is a scalar, which does not affect the symmetry properties of $K(\mathbf{r},\mathbf{r}')$, and $A(\mathbf{r})$ is a scalar function, which regilarizes the diagonal part of the kernel.

6.3.1 Cylindrical Symmetry

If the Hamiltonian is symmetric under rotations about a single axis it is convenient to introduce a cylindrical coordinate system with ρ measuring the distance

from the the symmetry axis $\hat{e}_z$, and where φ is the azimuthal angle around this axis. The superfluid order parameter can be written as $\Delta(\mathbf{r}) = |\Delta(\rho)|e^{-i\kappa\varphi}$. When a singly quantized vortex line is penetrating the gas $\kappa = 1$, whereas $\kappa = 0$ is the superfluid is in a state of zero circulation. The symmetry of the order parameter imposes specific requirements on the symmetry of the kernel, as we shall now see.

Taking the gas to be confined in a cylinder of radius R, the single-particle states of the normal state Hamiltonian are eigenstates of the angular momentum operator L_z, and of the axial momentum operator, with eigenvalues $m\hbar$ and $\hbar k$, respectively:

$$\phi_\eta(\mathbf{r}) = R_{nm}(\rho)\frac{e^{im\varphi}}{\sqrt{2\pi}}\frac{e^{ikz}}{\sqrt{L}}. \tag{6.32}$$

The linearized gap equation then becomes

$$\begin{aligned}\Delta(\mathbf{r})(1 - A(\mathbf{r})) &= \int_0^R d\rho'\,\rho' \sum_{\eta\eta'} \frac{F_{\eta\eta'}}{2\pi L} R_{n'm'}(\rho)R_{n'm'}(\rho')R_{nm}(\rho')R_{nm}(\rho) \\ &\quad \times e^{i(m+m')\varphi}e^{i(k+k')z}|\Delta(\rho')|\delta_{m+m'+\kappa,0}\delta_{k+k',0}. \end{aligned}\tag{6.33}$$

The cylindrical symmetry thus enforces the following selection rules on the Kernel:

$$\begin{aligned} m + m' + \kappa &= 0, \\ k + k' &= 0. \end{aligned}$$

Below we present the results of calculations of the transition temperature in for a Fermi gas in a cylinder with and without a vortex.

6.3.2 Spherical Symmetry

In the case of $SO(3)$ symmetry we express all quantities in terms of spherical coordinates $\{r, \theta, \varphi\}$, where $r = \sqrt{x^2 + y^2 + z^2}$ is the distance from the origin, θ is the polar angle between $\mathbf{r}$ and $\hat{e_z}$, and φ the azimuthal angle about the z-axis. We can then express the normal state wavefunctions as

$$\phi_\eta(\mathbf{r}) = R_{nl}(r)Y_{lm}(\theta, \varphi). \tag{6.34}$$

The radial function $R_{nl}(r)$ satisfies a Schrödinger equation in r, and the spherical harmonic $Y_{lm}(\theta, \varphi)$ is the eigenfunction of the angular momentum operator $\mathbf{L}^2$, and its projection onto the z-axis L_z, with eigenvalues $l(l+1)\hbar^2$ and $m\hbar$, respectively. Assuming that no current flow, the order parameter $\Delta(\mathbf{r}) = \Delta(r)$ can be chosen to be real. For the linearized gap equation we then have

$$\begin{aligned}\Delta(r)(1 - A(r)) &= \int_0^\infty dr' r'^2 \sum_{\eta\eta'} F_{\eta\eta'} R_{n'l'}(r) R_{n'l'}(r') R_{nl}(r') R_{nl}(r) \\ &\quad \times Y_{l'm'}(\theta, \varphi) Y_{lm}(\theta, \varphi) \Delta(r) \delta_{l-l',0} \delta_{m+m',0} (-1)^m. \end{aligned} \tag{6.35}$$

This gives us the selection rules limiting the number of contributing terms in the double sum over quasi-particle states in (6.28)

$$\begin{aligned} l - l' &= 0, \\ m + m' &= 0. \end{aligned}$$

We have not performed a calculation of the transition temperature for a spherically symmetric potential, but we chose to include this discussion for completeness.

6.4 Numerical Implementation

When solving the integral gap equation we utilize the DVR method, which is described in Appendix B. In essence this entails repesenting the kernel as a matrix $\mathbf{K}$, whos matrix elements $K_{\alpha\beta}$ are given in terms of the DVR basis functions, which themselves are in a ono to one correspondence with a spatial grid. Since the DVR grid is associated with a numerical quadrature the integral gap equations becomes:

$$\Delta_\alpha = \sum_\beta K_{\alpha\beta}\Delta_\beta, \tag{6.36}$$

where Δ_α is the value of the pairing field at the bα'th mesh point. The quadrature weights are included in the expression for kernel matrix on the grid. This matrix gap equation first has a solution when the largest eigenvalue $\lambda_{\max}$ of $\mathbf{K}$ iequals one. In Fig. 6.1 we plot a typicalexample of the temperature evolution of $\lambda_{\max}$ for asuperfluid in a cylinder with and without a vortex. The linearized gap equation gives the correct bulk transition temperature, *i.e.* $\lambda_{\max}$ crosses one at $T \simeq T_{c0}$, while the presence of the vortex is observed to cause a negative shift in the value of T_c. We will elaborate on this effect in Section 6.5. It is important to note that $K_{\alpha\beta}$ depends only on the normal state wavefunctions, which are found self-consistently much faster than the quasi-particle modes in the superfluid state (especially close to T_c). Therefore the linearized gap equation is an extremely efficient method for finding the transition point. From data sets like those shown in Fig. 6.1 the value of T_c is determined by cubic spline interpolation [215] to find the precise temperature, where $\lambda_{\max}$ cross one.

We have investigated the dependence of T_c as given by the linearized gap equation on $k_{\mathrm{F}}|a|$. For a fixed cylinder radius $R = 28.5$ μm and ^{6}Li parameters,

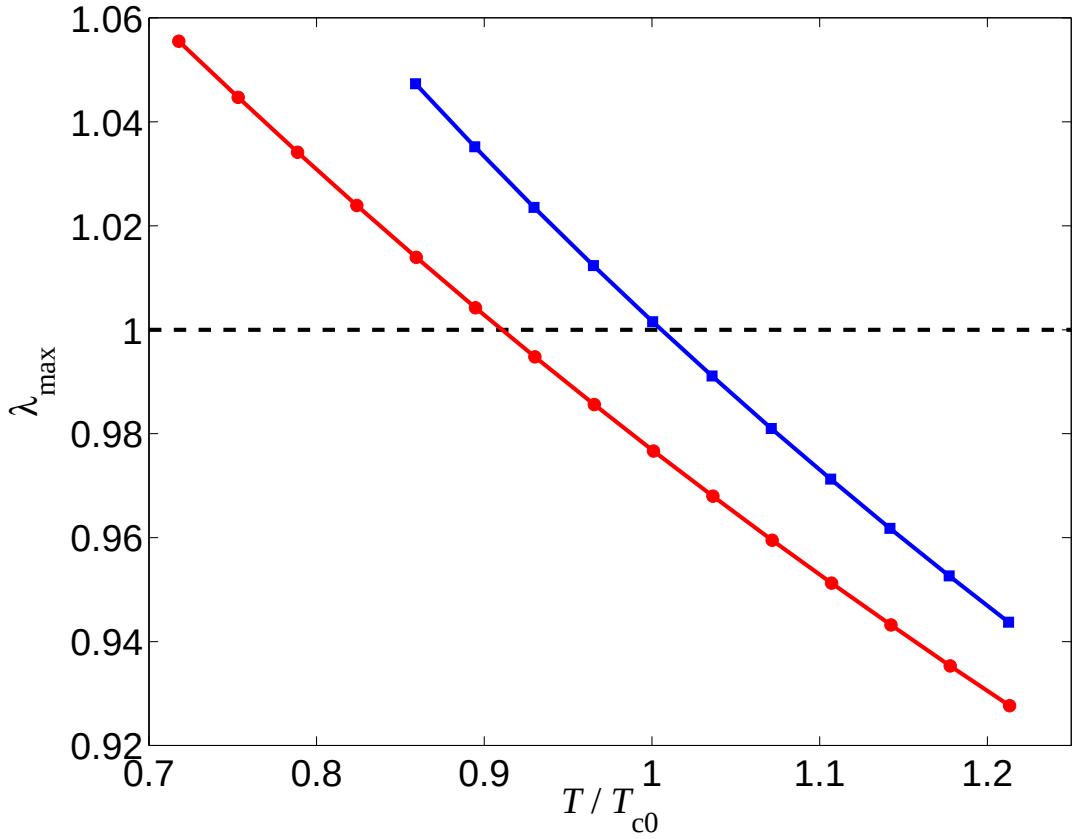

Figure 6.1: The largest eigenvalue of the kernel as a function of temperature in an interval around the bulk value of T_c. The transition temperature is found as the temperature at which $\lambda_{\max}$ crosses one. Results for both a superfluid at rest (■'s) and a vortex state (●'s) are shown with lines to guide the eye. The vortex state causes a shift in T_c, which we investigate in detail below.

we compare in Fig. 6.2 the transition temperature found by the method described above. The agreement is excellent over a large range of $k_{\rm F}|a|$, where the transition temperature varies exponentially. This demomstrates the effectiveness of the linearized approach.

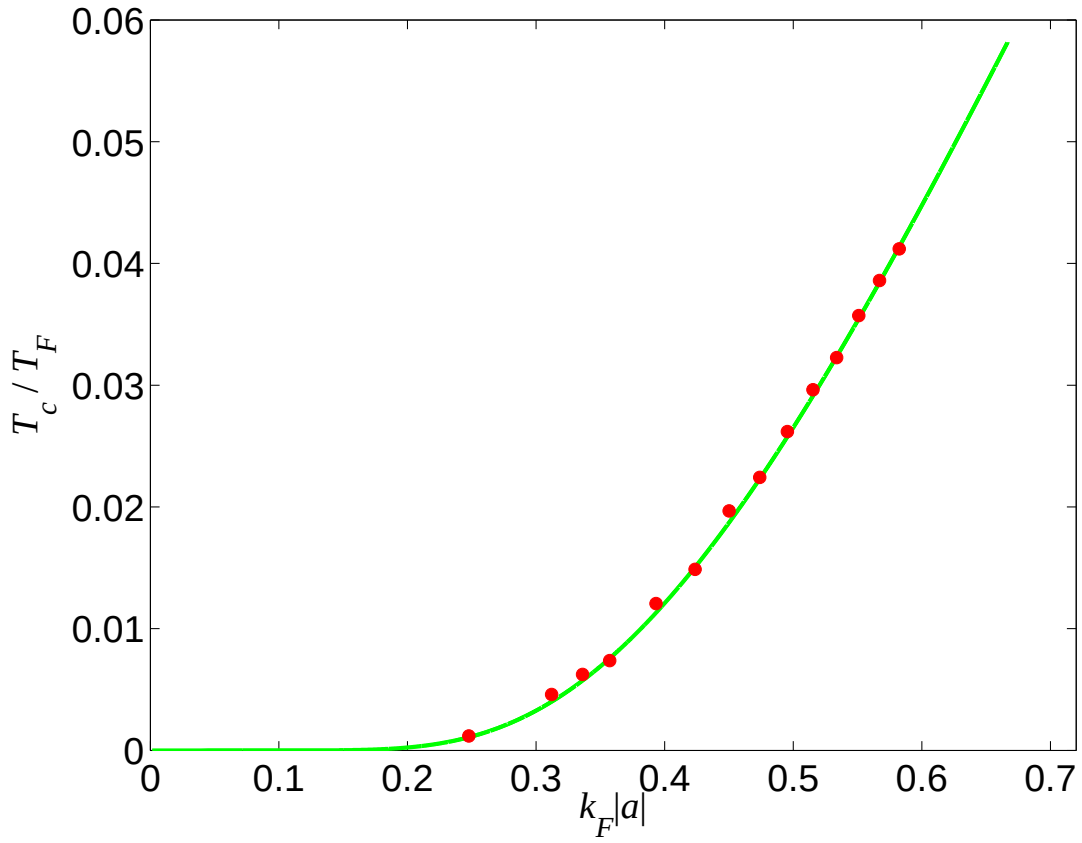

Figure 6.2: Critical temperature for superfluid Fermi gas in a cylinder. Results from the linearized gap equation (•) are compared with the analytical expression for a bulk system (*green line*).

6.5 Shift of T_c for a Vortex

As we indicated in Section 5.4, the critical temperature for the vortex phase T_{cv} is lower than that of the bulk superfluid phase without a vortex T_{c0}. For the specific parameters used in Chapter 5, the difference is $1 - T_{cv}/T_{c0} \simeq 0.1$. This difference can be understood as follows: The vortex phase becomes unstable with respect to the normal phase when the extent of the vortex core becomes comparable to the radius R of the system. Since the size of the vortex is $\mathcal{O}(\xi_{\rm BCS})$,

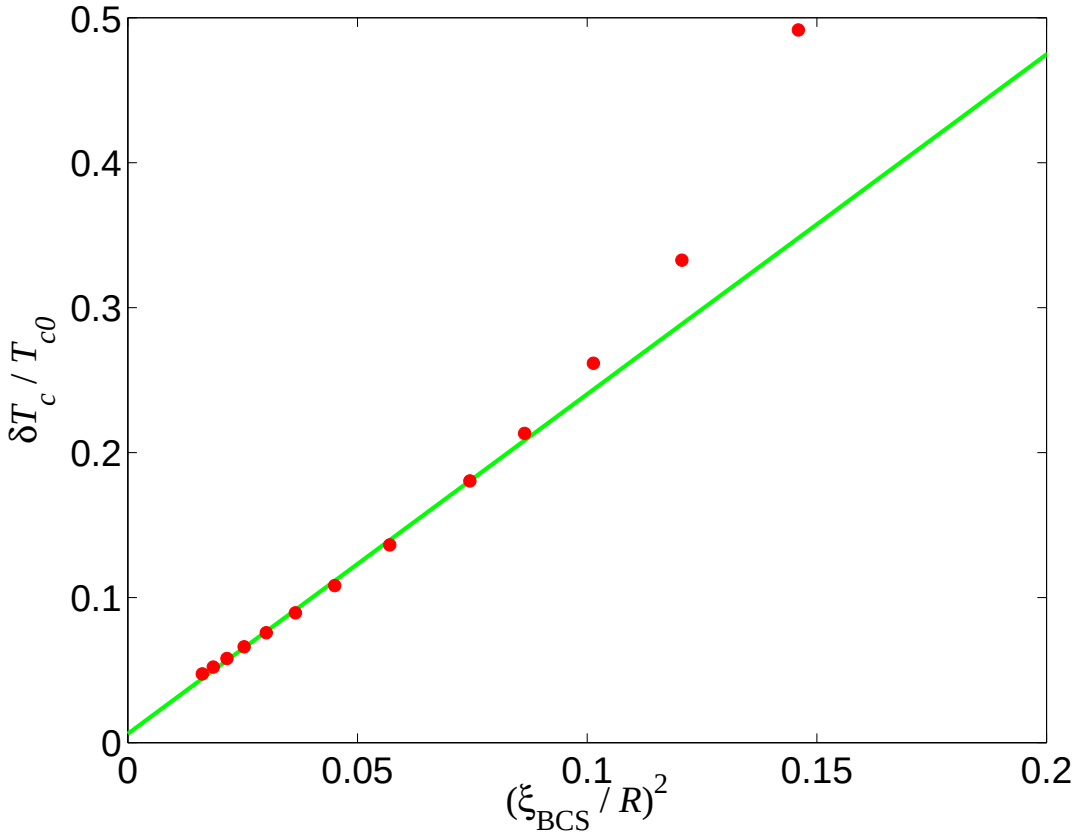

Figure 6.3: The shift in superfluid transition temperature for a vortex state $\delta T_c/T_{c0}$ (•), as a function of the radius of the confinig cylinder at fixed denisty. The green line is a linear fit to the simple model (6.37) with the parameters given in the text. The data points for the three smallest cylinders were not included in the fit.

we can estimate T_{cv} from the condition $\xi_{\rm BCS}(T_{cv}) \sim \mathcal{O}(R)$. Using $\Delta_0(T) \simeq 1.7\Delta_0(0)(1-T/T_{c0})^{1/2}$ [70] for $0 < 1 - T/T_{c0} \ll 1$, this yields

$$\frac{\delta T_c}{T_{c0}} \equiv 1 - \frac{T_{cv}}{T_{c0}} \sim \frac{\xi_{\rm BCS}(0)^2}{R^2}\alpha_2 \tag{6.37}$$

where α_2 is a number of order one.

We now test this expression and determine the constant α_2 by numerically

calculating the shift in the critical temperature $\delta T_c/T_{c0}$ due to the presence of a vortex for various radii of the system, keeping the density fixed such that the value of the BCS coherence length, and the bulk transition temperature are unchanged. The result is shown in Fig. 6.3, where the relative shift of the superfluid transition temperature in the vortex state is plotted versus $(\xi_{\rm BCS}/R)^2$. We see that we get excellent agreement with Eq. (6.37) for large radii, but that $\delta T_c/T_{c0}$ deviates substantially from our simple model prediction, when the size of the cylinder is decreased. For a cylinder radius not much larger than $\xi_{\rm BCS}$ the vortex state can no longer be stabilized and the vortex transition temperature decreases towards zero. We have fitted the data to a linear function of $(\xi_{\rm BCS}/R)^2$, excluding the data points for the three smallest cylinders from the fit. The result which gives $\alpha_2 \simeq 2.3$ is also plotted in Fig. 6.3. The fit gives a small offset of 0.006, while we would expect the shift to vanish in the limit of $R \to \infty$. However, this small error is on the order of the accuracy of the numerical scheme as is clear from the scatter of points in Fig. 6.2. So one can understand the decrease in T_c due to the presence of the vortex as a finite size effect which scales as $\xi_{\rm BCS}(0)^2/R^2$.

Chapter 7

Conclusion

7.1 Summary

In the work presented here we have investigated the properties of a superfluid atomic Fermi gas within the confines of a weak-coupling mean-field theory. Special attention has been paid to the bulk system, exemplified by a gas held in a cylindrical box of radius larger than the BCS coherence length. In such a geometry the vortex state of the gas was studied in great detail. The vortex is an excited state of the superfluid system, thermodynamically unstable in the absence of rotation. However, once created the rotational currents of the vortex can persist as meta-stable flow for extended periods, thus providing a prime example of superfluidity. This is due to the macroscopic coherence of the system in the superfluid phase, which enforces a quantization of the circulation.

We have presented the first microscopic calculation of the energy difference between the superfluid at rest and the state with a single, central vortex of unit circulation. This energy is directly related to the critical rotation frequency, required to stabilize the vortex state. Our result is of fundamental importance

to vortex physics, and should be of relevance in a wide range of Fermi systems. The calculation showed that the important length scale that characterizes the size of the vortex core region, where superfluidity is suppressed, is the BCS coherence length of the system.

Furthermore, we have studied the thermodynamics of the vortex state, and shown how the presence of low-lying modes, with energies below the bulk value of the gap, leads to a linear contribution to the specific heat at low temperatures, in contrast with the non-vortex state where the low temperature specific heat is exponentially suppressed due to the energy gap. These modes are bound quasi-particle states in the vortex core, and their occupation implies that the vortex core is comprised of atoms in the normal state. As a consequence the vortex does not cause a significant suppression of the atomic density, and we predict that a direct observation of the vortex core, as has been done for atomic Bose-Einstein condensates, is unlikely for a superfluid Fermi gas in the weak-coupling limit. Instead we propose to observe the rotational currents associated with the vortex through a laser probing method, which under the right experimental circumstances can detect the bound states in the vortex core spectroscopically. The laser probing method, which is akin to a STM measurement on a superconductor, is also a solid candidate for experimental detection of the energy gap in the system, as we have shown by calculating the response of a bulk system to the probing field in the absence of a vortex. A direct calculation of the transition temperature of the gas showed that the vortex can significantly suppress the value of T_c. We demonstrated how this can be understood as a finite size effect; the vortex becomes unstable if the size of its core becomes comparable to the radius of the confining vessel.

In addition to the calculations of the properties of a bulk Fermi gas, which are of importance from an elemental perspective, we have also studied the effect of a superfluid Fermi gas under external harmonic confinement as this situation relates directly to the ongoing experiments. Our analysis indicates that a vortex in a trapped gas may be directly observable, but since these calculations were performed at the limit of the range of validity of our mean-field approach, a theory treating the effect of strong interactions would be needed to substantiate this prediction.

In the many-body theory of dilute quantum gases the atomic interaction can be replaced with a simplified model potential, which reproduces the correct asymptotic scattering physics. In the ultracold regime, where the scattering is essentially occurring at zero energy, the details of the interatomic potential are irrelevant, and a shape independent approximation can be adopted, in which the potential is parameterized by a single physical parameter, the s-wave scattering length, and the potential taken to be of zero range. An essential aspect of the theory presented here is the derivation of a properly regularized gap equation, for the superfluid order parameter, which is free of the ultraviolet divergences stemming from the use of a contact potential with no implicit momentum cutoff. This procedure directly relates the strength of the model potential with the physical scattering parameter, and results in a first principles theoretical description with no free parameters. Therefore the comparison of the theoretical predictions with future experiments will be straightforward and direct, with no adjustable factors.

Finally, we have characterized the nature of superfluidity in the system, performing the first derivation of the spatial variation of the superfluid density.

This was defined in terms of the response of the system to a rotation, effectively twisting the phase of the order parameter The superfluid density was shown to be related directly to the strain energy of the gas under this phase twist, in a way similar to the elasticity of a solid under sheer stress. In the limit of a small phase twist the superfluid density was found perturbatively from the mean-field theory. An important future endeavor will be to devise a method for probing directly the superfluid density of the gas.

Having thus summarized the principal conclusions reached in this thesis, it is appropriate to look ahead, and attempt to put our work in perspective.

7.2 Outlook

We consider the work presented here timely with respect to the ongoing experimental effort to achieve a phase transition to a superfluid state in a trapped atomic Fermi gas. Since the first cooling of a dilute gas to Fermi degeneracy in 1999 the experimental progress has been swift, and presently several research groups seem to be on the verge of achieving pairing superfluidity. An important theoretical question which has not yet been answered beyond reproach is how to determine unambiguously if the gas is in the superfluid state. In the weak-coupling limit the bulk properties like the density and energy are mostly unaffected by the superfluid phase transition, while for a gas with strong interactions it is often impossible to distinguish the effects of superfluidity and collisional hydrodynamics. Such problems arise when analyzing both the collective oscillations, and the mode of expansion of the gas. It is quite possible that several experiments have already formed a superfluid Fermi gas, but the

signatures may be so subtle that they have thus far been undetectable. Instead experimentalist will likely need to focus on the macroscopic quantum effects, which are manifestations of superfluidity in the system. An example of these is quantized circulation, as in the vortex state we have studied. Indeed, this can be regarded as one of the hallmarks of superfluidity, and thus the creation and subsequent detection of a quantized vortex in a Fermi gas, would be a "smoking gun" for superfluid behavior.

Presently, the attainable experimental temperatures are an order of magnitude higher than the predicted BCS transition temperature in the weak-coupling limit. Several theoretical suggestions for enhancing pairing are actively being investigated in the laboratory. All involve increasing the effective coupling parameter $k_{\mathrm{F}}|a|$, on which T_c depends exponentially in the mean-field theory. One way to accomplish this is to load the Fermi atoms into an optical lattice. The density of states available for pairing is then directly related to the depth of the lattice. There is also a real possibility that fermions in such periodic structures could have applications in quantum information processing.

Other proposals involve increasing the strength of the two-body interaction. This can be achieved in three different ways which all entail an effective attraction between two Fermi atoms mediated by a bosonic intermediary. The main experimental focus is on using a Feshbach resonance to increase the effective fermion-fermion scattering length via a resonant coupling to a molecular bosonic bound state, controlled by adjusting a magnetic field. The reversible production of molecules from the atomic sample, and tunability of the interaction strength have been demonstrated in recent experiments. Additionally, it has been proposed to create bosonic dimers directly out of the atomic Fermi gas us-

ing photoassociation, a technique which has already been successfully applied as a means for generating cold molecules in a Bose condensed gas. Important questions which remain to be answered relate to the kinetics of molecule formation and equilibration. A particular issue of fundamental importance is the possible production of a Bose-Einstein condensate of molecules. Ultracold molecules could provide a test-bed for probing the fundamental interactions in chemistry. The possibility of inducing macroscopic quantum oscillations between atomic and molecular forms through the resonant coupling; such coherent chemical reactions would herald a new regime for molecular physics. The last scheme being pursued experimentally involves immersing the Fermi atoms in a condensed cloud of bosons. The fermions can then interact by exchanging density fluctuations of the boson component. By tuning the boson-fermion interaction on the other hand, through a Feshbach resonance, the formation of heteronuclear molecules with a permanent electric dipole moment is foreseen.

Even beyond the relevance for achieving superfluidity the tuning of the atomic interaction have important implications since it brings the gas into a strongly-interacting regime, where new and interesting physics emerges. An example is the absence of a density dependent mean-field shift of RF transitions in this regime, which is potentially relevant for the construction of more accurate atomic clocks. Furthermore, when the size of the scattering length exceeds the inter-particle spacing the simple picture of two-body collisions, which we have used in the present theory, breaks down. In the strong interaction limit the scattering is unitarity limited, and the mean-field energy, and the pairing gap both approach a constant fraction of the Fermi energy of the system. In this limit the inter-particle spacing is the only relevant length scale of the problem, and it is thus

expected that all strongly interacting Fermi systems will behave universally, independent of the details of the interaction.

Tabletop experiments at ultralow temperatures thus promise to allow us to study in a controlled manner a strongly interacting Fermi gas, and can therefore provide a model system for advancing our knowledge of this system. The impact would reach far beyond the atomic physics community, as the physics of strongly interacting fermions govern the properties of high temperature superconductors, the equation of state of nuclear matter, and the interior of compact stars to name but a few examples. The many-body theory of such strongly interacting systems is not well-established, and we anticipate a climate where experiment and theory are mutually conducive.

If the achievement of Bose-Einstein condensation offers a guideline, the future of the atomic physics community looks bright; that discovery sparked a frantic research effort with the aim to understand and manipulate the new state of matter. This had already led to numerous basic discoveries. Similarly, ultracold Fermi gases have the potential for a substantial impact due their scientific and technological relevance. In conclusion there is a host of interesting research question of fundamental importance ahead, and in answering them we have every reason to expect the continuation of a stimulating intellectual journey.

Appendix A

The Pseudopotential Approximation

The pseudopotential method of Huang and Yang was developed to describe the interaction properties of imperfect gases at low temperatures [26, 216], building on earlier work by Fermi [217] and Breit [218] on scattering of slow neutrons by protons. In a dilute and cold gas only binary collisions are relevant at low energies. Furthermore, at low energies the centrifugal barrier effectively attenuates the amplitude of scattering in channels with a finite angular momentum. The interaction properties of the gas can then be acurately described by a single parameter; the s-wave scattering length a, the interaction turn out to be independent of the specific shape of the two-body potential.

The sign and size of the scattering length is of course determined by the details of the potential, and for neutral atoms it is the van der Waals interaction $\sim r^{-6}$ that is responsible for the low energy scattering (here and in the following r is the distance between the two scattering particles). In particular the value of a is quite sensitive to the location of the last bound state in the potential. The validity of the shape independent approximation is based on the condition that both the thermal wavelength λ and the average distance between the atoms

$\sim n^{-1/3}$ is much larger than all other relevant length scales in the problem, in particular the range of the interaction potential. If this is satisfied the details of the potential are unimportant as the particles are 'smeared out' and see only the average effect of the interaction. Likewise they experience an effective interaction that is very small, even though the potential may have large values, thus the interaction can be treated as a pertubation to the ideal gas case. The idea of the pseudopotential approximation is to replace the exact two-body interaction with a model potential, which is chosen such that it hugely simplifies the scattering problem, while correctly reproducing the asymptotic scattering wavefunction. The details of the wavefunction close to the scattering center will not be captured correctly in this approach, but at long wavelengths the physics is insensitive to these short length scale oscillations. The scattering length a characterizes the net effect of the short-range interactions. In the zero energy limit the asymptotic part of the wavefunction must be proportional to $1 - (a/r)$. We review the derivation of this well known result below, since it elucidates the basic scattering features, which the definition of the approximate model potential must be able to reproduce. As we shall see the introduction of the approximate pseudopotential can be viewed as changing the boundary condition of the scattering wavefunction at small interparticle distances, such that it has a node at $r = a$ instead of $r = 0$.

We consider in the following a general two-body, finite ranged scattering potential via which particles of masses m_1 and m_2 interact. In the center of mass reference frame, defined by the center of mass coordinate $\mathbf{R}$ and the relative coordinate $\mathbf{r}$

$$\begin{aligned} \mathbf{R} &= \frac{1}{2}(\mathbf{r}_1 + \mathbf{r}_2) \\ \mathbf{r} &= \mathbf{r}_2 - \mathbf{r}_1, \end{aligned} \tag{A.1}$$

the Schrödinger equation for the relative wavefunction is

$$\left(\nabla^2 + k^2\right)\psi(\mathbf{r}) = v(r)\psi(\mathbf{r}), \tag{A.2}$$

where $m_r = m_1 m_2/(m_1 + m_2)$ and $v(r) = (2m_r/\hbar^2)V(r)$ is the reduced mass and reduced potential, respectively.

The total wavefunction is given by

$$\Psi(\mathbf{r}_1, \mathbf{r}_2) = e^{i\mathbf{P}\cdot\mathbf{R}}\psi(\mathbf{r}), \tag{A.3}$$

with the total momentum $\mathbf{P}$ defining the free motion of the center of mass. At sufficiently low energies that only s-wave scattering is important it suffices to consider only solutions which are spherically symmetric. We thus take

$$u(r) = r\psi(r), \tag{A.4}$$

where the boundary consition is $u(r) \to 0$ for $r \to 0$, such that $\psi(r)$ remains finite at the origin. Then the Schrödinger equation (A.2) reduces to a radial equation for u

$$\frac{d^2u(r)}{dr^2} + k^2u(r) = v(r)u(r). \tag{A.5}$$

Under the assumption that $v(r)$ is of finite range, the radial function is asymptotically (*i.e.* for large interparticle separation) that of a free particle, phase shifted compared to the relative wavefunction of two non-interacting paticles. Choosing a special normalization we have

$$\lim_{r\to\infty} u(r) = u_\infty(r) = r\psi_\infty(r) = \frac{\sin(kr + \delta_0(k))}{\sin\ \delta_0(k)}, \tag{A.6}$$

where $\delta_0(k)$ is the s-wave phase shift [219]. In the low energy limit, *i.e.* $k \to 0$ we have

$$u_\infty(r) = \frac{\cos kr \sin\delta_0(k) + \sin kr \cos\delta_0(k)}{\sin\delta_0(k)} \sim 1 + kr\ \cot\ \delta_0(k), \tag{A.7}$$

as seen by expanding the sine and cosine terms to first order in kr. The low energy behavior of the phase shift being determined by the expansion [64]

$$\lim_{k\to 0} k \cot\ \delta_0(k) = -\frac{1}{a} + \frac{1}{2} r_e k^2 + \cdots, \tag{A.8}$$

where r_e is the effective range of the potential, and a is the scattering length. At the temperatures of interest we may neglect all terms beyond the first in (A.8), and we thus have to the zeroth order in k

$$-\frac{1}{k \cot\ \delta_0(k)} \approx a, \tag{A.9}$$

which demonstrates that in the zero energy limit the asymptotic wavefunction behaves like $\psi_\infty \sim (1 - a/r)$. We can understand this by looking at the nodes of $u_\infty \propto \sin(kr + \delta_0(k)))$, which are located at $r_n = (n\pi - \delta_0(k))/k$, with $n \in \mathbb{Z}$. When k approaches zero, all the nodes r_n go to $\pm\infty$, except one which tends to a. Our aim is therefore to introduce a model potential which ensures exactly this boundary condition. We now define as the eigenfunction of our model potential the wavefunction $\phi(r)$ over all values of r except $r = 0$, in such a way that

$$\left(\nabla^2 + k^2\right) \phi(r) = 0, \tag{A.10}$$

with the boundary condition

$$\phi(a) = 0. \tag{A.11}$$

That is, we choose the model potential such that $\phi(r)$ vanishes at the same point as the asymptotic wavefunction of the full potential, in effect imposing a hard wall boundary condition at $r = a$. In the low energy limit the form of our new function must be

$$\phi(r) = \left(1 - \frac{a}{r}\right) \chi, \tag{A.12}$$

in order for it to correctly describe the scattering physics in the far region. Here χ is a constant. It is clear from (A.12) that

$$\chi = \left[\frac{\partial(r'\phi(r'))}{\partial r'}\right]_{r'=0}. \tag{A.13}$$

To find the behavior of $\phi(r)$ at the origin we use (A.12) and operate on $\phi(r)$ with $\nabla^2 + k^2$. In the limit of $k \to 0$ it follows that

$$(\nabla^2 + k^2)\phi(r) = 4\pi a\delta(\mathbf{r})\chi. \tag{A.14}$$

We therefore find that the function ϕ satisfies the equation

$$\left(\nabla^2 + k^2\right)\phi(r) = 4\pi a\delta(\mathbf{r})\frac{\partial}{\partial r}\left(r\phi(r)\right). \tag{A.15}$$

at all r. The operator $4\pi a\delta(\mathbf{r})\partial_r(r\cdot)$ plays the part of an effective reduced potential and it is called the pseudopotential. We stress here that (A.15) is not the exact Schrödinger equation of the physical problem as only the s-wave solutions ϕ for low energies coincides with ψ. However it can be shown that (A.15) is correct to the second order in the scattering length. Taking as the two-body potential

$$V(r) = \left(\frac{\hbar^2}{2m_r}\right)v(r) = \frac{4\pi a\hbar^2}{m_a}\delta(\mathbf{r})\frac{\partial}{\partial r}(r\cdot), \tag{A.16}$$

for particles of equal mass $m_1 = m_2 = m_a$, we get energy eigenvalues for the inperfect gas which are correct to the lowest order in a. Since the pseudopotential has the same sign as the scattering length we see that $a < 0$ ($a > 0$) corresponds to an effectively attractive (repulsive) potential. In this thesis we will be concerned with the attractive case only. We stress again that the pseudopotential approximation is only valid for a dilute gas, *i.e.* when $n|a|^3 \ll 1$, or equivalently $k_{\mathrm{F}}|a| \ll 1$, for a Fermi gas.

It is instructive to calculate the scattering amplitude for elastic scattering via the pseudopotential:

$$\begin{aligned} f_k^{l=0} &= -\frac{2m_r}{4\pi\hbar^2}\int d^3r'\, e^{i\mathbf{k}\cdot\mathbf{r}'}V(\mathbf{r}')\psi(\mathbf{r}') = -a\int d^3r'\,\delta(\mathbf{r}')\frac{\partial}{\partial r'}(r'\psi(\mathbf{r}')) \\ &= -a\left[\frac{\partial(r'\psi(\mathbf{r}'))}{\partial r'}\right]_{r'=0} = -a\chi. \end{aligned} \tag{A.17}$$

We therefore have for the asymptotic scattering wavefunction

$$\psi(\mathbf{r}) = e^{i\mathbf{k}\cdot\mathbf{r}} - a\frac{e^{ikr}}{r}\chi. \tag{A.18}$$

To find the value of the constant χ we multiply (A.18) by r, take the derivative with respect to r, and set r to zero. This gives us

$$\chi = 1 - a\chi ik, \tag{A.19}$$

or $\chi = 1/(1+ika)$. Thus the s-wave scattering amplitude of the regularized pseudopotential is

$$f_k^{l=0} = -\frac{a}{1+ika}, \tag{A.20}$$

such that the cross section for scattering of non-identical particles is

$$\sigma(k) = 4\pi|f_k^{l=0}|^2 = \frac{4\pi a^2}{1+k^2a^2}. \tag{A.21}$$

To distinguish the model potential described in detail above from the replacement of the interatomic potential with a simple contact potential, which is also commonly referred to as the pseudopotential approximation, we will often speak of the *regularized pseudopotential*, and call the $\partial_r(r\cdot)$ the *regularization operator*. In most cases the scattering wavefunction is regular at the origin and the the differential operator may be replaced by unity, such that the inter-particle potential is well approximated by a delta function potential of of strength $4\pi a\hbar^2/m_a$.

However, as we show in Chapter 3 pairing correlations as in a superfluid Fermi gas give rise to two-body states which diverge as r^{-1} at small separations. In that case the inclusion of the regularization operator is crucial to guarantee the correct physical behavior. One can also use a contact potential with a bare coupling strength g_0, *i.e.* $V(\mathbf{r}) = g_0\delta(\mathbf{r})$ in this case, but the value of g_0 has to be regualrized through the Lippmann-Schwinger equation for the two-body T-matrix to eliminate the high energy states responsible for the divergent behavior. At a scattering energy E, the T-matrix is defined as $T_{\mathbf{k}',\mathbf{k}}(E) \equiv \langle \mathbf{k}'|\hat{V}|\psi\rangle$, and the Lippmann-Schwinger equation reads [31]

$$T_{\mathbf{k}'\mathbf{k}}(E) = U_{\mathbf{k}'\mathbf{k}} + \frac{1}{V}\sum_{\mathbf{k}''} U_{\mathbf{k}'\mathbf{k}''}\left(E - \frac{\hbar^2 k''^2}{m_a} + i\delta\right)^{-1} T_{\mathbf{k}''\mathbf{k}}(E). \tag{A.22}$$

The positive infinitesimal δ ensures only outgoing scattered waves, and $U_{\mathbf{k}'\mathbf{k}}$ is the Fourier transform of the potential, $U_{\mathbf{k}'\mathbf{k}} = g_0$ for a contact interaction. We are interested in elastic scattering, *i.e.* $k = k' = \sqrt{m_a E_k/\hbar^2}$, for which the T-matrix is said to be evaluated *on the energy shell*. For the contact potential the equation for the T-matrix then becomes:

$$T_{\mathbf{k}\mathbf{k}}(E_k) = g_0 + \frac{g_0}{V}\sum_{\mathbf{k}'}\left(E_k - \frac{\hbar^2 k'^2}{m_a} + i\delta\right)^{-1} T_{\mathbf{k}'\mathbf{k}}(E_k). \tag{A.23}$$

This equation can be solved by iteration: the zeroth order expression for $T_{\mathbf{k}\mathbf{k}}(E_k)$ is simply g_0, and successive order can be generated by inserting the lower order expression for the T-matrix on the right hand side of (A.23). For example the first and second order terms are

$$T^{(1)}_{\mathbf{k}\mathbf{k}}(E_k) = g_0 + \frac{g_0}{V}\sum_{\mathbf{k}'}\left(E_k - \frac{\hbar^2 k'^2}{m_a} + i\delta\right)^{-1} g_0, \tag{A.24}$$

$$T^{(2)}_{\mathbf{k}\mathbf{k}}(E_k) = g_0 + \frac{g_0}{V}\sum_{\mathbf{k}'}\left(E_k - \frac{\hbar^2 k'^2}{m_a} + i\delta\right)^{-1} T^{(1)}_{\mathbf{k}\mathbf{k}}(E_k), \tag{A.25}$$

This generates the Born-Series, and we can solve the Lippmann-Schwinger equation exactly by summing the Born series to all orders, recognizing that this represents a geometric series

$$T_{\mathbf{kk}}(E_k) = g_0 \sum_{n=0}^{\infty} \left(\frac{g_0}{V} \sum_{\mathbf{k}'} \frac{1}{\frac{\hbar^2 k^2}{m_a} - \frac{\hbar^2 k'^2}{m_a} + i\delta} \right)^n = g_0 \sum_{n=0}^{\infty} \left(g_0 \mathcal{I}(k, k_c) \right)^n , \quad \text{(A.26)}$$

where we have taken the continuum limit and introduced the integral

$$\mathcal{I}(k, k_c) \equiv \frac{1}{2\pi^2} \int_0^{k_c} dk' \, \frac{k'^2}{\frac{\hbar^2 k^2}{m_a} - \frac{\hbar^2 k'^2}{m_a} + i\delta}. \quad \text{(A.27)}$$

Notice that a specific momentum cutoff k_c has been introduced in the integral, and that the value of the integral will depend not only on k, but also k_c. Returning to the expression (A.26) for the T-matrix, we observe that provided $|g_0 \mathcal{I}(k, k_c)| < 1$ (see below) the sum is convergent, and we find that

$$T_{\mathbf{kk}}(E_k) = \frac{g_0}{1 - g_0 \mathcal{I}(k, k_c)}. \quad \text{(A.28)}$$

The integral can be evaluated analytically, which is done in Appendix F, where we find that

$$\begin{aligned} \mathcal{I}(k, k_c) &= \frac{m_a}{4\pi^2 \hbar^2} \left[k \ln \left(\frac{k_c + k}{k_c - k} - 2k_c - i\pi k \right) \right] \\ &= \frac{m_a k_c}{4\pi^2 \hbar^2} \left[2 \frac{k}{k_c} \tanh^{-1} \frac{k}{k_c} - 2 - i\pi \frac{k}{k_c} \right] \\ &\simeq -\frac{m_a k_c}{4\pi^2 \hbar^2} \left(2 + i\pi \frac{k}{k_c} \right), \end{aligned} \quad \text{(A.29)}$$

where the first equality implies that $k_c > k$, and the last line follows from a Taylor expansion of $\tanh^{-1}$, and neglecting terms of order k/k_c compared with $(k/k_c)^2$.

To relate the value of the bare coupling constant g_0 to the physical scattering length, we consider the zero energy limit ($k \to 0$) of the T-matrix. Under the

condition that the scattering length of the contact potential be equal to the scattering length of the real interatomic potential, a, the zero energy limit of the T-matrix must be $T_{00}(0) = 4\pi\hbar^2 a/m_a \equiv g$ [31]. From (A.28) and (A.29) we therefore have

$$g_0 = \frac{g}{1 - g\mathcal{I}(k, k_c)} = \frac{g}{1 - \frac{m_a g k_c}{2\pi^2\hbar^2}}. \tag{A.30}$$

The importance of the momentum cutoff k_c is now clear: if $k_c \to \infty$ the T-matrix of the contact potential $g_0(1+g_0 m_a k_c/2\pi^2\hbar^2)^{-1}$ vanishes. This is simply the well know result that a delta function potential in three dimensions does not lead to any scattering. Only with an explicit momentum cutoff do we obtain a finite scattering amplitude for the unregularized pseudopotential.

Having fixed the value of g_0 by requiring the T-matrix to match that of the real potential at zero scattering energy, we can find evalute $T_{\mathbf{kk}}(E_k)$ at finite energies. Using (A.30) in expression (A.28) we then have after a few manipulations the simple result

$$T_{\mathbf{kk}}(E_k) = \frac{g}{1 + ika}. \tag{A.31}$$

The validity of this relation is determined by our assumption that $|g_0\mathcal{I}(k, k_c)| < 1$, such that the Born series to converges. From the expression for the bare coupling constant in term of the physical scattering length, and using the value of the momentum integral, this leads to the condition that $k|a| < 2k_c/\pi k$. We make use of this regularization procedure (*i.e.* delta function with a finite energy cutoff) when discussing Cooper pairing in a homogeneous system, but for situations, where the pair wavefunction varies in space, we have found it most useful to implement the regularized pseudopotential.

We end this discussion by comparing the scattering properties of the regularized pseudopotential with those of the contact potential (unregularized pseu-

dopotential) with an explicit momentum cutoff. Since the T-matrix on the energy shell is the scattering amplitude for elastic collisions

$$T_{\mathbf{kk}}(E = \frac{\hbar^2 k^2}{m_a}) = -\frac{4\pi\hbar^2}{m_a} f_k^{l=0}, \tag{A.32}$$

we conclude by comparing (A.31) with (A.20) that the contact potential with a momentum cutoff produces the same scattering states as the regularized pseudotential.

Appendix B

Numerical Methods

The development of efficient numerical methods to self-consistently solve the BdG equations constitutes a substantial part of the work presented in this thesis. The purpose of this appendix is to detail the procedures we have used to generate the numerical results. Our focus has been to find an efficient and reliable way to solve the non-linear eigenvalue problem (3.36). This involves two elements: diagonalization of the BdG equations for a given set of mean-field potentials, which yields the single-particle states from which new guesses for the fields can be generated and iteration of the solution until these potentials have converged to self-consistency. Though the iteration procedure is straightforward we will discuss in further detail below. The main part of this chapter though is devoted to discussing our method of choice for numerically representing the BdG matrix. For reasons on which we elaborate in the next section, we have utilized a Discrete Variable Representation (DVR) of the BdG Hamiltonian. In our view a DVR represents an optimal compromise between grid based and spectral methods, and is particularly well suited for problems requiring an iterative approach.

B.1 Discrete Variable Representation

The BdG equations in general must be solved numerically. Some of the effects that we are interested in, such as the shifts in the critical temperature T_c and in the ground state energy of the gas associated with the vortex state, are quite hard to calculate numerically as they are very small compared with the corresponding bulk values. For example, to obtain the vortex energy one needs to subtract two large numbers to get a small number. This requires a very accurate numerical scheme to solve the BdG equations. Such a scheme is provided by the DVR method. DVRs are representations on a basis of functions localized about discrete values of the coordinate. This property ensures that local functions of the coordinate operator are approximately diagonal within the DVR basis, making DVRs ideally suited for solving self-consistent problems like the present one, where the matrix elements of the pairing and Hartree fields (local functions) have to be evaluated at each iteration. In addition the representation of the kinetic energy operator is exact. The literature on DVRs is extensive and we shall only convey the central points here, focusing on the basic features of the methodology. A detailed review of the technique can be found in [220, 221].

B.1.1 General Framework

Since the DVR method is a completely universal approach to solving the quantum eigenvalue problem, we will keep the discussion general, and only remark on the specific implementation for BdG equations when needed. We seek a solution to an effectively one-dimensional Schrödinger equation with a local potential $\hat{V}$

$$\hat{H}|\Psi\rangle = (\hat{T} + \hat{V})|\Psi\rangle = E|\Psi\rangle. \tag{B.1}$$

The kinetic energy operator is denoted by $\hat{T}$. There are two common approaches to solving this equation: one involves representing it in coordinate space, *i.e.* defining the wavefunction $\Psi(x_\alpha) = \langle x_\alpha|\Psi\rangle$ on a finite set of N grid points $\{x_\alpha, \alpha = 1, \ldots, N\}$. By inserting the approximate completeness relation $\sum_\alpha |x_\alpha\rangle\langle x_\alpha| \approx 1$, we achieve a matrix representation of the Hamiltonian on the grid. The potential is diagonal (under the assumption that it is a local function of $\hat{x}$), but the derivative operator must be approximated, typically by a finite difference formula. We call this procedure for solving (B.1) the *grid-based method*. Alternatively, we can choose a complete square-integrable basis set of functions $\{\phi_n(x), n = 1, \ldots, \infty\}$, and expand the wavefunction in terms of these (throughout this discussion we will use Latin letters to enumerate basis functions, and Greek letters for identifying grid points). This leads to the so-called *variational basis representation* (VBR). As the derivatives of the basis functions are known, we can evaluate the matrix elements of the kinetic energy operator exactly in the VBR. The matrix elements of the potential are

$$V_{ij}^{\mathrm{VBR}} = \langle\phi_i|\hat{V}|\phi_j\rangle. \tag{B.2}$$

In general this expression has to be evaluated by numerical quadrature, which can be done to arbitrary accuracy. Therefore the only source of error in the VBR is the truncation to a finite basis $\{\phi_n(x), n = 1, \ldots, N\}$. We note that the name underscores the fact that the eigenvalues of the VBR Hamiltonian matrix are variational upper bounds on the exact spectrum.

Since the accurate evaluation of (B.2) can be computationally heavy it is often desirable to introduce a further approximation in constructing the Hamiltonian matrix. It involves the construction of a special basis $\{u_\alpha, \alpha = 1, \ldots, M\}$ which diagonalizes the coordinate operator. Denote by $\mathbf{Q}$ the position matrix in the

truncated basis

$$Q_{ij} = \langle \phi_i | \hat{x} | \phi_j \rangle, \tag{B.3}$$

we then seek a transformation $\mathbf{U}$, such that

$$\mathbf{X} = \mathbf{U}^\dagger \mathbf{Q} \mathbf{U}, \tag{B.4}$$

where $\mathbf{X}$ is a diagonal matrix $X_{\alpha\beta} = \langle u_\alpha | \hat{x} | u_\beta \rangle = x_\alpha \delta_{\alpha\beta}$, whos eigenvalues define a set of M grid points. The unitary transformation matrix is given by $U_{n\alpha} = \langle \phi_n | u_\alpha \rangle$. If we assume that the potential can be written as a power series of the coordinate operator:

$$\hat{V} = a_0 + a_1 \hat{x} + a_2 \hat{x}^2 + \cdots, \tag{B.5}$$

then the matrix elements of $\hat{V}$ is simply the sum of matrix elements of powers of $\hat{x}$. For the sake of argument we focus on the quadratic term. By inserting the *approximate* completeness relation of the coordinate eigenstates three times we obtain

$$\begin{aligned} \langle \phi_i | \hat{x}^2 | \phi_j \rangle &\approx \sum_{\alpha=1}^{M} \sum_{\beta=1}^{M} \sum_{\gamma=1}^{M} \langle \phi_i | u_\alpha \rangle \langle u_\alpha | \hat{x} | u_\beta \rangle \langle u_\beta | \hat{x} | u_\gamma \rangle \langle u_\gamma | \phi_j \rangle \\ &= \sum_{\alpha=1}^{M} \langle \phi_i | u_\alpha \rangle x_\alpha^2 \langle u_\alpha | \phi_j \rangle = \sum_{\alpha=1}^{M} U_{i\alpha} x_\alpha^2 U_{\alpha j}^*. \end{aligned} \tag{B.6}$$

This approximation is referred to as the *finite basis-set representation* (FBR). In the limit of $M \to \infty$ the completeness relation becomes exact and the FBR is identical to the VBR. A similar procedure can be carried out on all terms in the expansion of the potential, and within the FBR the potential matrix elements can therefore be written as

$$V_{ij}^{\mathrm{FBR}} = \sum_{\alpha=1}^{M} U_{i\alpha} V(x_\alpha) U_{\alpha j}^*. \tag{B.7}$$

This ensures an efficient evaluation of potential energy matrix elements. Both the VBR and FBR are *spectral methods* for solving the Schrödinger equation. We will now introduce the DVR method, which in some sense combines the virtues of the spectral method (exact evaluation of the kinetic energy) with those of grid-based methods (easy representation of the potential).

The FBR potential matrix element (B.7) looks conspicuously like a quadrature formula [222]

$$\langle f|g\rangle \equiv \int_a^b dx\, w(x) f(x) g(x) \equiv \sum_{k=1}^{N} w_k f(x_k) g(x_k), \tag{B.8}$$

where we have introduced an explicit weight function $w(x)$. A DVR exists if the spectral basis of N functions $\phi_n(x)$, orthogonal over a range $[a, b]$ with weight function $w(x)$, are chosen such that there is an associated quadrature rule with N points x_α and weights w_α ensuring that the overlap integral can be evaluated *exactly* by quadrature:

$$\langle \phi_i|\phi_j\rangle \equiv \int_a^b dx\, w(x) \phi_i^*(x) \phi_j(x) = \sum_{\alpha=1}^{N} w_\alpha \phi^*(x_\alpha) \phi_j(x_\alpha) = \delta_{ij}, \tag{B.9}$$

and that they additionally fulfill the discrete completeness relation

$$\sum_{n=1}^{N} \phi_n^*(x_\alpha) \phi_n(x_\beta) = \frac{\delta_{\alpha\beta}}{w_\alpha}. \tag{B.10}$$

We then define coordinate eigenfunctions, or DVR functions, as functions with the property

$$\chi_\alpha(x_\beta) = \frac{\delta_{\alpha\beta}}{\sqrt{w_\alpha}}, \tag{B.11}$$

i.e. they vanish on all but one quadrature points. The DVR functions can be expanded in the spectral basis:

$$\chi_\alpha = \langle x|\chi_\alpha\rangle = \sum_{n=1}^{N} \phi_n(x) \langle \phi_n|\chi_\alpha\rangle. \tag{B.12}$$

The expansion coefficients are determined by

$$\langle \phi_n | \chi_\alpha \rangle = \int dx\, w(x) \phi_n^*(x) \chi_\alpha(x) = \sum_{\beta=1}^{N} w_\beta \phi_n^*(x_\beta) \chi_\alpha(x_\beta) = \sqrt{w_\alpha} \phi_n^*(x_\alpha), \quad \text{(B.13)}$$

where we have employed the underlying quadrature integration rule and the property of the DVR functions (B.11). The discrete variable and finite basis-set representations are therefore connected through a unitary transformation $\mathbf{U}$

$$U_{n\alpha} = \langle \phi_n | \chi_\alpha \rangle = \sqrt{w_\alpha} \phi_n^*(x_\alpha). \quad \text{(B.14)}$$

It is important to note that this is a square matrix; there are the same number of basis functions as quadrature points and weights.

The coordinate eigenfunctions are given by

$$\chi_\alpha(x) = \sum_{n=1}^{N} \phi_n(x) U_{n\alpha} = \sum_{n=1}^{N} \phi_n(x) \phi_n^*(x_\alpha) \sqrt{w_\alpha}. \quad \text{(B.15)}$$

The Hamiltonian can then be transformed from the FBR to the DVR basis. For the kinetic energy operator we have

$$T_{\alpha\beta}^{\mathrm{DVR}} = \langle \chi_\alpha | \hat{T} | \chi_\beta \rangle = \left(\mathbf{U}^\dagger \mathbf{T}^{\mathrm{FBR}} \mathbf{U} \right)_{\alpha\beta}, \quad \text{(B.16)}$$

where $T_{ij}^{\mathrm{FBR}} = \langle \phi_i | \hat{T} | \phi_j \rangle$. Since we stipulated that T_{ij}^{FBR} can be evaluated exactly, the same holds true for the matrix elements of $\hat{T}$ in the DVR basis. For the potential we find that

$$V_{\alpha\beta}^{\mathrm{DVR}} = \langle \chi_\alpha | \hat{V} | \chi_\beta \rangle = \left(\mathbf{U}^\dagger \mathbf{V}^{\mathrm{FBR}} \mathbf{U} \right)_{\alpha\beta}. \quad \text{(B.17)}$$

Due to the approximation introduces when expressing the potential operator in the FBR basis as discussed above, this equality only holds approximately. However, the big advantage of the DVR immediately follows from (B.7), and (B.17):

$$V_{\alpha\beta}^{\mathrm{DVR}} \simeq V(x_\alpha) \delta_{\alpha\beta}. \quad \text{(B.18)}$$

Furthermore, the representation of the wavefunction is extraordinarily simple in the DVR basis. We expand it in terms of the the coordinate eigenfunctions:

$$\Psi(x) = \sum_{\alpha=1}^{N} \gamma_\alpha \chi_\alpha(x), \tag{B.19}$$

this will give us a set of linear equations for the expansion coefficients γ_α. The value of the wavefunction on the mesh points is then given as

$$\Psi(x_\alpha) = \frac{\gamma_\alpha}{\sqrt{w_\alpha}}. \tag{B.20}$$

The discretized Schrödinger equation becomes

$$\sum_{\beta=1}^{N} (T_{\alpha\beta} + V_{\alpha\beta})\gamma_\beta = E\gamma_\alpha. \tag{B.21}$$

Given the expansion of the wavefunction (B.19) it is simple to interpolate it onto any other mesh $\{y_k, k = 1, \ldots, M\}$

$$\Psi(y_k) = \sum_{\alpha=1}^{N} \gamma_\alpha \chi_\alpha(y_k). \tag{B.22}$$

The fact that the potential operator is (approximately) diagonal in the DVR basis is what makes the method useful for us, since we are solving an iterative eigenvalue problem. We obtain a significant improvement in computational efficiency by representing the Hamiltonian on a grid, eliminating the need to re-evaluate matrix elements of $\hat{V}$ at each iteration step. In addition to the simple form of the potential the kinetic energy operator is accurately represented, even for small grids. Having presented the general features of the DVR scheme we now turn to specific examples. There are many ways to construct a DVR, in general the appropriate form will be determined by the problem at hand. We focus below on DVR's tailored specifically to solve problems with cylindrical or spherical symmetry.

B.1.2 Bessel Function DVR

We first consider a DVR basis built on Bessel functions of integer order. This is particularly well suited for describing systems with cylindrical symmetries since the eigenstates of the Laplacian in 2 dimensions are products of Bessel functions for the radial part (ρ) and Fourier functions for the angular part (φ):

$$\Psi_{nm}(\rho,\varphi) = N_{nm} J_m(k_n \rho) \frac{e^{im\varphi}}{2\pi}, \tag{B.23}$$

with eigenvalues $-k_n^2$ [223]. The angular momentum quantum number m is restricted to integer values. The coordinate ρ is defined on the interval $[0, R]$. We must chose the weight function to be $w(\rho) = \rho$ since the the orthogonality condition of the Bessel functions is

$$\int_0^R d\rho\, \rho\, J_m(k_i \rho) J_m(k_j \rho) = \frac{\delta_{ij}}{N'^2_{im}}, \tag{B.24}$$

where the coordinate normalization constant (see below) is given by [128]

$$N'_{im} = \frac{\sqrt{2}}{R J_{m+1}(k_i R)}. \tag{B.25}$$

Similarly, the Bessel functions are also orthogonal in coordinate space, when integrated over the momentum interval $[0, K]$:

$$\int_0^K dk\, k\, J_m(k \rho_\alpha) J_m(k \rho_\beta) = \frac{\delta_{\alpha\beta}}{N^2_{\alpha m}}, \tag{B.26}$$

with the momentum normalization

$$N_{\alpha m} = \frac{\sqrt{2}}{K J_{m+1}(K \rho_\alpha)}. \tag{B.27}$$

In order to define the N quadrature points we impose a hard wall boundary condition at $\rho = R$. This implies that the coordinate eigenfunctions must vanish at the boundary, and the grid is then related to the first N zeros of the order

m Bessel function. Because of the boundary condition the last grid point is superfluous, and the actual order of the quadrature is $N-1$. As is the case for the discrete Fourier representation, to which the Bessel function DVR can be related [223], the boundary condition must be simultaneously satisfied in momentum space. We thus obtain the radial and momentum grids as $\rho_\alpha = z_\alpha/K$, and $k_i = z_i/R$, respectively, where $\{z_i, i = 1, \ldots, N\}$ are defined through $J_m(z_i) = 0$. Note that since $k_N = z_N/R = K$, and $\rho_N = z_N/K = R$, the maximum momentum and the maximum value of ρ are not independent, but are inversely related to each other by the relation $RK = z_N$.

We must now determine the weights such that the quadrature integration rule can be applied. To do this we define the symmetric matrix

$$U^m_{i\alpha} = N'_{im} N_{\alpha m} J_m(k_i \rho_\alpha) = \frac{2}{z_N} \frac{J_m(z_i z_\alpha / z_N)}{J_{m+1}(z_i) J_{m+1}(z_\alpha)}, \tag{B.28}$$

(in the following it will be understood that the quadrature is based on the m'th order Bessel function and we shall drop the index m on U and on the normalization constants N_α, N'_i whenever there is no ambiguity). It can be shown that $U^\dagger$ is the matrix defining the transformation from the coordinate representation to a momentum space basis. It has not been proven rigorously that this transformation is unitary, *i.e.* $(UU^\dagger)_{ij} = \delta_{ij}$, but numerical studies show that the matrix product is quasi-unitary, in the sense that the deviations from unitarity become negligible in the limit of large N [223]. We obtain the weights for integration in coordinate space by demanding that the normalization condition (B.24) still holds

$$\int_0^R d\rho\, \rho\, J_m(k_i \rho) J_m(k_j \rho) \;\simeq\; \sum_{\alpha=1}^{N} w_\alpha\, J_m(k_i \rho_\alpha) J_m(k_j \rho_\alpha)$$

$$= \sum_{\alpha=1}^{N} \frac{w_\alpha}{N'_i N'_j N_\alpha^2} U_{i\alpha} U_{j\alpha} = \frac{\delta_{ij}}{N'^2_i}. \qquad \text{(B.29)}$$

But $U_{i\alpha}U_{j\alpha} = U_{i\alpha}U^\dagger_{\alpha j}$, and since $\sum_\alpha U_{i\alpha}U^\dagger_{\alpha j} = \delta_{ij}$, it is clear that the quadrature rule works if the weights are chosen to be:

$$w_\alpha = N_\alpha^2 = \frac{2}{K^2 J^2_{m+1}(z_\alpha)}. \qquad \text{(B.30)}$$

Similarly, we find the weights relevant for applying the quadrature rule to integration over the momentum variable to be

$$w'_i = N'^2_i = \frac{2}{R^2 J^2_{m+1}(z_i)}. \qquad \text{(B.31)}$$

With the Bessel function quadrature in place we can go ahead and construct a DVR basis. As our orthonormal basis functions we chose

$$\phi_i(\rho) = \sqrt{w'_i} J_m(k_i \rho), \qquad \text{(B.32)}$$

where the $\sqrt{w'_i}$ is necessary to ensure that the basis set is orthonormal, *i.e.* $\langle \phi_m | \phi_n \rangle = \delta_{mn}$. From (B.15) we thus have for the coordinate eigenfunctions

$$\chi_\alpha(\rho) = \sum_{n=1}^{N} \sqrt{w'_n} J_m(k_n \rho) U_{n\alpha} = \sum_{n=1}^{N} \sqrt{w_\alpha} w'_n \, J_m(k_n \rho) J_m(k_n \rho_\alpha). \qquad \text{(B.33)}$$

It is easy to check that the $\chi' s$ do indeed diagonalize the coordinate operator

$$\begin{aligned} \chi_\alpha(\rho_\beta) &= \sum_{n=1}^{N} \sqrt{w_\alpha} w'_n \, J_m(k_n \rho_\beta) J_m(k_n \rho_\alpha) \\ &= \frac{1}{\sqrt{w_\beta}} \sum_{n=1}^{N} U^\dagger_{\beta n} U_{n\alpha} = \frac{\delta_{\alpha\beta}}{\sqrt{w_\alpha}}, \end{aligned} \qquad \text{(B.34)}$$

and that they are orthonormal

$$\begin{aligned} \langle \chi_\alpha | \chi_\beta \rangle &= \sum_{\gamma=1}^{N} w_\gamma \sum_{n=1}^{N} \sum_{s=1}^{N} \sqrt{w_\alpha w_\beta} \, w'_n w'_s \, J_m(k_n \rho_\gamma) J_m(k_n \rho_\alpha) J_m(k_s \rho_\gamma) J_m(k_s \rho_\beta) \\ &= \sum_{\gamma=1}^{N} \sum_{n=1}^{N} \sum_{s=1}^{N} U^\dagger_{\gamma n} U_{n\alpha} U^\dagger_{\gamma s} U_{s\beta} = \sum_{\gamma=1}^{N} \delta_{\alpha\gamma} \delta_{\beta\gamma} = \delta_{\alpha\beta}. \end{aligned} \qquad \text{(B.35)}$$

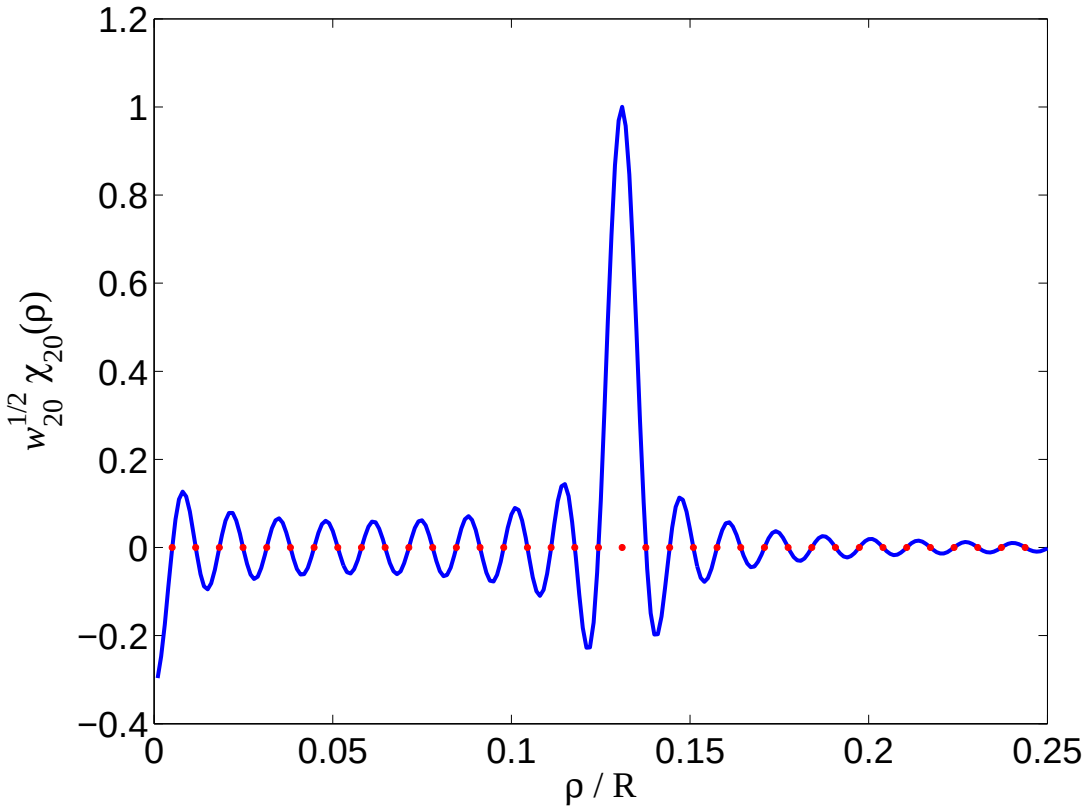

Figure B.1: Example of a coordinate eigenfunction $\chi_\alpha(\rho)$ for a Bessel function DVR based on J_0 with $N = 150$ (*blue line*). For the particular function plotted $\alpha = 20$, and the discrete delta function property (B.11) of the DVR function is clearly visible, as it is equal to $\sqrt{w_\alpha}$ at $\rho = \rho_\alpha$, while vanishing on all other DVR points (•'s). Since $z_N = 473.59$ the first DVR grid point is at $\rho = z_0/z_N = 2.4048/z_N = 5.0778\ 10^{-3}$.

An example of a DVR function for a grid based on the roots of the 0'th order Bessel function is plotted in Fig. B.1. As is seen in the figure the DVR function vanishes on all but one grid point, about which it is localized, but it is non-zero between the DVR points. Hence it has a discrete delta function property.

The discretization of the Schrödinger equation has the simple properties de-

scribed above. We calculate the matrix elements of the kinetic energy operator explicitly:

$$\begin{aligned} T_{\alpha\beta} &= \langle\chi_\alpha|\hat{T}|\chi_\beta\rangle \\ &= \int_0^R d\rho\rho\,\sqrt{w_\alpha w_\beta}\sum_{n=1}^{N}\sum_{s=1}^{N} w'_n w'_s\, J_m(k_n\rho)J_m(k_n\rho_\alpha) \\ &\quad \times\hat{T}\,J_m(k_s\rho), J_m(k_s\rho_\beta) \end{aligned} \tag{B.36}$$

we recall that the Bessel functions are eigenfunctions of the kinetic energy operator, $\hat{T}\,J_m(k_s\rho) = \frac{1}{2}k_s^2 J_m(k_s\rho)$, so the matrix elements can be evaluated analytically (within the quadrature approximation to the integral):

$$\begin{aligned} T_{\alpha\beta} &= \sum_{\gamma=1}^{N}\sum_{n=1}^{N}\sum_{s=1}^{N} w_\gamma\sqrt{w_\alpha w_\beta}w'_n w'_s J_m(k_n\rho_\gamma)J_m(k_n\rho)\alpha\,\frac{k_s^2}{2}\,J_m(k_s\rho_\gamma)J_m(k_s\rho_\beta) \\ &= \sum_{\gamma=1}^{1}\sum_{n=1}^{N}\sum_{s=1}^{N}\frac{k_s^2}{2}\,U^\dagger_{\gamma n}U_{n\alpha}U_{\gamma s}U_{s\beta} = \sum_{s=1}^{N} U^\dagger_{i\alpha s}\,\frac{k_s^2}{2}\,U_{s\beta} \\ &= U^\dagger\,\frac{\mathbf{k}^2}{2}\,U = U\,\frac{\mathbf{k}^2}{2}\,U^\dagger. \end{aligned} \tag{B.37}$$

Likewise, it is easy to show that the potential is diagonal in the DVR basis.

Although it appears that a separate grid is needed for each m value, we have found that in practice only two grids are needed, one based on J_0 for even and one based on J_1 for odd m. Hence we have two sets of DVR functions $\{\chi^0_\alpha(\rho), \alpha = 1,\ldots,N\}$ and $\{\chi^1_\alpha(\rho), \alpha = 1,\ldots,N\}$. The associated quadrature points are ρ^0_α (ρ^1_α) and the weights w^0_α (w^1_α), where the superscripts indicate whether the grids are derived from the roots of J_0 and J_1, respectively. When solving the BdG equations for a vortex state, special care must be taken to represent the off-diagonal terms correctly, since they will mix different angular momentum components, and hence functions on both spatial grids. We write the BdG equations for a single quantum state of the system in the compact form

(suppressing the indices labeling the quantum numbers of the state):

$$\mathcal{L}_m u + \Delta v = 0, \tag{B.38}$$

$$-\mathcal{L}_{m+1} v + \Delta u = 0, \tag{B.39}$$

where $\mathcal{L}_m = T_m + V_{\rm ext}(\mathbf{r}) + g n_\sigma(\mathbf{r}) - \mu - E$, with T_m being the kinetic energy corresponding to angular momentum m, meaning the centrifugal potential is $m^2/2\rho^2$ in dimensionless units. The remaining terms in $\mathcal{L}_m$ represents the external potential, the Hartree field, the chemical potential and the excitation energy of the single-particle state in question, respectively. We start by finding the matrix elements of $\Delta(\mathbf{r})$ for the case where m is even. The appropriate expansion of u and v is then:

$$\begin{aligned} u(\rho) &= \sum_{\alpha=1}^{N} \gamma_\alpha \chi^0(\rho), \\ v(\rho) &= \sum_{\beta=1}^{N} \gamma_\beta \chi^1_\beta(\rho), \end{aligned} \tag{B.40}$$

Inserting the expansion of u, v into (B.38) and multiplying by $\chi^0_\alpha(\rho)$ followed by an integration over $\rho d\rho$ we obtain for the off-diagonal (overlap) matrix elements

$$\Delta_{\alpha\beta} = \int_0^R d\rho\rho\, \chi^0_\alpha(\rho)\Delta(\rho)\chi^1_\beta(\rho). \tag{B.41}$$

Substituting for $\chi^0_\alpha(\rho)$ and $\chi^1_\beta(\rho)$ and using the quadrature integration rule on the 'even' grid, *i.e.* $\int d\rho\rho\, F(\rho) = \sum_\alpha w^0_\alpha F(\rho^0_\alpha)$, we get

$$\begin{aligned} \Delta_{\alpha\beta} &= \sum_{\gamma=1}^{N}\sum_{m=1}^{N}\sum_{n=1}^{N} w^0_\gamma \sqrt{w^0_\alpha w^1_\beta}\, w^{0'}_n w^{1'}_m J_0(k^0_n\rho^0_\gamma) J_0(k^0_n\rho^0_\alpha) J_1(k^1_m\rho^0_\gamma) J_1(k^1_m\rho^1_\beta)\Delta(\rho^0_\gamma), \\ &= \sum_{\gamma=1}^{N}\sum_{m=1}^{N}\sum_{n=1}^{N} \sqrt{w^0_\gamma w^1_\beta}\, w^{1'}_m U^0_{n\gamma} U^0_{n\alpha} J_1(k^1_m\rho^0_\gamma) J_1(k^1_m\rho^1_\beta)\Delta(\rho^0_\gamma), \\ &= \sum_{\gamma=1}^{N}\sum_{m=1}^{N} \sqrt{w^0_\gamma w^1_\beta}\, w^{1'}_m \delta_{\alpha\gamma} J_1(k^1_m\rho^0_\gamma) J_1(k^1_m\rho^1_\beta)\Delta(\rho^0_\gamma), \end{aligned}$$

$$= \sum_{m=1}^{N} \sqrt{w_\alpha^0 w_\beta^1} w_m^{1'} J_1(k_m^1 \rho_\alpha^0) J_1(k_m^1 \rho_\beta^1) \Delta(\rho_\alpha^0), \tag{B.42}$$

where we have utilized the unitarity of the U-matrices. Similarly, the matrix elements of the 3rd quadrant of the BdG Hamiltonian are found by expanding $u(\rho)$ and performing the overlap integral with $\chi_\alpha^1(\rho)$, using the *same* quadrature rule as before to evaluate the integral

$$\begin{aligned}
\Delta_{\alpha\beta} &= \int d\rho\, \chi_\alpha^1(\rho) \Delta(\rho) \chi_\beta^0(\rho) \\
&= \sum_{\gamma=1}^{N} \sum_{m=1}^{N} \sum_{n=1}^{N} w_\gamma^0 \sqrt{w_\alpha^1 w_\beta^0} w_n^{0'} w_m^{1'} J_0(k_n^0 \rho_\gamma^0) J_0(k_n^0 \rho_\beta^0) J_1(k_m^1 \rho_\gamma^0) J_1(k_m^1 \rho_\alpha^1) \Delta(\rho_\gamma^0), \\
&= \sum_{\gamma=1}^{N} \sum_{m=1}^{N} \sum_{n=1}^{N} \sqrt{w_\gamma^0 w_\alpha^1} w_m^{1'} U_{n\gamma}^0 U_{n\beta}^0 J_1(k_m^1 \rho_\gamma^0) J_1(k_m^1 \rho_\alpha^1) \Delta(\rho_\gamma^0), \\
&= \sum_{\gamma=1}^{N} \sum_{m=1}^{N} \sqrt{w_\gamma^0 w_\alpha^1} w_m^{1'} \delta_{\beta\gamma} J_1(k_m^1 \rho_\gamma^0) J_1(k_m^1 \rho_\alpha^1) \Delta(\rho_\gamma^0), \\
&= \sum_{m=1}^{N} \sqrt{w_\gamma^0 w_\alpha^1} w_m^{1'} J_1(k_m^1 \rho_\beta^0) J_1(k_m^1 \rho_\alpha^1) \Delta(\rho_\beta^0),
\end{aligned} \tag{B.43}$$

which is the transpose of the expression given above, as expected. Had we used a different quadrature rule in the 3rd quadrant (*e.g.* the integration rule associated with the 'odd' grid) we would have ended a non-symmetric BdG matrix. It does not matter if we choose the 'even' or 'odd' grid quadrature rule, as long as we are consistent. It is easily seen that in the case where the two grids are the same, *i.e.* when $\rho_\alpha^0 = \rho_\alpha^1$, $w_\alpha^0 = w_\alpha^1$, and $k_\alpha^0 = k_\alpha^1$ for all α, the overlap matrix elements become diagonal so that $\Delta_{\alpha\beta} = \Delta(\rho_\alpha^0)\delta_{\alpha\beta}$. The matrix elements for the case of m odd are the same as those found above, but with the expressions in the 2nd and 3rd quadrant reversed.

B.1.3 Orthogonal Polynomial DVR

We now consider a special class of DVRs, where the underlying spectral basis functions are defined in terms of a classical orthogonal polynomial such that

$$\phi_n(x) = \sqrt{w(x)}\, p_{n-1}(x), \tag{B.44}$$

where $w(x)$ is a non-negative weight function, and $\{p_n, n = 0, 1, \ldots\}$ are polynomials of degree n, orthogonal to each other over a range $[a, b]$ with respect to $w(x)$, *i.e.*

$$\int_a^b dx\, w(x) p_m(x) p_n(x) = \delta_{mn}. \tag{B.45}$$

Depending on the orthogonal polynomial in question the interval can be either finite, semi-infinite or infinite. Including the weight function directly in the basis functions slightly modifies the definition of the DVR functions:

$$\chi_\alpha(x) = \sum_{n=1}^{N} \phi_n(x) \phi_n^*(x_\alpha) \sqrt{\frac{w_\alpha}{w(x_\alpha)}}, \tag{B.46}$$

as is easily demonstrated. The DVR functions are therefore the product of a polynomial of order $N - 1$ by the square root of the weight function. The special property of the orthogonal polynomials is that the associated quadrature is of the Gauss-Jacobi type. Hence for a quadrature specified on N points the integration rule (B.8) is *exact* when the integrand is a polynomial of degree $2N - 1$ or less [222, 224]. We will now determine the DVR grid points and the quadrature weights.

The orthogonal polynomials are known to satisfy the Christoffel-Darboux sum formula [224, 225]

$$\sum_{m=0}^{n} p_m(x) p_m(y) = \frac{k_n}{k_{n+1}} \frac{p_{n+1}(x) p_n(y) - p_n(x) p_{n+1}(y)}{x - y}, \tag{B.47}$$

where k_n is the coefficient of x^n in $p_n(x)$. An equivalent formula holds for the basis functions (B.44)

$$\sum_{m=1}^{N} \phi_m(x)\phi_m(y) = \frac{k_{N-1}}{k_N} \frac{\phi_{N+1}(x)\phi_N(y) - \phi_N(x)\phi_{N+1}(y)}{x-y}, \tag{B.48}$$

as is seen by multiplying both sides of (B.47) by $\sqrt{w(x)w(y)}$. The condition of discrete completeness (B.10) of the basis functions ϕ_n is then fulfilled for a given family of orthogonal polynomials if

$$\phi_{N+1} = 0 \implies p_N(x_\alpha) = 0. \tag{B.49}$$

This defines the mesh points. To determine the quadrature weights we follow the discussion in Szegö [224]: Setting $y = x_\alpha$ in (B.48), and integrating over the interval. We evaluate the left hand side first:

$$\begin{aligned} \int_a^b dx \sum_{m=1}^{N} \phi_m(x)\phi_m(x_\alpha) &= \sum_{n=0}^{N-1} \left(\int_a^b dx\, w(x) p_n(x) p_0(x) \right) \frac{p_n(x_\alpha)}{p_0(x)} \\ &= \sum_{n=0}^{N-1} \delta_{n0} \frac{p_n(x_\alpha)}{p_0(x)} = 1, \end{aligned} \tag{B.50}$$

using the fact that $p_o(x)$ is constant and non-vanishing. On the right hand side the second term vanishes since $\phi_{N+1}(x_\alpha) = 0$, and we are left with

$$\begin{aligned} 1 &= \frac{k_{N-1}}{k_N} \int_a^b dx \frac{\phi_{N+1}(x)\phi_N(x_\alpha)}{x - x_\alpha} \\ &= \frac{k_{N-1}}{k_N} \int_a^b dx\, w(x) \frac{p_N(x) p_{N-1}(x_\alpha)}{x - x_\alpha} = \frac{k_{N-1}}{k_N} \sum_\beta w_\beta \frac{p_N(x_\beta) p_{N-1}(x_\alpha)}{x_\beta - x_\alpha} \\ &= \frac{k_{N-1}}{k_N} p'_N(x_\alpha) p_{N-1}(x_\alpha) w_\alpha. \end{aligned} \tag{B.51}$$

The weights are then given by

$$w_\alpha = \frac{k_N}{k_{N-1}} \frac{1}{p_{N-1}(x_\alpha) p'_N(x_\alpha)}. \tag{B.52}$$

Going back to the expansion of the coordinate eigenfunctions (B.46) we find from the Christoffel-Darboux formula for the basis functions (B.48) that the DVR functions can be expressed as

$$\chi_\alpha(x) = \sqrt{\frac{w_\alpha}{w(x_\alpha)}}\,\frac{k_{N-1}}{k_N}\,\frac{\phi_{N+1}(x)\phi_N(x_\alpha)}{x - x_\alpha} = \frac{p_N(x)}{p'_N(x_\alpha)(x - x_\alpha)}\sqrt{\frac{w(x)}{w_\alpha}}. \tag{B.53}$$

We note that the orthogonal polynomial of order N can expressed as

$$p_N(x) = k_N \prod_{\alpha=1}^{N}(x - x_\alpha), \tag{B.54}$$

where $p_N(x_\alpha) = 0$. The derivative of $p_N(x)$ is easily calculated

$$\phi'_N(x) = \sum_{\alpha=1}^{N}\frac{p_N(x)}{x - x_\alpha}, \tag{B.55}$$

and specifically on the mesh points it takes the values

$$\phi'_N(x_\alpha) = k_N \prod_{\beta=1}^{N}{}'\,(x_\alpha - x_\beta), \tag{B.56}$$

where the prime denotes the exclusion of the point $x_\beta = x_\alpha$ in the product. The expression for the DVR functions can therefore be reduced to the simple form

$$\chi_\alpha(x) = v_\alpha(x)\sqrt{\frac{w(x)}{w_\alpha}}, \tag{B.57}$$

where $v_\alpha(x)$ are the Lagrange interpolating functions defined at the associated quadrature points

$$v_\alpha(x) = \prod_{\beta=1}^{N}{}'\,\frac{x - x_\beta}{x_\alpha - x_\beta}. \tag{B.58}$$

Matrix elements of the derivative operator are easily found as $v_\alpha(x)$ and its derivatives can be tabulated. We remark that an alternative, yet less straightforward way to evaluate the kinetic energy matrix elements, is to use the known properties of the orthogonal polynomials and their derivatives. For each particular orthogonal polynomial DVR analytical formulas for $T_{\alpha\beta}$ can then be derived [220].

B.1.4 One Grid to Rule Them All

We end our exploration of the DVR method by giving an example of a DVR based on an orthogonal polynomial. For solving the BdG equations in a system with radial harmonic confinement, we have found it efficient to use a DVR based on associated Laguerre polynomials $L_n^k(x)$, where k is an integer. These are orthogonal over the interval $[0, \infty]$ with weight function $w(x) = x^k e^{-x}$. In our experience this approach works very well for solving the radial Schrödinger equation for potentials with both cylindrical and spherical symmetry. The basis functions $\phi_n(x) = x^{k/2} e^{-x/2} L_n^k(x)$ can be shown to be associated with the kinetic energy operator [220]

$$T = -\frac{1}{2}\frac{d^2}{dx^2} + \frac{k(k-2)}{8x^2}. \tag{B.59}$$

Choosing $k = 2l + 2$ we find that this is equivalent to the radial kinetic energy operator of a particle with angular momentum l represented in spherical coordinates. The odd integer values $k = 2|m| + 1$ reduces (B.59) to the radial kinetic energy in cylindrical coordinates for angular momentum m. The important point is that in both cases the singular centrifugal potential is included in T such that its matrix elements will be exactly calculated.

It may seem that a separate grid is needed for each value of l (m). However, we have found that this is doing unnecessary work. Indeed it is possible to solve the radial Schrödinger equation with great precision using only a single value of k for *all* values of the angular momentum, and including the centrifugal barrier $l(l+1)/2x^2$ ($m^2/2x^2$) as an additional term in the Hamiltonian. For a system with spherical symmetry we choose $k = 2$, such that the second term in (B.59) vanishes. However, the inclusion of $\sqrt{w(x)} = x^{k/2} e^{-x/2}$ in the DVR function ensures that it vanishes like x at the origin, and consequently the matrix

elements of the centrifugal term are all regular at the origin. For cylindrical symmetry we use $k = 1$, in which case the second term in (B.59) becomes $-1/8x^2$, so this part of the singular potential is treated explicitly. The behavior of the DVR functions at the origin is $x^{1/2}$, which enforces regularity on all matrix elements of $m^2/2x^2$. As a example of the performance of the method we plot in Fig. B.2 the relative error on the calculated eigenvalues for both a spherically and cylindrically symmetric harmonic oscillator for several different values of the angular momentum. The plots show that a single grid for each symmetry (spherical or cylindrical) is capable of accurately representing the Hamiltonian for the considered example, finding eigenstates with energies up to $E_n \simeq 125\ \hbar\omega$ with a relative error of less than 10^{-6}. For reasons which are not entirely clear to us the accuracy of the eigenvalues for $l = 1$ ($m = 1$) are significantly worse than for all other values of the angular momentum. However, the error on these states is still well within what we believe is acceptable.

We have only applied this particular DVR for potentials with radial harmonic confinement, where we find it to work extremely well. In order to maximize the number of eigenvalues that are captured accurately for a given number of grid points, we rescale the grid by a scaling factor, such that $x'_\alpha = hx_\alpha$, to concentrate the points in the region of physical interest, where the wavefunction is finite. For $N \simeq 150$ we find that the optimal value of h is around 20 for both the cylindrical and spherical grids. We remark that while the centrifugal term formally will not be treated exactly since its matrix elements are non-polynomial, and hence outside the scope of the quadrature, by concentrating the quadrature points in the region close to the origin, we can still achieve great accuracy.

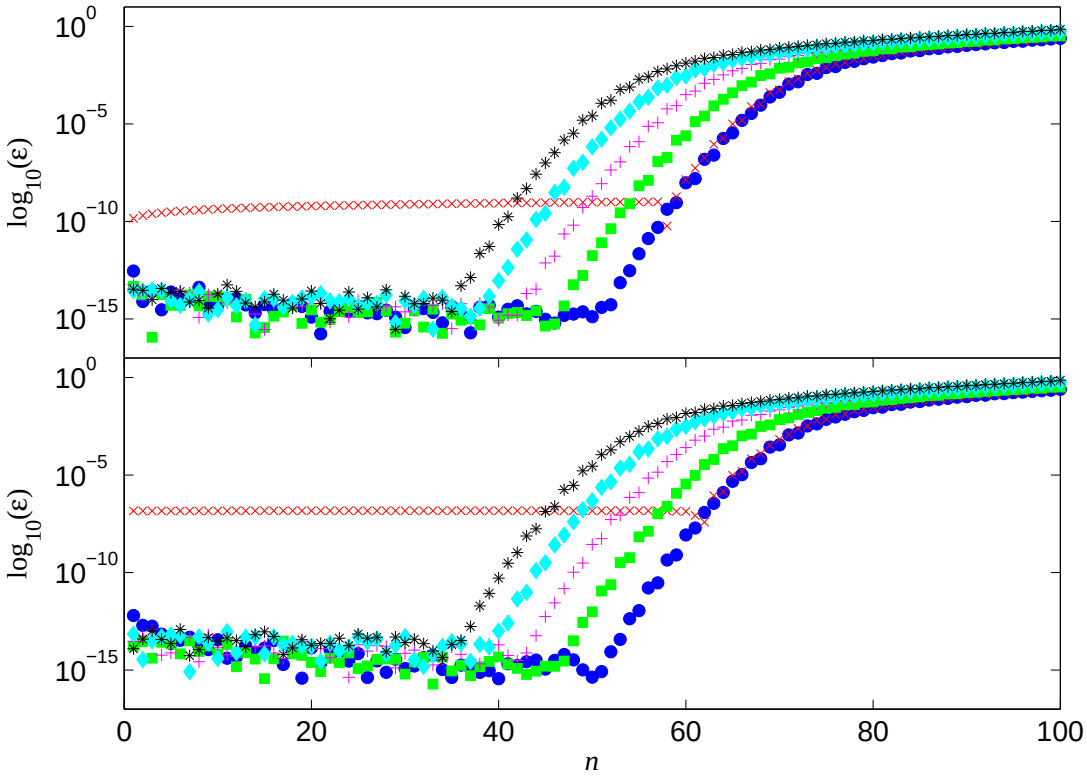

Figure B.2: Plot of the relative error $\varepsilon \equiv |E_n^{\text{num}} - E_n|/E_n$ of the eigenvalues of a spherical (*top panel*) and a cylindrical (*bottom panel*) harmonic oscillator potential as a function of the radial quantum number n. The Schrödinger equation was solved using the Laguerre DVR method with $N = 150$, and grid scaling factor $h = 20$. In the upper panel the symbols are $l = 0$ (●'s), $l = 1$ (×'s), $l = 10$ (■'s), $l = 20$ (+'s), $l = 30$ (♦'s), and $l = 50$ (∗'s). In the lower panel the symbols correspond to the same values of m.

B.2 Self-consistency

As stated several times the BdG equations (3.36) constitute a non-linear eigenvalue problem in that the solutions for the quasi-particle amplitudes $u_\eta(\mathbf{r})$ and $v_\eta(\mathbf{r})$, and their energies E_η depend on the mean-field potentials $\Delta(\mathbf{r})$, and the

atomic density $n_\sigma(\mathbf{r})$, which themselves are determined from the quasi-particle modes, *i.e.*

$$\Delta = \Delta(\{u_\eta(\Delta, n_\sigma), v_\eta(\Delta, n_\sigma), E_\eta(\Delta, n_\sigma)\}), \tag{B.60}$$

and likewise for the density. To solve this set of equation we adopt an iterative procedure. That is we start from an initial guess for the mean-fields at a given temperature, which is inserted into the BdG equations. Solving these then gives us a set of quasiparticle states from which new mean-fields can be constructed. These updated potentials are then inserted back into the BdG equations, and step by step the system of equations converges towards a self-consistent solution. This algorithm is illustrated schematically in Fig. B.3. Our test of convergence consists of comparing the integrated mean fields $\int d^3r\, \Delta(\mathbf{r})$ and $\int d^3r\, n_\sigma(\mathbf{r})$ with the values of those integrals from the previous iteration step. If the relative change in both is less than a set tolerance level, we accept the present values of the gap function and density as converged. Typically the tolerance level is set at 10^{-6}. We have found that in general the Hartree field converges much faster than the order parameter function $\Delta(\mathbf{r})$. Furthermore, the convergence of the integrated values of the gap and the density is almost always monotonic. This means that it is never a good idea to construct the next guess on $\Delta(\mathbf{r})$ and $n_\sigma(\mathbf{r})$ by mixing values from several iteration steps. The latest values are always the best guess, and ensures the fastest convergence. We speculate that if some other convergence criteria could be found, where the value of the observed parameter oscillates between from iteration to iteration, more sophisticated schemes could be successfully applied to damp out these fluctuations in an optimized fashion.

Often we desire to obtain a solution with a specified number of particles. A simple extension of out iteration scheme allows us to this, by introducing a

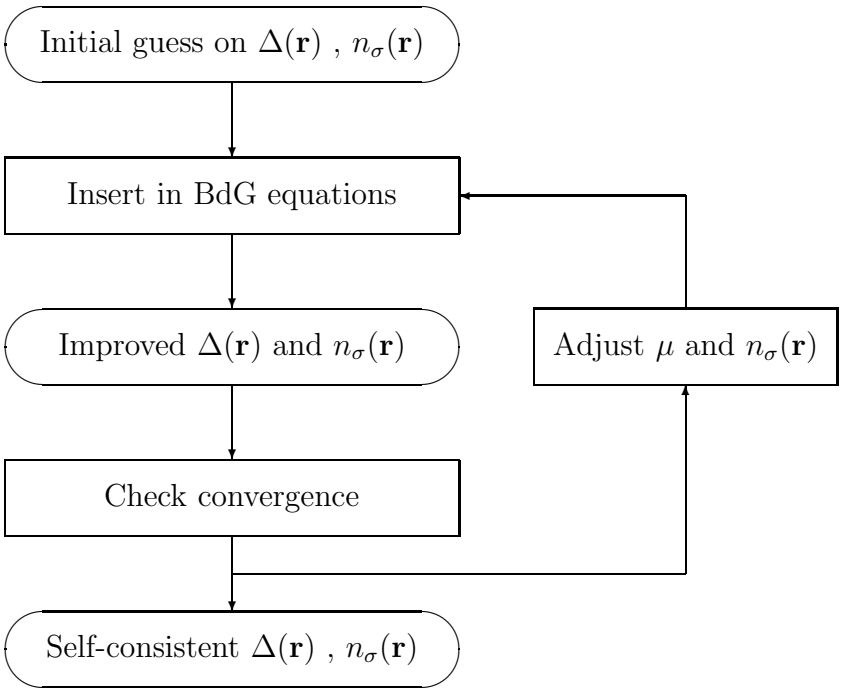

Figure B.3: The pairing field $\Delta(\mathbf{r})$ and the density distribution $n_\sigma(\mathbf{r})$ satisfy a set of coupled equations which have to be solved by iteration. The procedure illustrated here has been used in the calculations presented in the text.

new constraint. When fixing the particle number to be some particular value N_σ we adjust the chemical potential and the atomic density distribution at each iteration step. Denoting by r_i the ratio between the sought atom number and the expectation value of $\hat{N}_\sigma$ at the i'th iteration step, $r = N_\sigma/N^i$, we construct the values of μ and $n_\sigma(\mathbf{r})$ to be used as input at the next iteration step to be

$$\begin{aligned} \mu^{i+1} &= r\,\mu^i, \\ n_\sigma^{i+1}(\mathbf{r}) &= r\,n_\sigma^i(\mathbf{r}). \end{aligned}$$

In our experience this method is both fast and works with very few exceptions.

A notable failure is for a normal state Fermi gas close to zero temperature, where shell effects causes a step structure in $\mu(N)$ as discussed in Section 5.4. In that case the method described here can lead to a situation where the chemical potential jumps back and forth cyclicly between two or more values, corresponding to different steps, without N_σ^i ever converging to N_σ. An alternative method to fixing the particle number would be to first converge the BdG solution to self-consistence at at fixed value of μ, and then change the chemical potential in the direction needed to make N_σ^i approach the desired value, repeating the entire self-consistent calculation at this new value of μ. Iterating this procedure one can implement a root finding procedure for the chemical potential. However, since each step involves a full solution of the BdG problem it is much more involved than simply adjusting μ 'on the fly' within the BdG solver. Furthermore, one is still subject to the problems posed by shell effects.

B.3 Parallelization

Since the Pauli exclusion principle mandates that no more than a single fermion can occupy any given quantum state, the number of quasi-particle states we generally need to generate is a few times the number of particles in the system. Typically this means tens of thousands of states. Luckily, the BdG equations for a system with cylindrical symmetry are block diagonal in the angular momentum quantum number m. Furthermore, for a system with free propagation along the symmetry axis, the axial momentum $\hbar k_z$ enters the Hamiltonian only parametrically. Hence the eigenvalue problem splits into the diagonalization of a large number of small matrices, one for each set of values (m, k_z). This problem

is ideally suited for parallelization, since mean-fields, *i.e.* the density and the gap function $\Delta(\mathbf{r})$, are the sum of contributions from quasi-particle states with different values of m and k_z, *e.g.*

$$\Delta(\mathbf{r}) = \sum_{mk_z} \Delta_{mk_z}(\mathbf{r}), \tag{B.61}$$

where the individual terms $\Delta_{mk_z}(\mathbf{r})$ can be calculated independently. The density distribution $n_\sigma(\mathbf{r})$ can be broken down in a similar fashion. The same holds true for a spherically symmetric system, where the Hamiltonian separates into sectors with different values of l, and $\Delta(\mathbf{r}) = \sum_l \Delta_l(\mathbf{r})$. We therefore parse out the calculation to several processors, which at a given iteration step independently calculate $\Delta_{mk_z}(\mathbf{r})$ (or $\Delta_l(\mathbf{r})$) for a small number of m (or l) values using the current values of the mean-fields as input. The results are then communicated back to a master processor, which combines them to created updated potentials, $\Delta(\mathbf{r})$ and $n_\sigma(\mathbf{r})$.

The individual matrices are very small (typically we use between 100 and 200 DVR points), but the calculation does not rely heavily on communications back and forth between the 'master' and the 'slaves'. Hence the limiting task is the diagonalization of thousands of matrices, and by distributing this task, we achieve almost perfect linear speed-up with the number of nodes. Therefore our numerical problem is the poster child for parallelization.

Appendix C

Finite Temperature Field Theory

This section serves to provide a super brief introduction to the concepts of finite temperature field theory as they apply to a superfluid Fermi gas. For a more thorough introduction the reader should consult a standard textbook (see for example [27, 46]).

As we have seen in chapter 3 the grand canonical ensemble provides the natural context in which to describe the superfluid Fermi system, since the particle number is not conserved in the condensed phase. The state of thermal equilibrium is then determined by minimizing the free energy under the constraint that the average particle number is fixed to be $N = \langle \hat{N} \rangle$. Introducing the operator

$$\hat{K} = \hat{H} - \mu \hat{N}, \tag{C.1}$$

this means that the thermal average of an operator $\hat{O}$ is

$$\langle \hat{O} \rangle = \frac{\mathrm{Tr}[e^{-\beta \hat{K}} \hat{O}]}{\mathrm{Tr}[e^{-\beta \hat{K}}]}, \tag{C.2}$$

where as usual $\beta = 1/k_{\mathrm{B}}T$. Since the statistical operator $\exp(-\beta \hat{K})$ is identical to the the quantum mechanical evolution operator evaluated at $t = -i\hbar\beta$, the thermal averaging can be thought of as a propagation in imaginary time $t = -i\tau$

from $\tau = 0$ to $\beta\hbar$. We define the modified Heisenberg picture

$$\hat{O}_H(\tau) = e^{\hat{K}\tau/\hbar} O e^{-\hat{K}\tau/\hbar}. \tag{C.3}$$

It turns out that this representation is a convenient starting point for perturbation expansions of physical quantities. To see this let us split $\hat{K}$ into a part $\hat{K}_0$, which can be diagonalized exactly, and a perturbation $\hat{H}'$. In analogy with time-dependent perturbation theory at zero temperature we introduce an interaction picture $\hat{O}_I(\tau)$ such that

$$\hat{O}_I(\tau) = e^{\hat{K}_0\tau/\hbar} O e^{-\hat{K}_0\tau/\hbar}. \tag{C.4}$$

This representation of the operator is related with the Heisenberg picture by a simple transformation

$$\hat{O}_I(\tau) = \mathcal{U}(\tau, 0)\hat{O}_H\mathcal{U}(0, \tau), \tag{C.5}$$

where

$$\mathcal{U}(\tau, 0) = e^{\hat{K}_0\tau/\hbar} e^{-\hat{K}\tau/\hbar}. \tag{C.6}$$

The transformation operator satisfies the Bloch equation

$$\hbar\frac{\partial\mathcal{U}(\tau, 0)}{\partial\tau} = e^{\hat{K}_0\tau/\hbar}\left(\hat{K}_0 - \hat{K}\right)e^{-\hat{K}\tau/\hbar} = -\hat{H}'_I(\tau)\mathcal{U}(\tau, 0). \tag{C.7}$$

The solution is easily found by integration, and yields an integral equation, which can be solved by iteration to give the perturbation series for $\mathcal{U}$

$$\mathcal{U}(\tau, 0) = \sum_{n=0}^{\infty}\frac{(-1/\hbar)^n}{n!}\int_0^\tau d\tau_1 \cdots \int_0^\tau d\tau_n\, T_\tau \hat{H}'(\tau_1)\cdots\hat{H}'(\tau_n), \tag{C.8}$$

where he symbol T_τ orders the operators such that τ decreases from left to right, and we have dropped the subscript on the interaction picture operators. The

perturbation expansion of the grand canonical partition function can then be found

$$\begin{aligned} e^{-\beta\Omega} &= \mathrm{Tr}[e^{-\beta\hat{K}}] = \mathrm{Tr}[e^{-\beta\hat{K}_0}\mathcal{U}(\beta\hbar,0)] \\ &= \sum_{n=0}^{\infty}\frac{(-1/\hbar)^n}{n!}\int_0^{\beta\hbar}d\tau_1\cdots\int_0^{\beta\hbar}d\tau_n\,\mathrm{Tr}[e^{-\beta\hat{K}_0}T_\tau\hat{H}'(\tau_1)\cdots\hat{H}'(\tau_n)], \end{aligned} \tag{C.9}$$

from which the linked cluster theorem for the ground state energy follows by purely combinatorial considerations when it is realized that only topologically distinct, connected diagrams contribute to the sum.

One can show that the single-particle Green's function for fermions (bosons) must be anti-periodic (periodic) in each τ variable with period $\beta\hbar$. This defines the Fourier transforms between the τ and so-called Matsubara frequency representations

$$F(i\omega_n) = \int_0^{\hbar\beta}d\tau\,e^{i\omega_n\tau}F(\tau), \tag{C.10}$$

$$F(\tau) = \frac{1}{\beta\hbar}\sum_n e^{-i\omega_n\tau}F(i\omega_n), \tag{C.11}$$

where the allowed frequencies form a discrete set. For fermions the Fourier series is restricted to include only odd terms

$$\omega_n = \frac{(2n+1)\pi}{\beta\hbar}, \tag{C.12}$$

whereas bosonic Matsubara frequencies are even

$$\omega_n = \frac{(2n)\pi}{\beta\hbar}. \tag{C.13}$$

C.1 Matsubara Sums

To evaluate sums over Matsubara frequencies

$$\frac{1}{\beta\hbar}\sum_{\omega_n}F(i\omega_n), \tag{C.14}$$

we apply the residue theorem [128] to the function $F(\omega)$, which has poles that all lie off the imaginary axis. Since the Fermi distribution function has first order poles at the complex frequencies $i(2n+1)\pi/\beta\hbar$, with $n \in \mathbb{Z}$ one may easily prove the equality

$$\oint_C d\omega\, F(\omega) f(\hbar\omega) = 2\pi i \sum_{\omega_n} \mathrm{Res}_n(F(\omega) f(\hbar\omega)) = -\frac{2\pi i}{\beta\hbar} \sum_{\omega_n} F(i\omega_n). \qquad \text{(C.15)}$$

The contour C encloses the imaginary axis, see Fig. (C.1), and we have utilized that the residue of $f(\hbar\omega)$ at $\omega = i\omega_n$ is $-1/\beta\hbar$. The integral over the contour C' enclosing not only the poles of $f(\hbar\omega)$, but also those of $F(\omega)$ can then be written as

$$\oint_{C'} d\omega\, F(\omega) f(\hbar\omega) = \oint_C d\omega\, F(\omega) f(\hbar\omega) + 2\pi i \sum_{\alpha} \mathrm{Res}_\alpha(F(\omega) f(\hbar\omega)), \qquad \text{(C.16)}$$

where α enumerate the poles of $F(\omega)$. Extending C' to infinity the integral on the left hand side of (C.16) vanishes, and we arrive at the identity

$$\frac{1}{\beta\hbar} \sum_{\omega_n} F(i\omega_n) = \sum_{\alpha} \mathrm{Res}_\alpha \left(F(\omega) f(\hbar\omega)\right). \qquad \text{(C.17)}$$

As an example we evaluate the commonly appearing sum

$$\frac{1}{\beta\hbar} \sum_{\omega_n} \frac{1}{i\omega_n + i\omega_m - E_\eta/\hbar} \frac{1}{i\omega_n + E_\nu/\hbar}, \qquad \text{(C.18)}$$

Where ω_m is a bosonic Matsubara frequency. In this particular case the function $F(\omega)$ is

$$F(\omega) = \frac{1}{\omega + i\omega_m - E_\eta/\hbar} \frac{1}{\omega + E_\nu/\hbar}, \qquad \text{(C.19)}$$

with poles located at $\omega_1 = E_\eta/\hbar - i\omega_m$, and $\omega_2 = -E_\nu$. For the residues in (C.17) we have

$$\begin{aligned} \mathrm{Res}_1 \left(F(\omega) f(\hbar\omega)\right) &= \frac{f(E_\eta)}{E_\eta/\hbar + E_\nu/\hbar - i\omega_m}, \\ \mathrm{Res}_2 \left(F(\omega) f(\hbar\omega)\right) &= \frac{1 - f(E_\nu)}{i\omega_m - E_\eta/\hbar - E_\nu\hbar}, \end{aligned}$$

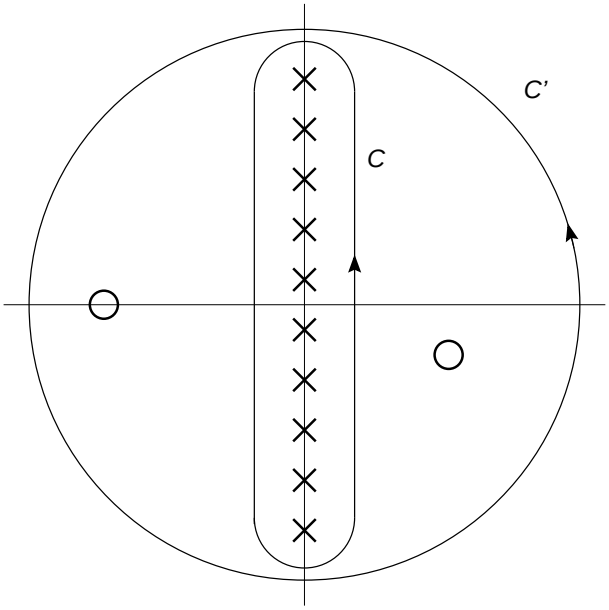

Figure C.1: Contours for evaluation of Matsubara sums. The crosses mark the poles of the Fermi function, while circles indicate the poles of the function $F(\omega)$ (see text).

using the relations $f(-E) = 1 - f(E)$, and $f(E - i\hbar\omega_m) = f(E)$, provided ω_m is a bosonic frequency.

C.2 Green's Functions

As is customary we shall denote the finite temperature Green's function by $\mathcal{G}$. This should not be confused with the symmetry group of the Hamiltonian for which we adopted the same symbol. We hope that the meaning will be clear from the context. In order to construct a perturbation theory which is valid in the condensed phase we must include in our description not only the "normal" propagator $\mathcal{G}$, but also anomalous propagators, $\mathcal{F}^\dagger$ and $\mathcal{F}$, describing the finite amplitude for creating and destroying a pair of particles in opposite spin states,

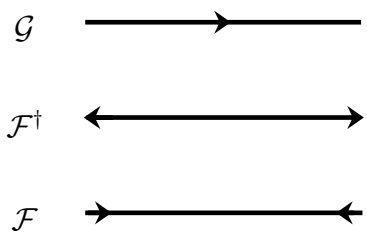

Figure C.2: Feynman diagrams for the Green's functions.

respectively [65]. The definitions of the relevant propagators are

$$\begin{aligned}
\mathcal{G}(\mathbf{r}\tau,\mathbf{r}'\tau') &= -\langle T_\tau \psi_\sigma(\mathbf{r},\tau)\psi^\dagger_\sigma(\mathbf{r}',\tau')\rangle, \\
\mathcal{F}(\mathbf{r}\tau,\mathbf{r}'\tau') &= -\langle T_\tau \psi_\uparrow(\mathbf{r},\tau)\psi_\downarrow(\mathbf{r}',\tau')\rangle, \\
\mathcal{F}^\dagger(\mathbf{r}\tau,\mathbf{r}'\tau') &= -\langle T_\tau \psi^\dagger_\downarrow(\mathbf{r},\tau)\psi^\dagger_\uparrow(\mathbf{r}',\tau')\rangle,
\end{aligned} \tag{C.20}$$

assuming both spin states are equally populated such that $\mathcal{G}_{\uparrow\uparrow} = \mathcal{G}_{\downarrow\downarrow} = \mathcal{G}$. Fig. (C.2) provides the graphical representation of the superfluid Green's functions.

The convention for evaluating the same time Green's functions is to take the limit $\tau' = \tau^+$, or equivalently, $\tau - \tau' = 0^-$ [46]. Using this, and the Matsubara rules "in reverse" we find that the Green's functions for a Fermi superfluid have the spectral decomposition

$$\begin{aligned}
\mathcal{G}(\mathbf{r},\mathbf{r}',i\omega_n) &= \sum_\eta \left[\frac{u_\eta(\mathbf{r})u^*_\eta(\mathbf{r}')}{i\omega_n - E_\eta/\hbar} + \frac{v_\eta(\mathbf{r}')v^*_\eta(\mathbf{r})}{i\omega_n + E_\eta/\hbar}\right], \\
\mathcal{F}(\mathbf{r},\mathbf{r}',i\omega_n) &= \sum_\eta \left[\frac{u_\eta(\mathbf{r})v^*_\eta(\mathbf{r}')}{i\omega_n - E_\eta/\hbar} - \frac{u_\eta(\mathbf{r}')v^*_\eta(\mathbf{r})}{i\omega_n + E_\eta/\hbar}\right], \\
\mathcal{F}^\dagger(\mathbf{r},\mathbf{r}',i\omega_n) &= \sum_\eta \left[\frac{u^*_\eta(\mathbf{r}')v_\eta(\mathbf{r})}{i\omega_n - E_\eta/\hbar} - \frac{u^*_\eta(\mathbf{r})v_\eta(\mathbf{r}')}{i\omega_n + E_\eta/\hbar}\right].
\end{aligned} \tag{C.21}$$

For a translationally invariant system one can go to the momentum representation and the forms of the Green's functions are then (assuming $\Delta = \Delta^*$)

$$\begin{aligned} \mathcal{G}(\mathbf{k}, i\omega_n) &= \frac{u_{\mathbf{k}}^2}{i\omega_n - E_{\mathbf{k}}/\hbar} + \frac{v_{\mathbf{k}}^2}{i\omega_n + E_{\mathbf{k}}/\hbar}, \\ \mathcal{F}(\mathbf{k}, i\omega_n) &= -u_{\mathbf{k}} v_{\mathbf{k}} \left[\frac{1}{i\omega_n - E_{\mathbf{k}}/\hbar} - \frac{1}{i\omega_n + E_{\mathbf{k}}/\hbar} \right], \end{aligned} \tag{C.22}$$

and in this case $\mathcal{F}^\dagger(\mathbf{k}, i\omega_n) = \mathcal{F}(\mathbf{k}, i\omega_n)$.

Appendix D

Wick's Theorem

We are often faced with the calculation of thermal averages of products of n operators

$$\langle \hat{A}_1 \hat{A}_2 \cdots \hat{A}_n \rangle = \mathrm{Tr}[\hat{\rho} \hat{A}_1 \hat{A}_2 \cdots \hat{A}_n], \tag{D.1}$$

where $\hat{A}_i$ denote either a creation operator $\hat{c}_i^\dagger$ or a destruction operator $\hat{c}_i$, and we have defined the distribution operator as

$$\hat{\rho} = \frac{e^{-\beta \hat{K}}}{\mathrm{Tr}[e^{-\beta \hat{K}}]}. \tag{D.2}$$

In general, ensemble averages like (D.1) are difficult to evaluate, but in the special case that the Hamiltonian is quadratic in the field operators, the expression can be greatly simplified by applying Wick's theorem [226]. Because of the form of the distribution operator when $\hat{K}$ s quadratic we will refer to this as a Gaussian ensemble. It is worth pointing out that a Gaussian ensemble is equivalent to a system of non-interacting particles.

Below we state Wick's theorem without proof. The interested reader is urged to consult Zubarev *et al.* for the proof [227]. A nice discussion can also be found in Fetter and Walecka [27]. While the derivations concern only the ensembles where the exponent of the distribution function contain *normal* pairs of the form

$\hat{c}_i^\dagger \hat{c}_j$, the theorem can also be applied to systems governed by a quadratic Hamiltonian, which includes *anomalous* terms like $\hat{c}_i \hat{c}_j$. As pointed out in Chapter 3 we can introduce a canonical transformation from the operators $\hat{c}_i$ to a new set of operators $\hat{\gamma}_\eta$, such that when $\hat{\rho}$ is written in the new basis it contains only normal pairs $\hat{\gamma}_\eta^\dagger \hat{\gamma}_\nu$. Since the transformation is linear, the theorem can thus be applied to any quadratic ensemble.

Defining the *pairing* of two operators as their average in the Gaussian ensemble $\langle \hat{A}_i \hat{A}_j \rangle_0$. The subscript 0 indicate that the average is taken in the quadratic ensemble. Furthermore we introduce the *complete system of pairings* for a product of operators, where the operators are paired in sequence, the first with the second, the third with the fourth, etc. For example the complete system of pairings of the operator product $\hat{A}_1 \hat{A}_2 \hat{A}_3 \hat{A}_4 = \langle \hat{A}_1 \hat{A}_2 \rangle_0 \langle \hat{A}_3 \hat{A}_4 \rangle_0$. If the number of operators are odd the complete system of pairings vanishes. Wick's theorem states that an average like D.1 calculated in a Gaussian ensemble is equal to the sum over all complete systems of pairing. In mathematical terms this can be written as

$$\langle \hat{A}_1 \hat{A}_2 \cdots \hat{A}_n \rangle_0 = \sum_{P_d} (\pm 1)^{\mathcal{P}} \langle \hat{A}_1 \hat{A}_2 \rangle_0 \langle \hat{A}_3 \hat{A}_4 \rangle_0 \cdots \langle \hat{A}_{n-1} \hat{A}_n \rangle_0. \tag{D.3}$$

The sum runs over all distinct permutations P_d of the indices. Each complete system of pairings acquire a phase factor $(\pm 1)^{\mathcal{P}}$, where $\mathcal{P}$ is the number of interchanges required to transform the original arrangement of the operators into the final one. The upper (lower) sign refer to bosons (fermions). As an example we evaluate the simplest non-trivial operator average, which consists of four operators

$$\langle \hat{A}_1 \hat{A}_2 \hat{A}_3 \hat{A}_4 \rangle_0 \;=\; \langle \hat{A}_1 \hat{A}_2 \rangle_0 \langle \hat{A}_3 \hat{A}_4 \rangle_0 \pm \langle \hat{A}_1 \hat{A}_3 \rangle_0 \langle \hat{A}_2 \hat{A}_4 \rangle_0$$

$$+\langle \hat{A}_1 \hat{A}_4 \rangle_0 \langle \hat{A}_2 \hat{A}_3 \rangle_0. \tag{D.4}$$

The form in which we most commonly encounter this in the theory of a two-component Fermi gas is

$$\begin{aligned} \langle \hat{\psi}^\dagger_\uparrow(\mathbf{r}) \hat{\psi}^\dagger_\downarrow(\mathbf{r}) \hat{\psi}_\downarrow(\mathbf{r}) \hat{\psi}_\uparrow(\mathbf{r}) \rangle_0 &= \langle \hat{\psi}^\dagger_\uparrow(\mathbf{r}) \hat{\psi}_\uparrow(\mathbf{r}) \rangle_0 \langle \hat{\psi}^\dagger_\downarrow(\mathbf{r}) \hat{\psi}_\downarrow(\mathbf{r}) \rangle_0 \\ &\quad + \langle \hat{\psi}^\dagger_\uparrow(\mathbf{r}) \hat{\psi}^\dagger_\downarrow(\mathbf{r}) \rangle_0 \langle \hat{\psi}_\downarrow(\mathbf{r}) \hat{\psi}_\uparrow(\mathbf{r}) \rangle_0 \\ &\quad - \langle \hat{\psi}^\dagger_\uparrow(\mathbf{r}) \hat{\psi}_\downarrow(\mathbf{r}) \rangle_0 \langle \hat{\psi}^\dagger_\downarrow(\mathbf{r}) \hat{\psi}_\uparrow(\mathbf{r}) \rangle_0. \end{aligned} \tag{D.5}$$

The first term is simply the product of the atomic densities in the two hyperfine states, while the second term is the squared modulus of the anomalous average defined in Chapter 3, it is non-vanishing only in the superfluid phase. The last term is indicative of an internal coherence or *magnetization* in the system and is usually neglected in theories of Fermi superfluidity.

Appendix E

Duality of the Quasi-Particle Modes

The prove the duality between the positive and negative energy branches of the Bogoliubov quasi-particle spectrum

$$E_{\eta\sigma} \rightarrow -E_{\eta-\sigma}, \quad \begin{pmatrix} u_\eta \\ v_\eta \end{pmatrix} \rightarrow \begin{pmatrix} v_\eta^* \\ -u_\eta^* \end{pmatrix}, \tag{E.1}$$

we first observe that

$$\begin{pmatrix} -1 & 0 \\ 0 & 1 \end{pmatrix} \left[\begin{pmatrix} -\mathcal{L}_{-\sigma}^* & \Delta^* \\ \Delta & \mathcal{L}_\sigma \end{pmatrix} \begin{pmatrix} v_\eta \\ u_\eta \end{pmatrix} \right]^* = \begin{pmatrix} \mathcal{L}_{-\sigma} & \Delta \\ \Delta^* & -\mathcal{L}_\sigma^* \end{pmatrix} \begin{pmatrix} v_\eta^* \\ -u_\eta^* \end{pmatrix}, \tag{E.2}$$

but using the Bogoliubov-de Gennes equations the left-hand side can also be written as

$$\begin{pmatrix} -1 & 0 \\ 0 & 1 \end{pmatrix} \left[\begin{pmatrix} -\mathcal{L}_{-\sigma}^* & \Delta^* \\ \Delta & \mathcal{L}_\sigma \end{pmatrix} \begin{pmatrix} v_\eta \\ u_\eta \end{pmatrix} \right]^* = \begin{pmatrix} -1 & 0 \\ 0 & 1 \end{pmatrix} E_{\eta\sigma} \begin{pmatrix} v_\eta^* \\ u_\mu^* \end{pmatrix}, \tag{E.3}$$

where we have used that the energies are all real (they are the eigenvalues of a Hermitian matrix), and so we find that

$$\begin{pmatrix} \mathcal{L}_{-\sigma} & \Delta \\ \Delta^* & -\mathcal{L}_\sigma^* \end{pmatrix} \begin{pmatrix} v_\eta^* \\ -u_\eta^* \end{pmatrix} = -E_{\eta\sigma} \begin{pmatrix} v_\eta^* \\ -u_\eta^* \end{pmatrix}, \tag{E.4}$$

which proves (E.1). Hence there is a duality between eigenstates in the '+' family ($E_{\eta\sigma} > 0$) and the '−' family ($E_{\eta\sigma} < 0$). Since the latter does not contribute any additional information we keep only the '+' family solutions.

In the case of a singly quantized vortex line the duality between the '+' and '−' family solutions can be shown to be:

$$E_{-m-1} \rightarrow -E_m, \quad \begin{pmatrix} u_{-m-1} \\ v_m \end{pmatrix} \rightarrow \begin{pmatrix} v^*_{-m-1} \\ -u^*_m \end{pmatrix}, \tag{E.5}$$

where for reasons of clarity we have only indicated the angular momentum quantum number of the quasi-particle states.

Appendix F

Evaluation of a Few Integrals

The purpose of this appendix is give the details of the evaluation of some of the integrals encountered in the body of the text.

F.1 Regular Part of Green's Function

To evaluate the integral I_1 we re-write it as (introducing $\tilde{\gamma} = 2m\gamma/\hbar^2$)

$$\begin{aligned} I_1 &= \frac{m_a}{\pi^2\hbar^2}\int_0^{k_c(\mathbf{r})} dk\, \frac{k^2}{k_{\rm F}^2(\mathbf{r}) - k^2 + i\tilde{\gamma}} \\ &= \frac{m_a}{\pi^2\hbar^2}\int_0^{k_c(\mathbf{r})} dk\, \frac{k}{2}\left(\frac{1}{k_{\rm F}(\mathbf{r}) - k + i\delta} - \frac{1}{k_{\rm F}(\mathbf{r}) + k + i\delta}\right) \\ &= \frac{m_a}{2\pi^2\hbar^2}\left(I_{1a} + I_{1b}\right), \end{aligned} \tag{F.1}$$

with $\delta = \tilde{\gamma}/2k_{\rm F}(\mathbf{r})$. With the help of the identity [228]

$$\lim_{\delta\to 0^+}\int \frac{dx f(x)}{x + i\delta} = {\rm P}\int \frac{dx f(x)}{x} - i\pi\int dx\, f(x)\delta(x), \tag{F.2}$$

we find that

$$\begin{aligned} I_{1a} &= {\rm P}\int_0^{k_c(\mathbf{r})} dk\, \frac{k}{k_{\rm F}(\mathbf{r}) - k} - i\pi\int_0^{k_c(\mathbf{r})} dk\, k\, \delta(k_{\rm F}(\mathbf{r}) - k) \\ &= -{\rm P}\int_0^{k_c(\mathbf{r})} dk\, \frac{k_{\rm F}(\mathbf{r}) - k}{k_{\rm F}(\mathbf{r}) - k} - k_{\rm F}(\mathbf{r})\ {\rm P}\int_0^{k_c(\mathbf{r})}\ \frac{d(k_{\rm F}(\mathbf{r}) - k)}{k_{\rm F}(\mathbf{r}) - k} - i\pi k_{\rm F}(\mathbf{r}) \end{aligned}$$

$$= \quad -k_c(\mathbf{r}) - k_{\rm F}(\mathbf{r}) \ln \frac{k_c(\mathbf{r}) - k_{\rm F}(\mathbf{r})}{k_{\rm F}(\mathbf{r})} - i\pi k_{\rm F}(\mathbf{r}), \tag{F.3}$$

since $0 \leq k_{\rm F}(\mathbf{r}) \leq k_c(\mathbf{r})$. Similarly, we get for I_{1b}

$$I_{1b} = -k_c(\mathbf{r}) + k_{\rm F}(\mathbf{r}) \ln \frac{k_c(\mathbf{r}) + k_{\rm F}(\mathbf{r})}{k_{\rm F}(\mathbf{r})}, \tag{F.4}$$

where there is no contribution from the delta function $\delta(k_{\rm F}(\mathbf{r}) + k)$, since k can not be negative. In summary, the integral which enters the regular part of the single-particle Green's function (3.63) is

$$I_1 = -\frac{m_a}{\pi^2\hbar^2} \left(k_c(\mathbf{r}) - \frac{k_{\rm F}(\mathbf{r})}{2} \ln \frac{k_c(\mathbf{r}) + k_{\rm F}(\mathbf{r})}{k_c(\mathbf{r}) - k_{\rm F}(\mathbf{r}} \right) - \frac{i m_a k_{\rm F}(\mathbf{r})}{2\pi\hbar^2}. \tag{F.5}$$

F.2 Zero Temperature Gap in LDA

We seek the value of $\Delta(\mathbf{r})$ which solves the zero temperature gap equation in a LDA setting

$$-\frac{1}{g} = I_2 - \frac{m_a}{2\pi^2\hbar^2} \left(k_c(\mathbf{r}) - \frac{k_{\rm F}(\mathbf{r})}{2} \ln \frac{k_c(\mathbf{r}) + k_{\rm F}(-\mathbf{r})}{k_c(\mathbf{r}) - k_{\rm F}(\mathbf{r}} \right), \tag{F.6}$$

where the momentum integral is given by

$$I_2 = \frac{1}{2\pi^2} \int_0^{k_c(\mathbf{r})} dk\, k^2\, \frac{1}{2E(\mathbf{r}, \mathbf{k})}. \tag{F.7}$$

With the substitution $\epsilon = \hbar^2 k^2 / 2m_a$ the integral becomes

$$I_2 = \frac{1}{\pi^2} \left(\frac{m_a}{2\hbar^2} \right)^{3/2} \int_0^{\epsilon_c(\mathbf{r})} \frac{d\epsilon\, \sqrt{\epsilon}}{\sqrt{(\epsilon - \mu(\mathbf{r}))^2 + |\Delta(\mathbf{r})|^2}} \tag{F.8}$$

where $\epsilon_c(\mathbf{r}) \equiv \hbar^2 k_c(\mathbf{r}) / 2m_a$. We define the dimensionless variable $x \equiv \epsilon / \mu(\mathbf{r})$, in terms of which the integral expression is

$$I_2 = \frac{m_a k_{\rm F}(\mathbf{r})}{4\pi^2\hbar^2} \int_0^{\epsilon_c(\mathbf{r})/\mu(\mathbf{r})} \frac{dx \sqrt{x}}{\sqrt{(x-1)^2 + |\tilde{\Delta}(\mathbf{r})|^2}}, \tag{F.9}$$

where we have introduced the parameter $\tilde{\Delta}(\mathbf{r}) \equiv \Delta(\mathbf{r})/\mu(\mathbf{r})$. In the weak-coupling limit this is a small quantity, and to property exploit this we split the integral into three regions

$$\begin{aligned} (i) \qquad & 0 < x < 1-\tau \\ (ii) \qquad & 1-\tau < x < 1+\tau \\ (ii) \qquad & 1+\tau < x < \epsilon_c(\mathbf{r})/\mu(\mathbf{r}). \end{aligned}$$

Here τ is a small parameter, defined such that $\tilde{\Delta}(\mathbf{r}) \ll \tau \ll 1$. By writing $\sqrt{x}$ as $(\sqrt{x}-1)+1$ we then have

$$\begin{aligned} I_2 \;\simeq\; & \frac{m_a k_{\rm F}(\mathbf{r})}{4\pi^2\hbar^2}\Big[\int_0^{1-\tau} dx\, \frac{(\sqrt{x}-1)+1}{\sqrt{(x-1)^2+|\tilde{\Delta}(\mathbf{r})|^2}} \\ & + \int_{1-\tau}^{1+\tau} dx\, \frac{1}{\sqrt{(x-1)^2+|\tilde{\Delta}(\mathbf{r})|^2}} \\ & + \int_{1+\tau}^{\epsilon_c(\mathbf{r})/\mu(\mathbf{r})} dx\, \frac{(\sqrt{x}-1)+1}{\sqrt{(x-1)^2+|\tilde{\Delta}(\mathbf{r})|^2}}\Big]. \end{aligned} \tag{F.10}$$

We have taken $\sqrt{x} \simeq 1$ in the middle integral, introducing an error or order τ^2. Collecting terms the integral expression is

$$\begin{aligned} I_2 \;\simeq\; & \frac{m_a k_{\rm F}(\mathbf{r})}{4\pi^2\hbar^2}\Big[\int_0^{\epsilon_c(\mathbf{r})/\mu(\mathbf{r})} \frac{dx}{\sqrt{(x-1)^2+|\tilde{\Delta}(\mathbf{r})|^2}} \\ & + \int_0^{1-\tau} \frac{\sqrt{x}-1}{\sqrt{(x-1)^2+|\tilde{\Delta}(\mathbf{r})|^2}} \\ & + \int_{1+\tau}^{\epsilon_c(\mathbf{r})/\mu(\mathbf{r})} dx\, \frac{\sqrt{x}-1}{\sqrt{(x-1)^2+|\tilde{\Delta}(\mathbf{r})|^2}}\Big]. \end{aligned} \tag{F.11}$$

Neglecting term of $(\tilde{\Delta}(\mathbf{r})/\tau)^2$, we can set $\tilde{\Delta}(\mathbf{r}) = 0$ in the last two integrals:

$$\begin{aligned} I_2 \;\simeq\; & \frac{m_a k_{\rm F}(\mathbf{r})}{4\pi^2\hbar^2}\Big[\int_0^{\epsilon_c(\mathbf{r})/\mu(\mathbf{r})} \frac{dx}{\sqrt{(x-1)^2+|\tilde{\Delta}(\mathbf{r})|^2}} \\ & - \int_0^{1-\tau} \frac{dx}{1+\sqrt{x}} + \int_{1+\tau}^{\epsilon_c(\mathbf{r})/\mu(\mathbf{r})} \frac{dx}{1+\sqrt{x}}\Big]. \end{aligned} \tag{F.12}$$

All these integrals can be evaluated analytically [229], and we find for I_2

$$\begin{aligned} I_2 = &= \frac{m_a k_{\rm F}(\mathbf{r})}{4\pi^2\hbar^2}\Big\{ \ln\left[\left(\frac{k_c^2(\mathbf{r})}{k_{\rm F}2(\mathbf{r})}-1\right)+\sqrt{\left(\frac{k_c^2(\mathbf{r})}{k_{\rm F}2(\mathbf{r})}-1\right)^2+|\tilde{\Delta}(\mathbf{r})|^2}\right] \\ &\quad -\ln\left(\sqrt{1+|\tilde{\Delta}(\mathbf{r})|^2}-1\right)-2\left(\sqrt{1-\tau}-\ln\left[1+\sqrt{1-\tau}\,\right]\right) \\ &\quad -2\left(\sqrt{1+\tau}-\ln\left[1+\sqrt{1+\tau}\right]\right) \\ &\quad +2\left(\frac{k_c(\mathbf{r})}{k_{\rm F}(\mathbf{r})}-\ln\left[1+\frac{k_c(\mathbf{r})}{k_{\rm F}(\mathbf{r})}\right]\right)\Big\}. \end{aligned} \tag{F.13}$$

We then expand the square roots, and throw away terms of order $|\tilde{\Delta}(\mathbf{r})|^4$ and τ^2, as well as neglecting $|\tilde{\Delta}(\mathbf{r})|^2$ when compared with $k_c^2(\mathbf{r})/k_{\rm F}2(\mathbf{r})-1$. This leaves us with

$$I_2 = \frac{m_a k_{\rm F}(\mathbf{r})}{4\pi^2\hbar^2}\left[5\ln 2-4-\ln\frac{k_c(\mathbf{r})+k_{\rm F}(\mathbf{r})}{k_c(\mathbf{r})-k_{\rm F}(\mathbf{r})}+\frac{2k_c(\mathbf{r})}{k_{\rm F}(\mathbf{r})}-\ln\frac{|\Delta(\mathbf{r})|^2}{2\mu^2(\mathbf{r})}\right]. \tag{F.14}$$

Inserting this into (F.6) we finally have for the zero temperature gap (assuming $\Delta(\mathbf{r})$ real)

$$\Delta(\mathbf{r}) = 8e^{-2}\mu(\mathbf{r})e^{1/N(\mathbf{r},0)g}. \tag{F.15}$$

F.3 Sum Rule for Laserprobe Current

We wish to evaluate the integral of the laserprobing current (5.36) over all detunings. Assuming the laserprofile is constant $\Omega(\mathbf{r}) = \Omega$ the equation for the current reduces to

$$\begin{aligned} I(\delta) = &- \frac{2\pi\Omega^2}{\hbar}\Big\{\sum_{\eta,n}\left|\int d^3r\, u_\eta(\mathbf{r})\phi_n^*(\mathbf{r})\right|^2 [f(E_\eta)-f(\xi_n)] \\ &\times \delta(E_\eta-\xi_n-\tilde{\delta})+\sum_{\eta,n}\left|\int d^3r\, v_\eta^*(\mathbf{r})\phi_n^*(\mathbf{r})\right|^2 \\ &\times [1-f(E_\eta)-f(\xi_n)]\,\delta(E_\eta+\xi_n+\tilde{\delta})\Big\}. \end{aligned} \tag{F.16}$$

The integral of the current over all detunings is then

$$\begin{aligned}\int d\delta\, I(\delta) &= -\frac{2\pi\Omega^2}{\hbar}\sum_{\eta,n}\Big\{\Big|\int d^3r\, u_\eta(\mathbf{r})\phi_n^*(\mathbf{r})\Big|^2\,[f(E_\eta)-f(\xi_n)] \\ &\quad +\Big|\int d^3r\, v_\eta^*(\mathbf{r})\phi_n^*(\mathbf{r})\Big|^2\,[1-f(E_\eta)-f(\xi_n)]\Big\} \\ &= -\frac{2\pi\Omega^2}{\hbar}\sum_{\eta,n}\int d^3r\int d^3r'\,\phi_n^*(\mathbf{r})\phi_n(\mathbf{r}') \\ &\quad \times\Big\{-f(\xi_n)\left[u_\eta(\mathbf{r})u_\eta^*(\mathbf{r}')+v_\eta^*(\mathbf{r})v_\eta(\mathbf{r}')\right] \\ &\quad +u_\eta(\mathbf{r})u_\eta^*(\mathbf{r}')f(E_\eta)+v_\eta^*(\mathbf{r})v_\eta(\mathbf{r}')[1-f(E_\eta)]\Big\}. \qquad \text{(F.17)}\end{aligned}$$

Utilizing the completeness of the quasi-particle amplitudes (3.30) in the first term, and that the normal state wavefunctions also form a complete set, *i.e.* $\sum_n \phi_n^*(\mathbf{r}')\phi_n(\mathbf{r}') = \delta(\mathbf{r}-\mathbf{r}')$, in the second term we obtain for the current:

$$\begin{aligned}\int d\delta\, I(\delta) &= -\frac{2\pi\Omega^2}{\hbar}\Big\{-\int d^3r\sum_n |\phi_n(\mathbf{r})|^2\, f(\xi_{\mathbf{k}}) \\ &\quad +\int d^3r\sum_\eta\left[|u_\eta(\mathbf{r})|^2 f(E_\eta)+|v_\eta(\mathbf{r})|^2(1-f(E_\eta))\right]\Big\} \\ &= \frac{2\pi\Omega^2}{\hbar}\,(N_e-N_\uparrow)\,. \qquad \text{(F.18)}\end{aligned}$$

Bibliography

[1] H. K. Onnes, Comm. Phys. Lab. Univ. Leiden **119**, **120**, **122** (1911).

[2] W. Meissner and R. Oschenfeld, Naturwissenschaften **21**, 787 (1933).

[3] P. Kapitza, Nature **141**, 74 (1938).

[4] J. F. Allen and A. D. Misener, Nature **141**, 75 (1938).

[5] J. F. Allen and H. Jones, Nature **141**, 243 (1938).

[6] V. Peshkov, J. Phys. (USSR) **8**, 381 (1944).

[7] F. London, Nature **141**, 643 (1938).

[8] L. Tisza, Nature **141**, 913 (1938).

[9] C. J. Gorter and H. Casimir, Phys. Z. **35**, 963 (1934).

[10] L. D. Landau, J. Phys. (USSR) **5**, 71 (1941).

[11] V. L. Ginzburg and L. D. Landau, Zh. Eksperim. i. Theor. Fiz. **20**, 1064 (1950).

[12] L. P. Pitaevskii, Sov. Phys. JETP **13**, 451 (1961).

[13] E. P. Gross, Il Nuovo Cimento **20**, 454 (1961).

[14] P. W. Anderson, Rev. Mod. Phys. **38**, 298 (1966).

[15] N. Bogolubov, J. Phys. **11**, 23 (1947).

[16] J. Bardeen, L. N. Cooper, and J. R. Schrieffer, Phys. Rev. **108**, 1175 (1957).

[17] D. D. Osheroff and R. C. R. ad D. M. Lee, Phys. Rev. Lett. **28**, 885 (1972).

[18] G. J. Bednorz and K. A. Müller, Z. Phys. B **64**, 189 (1986).

[19] M. H. Anderson, J. R. Ensher, M. R. Matthews, C. E. Wieman, and E. A. Cornell, Science **269**, 198 (1995).

[20] K. B. Davis, M.-O. Mewes, M. R. Andrews, N. J. van Druten, D. S. Durfee, D. M. Kurn, and W. Ketterle, Phys. Rev. Lett. **75**, 3969 (1995).

[21] C. C. Bradley, C. A. Sackett, J. J. Tollett, and R. G. Hulet, Phys. Rev. Lett. **75**, 1687 (1995), *ibid.* **79**, 1170 (1997).

[22] W. Pauli, Phys. Rev. **58**, 716 (1940).

[23] J. P. Elliott and P. G. Dawber, *Symmetry in Physics* (Oxford University Press, New York, 1979), Vol. 2.

[24] E. C. Stoner, Phil Mag. **48**, 719 (1924).

[25] W. Pauli, jr., Z. Phys. **31**, 765 (1925).

[26] K. Huang, *Statistical Mechanics*, 2nd ed. (Wiley, New York, 1987).

[27] A. L. Fetter and J. D. Walecka, *Quantum theory of many-particle systems* (McGraw-Hill, New York, 1971).

[28] E. Fermi, Rend. Licei **3**, 145 (1926), translated by Alberto Zannoni, http://arxiv.org/cond-mat/9912229.

[29] E. Fermi, Z. Physik **36**, 902 (1926).

[30] P. Ehrenfest and J. R. Oppenheimer, Phys. Rev. **37**, 333 (1931).

[31] C. J. Pethick and H. Smith, *Bose-Einstein Condensation in Dilute Gases* (Cambridge University Press, Cambridge, 2002).

[32] A. Einstein, Sitzungber. Preuss. Akad. Wiss. **1925**, 3 (1925).

[33] S. Bose, Z. Phys. **26**, 178 (1924).

[34] T. J. Greytak, in *Bose-Einstein Condensation*, edited by A. Griffin, D. W. Snoke, and S. Stringari (Cambridge University Press, Cambridge, 1995), Chap. 7, p. 131.

[35] J. R. Anglin and W. Ketterle, Nature **416**, 211 (2002).

[36] C. S. Adams and E. Riis, Prog. Quant. Electr. **21**, 1 (1997).

[37] in *Bose-Einstein Condensation in Atomic Gases*, *International School of Physics "Enrico Fermi", Course CXL*, edited by M. Inguscio, S. Stringari, and C. E. Wieman (IOS Press, Amsterdam, 1999).

[38] E. A. Cornell and C. E. Wieman, Rev. Mod. Phys. **74**, 875 (2002).

[39] W. Ketterle, Rev. Mod. Phys. **74**, 1131 (2002).

[40] B. DeMarco, J. L. Bohn, J. P. B. Jr., M. Holland, and D. S. Jin, Phys. Rev. Lett. **82**, 4208 (1999).

[41] S. L. Shapiro and S. A. Teukolsky, *Black Holes, White Dwarfs, and Neutron Stars* (John Wiley & Sons, New York, 1983).

[42] A. W. Truscott, K. E. Strecker, W. I. McAlexander, G. B. Partridge, and R. G. Hulet, Science **291**, 2570 (2001).

[43] B. DeMarco and D. S. Jin, Science **285**, 1703 (1999).

[44] J. Schneider and H. Wallis, Phys. Rev. A **57**, 1253 (1998).

[45] D. A. Butts and D. S. Rokhsar, Phys. Rev. A **55**, 4346 (1997).

[46] G. D. Mahan, *Many-Body Physics*, 3rd ed. (Kluwer Academics/Plenum Publishers, New York, 2000).

[47] R. D. Mattuck, *A Guide to Feynman Diagrams in the Many-Body Problem*, 2nd ed. (Dover Publications, Inc., New York, 1976).

[48] G. M. Bruun and K. Burnett, Phys. Rev. A **58**, 2427 (1998).

[49] H. T. C. Stoof, M. Houbiers, C. A. Sackett, and R. G. Hulet, Phys. Rev. Lett. **76**, 10 (1996).

[50] M. Houbiers, R. Ferwerda, H. T. C. Stoof, W. I. McAlexander, C. A. Sackett, and R. G. Hulet, Phys. Rev. A **56**, 4864 (1997).

[51] R. Roth and H. Feldmeier, Phys. Rev. A **64**, 043603 (2001).

[52] H. Heiselberg, Phys. Rev. A **63**, 043606 (2001).

[53] M. E. Gehm, S. L. Hemmer, S. R. Granade, K. M. O'Hara, and J. E. Thomas, Phys. Rev. A **68**, 011401(R) (2003).

[54] M. R. Schafroth, Phys. Rev. **96**, 1149 (1954).

[55] M. R. Schafroth, Phys. Rev. **100**, 502 (1955).

[56] M. R. Schafroth and J. M. Blatt, Phys. Rev. **100**, 1221 (1955).

[57] D. D. Osheroff, Rev. Mod. Phys. **69**, 667 (1997).

[58] A. J. Leggett, Rev. Mod. Phys. **47**, 331 (1975).

[59] A. Bohr, B. R. Mottelson, and D. Pines, Phys. Rev. **110**, 936 (1958).

[60] P. Ring and P. Schuck, *The Nuclear Many-Body Problem* (Springer-Verlag, New York, 1980).

[61] E. Gubankova, W. V. Liu, and F. Wilczek, Phys. Rev. Lett. **91**, 032001 (2003).

[62] E. W. Kolb and M. S. Turner, *The Early Universe* (Addison Wesley, Reading, 1990).

[63] L. N. Cooper, Phys. Rev. **104**, 1189 (1956).

[64] J. R. Taylor, *Scattering Theory*, 3rd ed. (John Wiley & Sons, Inc., New York, 1987).

[65] R. D. Mattuck and B. Johansson, Adv. in Phys. **17**, 509 (1968).

[66] J.-P. Blaizot and G. Ripka, *Quantum Theory of Finite Systems* (MIP press, Cambridge, 1986).

[67] G. Bruun, Y. Castin, R. Dum, and K. Burnett, Euro. Phys. J. D **7**, 433 (1999).

[68] N. N. Bogoliubov, Sov. Phys. JETP **34**, 41 (1958).

[69] J. G. Valatin, Il Nuovo Cimento **8**, 843 (1958).

[70] P. G. de Gennes, *Superconductivity of metals and alloys* (Addison-Wesley, New York, 1989).

[71] P. Anderson, Phys. Rev. **112**, 1900 (1958).

[72] P. C. Martin, in *Superconductivity*, edited by R. D. Parks (Marcel Dekker, Inc., New York, 1969), Vol. I.

[73] G. M. Bruun and B. R. Mottelson, Phys. Rev. Lett. **87**, 063606 (2001).

[74] G. M. Bruun, Phys. Rev. Lett **89**, 263002 (2002).

[75] M. A. Baranov and D. S. Petrov, Phys. Rev. A **62**, 04601 (2000).

[76] A. Griffin, *Excitations in a Bose-Condensed Liquid* (Cambridge University Press, Cambridge, 1993).

[77] M. Tinkham, *Introduction to superconductivity*, 2nd ed. (McGraw-Hill, Inc., New York, 1996).

[78] A. Bulgac and Y. Yu, Phys. Rev. Lett. **88**, 043504 (2002).

[79] M. Grasso and M. Urban, Phys. Rev. A **68**, 033610 (2003).

[80] A. Bulgac, Phys. Rev. C **65**, 051305 (2001).

[81] M. Randeria, in *Bose-Einstein Condensation*, edited by A. Griffin, D. W. Snoke, and S. Stringari (Cambridge University Press, Cambridge, 1995), Chap. 15, p. 355.

[82] L. P. Gorkov and T. K. Melik-Barkhudarov, Sov. Phys. JETP **13**, 1018 (1961).

[83] H. Heiselberg, C. J. Pethick, H. Smith, and L. Viverit, Phys. Rev. Lett. **85**, 2418 (2000).

[84] Z. Hadzibabic, C. A. Stan, C. H. Schunck, M. W. Z. K. Dieckmann, and W. Ketterle, Phys. Rev. Lett. **91**, 160401 (2003).

[85] A. E. Leanhardt, T. A. Pasquini, M. Saba, A. Schirotzek, Y. Shin, D. Kielpinski, D. E. Pritchard, and W. Ketterle, Science **301**, 1513 (2003).

[86] W. Hofstetter, J. I. Cirac, P. Zoller, E. Demler, and M. D. Lukin, Phys. Rev. Lett. **89**, 220407 (2002).

[87] R. Micnas, J. Ranninger, and S. Robaszkiewicz, Rev. Mod. Phys. **62**, 113 (1990).

[88] M. Greiner, O. Mandel, T. Esslinger, T. W. Hänsch, and I. Bloch, Nature (London) **415**, 39 (2002).

[89] L. Viverit, Phys. Rev. A **66**, 023605 (2002).

[90] G. Modugno, G. Roati, F. Riboli, F. Ferlaino, R. J. Brecha, and M. Imguscio, Scince **297**, 2240 (2002).

[91] A. J.Moerdijk, B. J. Verhaar, and A. Axelson, Phys. Rev. A **51**, 4852 (1995).

[92] S. Inouye, M. R. Andrews, J. Stenger, H.-J. Miesner, D. M. Stamper-Kurn, and W. Ketterle, Nature **392**, 151 (1998).

[93] K. M. O'Hara, S. L. Hemmer, M. E. Gehm, S. R. Granade, , and J. E. Thomas, Scince **298**, 2179 (2002).

[94] C. A. Regal, C. Ticknor, J. L. Bohn, and D. S. Jin, Nature **424**, 47 (2003).

[95] T. Bourdel, J. Cubizolles, L. Khaykovich, K. M. F. Magalhães, S. J. J. M. F. Kokkelmans, G. V. Shlyapnikov, and C. Salomon, Phys. Rev. Lett. **91**, 020402 (2003).

[96] K. E. Strecker, G. B. Partridge, and R. G. Hulet, Phys. Rev. Lett. **91**, 080406 (2003).

[97] J. Cubizolles, T. Bourdel, S. J. J. M. F. Kokkelmans, G. V. Shlyapnikov, and C. Salomon, http://arxiv.org/cond-mat/0308018 (2003).

[98] S. Jochim, M. Bartenstein, G. Hendl, C. Chin, J. H. Denschlag, and R. Grimm, http://arxiv.org/cond-mat/0308095 (2003).

[99] K. Xu, T. Mukaiyama, J. R. Abo-Shaeer, J. K. Chin, D. Miller, and W. Ketterle, http://arxiv.org/cond-mat/0310027 (2003).

[100] M. Mackie, E. Timmermans, R. Côté, and J. Javanainen, Optics Express **8**, 118 (2001).

[101] C. McKenzie, J. H. Denschlag, H. Häffner, A. Browaeys, L. E. E. de Araujo, F. K. Fatemi, K. M. Jones, J. E. Simsarian, D. Cho, A. Simoni, E. Tiesinga, P. S. Julienne, K. Helmerson, P. D. Lett, S. L. Rolston, and W. D. Phillips, Phys. Rev. Lett. **88**, 120403 (2002).

[102] R. Friedberg and R. D. Lee, Phys. Lett. A **138**, 423 (1989).

[103] R. Friedberg and R. D. Lee, Phys. Rev. B **40**, 6745 (1989).

[104] E. Timmermans, K. Furuya, P. W. Milonni, and A. K. Kerman, Phys. Lett. A **285**, 228 (2001).

[105] M. Holland, S. J. J. M. F. Kokkelmans, M. L. Chiofalo, and R. Walser, Phys. Rev. Lett. **87**, 120406 (2001).

[106] Y. Ohashi1, , and A. Griffin, Phys. Rev. Lett. **89**, 130402 (2002).

[107] J. N. Milstein, S. J. J. M. F. Kokkelmans, and M. J. Holland, Phys. Rev. A **66**, 043604 (2002).

[108] M. Greiner, C. A. Regal, and D. S. Jin, http://arxiv.org/cond-mat/0311172 (2003).

[109] S. Jochim, M. Bartenstein, A. Altmeyer, G. Hendl, S. Riedl, C. Chin, J. D. Denschlag, and R. Grimm, Science (2003).

[110] G. M. Bruun and H. Heiselberg, Phys. Rev. A **65**, 053407 (2002).

[111] G. M. Bruun, Phys. Rev. A **66**, 041602 (2002).

[112] H. Heiselberg and B. Mottelson, Phys. Rev. Lett. **88**, 190401 (2002).

[113] H. Heiselberg, physics/0304005 (2003).

[114] C. A. R. Sá de Melo, M. Randeria, and J. R. Engelbrecht, Phys. Rev. Lett. **71**, 3202 (1993).

[115] F. London, *Superfluids* (John Wiley & Sons, Inc., New York, 1950), Vol. I.

[116] G. Baym, in *Mathematical Methods in Solid State and Superfluid Theory*, edited by R. C. Clark and G. H. Derrick (Oliver and Boyd, Edinburgh, 1969).

[117] L. Landau, Phys. Rev. **60**, 356 (1941).

[118] W. F. Vinen, in *Superconductivity*, edited by R. D. Parks (Marcel Dekker, Inc., New York, 1969), Vol. I.

[119] P. M. Chaikin and T. C. Lubensky, *Principles of condensed matter physics* (Cambridge University Press, Cambridge, 1995).

[120] V. P. Gusynin, V. M. Loktev, and S. G. Sharapov, JETP **88**, 685 (1999).

[121] V. P. Gusynin, V. M. Loktev, R. M. Quick, and S. G. Sharapov, Int. J. Mod. Phys. B **12**, 3035 (1999).

[122] V. J. Emery and S. A. Kivelson, Nature **374**, 434 (1995).

[123] M. E. Fisher, M. N. Barber, and D. Jasnow, Phys. Rev. A **8**, 1111 (1973).

[124] B. S. Deaver, Jr. and W. M. Fairbank, Phys. Rev. Lett. **7**, 43 (1961).

[125] N. Byers and C. N. Yang, Phys. Rev. Lett. **7**, 46 (1961).

[126] L. Onsager, Phys. Rev. Lett. **7**, 50 (1961).

[127] R. Doll and M. Näbauer, Phys. Rev. Lett. **7**, 51 (1961).

[128] G. B. Arfken and H. J. Weber, *Mathematical Methods for Physicists*, 4th ed. (Academic Press, San Diego, 1995).

[129] G. B. Hess and W. M. Fairbank, Phys. Rev. Lett. **19**, 216 (1967).

[130] A. Bohr and B. R. Mottelson, Phys. Rev. **125**, 495 (1962).

[131] J. C. Garrison, J. Wong, and H. L. Morrison, Phys. Rev. A **2**, 491 (1970).

[132] J. S. Langer and M. E. Fisher, Phys. Rev. Lett. **19**, 560 (1967).

[133] N. V. Prokof'ev and B. V. Svistunov, Phys. Rev. B **61**, 11282 (2000).

[134] B. S. Shastry and B. Sutherland, Phys. Rev. B **65**, 243 (1990).

[135] E. L. Pollock and D. M. Ceperley, Phys. Rev. B **36**, 8343 (1987).

[136] E. H. Lieb, R. Seiringer, and J. Yngvason, Phys. Rev. B **66**, 134529 (2002).

[137] A. Paramekanti, N. Trivedi, and M. Randeria, Phys. Rev. B **57**, 11639 (1998).

[138] D. Poilblanc, Phys. Rev. B **44**, 9562 (1991).

[139] D. J. Scalapino, S. R. White, and S. Zhang, Phys. Rev. B **47**, 7995 (1993).

[140] W. Krauth, Phys. Rev. B **44**, 9772 (1991).

[141] K. G. Singh and D. S. Rokhsar, Phys. Rev. B **49**, 9013 (1994).

[142] A. M. Rey, K. Burnett, R. Roth, M. Edwards, C. J. Williams, and C. W. Clark, J. Phys. B **36**, 825 (2003).

[143] R. Roth and K. Burnett, Phys. Rev. A **68**, 023604 (2003).

[144] J. J. Sakurai, *Modern Quantum Mechanics* (Addison-Wesley, Massachusetts, 1994).

[145] A. L. Fetter, in *Superconductivity*, edited by R. D. Parks (Marcel Dekker, Inc., New York, 1969), Vol. I.

[146] R. J. Donnelly, *Quantized vortices in helium II* (Cambridge University Press, Cambridge, 1991).

[147] O. V. Lounsamaa and E. Thuneberg, Proc. Natl. Acad. Sci. **96**, 7790 (1999).

[148] R. E. Packard, Phys. Rev. Lett. **28**, 1080 (1972).

[149] P. W. Anderson and N. Itoh, Nature **256**, 25 (1975).

[150] F. V. D. Blasio and Ø. Elgaøy, Phys. Rev. Lett. **82**, 1815 (1999).

[151] Ø. Elgarøy and F. V. D. Blasio, Astronomy and Astrophysics **370**, 939 (2001).

[152] A. A. Svidzinsky, Astrophys. J. **590**, 386 (2003).

[153] M. R. Matthews, B. P. Anderson, P. C. Haljan, D. S. Hall, C. E. Wieman, and E. A. Cornell, Phys. Rev. Lett. **83**, 2498 (1999).

[154] K. W. Madison, F. Chevy, W. Wohlleben, and J. Dalibard, Phys. Rev. Lett. **84**, 806 (2000).

[155] J. R. Abo-Shaeer, C. Raman, J. M. Vogels, and W. Ketterle, Scince **292**, 476 (2001).

[156] A. L. Fetter and A. A. Svidzinsky, J. Phys.: Condens. Matt. **13**, R135 (2001).

[157] H. L. F. von Helmholtz, Crelle **4**, 1 (1858).

[158] Gustav Kirchhoff, *Vorlesungen über Mathematische Physik: Mechanik*, 4th ed. (Leipzig, 1897).

[159] J. D. Jackson, *Classical Electrodynamics*, 2nd ed. (Wiley, New York, 1975).

[160] A. A. Abrikosov, Sov. Phys. JETP **5**, 1174 (1957).

[161] P. Haljan, I. Coddington, P. Engels, and E. A. Cornell, Phys. Rev. Lett. **87**, 210403 (2003).

[162] I. Coddington, P. Engels, V. Schweikhard, and E. A. Cornell, Phys. Rev. Lett. **91**, 100402 (2003).

[163] E. B. Sonin, Phys. Rev. Lett. **59**, 87 (1987).

[164] J. R. Scrieffer, *Superconductivity* (Benjamin, New York, 1964).

[165] A. Andersen, T. Bohr, B. Stennum, J. J. Rasmussen, and B. Lautrup, Phys. Rev. Lett. **91**, 104502 (2003).

[166] J. E. Williams and M. J. Holland, Nature **401**, 568 (1999).

[167] E. L. Andronikashvili and Y. G. Mamaladze, Rev. Mod. Phys. **38**, 567 (1966).

[168] H. Alles, J. P. Ruutu, A. V. Babkin, P. J. Hakonen, O. V. Lounasmaa, and E. B. Sonin, Phys. Rev. Lett. **74**, 2744 (1995).

[169] M. Basta, V. Piciarelli, and R. Stella, Phys. Educ. **35**, 120 (2000).

[170] D. L. Feder, C. W. Clark, and B. I. Schneider, Phys. Rev. A **61**, 011601R (1999).

[171] F. Dalfovo and S. Stringari, Phys. Rev. Lett. **63**, 011601 (2000).

[172] T. P. Simula, S. M. M. Virtanen, and M. M. Salomaa, Phys. Rev. A. **66**, 035601 (2002).

[173] P. Nozières and D. Pines, *The Theory of Quantum Liquids* (Perseus Books, Cambridge, 1999), Vol. II.

[174] D. A. Huse, M. P. A. Fisher, and D. S. Fisher, Nature **358**, 553 (1992).

[175] V. L. Ginzburg and L. P. Pitaevskii, Sov. Phys. JETP **34**, 1240 (1958).

[176] V. L. Ginzburg and L. P. Pitaevskii, Sov. Phys. JETP **7**, 858 (1958).

[177] D. A. Butts and D. S. Rokhsar, Nature **397**, 327 (1999).

[178] H. Pu, C. K. Law, J. H. Eberly, and N. Bigelow, Phys. Rev. A **59**, 1533 (1999).

[179] M. Möttönen, T. Mizushima, T. Isoshima, M. M. Salomaa, and K. Machida, Phys. Rev. A **68**, 023611 (2003).

[180] R. Blauwgeers, V. B. Eltsov, M. Krusius, J. J. Ruohio, R. Schanen, and G. E. Volovik, Nature **404**, 471 (2000).

[181] P. L. Marston and W. M. Fairbank, Phys. Rev. Lett. **39**, 1208 (1977).

[182] P. Engels, I. Coddington, P. C. Haljan, V. Schweikhard, , and E. A. Cornell, Phys. Rev. Lett. **90**, 170405 (2003).

[183] G. M. Bruun and L. Viverit, Phys. Rev. A **64**, 063606 (2001).

[184] Ø. Elgarøy, http://arxiv.org/cond-mat/0111440 (2001).

[185] L. Kramer and W. Pesch, Z. Phys. **269**, 59 (1974).

[186] F. Gygi and M. Schlüter, Phys. Rev. B **43**, 7609 (1991).

[187] N. Nygaard, G. M. Bruun, C. W. Clark, and D. L. Feder, Phys. Rev. Lett. **90**, 210402 (2003).

[188] C. Caroli, P. G. D. Gennes, and J. Matricon, Phys. Lett. **9**, 307 (1964).

[189] J. Bardeen, R. Kümmel, A. E. Jacobs, and L. Tewordt, Phys. Rev. **187**, 556 (1969).

[190] H. F. Hess, R. B. Robinson, R. C. Dynes, J. M. Valles, Jr., and J. V. Waszczak, Phys. Rev. Lett. **62**, 214 (1989).

[191] H. F. Hess, R. B. Robinson, and J. V. Waszczak, Phys. Rev. Lett. **64**, 2711 (1990).

[192] F. Gygi and M. Schlüter, Phys. Rev. B **41**, 822 (1990).

[193] J. D. Shore, M. Huang, A. T. Dorsey, and J. P. Sethna, Phys. Rev. Lett. **62**, 3089 (1989).

[194] U. Klein, Phys. Rev. B **41**, 4819 (1990).

[195] S. Ullah, A. T. Dorsey, and L. B. Buchholtz, Phys. Rev. B **42**, 9950 (1990).

[196] A. L. Fetter, Phys. Rev. Lett. **27**, 986 (1971).

[197] N. W. Ashcroft and N. D. Mermin, *Solid State Physics* (Saunders College Publishing, Orlando, 1976).

[198] P. H. Keesom and R. Radebaugh, Phys. Rev. Lett. **13**, 685 (1964).

[199] S. Stringari, Phys. Rev. Lett. **82**, 4371 (1999).

[200] J. C. Wynn, D. A. Bonn, B. W. Gardner, Y.-J. Lin, R. Liang, W. N. Hardy, J. R. Kirtley, and K. A. Moler, Phys. Rev. Lett. **87**, 197002 (2001).

[201] E. J. Yarmchuk, M. J. V. Gordon, and R. E. Packard, Phys. Rev. Lett. **43**, 214 (1979).

[202] P. Törma and P. Zoller, Phys. Rev. Lett. **85**, 487 (2000).

[203] G. M. Bruun, P. Törma, M. Rodriguez, and P. Zoller, Phys. Rev. A **64**, 033609 (2001).

[204] N. Hayashi, M. Icioka, and K. Machida, Phys. Rev. Lett. **77**, 4074 (1996).

[205] F. Zambelli and S. Stringari, Phys. Rev. Lett. **81**, 1754 (1998).

[206] S. Sinha, Phys. Rev. A **55**, 4325 (1997).

[207] R. J. Dodd, K. Burnett, M. Edwards, and C. W. Clark, Phys. Rev.A **56**, 587 (1997).

[208] A. A. Svidzinsky and A. L. Fetter, Phys. Rev. A **58**, 3168 (1998).

[209] F. Chevy, K. W. Madison, and J. Dalibard, Phys. Rev. Lett. **85**, 2223 (2000).

[210] S. Stringari, Phys. Rev. Lett. **86**, 4725 (2001).

[211] E. Hodby, S. A. Hopkins, G. Hechenbalikner, N. L. Smith, and C. J. Foot, Phys. Rev. Lett. **91**, 090403 (2003).

[212] P. B. Blakie and R. J. Ballagh, Phys. Rev. Lett. **86**, 3930 (2001).

[213] K. E. Strecker, G. B. Partridge, A. G. Truscott, and R. G. Hulet, Nature **417**, 150 (2002).

[214] M. Rodriguez, G.-S. Paranoanu, and P. Törma, Phys. Rev. Lett. **87**, 100402 (2001).

[215] W. H. Press, B. P. Flannery, S. A. Teukolsky, and W. T. Vetterling, *Numerical Recipes* (Cambridge University Press, Cambridge, 1989).

[216] K. Huang and C. N. Yang, Phys. Rev. **105**, 767 (1957).

[217] E. Fermi, Ricerca. Scient. **7**, 13 (1936).

[218] G. Breit, Phys. Rev. **71**, 215 (1947).

[219] J. M. Blatt and V. F. Weisskopf, *Theoretical Nuclear Physics* (Wiley, New York, 1952).

[220] D. Baye and P.-H. Heenen, J. Phys. A: Math. Gen. **19**, 2041 (1986).

[221] J. C. Light and T. Carrington, Jr., Adv. Chem. Phys. **114**, 263 (2000).

[222] S. E. Koonin and D. C. Meredith, *Computational Physics* (Addison-Wesley, Reading, Masachusetts, 1990).

[223] D. Lemoine, J. Chem. Phys. **101**, 1 (1994).

[224] G. Szegö, *Orthogonal Polynomials*, Vol. XXIII of *American Mathematical Society Colloqium Publications* (American Mathematical Society, New York, 1939).

[225] M. Abramowitz and I. Stegun, *Handbook of Mathematical Functions* (Dover, New York, 1970).

[226] G. C. Wick, Phys. Rev. **50**, 268 (1950).

[227] D. Zubarev, V. Morozov, and G. Röpke, *Statistical Mechanics of Nonequilibrium Processes* (Akademie Verlag, Berlin, 1996), Vol. 1.

[228] P. Dennery and A. Krzywicki, *Mathematics for Physicists* (Dover, New York, 1995).

[229] I. S. Gradshteyn and I. M. Ryzhik, *Table of Integrals, Series, and Products* (Academic Press, Inc., San Diego, 1965).